Application of Variable Geometry Turbine on Gasoline Engines and the Optimisation of Transient Behaviours

Tang, Huayin

Award date:
2016

Awarding institution:
University of Bath

Application of Variable Geometry Turbine on Gasoline Engines and the Optimisation of Transient Behaviours

Huayin Tang

A thesis submitted for the degree of Doctor of Philosophy

University of Bath
Department of Mechanical Engineering

February 2016

Abstract

Downsizing of the internal combustion engine (ICE) through turbocharging is one of the primary approaches to reduce fuel consumption (FC) and emissions. The challenges for turbocharged engines include meeting low-end torque and transient torque response. While the Variable Geometry Turbine (VGT) is a proven measure for Diesel engines, quantitative understanding is still required to optimise the use of VGT on gasoline engines.

The accuracy of engine simulation, which is crucial in the design process, is largely affected by turbocharger modelling. Therefore, a novel turbocharger on-engine mapping facility was developed to improve the understanding and simulation accuracy of turbocharging system operating under variable pulsating and thermal conditions.

Experimental results demonstrated a 48Nm (17.7%) improvement in maximum torque and 4% FC improvement in the boosted region at 2000rpm through replacing the Fixed Geometry Turbine (FGT) with VGT on a 2.0 litter direct injection gasoline engine. Simulation was carried out using GT-Power to analyse the improvements. A 2.3% FC improvement was predicted with 0.6% from reduction in pumping work, 1.5% from combustion thermal efficiency and 0.2% from variation of compressor efficiency.

To investigate the effects of turbine size, three VGT sizes were selected and simulated. Depending on the size of VGT, the FC at engine speeds 3500rpm and below was reduced by 0.5 - 1% from the reduction of pumping work. The engine torque knee-point was advanced by 100 - 250rpm, and the transient response was improved by up to 4 seconds (73.4%). Therefore, further downsizing can be enabled by using VGT. To achieve the full potential especially the FC benefits at high speeds, a variable nozzle type VGT assisted by an additional waste-gate was proposed.

It is challenging to manage VGT during transients efficiently primarily because of the non-monotonic characteristics of the turbine response to VGT position. A methodology was established to investigate and optimise the transient response. To overcome the challenges and to reduce calibration effort, a semi-physical control strategy was developed. The optimum VGT trajectories were captured by this control strategy, while PID controller could not reach target engine torque in four of six cases simulated. Compared with PID controller, the turbocharger response time was improved by 15-19% in the two cases where PID controller can reach the target. This novel structure is also applicable to other complex systems such as two-stage turbocharging system and Diesel air-path system.

Acknowledgements

Firstly, I would like to express my appreciation to my supervisors, Professor Chris Brace and Dr Sam Akehurst for their patience and support. They have always been ready to provide help and suggestions whenever I was in need, regardless of the nature of the problem (research, life, career, finances). Having witnessed Chris's experience of raising six children I know I will not have more than three, although he has always encouraged me to have more!

I am also grateful to Dr Richard Burke, Dr Colin Copeland, Dr Chris Bannister and my other supervisors who gave me the opportunity to advance in my career and to work in the TSB project Torotrak V-Charge. This has made my last year at the University of Bath much more productive and fruitful. This high-quality project has taught me the product development in a commercial environment.

I thank also the Graduate School Scholarship from the Faculty of Engineering and Design at the University of Bath, especially Professor Gary Hawley for offering me the scholarship. I must thank all my colleagues at the Powertrain and Vehicle Research Centre at Bath. This is undoubtedly a capable and enthusiastic team.

I would like to thank Jaguar Land Rover Ltd for sponsoring my PhD. I very much appreciate the guidance from my industry supervisor – Dr Les Smith from Jaguar Land Rover Ltd, who became my supervisor in my subsequent career. It makes me feel embarrassed to look back at what I have reported in project meetings. I was surprised when he offered me a job to work in his elite team at JLR.

I have been very privileged to work with Jaguar Land Rover Ltd, Ford Motor Company, Cummins Turbo Technologies and Honeywell Turbo Technologies in the first and second phases of the TurboCentre project. The testing and analysis were carried out at the university. The turbochargers and engines were provided by the manufacturers and the OEMs. I am grateful to Dr Geoff Capon from Ford for his

help. His inspiring book "Turbocharging the Automotive Diesel Engine" was one of the most significant books in this field. Thanks to Professor Brace and Dr Capon who are big fans of curries, I did not have much of other cuisines in our gathering events.

I want to also thank Peter Davis and Ludek Pohorelsky from HTT, and also Dr Kai Zhang, Dr Ganesan Subramanian and Stephen Garrett from CTT for their support and the knowledge they shared with me.

I would also like to thank Emanuele Servetto from Powertech Engineering S.r.l. for the support and advices. Unfortunately, I did not manage to learn Italian.

I have also enjoyed working with Matt Smith from Sierra-CP Engineering who helped with setting up the connection between Matlab and the test cell control system. I hope that, in the future, I will be able to control the test systems from my office remotely.

I would not have been able to complete my work without assistance from our great technician team. I give special thanks to Bob Gusthart, Jim Cansell, Graham Rattley and James Burge. Surprisingly, they are also excellent English teachers who taught me words I could not have learned from text books.

To my friends, Deepak Hari, Qingning Zhang, Karl Giles, Dian Liu, Dr Andy Lewis, Calogero Avola, Dominic Parsons, Bo Hu and Tomasz Duda who have consistently supported me throughout my PhD. And to my other friends from China, Qiyou Deng, Zhihang Chen, Pengfei Lu, Pin Lv and Dai Liu, who were always with me – when they wanted to test the ability to metabolise alcohol.

Finally and most importantly, I deeply appreciate my family's support and understanding. For them to allow their only child to be away from home for several years is not an easy decision to make. Thankfully, I met Becky Di Bao without whom I would not need to travel between Bath and London that often. Our marriage will be the most important event in 2015, since holding my child at my graduation ceremony is unlikely.

Table of Contents

Abstract ……i

Acknowledgements ……ii

Table of Contents ……..iv

List of Figures ……ix

List of Tables ……..xv

Notations ……xvii

Chapter 1 - Introduction 1

1.1. Background 2

1.2. Downsizing and turbocharging of internal combustion engine 3

1.3. Aim and objectives 5

1.4. Scope of thesis 6

Chapter 2 - Review of the application of VGT to the downsized gasoline Engine 9

2.1. Fundamentals and Types of VGT 10

2.2. Challenges of Gasoline VGT Application 16

2.3. Downsized Gasoline Engines 19

2.4. Gasoline VGT Studies 26

2.5. Control Strategy 34

2.6. Summary 36

2.7. Conclusions 37

Chapter 3 - *Experimental facilities and testing procedures* 39

3.1. Engine hardware 40

3.2. Purposes and requirements for the experimental campaign 42

3.3. Test cell setup 43

3.3.1 Test control system 43

3.3.2 Measurement system 45

3.3.3. Test procedures 45

3.3.3.1. Steady state tests 47

3.3.3.2. Transient tests 49

3.4. Conclusions 50

Chapter 4 - Turbocharger On-Engine Mapping Facility 52

4.1. Introduction 53

4.1.1. Challenges in using conventional turbocharger performance maps in engine simulation 53

4.1.2. Measures to investigate and overcome the challenges 55

4.2. Facility description 59

4.2.1. Objectives of the test facility 59

4.2.2. Layout of the facility 60

4.2.3. Measurement system 62

4.2.4. Test procedure 63

4.3. Test results 67

4.3.1. Repeatability 67

4.3.2. Turbine mapping 69

4.3.3. Compressor mapping 74

4.4. Future improvement on the facility 76

4.5. Conclusions 78

Chapter 5 - Simulation Methodology 80

5.1. Introduction 81

5.1.1. Engine modelling 81

5.1.2. GT-Power 82

5.2. Modelling techniques and simulation validation at steady state operating points 83

5.2.1. Combustion modelling 83
5.2.1.1. Available models in GT-Power 83
5.2.1.2. Three pressure analysis 84
5.2.1.3. Combustion model validation 87
5.2.1.4. Critiques on combustion model calibration 93
5.2.2. Gas dynamics modelling 94
5.2.2.1. Flow modelling in GT-Power 94
5.2.2.2. Flowsplit element 96
5.2.2.3. Model set up 98
5.2.2.4. Model validation 99
5.2.3. Turbocharger modelling 102
5.2.3.1. Representation of turbocharger elements 102
5.2.3.2. Compressor model in GT-Power 105
5.2.3.3. Turbine model in GT-Power 106
5.2.3.4. Scaling of turbocharger performance map 107
5.2.3.5. Turbocharger model validation 109
5.2.3.6. Critique of turbocharger simulation 111
5.3. Validation of transient simulation 112
5.3.1. Overall performance 112
5.3.2. Combustion system 114
5.3.3. Turbocharging system 116
5.3.4. Final validation 125
5.4. Conclusions 127
Chapter 6 - Steady state behaviour 129
6.1. Trade-off between fuel consumption and turbine inlet temperature 130
6.2. Comparison of FGT and VGT 137
6.2.1. Experimental results 137

6.2.2. Simulation results 139

6.2.3.1. Effect of changes in exhaust manifold 140

6.2.3.2. Effect of changes in knock-limited spark timing 142

6.2.3.3. Effect of changes of turbine 142

6.2.3.4. Effect of changes of compressor 143

6.2.3.5. Distribution of fuel consumption improvement 144

6.3. Turbine matching for steady state performance and comparison between FGT and VGT 145

6.3.1. Turbine matching criteria 145

6.3.2. Comparison of engine steady state performance 150

6.3.2.1. Engine fuel consumption 150

6.3.2.2. Maximum torque at low engine speeds 154

6.3.2.3. Trade-off between low-end torque and fuel consumption 157

6.4. Conclusions 160

Chapter 7 - Transient behaviour 163

7.1. Optimisation of transient response in experiments 164

7.1.1. Experimental approach 164

7.1.2. Experimental results 166

7.1.2.1. Response of engine brake torque 166

7.1.2.2. Response of turbocharger speed 168

7.1.2.3. Optimisation of the transient operation 169

7.2. Optimisation of transient response in simulations 176

7.3. Investigation of transient response 180

7.4. Turbine matching for transient response and comparison between FGT and VGT 190

7.5. Conclusions 200

Chapter 8 - Transient control strategy 203

8.1. Selection of control strategy 204

8.2. Development of the semi-physical control strategy 208

8.3. Validation of the control strategy 212

8.4. Conclusions 216

Chapter 9 - Conclusions 218

9.1. Summary 219

9.2. Outlook 223

References 224

List of Figures

Figure 2.1: VGT types which vary area radially 11
Figure 2.2: Construction of a typical VGT 12
Figure 2.3: VGT types which vary area axially 14
Figure 2.4: Apparent turbine efficiency against normalized total mass flow rate [31] 14
Figure 2.5: Effects of nozzle clearance on turbine efficiency [54] 16
Figure 2.6: VNT mechanism [60] 17
Figure 2.7: Schematic of the control system of the Honda VFT turbocharged engine [37] 23
Figure 2.8: Control strategy of the VFT valve and the waste-gate [37] 24
Figure 2.9: Comparison of VGT and FGT turbochargers [37] 24
Figure 2.10: Effect of EGR rate on Lambda and spark advance [81] 25
Figure 2.11: Effect of WCEM on BMEP [64] 28
Figure 2.12: Over-fuelling requirements and BSFC comparison [64] 28
Figure 2.13: Transient response comparison [37] 30
Figure 2.14: Full load apparent turbine efficiency comparison between FGT and VNT [40] 31
Figure 2.15: Comparison of BSFC between VFT and VGT [40] 32
Figure 2.16: The operating range (specified with dashed lines) in which the load can be controlled by the vane position [90] 35
Figure 2.17: Transient vane position control strategies [91] 36
Figure 3.1: Photograph of experimental facility 41
Figure 3.2: Test control systems 44
Figure 3.3: Target and actual VGT trajectories 44
Figure 3.4: Layout of the test facilty 47
Figure 3.5: Engine operating points for steady state 48
Figure 4.1: Layout of the on-engine turbocharger mapping facility 61
Figure 4.2: Repeatability of turbine efficiency 68

Figure 4.3: Repeatability of compressor efficiency 69
Figure 4.4: Turbine flow characteristics at different VGT positions 70
Figure 4.5: Turbine efficiency measured at three different engine speeds..... 70
Figure 4.6: Instantaneous turbine inlet pressures at three engine speeds..... 71
Figure 4.7: Calculated turbine efficiency at VGT fully closed 73
Figure 4.8: Compressor efficiency contour map generated from cold test 75
Figure 4.9: Comparison of compressor efficiency under fired and unfired conditions 76
Figure 5.1: Three pressure analysis……...….85
Figure 5.2: Cyclic variation in cylinder 1 at 32Nm 88
Figure 5.3: Simulated cylinder pressure from TPA and measured pressure at 32Nm 89
Figure 5.4: Measured and simulated cylinder pressure at 229Nm with VGT turbocharger 91
Figure 5.5: Measured and simulated cylinder pressure at 319Nm with VGT turbocharger 92
Figure 5.6: Example of a flowsplit element 97
Figure 5.7: Exhaust manifold for VGT 98
Figure 5.8: Mass flow entering flowsplit element (FGT turbocharger, 2200rpm full load)..... .99
Figure 5.9: Engine model without turbocharger 100
Figure 5.10: Instantaneous pressure at exhaust port of cylinder 1, 2000rpm 32Nm 100
Figure 5.11: Instantaneous pressure at exhaust port of cylinder 1, 2000rpm 229Nm 101
Figure 5.12: Instantaneous pressure at exhaust port of cylinder 1, 2000rpm 319Nm 101
Figure 5.13: Effects of expansion diameter and characteristic length on exhaust port instantaneous pressure..... 102
Figure 5.14: Measured and simulated turbine expansion ratio 110
Figure 5.15: Instantaneous pressure at turbine inlet and outlet measured at 2200rpm 112
Figure 5.16: Comparison between measurements and simulation results of transient performance with imposed turbocharger rotational speed 113
Figure 5.17: Predictions of residual gas fraction during transient 114

Figure 5.18: Measured and simulated 10-90% burn duration during transient 115
Figure 5.19: Measured and simulated peak pressure in cylinder 1 during transient 115
Figure 5.20: Measured and simulated gross IMEP at cylinder 1 during transient ... 116
Figure 5.21: Instantaneous turbine expansion ratio during transient, VGT 60% closed 117
Figure 5.22: Fitted curves of normalised turbine efficiency against normalised blade speed ratio 118
Figure 5.23: Comparison between measured and simulated turbocharger rotational acceleration 120
Figure 5.24: Compressor pressure ratio during transient (VGT 75% closed after tip-in) 120
Figure 5.25: Predicted compressor power during transient (VGT 75% closed after tip-in)..... 121
Figure 5.26: Predicted normalised blade speed ratio 123
Figure 5.27: Turbine operating points during transient, VGT 60% closed after tip-in 123
Figure 5.28: Effects of changing turbine efficiency shape factor at low blade speed ratio on the simulated turbocharger rotational acceleration 124
Figure 5.29: Mass air flow during transient (simulations with connected turbocharger shaft)..... 125
Figure 5.30: Turbocharger speed during transient (simulations with connected turbocharger shaft) 125
Figure 5.31: Comparison between simulations with original map and modified map 127
Figure 6.1: Spark timing and Lambda test points 131
Figure 6.2: BSFC at various equivalence ratios..... 132
Figure 6.3: BSFC and TIT at various operating conditions 133
Figure 6.4: P-V diagram of the most advanced spark timing settings at each Lambda target..... 133
Figure 6.5: Constrained engine load with stoichiometric combustion for different TIT limits..... 135
Figure 6.6: Engine operating points in NEDC test 136
Figure 6.7: Comparison of engine operating window at 2000rpm WOT 138

Figure 6.8: Comparison of engine fuel consumption 139
Figure 6.9: Measured instantaneous pressures at exhaust port of cylinder 1 140
Figure 6.10: Layout of exhaust system in 1-D engine model 141
Figure 6.11: Simulated instantaneous pressures at exhaust port of cylinder 1 141
Figure 6.12: Distribution of fuel consumption improvement 145
Figure 6.13: Effect of turbine size on exhaust manifold pressure 148
Figure 6.14: Contour plot of turbine efficiency (%) and full load turbine operating points on the large and small VGTs 149
Figure 6.15: Contour plot of turbine efficiency (%) and full load turbine operating points for the medium VGT 149
Figure 6.16: Contour plot of turbine efficiency (%) and full load turbine operating points for the original FGT 150
Figure 6.17: Fuel consumption benefits compared to FGT – full load 151
Figure 6.18: Turbine efficiency comparison at full load (VGT turbines with waste-gate if necessary) 152
Figure 6.19: Fuel consumption benefits compared to FGT – part load 152
Figure 6.20: Predicted engine low-end torque 155
Figure 6.21: Simulated compressor operating points at 1300rpm engine speed 156
Figure 6.22: Contour plot of turbine efficiency (%) and 1300rpm maximum load . 156
Figure 6.23: Normalised power weighted turbine efficiency and vane position 157
Figure 6.24: Trade-off between torque knee-point and fuel consumption at high speeds 159
Figure 6.25: Trade-off between torque knee-point and fuel consumption at high speeds 159
Figure 7.1: Torque responses of single step change VGT actuator trajectories 165
Figure 7.2: Torque responses of the six tests with different VGT settings; the measured torque has been smoothed using 10-points smoothing 166
Figure 7.3: Torque responses at the second stage (0.5 – 1.0 s); the measured torque has been smoothed using 10-points smoothing 167
Figure 7.4: Instantaneous turbine inlet pressures at the second stage of three tests 167
Figure 7.5: Turbine total-to-static pressure ratio and engine volumetric efficiency 168
Figure 7.6: Fitted responses of the turbocharger speed at 1.5 s and turbocharger speed at 1.0 s with VGT 75% closed 169

Figure 7.7: Response curve between the turbocharger speed at the end of the first stage and the torque rise in the first stage. 170
Figure 7.8: Trade-off between the turbocharger speed at 1.5 s and T_{50} 172
Figure 7.9: Pareto optimal front of the trade-off between turbocharger speed at 1.5 s and T_{50} 172
Figure 7.10: Torque responses of trajectories in Pareto optimal curve region 1 173
Figure 7.11: Comparison of the optimised trajectories and the reference trajectory 175
Figure 7.12: Simulated responses of the turbocharger and engine during transient 177
Figure 7.13: Simulated turbocharger acceleration against T_{50} (VGT 70% closed at first stage in transient) 178
Figure 7.14: Simulated turbocharger acceleration against T_{50} (all VGT openings at first stage in transient) 178
Figure 7.15: Comparison between experimental data and simulation results 179
Figure 7.16: Simulated response of engine torque and turbocharger speed (Small VGT, 1500rpm) 181
Figure 7.17: Transient simulation results of single step change VGT trajectories (Small VGT, 1500rpm) 182
Figure 7.18: Comparison of turbocharger speed rise between single step change simulations and full DOE simulations (Small VGT, 1500rpm) 182
Figure 7.19: Simulated optimum VGT trajectory for small VGT at 1500rpm 183
Figure 7.20: Simulated responses of key parameters during the first stage of transient (Small VGT, 1500rpm) 184
Figure 7.21: Simulated turbine isentropic power at first 1 second after tip-in (Small VGT, 1500rpm) 185
Figure 7.22: Simulated responses of key parameters during entire transient (Small VGT, 1500rpm) 185
Figure 7.23: Prediction of the engine volumetric efficiency using the input of engine mass air flow and pressure ratio across engine block (1500rpm) 186
Figure 7.24: Prediction of the engine volumetric efficiency at two engine mass flow levels (1500rpm) 187
Figure 7.25: Simulated ratio of compressor power to turbine power during transient (Small VGT, 1500rpm) 188
Figure 7.26: Three stages during transient (Small VGT, 1500rpm) 189

Figure 7.27: Simulated response of engine torque (Small VGT, 1500rpm) 190
Figure 7.28: Simulated turbocharger speed rise of the three VGTs during transient at 1500rpm and 2000rpm 191
Figure 7.29: Comparison of turbocharger speed rise between single step change simulations and full DOE simulations (Small VGT, 2000rpm) 192
Figure 7.30: Optimum VGT trajectories from simulation results 192
Figure 7.31: Flow characteristics of the optimum VGT settings at first stage during transient simulation 193
Figure 7.32: Simulated turbocharger response during transient with optimum trajectories 196
Figure 7.33: Simulated engine torque knee point and improvement in turbocharger response time 196
Figure 7.34: Trade-off between turbocharger response time and averaged fuel consumption at low speeds 197
Figure 7.35: Trade-off between turbocharger response time and averaged fuel consumption at high speeds 198
Figure 7.36: Radar charts showing normalised improvements of each VGT system compared with the FGT 199
Figure 8.1: Correlation between maximum turbocharger speed rise and the engine pressure ratio 207
Figure 8.2: Correlation between maximum turbocharger speed rise and the engine delta pressure 207
Figure 8.3: Diagram of the estimation of turbine power for each VGT opening 210
Figure 8.4: Integration of the engine model and the control strategy 211
Figure 8.5: Comparison of the VGT trajectories 212
Figure 8.6: Comparison of the turbocharger response 213
Figure 8.7: Comparison of the engine brake torque response 213
Figure 8.8: Data points used to calibrate the engine volumetric efficiency model at 1500rpm 214

List of Tables

Table 2.1: Comparison of applications for various types of VGT turbocharger on the gasoline engine……19
Table 2.2: Typical downsized and turbocharged gasoline engines……20
Table 2.3: Comparison between VGT and FGT on a 2.0 L gasoline engine (approximation) [57]……..32
Table 2.4: Vehicle acceleration performance comparison: FGT vs. VAT [24]……..33
Table 2.5: Summary of VGT and FGT comparisons……..37
Table 3.1: Key measurement channels 46
Table 4.1: Turbocharger mapping facilities 58
Table 4.2: Control actuators and the primary functions 63
Table 5.1: Operating points for combustion model validation 88
Table 5.2: TPA simulation results at 2000rpm 32Nm 90
Table 5.3: Measured data and simulation results at 229Nm 91
Table 5.4: Measured data and simulation results at 319Nm 92
Table 5.5: Summary of combustion model validation at 2000rpm 93
Table 5.6: Comparison between measured data and simulated results of the engine model without turbocharging system 102
Table 5.7: Comparison between measured data and simulated results of full engine model with turbocharging system at 2000rpm 229 Nm 110
Table 5.8: Comparison between turbine efficiency fitting factors with default settings and modified settings 126
Table 6.1: Summary statistics for the TIT response model 134
Table 6.2: Turbine matching criteria for investigation 147
Table 6.3: Turbine scaling factors 149
Table 6.4: Fuel consumption improvement comparison at high speeds and low speeds 153
Table 6.5: VGT selection criteria based on steady state performance 160

Table 7.1: Comparison of the optimised strategies 175
Table 7.2: Simulation results of time required to reach target turbocharger speed .. 195
Table 7.3: Selection criteria for VGT configurations 200
Table 8.1: List of three possible structures of control strategy 206
Table 8.2: Summary of the parameters required to measure and model for this control strategy 211
Table 8.3: Summary of the parameters required to measure and model for this control strategy 215

Notation

A	Turbine housing throat area
BDC	Bottom dead centre
BSFC	Brake specific fuel consumption
BMEP	Brake mean effective pressure
CAD	Computer-aided design
CFD	Computational fluid dynamics
CO_2	Carbon dioxide
DI	Direct-injection
ECU	Engine control unit
EGR	Exhaust gas recirculation
ER	Expansion ratio
FC	Fuel consumption
FGT	Fixed geometry turbine
FMEP	Friction mean effective pressure
HP	High pressure
ICE	Internal combustion engine
IMEP	Indicated mean effective pressure
LP	Low pressure
NEDC	New European Drive Cycle
NO_x	Oxides of nitrogen
PI	Port injection
PMEP	Pumping mean effective pressure
PR	Pressure ratio
PRESS	Predicted residual error sum of squares
PWM	Pulse width modulation
R	Turbine housing radius
RMSE	Residual mean square error
SGDI	Spray guided direct injection
TDC	Top dead centre
TIT	Turbine inlet temperature
TPA	Three pressure analysis
VAT	variable turbine housing throat area
VFT	Variable flow turbine
VGT	Variable Geometry Turbine
VNT	Variable geometry nozzle turbine
VVT	Variable valve timing
WOT	Wide-open-throttle
WCEM	Water-cooled exhaust manifold

Chapter 1 - *Introduction*

Downsizing through turbocharging is a primary approach to improve the fuel economy of internal combustion engines. The Variable geometry turbine (VGT) turbocharger, which has the potential to further downsize and improve gasoline engines, will be investigated in this thesis. This was achieved through the development and use of advanced experiments and modelling techniques which improved the understanding of turbocharging systems. A new control strategy was also developed to implement advanced boosting on internal combustion engines.

This chapter lays out the background for this project. The aims and principle objectives of the thesis will be presented according to the background. This will be followed by a description of each chapter in this thesis, highlighting the contribution and impact of this work.

1.1. Background

Vehicle emission and fuel consumption legislation worldwide are driving evolutionary technologies in powertrain development. Despite the differences between each local regulations in the past, regulations on fleet averaged CO_2 emission are generally converging to around 100g/km by 2020 [1]. This demonstrated the importance and global awareness of vehicle emissions. In fact, meeting these increasingly tightening regulations in a cost-effective manner is the biggest challenge for the automotive industry nowadays.

However, there is no single solution for the powertrain design [2]. The selection of the powertrain technologies will largely depend on the target market, the applied vehicle and the maturity of technologies. A clear trade-off between the payback time and CO2 saving has been demonstrated [3]. Therefore, intelligent selection and combination of powertrain technologies are crucial. It has been stated that "Detailed analysis shows that the Internal Combustion Engine, operating on low carbon fuels, with varying degrees of electrification, is the most logical route to future on & off highway regulatory & commercial needs" [4].

Roadmaps have been drawn to foresee the potential automotive technology trends by 2050 [2, 5]. It was predicted that the level of electrification will grow continuously. The electric and plug-in hybrid vehicles will play important roles by 2050, dependent on the life cycle emissions and the breakthroughs in low cost and high energy density battery technologies. The alternative fuels/gases will also be an important part of the energy roadmap. In addition, the ICE technologies will still be a prevalent part of the powertrain.

The fact that the cumulative small improvements on ICE efficiency had been much greater than expected [6] has led to significant investments and R&D in future ICE with very high specific power and efficiency. Relative to Euro 4 gasoline engine technologies, downsizing of ICE offers potential of over 30% improvement in fuel economy at a cost/improvement rate of approximately $24 per gram(CO2)/mile [7, 8]. On top of this, another 20% fuel economy improvement can be achieved through

hybridisation at a rate of approximately $80 per gram(CO2)/mile. As the Real Driving Emission legislation will be implemented in future emission regulation, effective and integrated synergy between ICE technologies and electrification are also potential solutions for low carbon propulsion system. Electric turbocharging systems can provide additional boost capability during transient events when the engine-out NOx emission control is particularly challenging on conventional Diesel engines. This will improve the trade-offs between transient response, smoke emission and NOx emission. Aftertreatment systems equipped with electric heater also has the potential to improve the cold start behaviours. In addition, novel hybrids between ICE, mechanical, electrical and hydraulic systems through the use of flywheels [9-11] and hydraulic energy storage [12] are also very reliable and cost-effective solutions. It was stated that "Both evolutionary and disruptive technologies are likely to be successful" [1]. Therefore, the combination of improvement of ICE and electrification and other new technologies, such as fuel cell system, will be the primary approach to reduce fuel consumption and emission.

Having reviewed these trends in the automotive industry, advanced technologies that can improve the efficiency of ICE are of key importance on the energy roadmap. These advanced technologies include downsizing & boosting, combustion and fuel, valve actuation & cylinder deactivation, thermal management & friction reduction, and control optimisation.

In this thesis, a research in the area of downsizing and boosting will be presented. This will include investigations into VGT turbocharging system, and necessary facilities and tools for understanding and implementing advanced boosting systems.

1.2. Downsizing and turbocharging of internal combustion engine

Downsizing is a proven approach to reducing the fuel consumption of internal combustion engines. Higher efficiency is achieved by moving the engine's fuel efficient zones closer to normal road driving conditions and shifting to a more

efficient operating region through reducing engine displacement whilst maintaining the full load capacity via air charging [13, 14]. Furthermore, the weight of the engine and hence that of the vehicle can be lowered [15, 16] and manufacturing costs can be reduced by turbocharging the same base engine [17].

Turbocharging is one of the primary routes of downsizing [18] and has been applied predominantly to the Diesel engine [19, 20]. Although the technology has also been applied to other engine types such as the homogeneous charge compression ignition engine [21], and also to throttle loss recovery on the gasoline engine [22], it had been used on passenger cars as a means to increase the output power of the baseline engines. Turbocharged gasoline engines were limited by its combustion system, due to knock issues. Recently, turbocharged gasoline engines gained renewed interest because of the need for lower fuel consumption and the use of direct injection system, which improves the combustion behaviours and knock resistance. Therefore, turbocharging can be used as an approach to downsize the ICE.

Since the mass air flow variation of a gasoline engine is significantly higher than that of a Diesel engine, matching a turbocharger to a gasoline engine is more challenging. An air mass flow ratio of over 80:1 from rated power to idle is required for gasoline engines in contrast to the 6:1 ratio for passenger car Diesel engines [23], highlighting the necessity of varying the characteristics of the boosting system [15]. The specific torque of downsized gasoline engines with single waste-gated turbochargers is high throughout the engine speed range except at lower flow rate levels because the turbocharger design is usually optimized for medium to high flow conditions, compromising the low speed performance [17]. Furthermore, the transient response of conventional turbocharged gasoline engines is usually slower than that of naturally aspired engines due to the time period required to accelerate the turbocharger, provide sufficient boost pressure, and to achieve the maximum engine output [24, 25]. In addition, as the downsizing trend continues towards more extreme boosting, the incremental fuel consumption benefit at part-load operating points becomes smaller and the cost of achieving such increments also increases [26].

However, there are now several advanced boosting system structures with the potential to fulfil the key requirements of a fast transient response and high efficiency over a wide range of flow rates. These technologies include two-stage boosting system, supercharging with variable speed drive system, low speed compressor [27-29], electrical boosting system and VGT turbocharger [15, 30]. In this project, the potential of VGT turbocharger on gasoline engines will be investigated.

Compared to the fixed geometry turbine (FGT) which acts as a set restriction in the exhaust system [31], the VGT can vary the gas velocity and flow angle according to the engine operating condition virtually instantaneously [32], thereby achieving higher turbine efficiency across a wider range of engine speeds and loads [31, 33]. Moreover, due to the larger flexibility afforded by varying the engine load via controlling the throttle and the VGT, control strategies can be implemented that yield improvements in both the steady state and transient performance [34, 35].

1.3. Aim and objectives

The principle aim of this project is to demonstrate the potential benefits of the application of VGT to gasoline engines, thus, to show if VGT system is worth development on gasoline applications provided that the high exhaust gas temperature can be coped with more costly material. This work will use a systematic approach to compare the two technologies, FGT and VGT, both experimentally and in simulations. In order to enhance the understanding of turbocharging systems on downsized engines, novel testing facilities and simulation techniques that have been developed in this project have been used to assist the investigation. In addition, a novel transient control strategy for complex turbocharging systems has been developed and optimised to achieve the maximum potential of the turbocharger system.

According to the project aim, the following objectives were laid out:

1. Review the literature in the field of engine downsizing and turbocharging, especially the use of VGT technologies on gasoline engines.

2. Define and implement required testing and data acquisition systems. Apply test procedures to achieve repeatable and reliable experimental results.

3. Develop an advanced turbocharger testing facility to enhance the understanding of turbocharger behaviours under complex operating conditions.

4. Calibrate and use engine models for simulation comparison, and to assist experimental investigation.

5. Develop thorough understanding of VGT behaviours at steady state. Demonstrate the potential of gasoline VGT technologies for engine steady state operation.

6. Develop thorough understanding of VGT behaviours at transient operating conditions. Demonstrate the potential of gasoline VGT technologies for engine transient operation, and illustrate the trade-offs between steady state performance and transient performance.

7. Propose and develop a transient control strategy to maximise the potential of complex turbocharging systems.

1.4. Scope of thesis

The work described in each chapter from Chapter 2 to Chapter 8 in accordance with the aims and objectives of the project, are presented below:

Chapter 2 details the fundamentals and compares various types of VGTs. The technologies for engine downsizing and the state of art VGT applications on gasoline engines are reviewed and summarised.

Chapter 3 describes the facilities and approaches used in the experimental testing. The test control system, data acquisition system and test procedures developed according the requirements of the experiment are presented.

Chapter 4 presents the novel experimental facility for turbocharger on-engine mapping developed in this project. The challenges in turbocharger mapping and the countermeasures are discussed. The capability of this facility is demonstrated by presenting experimental results and investigations. Future improvements are also suggested so as to enhance the capability of this facility.

Chapter 5 demonstrates the procedure that was followed to calibrate an engine model for both steady state and transient simulations. The simulation result is validated against experimental data. The approaches and modelling techniques are discussed. Recommendations are also given for future work.

Chapter 6 presents the steady state comparison between the FGT and VGT turbochargers. The investigations are performed in both experiments and simulations. Finally, the trade-offs between steady state performances have been demonstrated. A novel configuration of variable nozzle type VGT, assisted by an additional waste-gate is proposed achieve the full potential.

Chapter 7 analyses the fundamentals of the transient behaviours of turbocharged engines. Optimisation of VGT transient trajectories are performed in both experiments and simulations, so a back-to-back comparison of transient performance can be made between FGT and VGT. Finally, the trade-offs between steady state and transient performances are presented for the selection of turbocharger technologies and turbine sizes.

Chapter 8 presents a novel transient control strategy proposed for VGT turbochargers and other complex turbocharging systems. The validation of the strategy is performed. The optimum trajectories can be achieved by this strategy, while a simple PID controller cannot reach the targets.

Chapter 9 summarises the key outcomes and conclusions of this thesis. Recommendations to the application of VGT on gasoline engines are given. In addition, the impacts and the contributions of this thesis are also summarised.

Chapter 2 - *Review of the application of VGT to the downsized gasoline Engine*

This chapter presents current downsized gasoline engines and the methods applied to achieve downsizing for fuel economy. The fundamentals of the VGT turbocharger will be detailed, followed by a summary and comparison of the various types of VGT suitable for gasoline engine boosting.

Despite the challenges, VGT technology has been used on production gasoline engines. This chapter will review the research and production examples of gasoline VGT applications. The results of these investigations will be compared and summarised in this chapter.

The comparison, discussion and summary in this chapter have been published in the form of a review article in the Institute of Mechanical Engineers International Journal of Engine Research [36].

2.1. Fundamentals and Types of VGT

The low speed performance and transient response of a turbine can be improved by using a housing with a smaller area-to-radius ratio - the ratio between the turbine housing throat area (A) to the radius (R) [37]. Lowering this ratio enables the exhaust gas flow to be accelerated to a higher velocity, thus increasing the kinetic energy; furthermore, the flow angle at the turbine tip is altered, moving the blade speed ratio (the ratio of blade tip velocity to the isentropic expansion velocity) to an optimum point, which is approximately 0.7 for an ideal radial flow turbine with a degree of reaction equal to 0.5 [38]. However, using a smaller turbine housing also reduces output at high engine speed because it acts as a restriction at high mass flow rates [39]. Since the appropriate area-to-radius ratio clearly depends on the engine speed, one of the main advantages of a VGT turbocharger is that the effective area-to-radius ratio and flow characteristics can be rapidly varied to achieve optimum turbine efficiency across a wide range of engine speeds. A further major benefit is that compared to the conventional waste-gate turbocharger that controls boost pressure by bypassing a portion of the exhaust gas, the VGT turbocharger can allow all the exhaust gas to pass through the turbine, reducing the wasted energy at the waste-gate [40, 41].

Several types of VGT are available for the gasoline engine boosting application, and include the variable geometry nozzle turbine (VNT) [42], variable turbine housing throat area (VAT) [43], variable flow turbine (VFT) [44], sliding wall with variable axial width [45], and twin scroll switching type [46]. These various forms of the VGT vary the effective flow area, either radially or axially.

The VNT, VAT and VFT, depicted in Figure 2.1, vary the throat or nozzle flow area in the radial plane. The vanes on the VNT (shown in Figure 2.2) can be closed to reduce the area between the vanes, altering the flow speed and the angle impinging

the turbine tip in order to increase the kinetic energy at low engine speeds where the exhaust gas flow and the contained energy are low [33, 44, 47]. Its flexibility means that a waste-gate is not usually required on VNT turbochargers [40]. Moreover, the VNT can deliver higher efficiency across the majority of the operating range and a larger flow rate ratio - the ratio of the maximum to minimum flow rate - than the other types of VGT [37, 38, 44, 47]. VNT turbochargers are already used on various gasoline engines such as the Porsche 911 Turbo S.

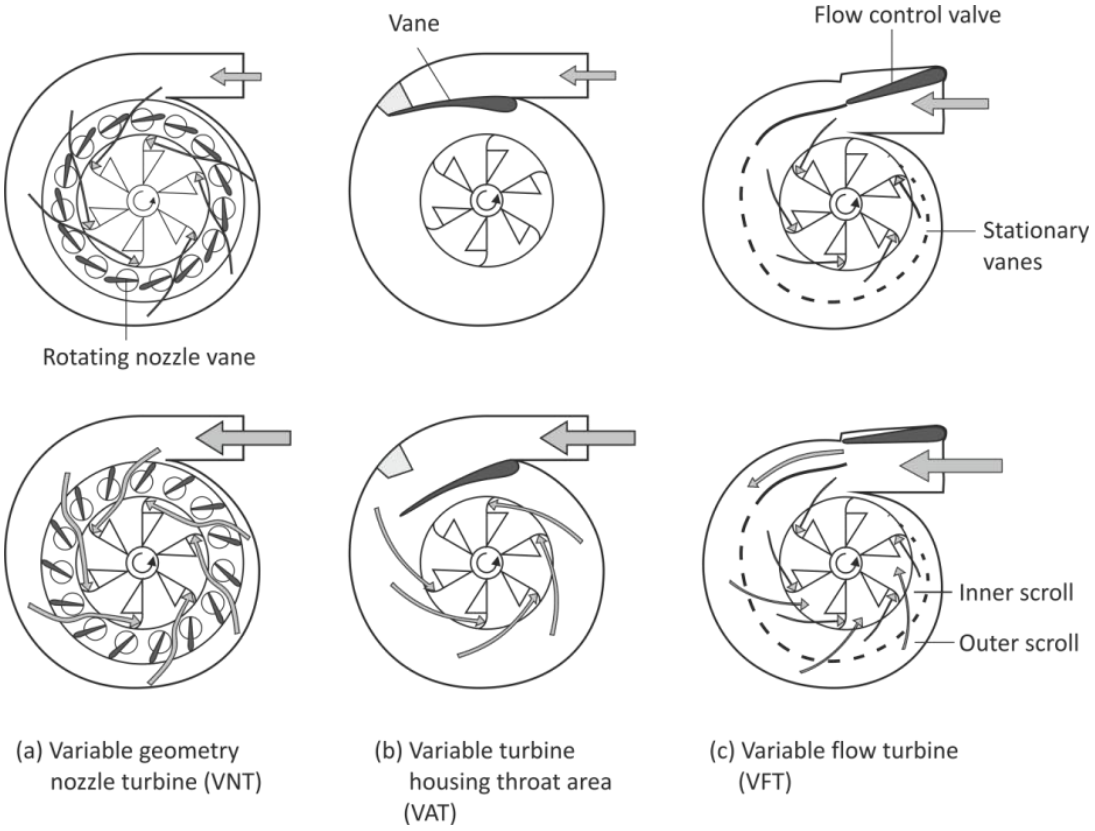

Figure 2.1: VGT types which vary area radially

Alternatively, by controlling the throat vane angle, the VAT varies the throat area, thereby changing the flow velocity and angle. Kawaguchi *et al*. [44] state that the flow rate ratio of VAT is generally lower than the VNT and that a waste-gate may thus be required to regulate the exhaust flow since the flow angle impinging the tip of the turbine cannot be varied to a large degree. Although lower efficiency and control difficulty may thus thwart VAT application, it has higher reliability and lower

cost owing to the simpler mechanism compared to the VNT.

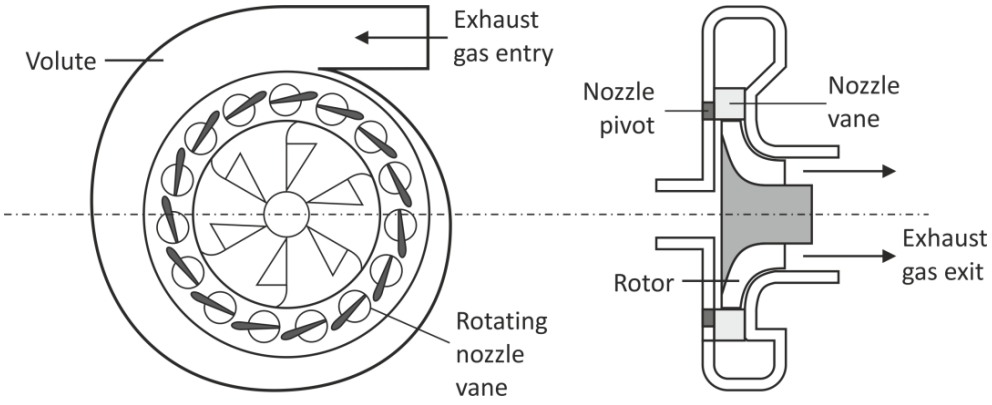

Figure 2.2: Construction of a typical VGT

Similarly, the VFT has a vane at the throat and a secondary scroll situated outside the primary scroll, with the flow within the two scrolls being controlled by the inter-scroll throat vane [33, 44, 47]. At low flow rates, the secondary scroll is closed and the exhaust gas flows through the primary scroll only, while at high flow rates, the secondary scroll is opened and the fixed vanes between the two scrolls change the flow angle of the exhaust gas; the boost pressure is controlled by continuously adjusting the flow control valve [33, 44, 47]. Kawaguchi *et al*. [44] propose a VFT turbocharger designed for gasoline engines and claim that the VFT structure is simpler than the conventional VNT, that the cost is lower, and that the device is more reliable since there are fewer moving components exposed to the high temperature corrosive exhaust gas [47]. A VFT turbocharger with an additional internal waste-gate is used on the Honda 2.3 L gasoline engine [37].

In contrast to the above-mentioned VNT, VAT and VFT configurations, devices with a sliding wall (Figure 2.3a) vary the throat area axially, and control of the exhaust gas flow velocity is achieved by changing the axial displacement of the sliding wall. Baines [48] reports that the gap between the sliding wall and the turbine housing causes efficiency losses. Petitjean *et al*. [17] propose a sliding wall VGT

turbocharger designed for gasoline engine applications in which the sliding wall mechanism is controlled by an actuator placed on the turbine housing. It has been claimed that its application on gasoline engines offers advantages over the VNT turbocharger in terms of cost and reliability.

The twin scroll switching type of turbocharger, shown in Figure 2.3b, has two scrolls along the axial direction of the turbine wheel, with one of the two scrolls being used at low flow rates to accelerate the flow. The twin scroll structure can clearly only provide limited flow rate control and accompanying efficiency improvements since the area cannot be varied continuously according to engine operating conditions [33]. Furthermore, the additional heat transfer area and friction losses are significant, especially at high engine speeds [44]. Capobianco and Gambarotta [49] showed that the efficiency of a twin-entry turbocharger under partial admission conditions is always lower than that under full admission conditions, with the interaction between the two air flow entries being highlighted. Hajilouy *et al*. [50] illustrated the same trend and highlighted flow separation and reverse flow under partial admission conditions due to the mixing of the two streams.

Compared to FGT, the flow characteristics of VGT can be varied to optimise the turbine operating point. Nevertheless, both the vane angle on VGT and the waste-gate position on FGT are actuators controlling boost pressure on turbocharged gasoline engines. Therefore, VGT turbochargers do not always operate at the optimum condition.

Capobianco and Gambarotta [31] tested a VNT (Garrett VNT 025), a VAT (Garrett VAT 025) turbine with the same turbine wheel and a FGT (Garrett TB025) with a similar turbine wheel. Their study shows that under steady flow conditions at the tested (corrected) turbocharger speed, the VNT and the VAT have an efficiency of over 50% in approximately 40% of the whole flow range, while the FGT has

comparable efficiency in only approximately 20% of the flow range, as shown in Figure 2.4 [31].

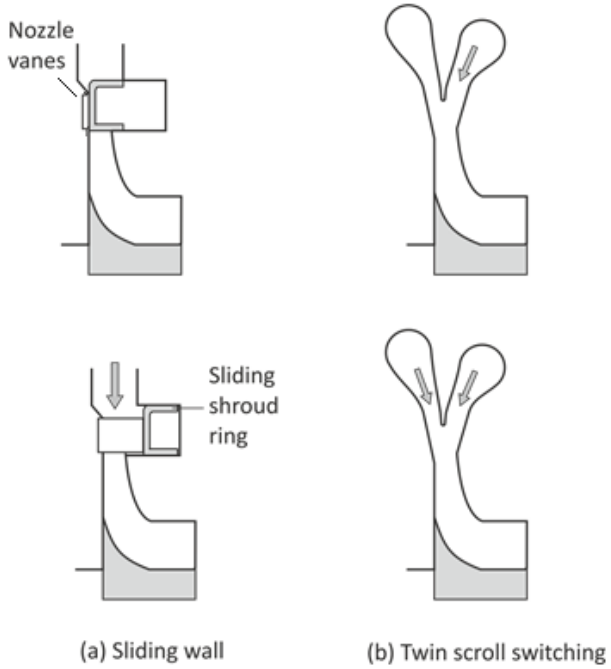

Figure 2.3: VGT types which vary area axially

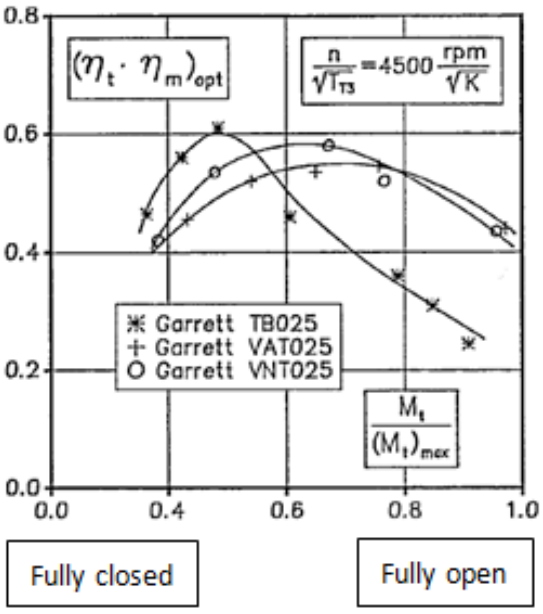

Figure 2.4: Turbine system efficiency against normalized total mass flow rate [31]

The optimum turbine system efficiency of FGT occurs when the waste-gate is almost fully closed such that most of the exhaust gas enthalpy can be utilised. On the other hand, the optimum turbine efficiency of VGT occurs at an intermediate opening as a result of the aerodynamic design of the turbine stage. With the fully closed VGT, the efficiency of VGT is lower than FGT due to the high velocity and Mach number at the nozzle and hence lower efficiency. However, the resultant high expansion ratio and higher isentropic power may lead to higher turbocharger power, which is favourable in terms of transient response and achievable boost pressure at low engine speed. With a fully opened VGT, the efficiency of turbine wheel is not optimum but the larger flow at the turbine rotor resulted in higher turbine system efficiency. It is also shown that the efficiency of the VNT is up to 5% higher than the VAT in approximately two thirds of the tested region. However, the peak efficiencies of the VAT and VNT are lower than the FGT at low vane positions, with both having peak efficiencies approximately 3% lower than the FGT.

Indeed, many authors [31, 40, 43, 51-53] have highlighted that the peak efficiency of the VGT is slightly lower than a waste-gate turbocharger due to surface friction, leakage losses through clearances, and the interaction and disturbance between the mechanism and the flow. In particular, Hu *et al*. [54] present a CFD comparison of turbine efficiency with different nozzle clearances, shown in Figure 2.5. It is clear that the large clearance on the VNT turbocharger results in a significant efficiency drop.

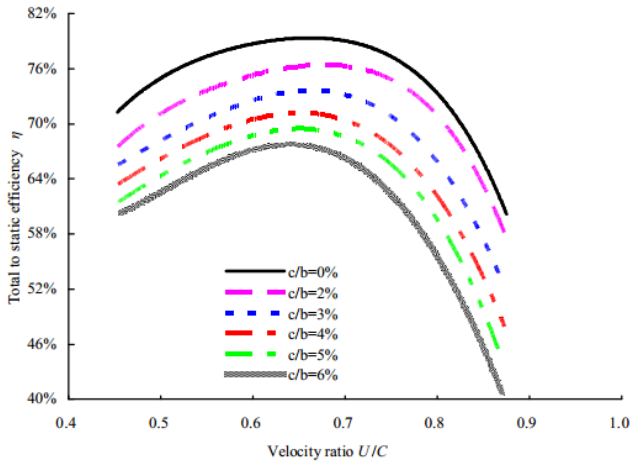

Figure 2.5: Effects of nozzle clearance on turbine efficiency [54]

2.2. Challenges of Gasoline VGT Application

Turbocharging the gasoline engine is, in general, more challenging than boosting its Diesel counterpart. The exhaust gas temperature of conventional gasoline engines can reach over 1000°C, over 200°C higher than that of Diesel engines [55, 56]. Conventional Diesel VGT turbocharger materials and construction cannot normally withstand these high temperatures and specialist design and construction are thus consequently required.

The VGT mechanism must operate not only at high temperatures but also in an oxidising environment with a high concentration of exhaust particles, and has to run at high speeds under high friction [32]. Indeed, Ito *et al*. [37] and Andersen *et al*. [57] affirm that conventional VGT mechanisms have a tendency to stick, causing failure when operating under high loads.

Due to the complexity of the VNT mechanism (Figure 2.6), its design is challenging [44, 58] and production costs can be higher and reliability lower in comparison with the other types of VGT [44, 47]. Shimizu *et al*. [33] state that larger free play is necessary to overcome the large thermal expansion; however, the correlation

between the actuator stroke and the vane position would also be affected. Arnold *et al*. [32] state that the clearance between the vanes and the housing must be larger to prevent vane sticking. Bender *et al*. [59] state that the turbine rotor of gasoline VGT turbochargers is typically larger and heavier than a standard waste-gate turbocharger turbine rotor due to the flow capacity requirement, leading to an unfavourable transient response.

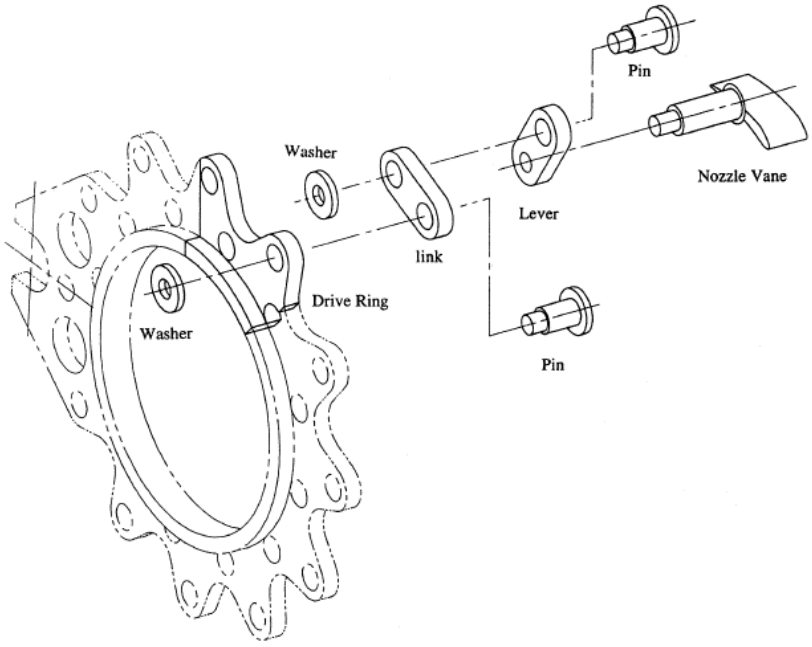

Figure 2.6: VNT mechanism [60]

In addition to the structural and material aspects of the design, Lezhew *et al*. [34] highlight the difficulties of controlling VGT turbochargers on gasoline engines. Gasoline engines use a throttle to control the load in contrast to Diesel engines which control the load mainly through the quantity of fuel injected into the combustion chamber. As a result, as the intake manifold pressure overshoot is more acceptable for Diesel engines, the focus is the speed of intake manifold pressure build-up. Conversely, any significant overshoot is undesirable on gasoline engines since this will result in a corresponding engine torque overshoot. Therefore, both the speed of intake manifold pressure build-up and the avoidance of overshoot are crucial control

targets of the gasoline application.

Moreover, the flow range of the VGT turbocharger is not always sufficient for gasoline engines. Shimizu *et al*. [33] tested a racing car gasoline engine with a VNT turbocharger. Due to the wide flow rate range, an additional waste-gate is required, further increasing the transient control challenge.

It has been suggested that exhaust gas pulsation is damped at low vane positions [22, 40]. Indeed, many authors have found this damping effect on Diesel VGT turbochargers [38, 61, 62] which can result in increased residual gas concentration, turbine inlet temperature and pumping losses [15]. This is because the exhaust back pressure can be reduced by exhaust gas pulsation, therefore, improving the exhaust process. In addition, Eichhorn *et al*. [22] state that the exhaust gas pulsation can also be distorted due to the large space between the nozzles and the turbine wheel. Arnold *et al*. [32] also affirm that the exhaust flow can become choked at very low vane positions due to the small area between the vanes. Hence, at very low vane positions, the efficiency of the turbine wheel is high while the efficiency of the vanes can be low. Nevertheless, Gabriel *et al*. [40] claim that the damping effect may, in fact, be beneficial under certain circumstances since transient compressor surge can be reduced due to the smaller exhaust gas pulsation [40].

In summary, table 2.1 shows a comparison of the key aspects of different types of VGT turbocharger for the gasoline engine. The VNT type has good efficiency over a wide range of flow rate conditions owing to the ability to vary the flow velocity and angle to a large extent but has lower reliability and higher cost due to its complex mechanism. On the other hand, the VFT and sliding wall types have acceptable performance and higher reliability due to their simpler structures.

Table 2.1: Comparison of applications for various types of VGT turbocharger on the gasoline engine

	VNT	VAT	VFT	Sliding wall	Scroll switching
Peak efficiency	High	Acceptable	Acceptable	Acceptable	Low
Flow range	Large	Low	Acceptable	Acceptable	Low
Reliability	Acceptable	Good	Good	Good	Good
Cost	High	Acceptable	Acceptable	Acceptable	Low
Existing prototype for gasoline engines	Yes [59]	-	Yes [37]	Yes [17]	-

2.3. Downsized Gasoline Engines

Despite the challenges of using VGT on gasoline engines, there are various commercial products available on the market, which are compared with other downsized gasoline engines in table 2.2. Among the listed engines, two-stage boosting systems are used on the three most heavily downsized engines, while single-stage boosting systems are used on the engines with the smallest specific power, highlighting the necessity of having a two-stage boosting system on highly downsized gasoline engines with over 100 kW/L specific power and over 30 bar brake mean effective pressure (BMEP) due to limited compressor flow range [63].

The Ultraboost engine utilises various synergetic technologies involving the combustion, boosting and exhaust systems, thereby achieving a high level of downsizing, and thus satisfactory low end torque and acceptable transient response. While it is claimed that this engine is cost effective, maintaining the rapid transient response and catalyst light-off is challenging since the two-stage variable valve lift system enables engine breathing to be improved at both low and high speeds.

	Ultraboost (target) [71, 72]	Mahle downsized two stage (target) [13, 70]	Ricardo Hyboost [68, 69]	Porsche 911 Turbo S engine [40, 59, 67]	Ford 1.0L ECOBOOST [65, 66]	Volkswagen 1.4TSI	Honda Acura RDX 2.3L engine [37]	Mahle downsized single stage [13, 64]
Specific power (kW/l)	142 (6500rpm)	120 (6500rpm)	105 (5500rpm)	103 (6250-6750rpm)	92	90	78 (6000rpm)	75 (6000rpm)
Peak BMEP (bar)	32 (3500rpm)	30 (2500-3000rpm)	29 (2500rpm)	23 (2100-4500rpm)	21 (1300-4500rpm)	22 (1750-4500rpm)	19 (4500rpm)	22 (2500-3000rpm)
Displacement (l)	2.0	1.2	1.0	3.8	1.0	1.4	2.3	1.2
Combustion system	DI + PI Dual VVT + two-stage variable valve lift	DI Dual VVT	DI Dual VVT	Multiple DI (up to three injections per cycle) VVT + two-stage intake valve lift	DI Dual VVT	DI Dual VVT	PI Dual VVT + one intake valve deactivate for tumble improvement	DI Dual VVT
Boosting system	Two stage supercharger + FGT	Two stage FGT + FGT	Two stage electric supercharger + FGT	Two VGTs in parallel	Single stage FGT	Two stage supercharger + FGT	Single stage VGT	Single stage VGT
BMEP at 1000 rpm (bar)	25	16	23 (with electric supercharger assisted)	21 (1950 rpm)	21 (1300 rpm)	16	10	10

Table 2.2 (a): Typical downsized and turbocharged gasoline engines

	Ultraboost (target) [71, 72]	Mahle downsized two stage (target) [13, 70]	Ricardo Hyboost [68, 69]	Porsche 911 Turbo S engine [40, 59, 67]	Ford 1.0L ECOBOOST [65, 66]	Volkswagen 1.4TSI	Honda Acura RDX 2.3L engine [37]	Mahle downsized single stage [13, 64]
Transient response	Better than JLR 3.0L Twin Turbo V6 Diesel	2bar BMEP to WOT at 1250rpm, 2bar boost achieved within 2.5s	-	-	-	2bar BMEP to WOT at 1250rpm, 2bar boost achieved within 2.5s	Low load to WOT at 2000rpm, max. boost achieved within 1.0s	-
Minimum BSFC (g/kWh)	-	235	-	-			-	235
BSFC at low load (g/kWh)	-	295 (2000rpm 4bar BMEP)	-	-	-	-	-	-
Type	Prototype	Prototype	Prototype	Production	Production	Production	Production	Prototype
Turbine inlet temperature limit (°C)	-	1025	-	1000	1050	980	-	850 (Diesel engine VGT)
Water-cooled exhaust manifold	Yes	No	-	No	Yes	No	Yes	Yes
Fuel enrichment	No	Yes (above 5000rpm)	No	-	Yes (minimum Lambda 0.95)	Yes	-	Yes
External EGR	Yes	Yes (HP)	Yes	No	No	No	No	Yes (HP)

Table 2.2 (b): Typical downsized and turbocharged gasoline engines

Further improvements can be realised via a more expensive fully variable valve actuation system [73], for example, the Fiat Multiair [74] and BMW Valvetronic systems [75]. It has been demonstrated that this type of system can reduce the throttle losses [76] and improve the full-load torque [73] by controlling valve opening and closing times, valve profile, and overlap period, thus enhancing fuel consumption and low end torque.

The Ricardo Hyboost engine achieves downsizing by integrating the engine into a micro-hybrid powertrain in which the electric supercharger typically operates for a short period of time (typically 1 – 3 s) [69]. Moreover, a water cooled intercooler is used on this engine in order to mitigate knock and maintain a stoichiometric air-fuel ratio through to full load.

The use of advanced turbocharger materials and improvements in gasoline engine design enabled the first application of the VGT turbocharger on a production gasoline engine, used on the Porsche 911 Turbo S [40]. This has a similar level of specific power but a lower peak BMEP compared to the Ricardo Hyboost engine, possibly because it is a production engine applied to a sports car. The maximum power of 390 kW is attained at engine speeds of 6250 – 6750 rpm [67]. If the turbocharger matching were moved towards lower engine speeds, the low end torque and transient response could be further improved.

The Honda 2.3 L engine is a production gasoline engine with a VGT turbocharger with the potential to replace a 3.5 L naturally aspirated engine. This engine is used on the Acura RDX, launched in the U.S. market in 2006 [37]. A VFT turbocharger is installed on the engine with a water-cooled exhaust manifold (WCEM) applied to limit the turbine inlet temperature [37]. Furthermore, an internal waste-gate (Figure 2.7), is used to bypass a portion of the exhaust gas flow at high speeds. Direct-injection (DI) is not used on this engine, and it is thus possible that the engine could

be further optimized if DI or a more advanced injection system were used. The VFT flow control valve and waste-gate are controlled using the boost pressure by two solenoid valves. The flow control valve and waste-gate control strategy are shown in Figure 2.8. While the flow range of the VFT the engine with the VFT turbocharger is smaller than that of the VNT, the production cost may also be increased due to the requirement of having an additional actuator. Nevertheless, it is shown in that although the achievable torque of the VFT turbocharger is almost equal to that of the FGT turbocharger at all operating points, high engine torque can be produced throughout a wider engine speed range.

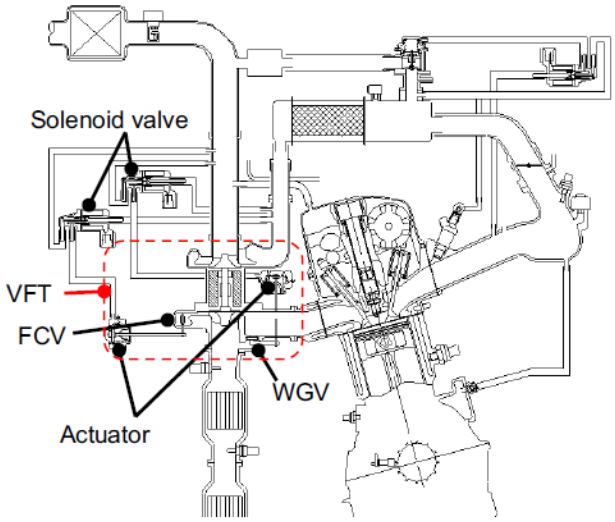

Figure 2.7: Schematic of the control system of the Honda VFT turbocharged engine [37]

The Mahle downsized single stage boosted engine is a prototype gasoline engine with a VGT turbocharger. A Diesel type VGT turbocharger, which has a design turbine inlet temperature limit of 850°C, is used [13]; a WCEM controls the turbine inlet temperature.

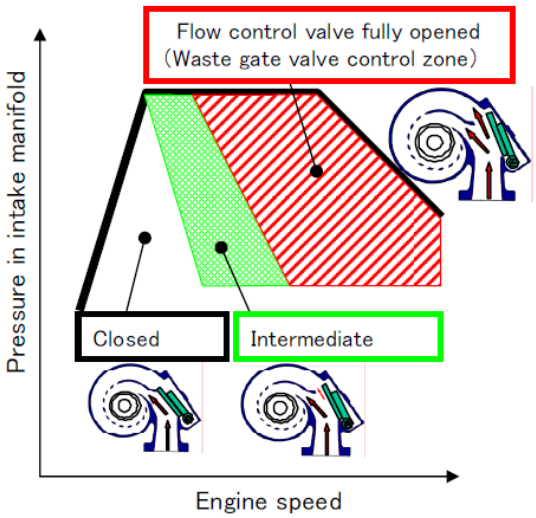

Figure 2.8: Control strategy of the VFT valve and the waste-gate [37]

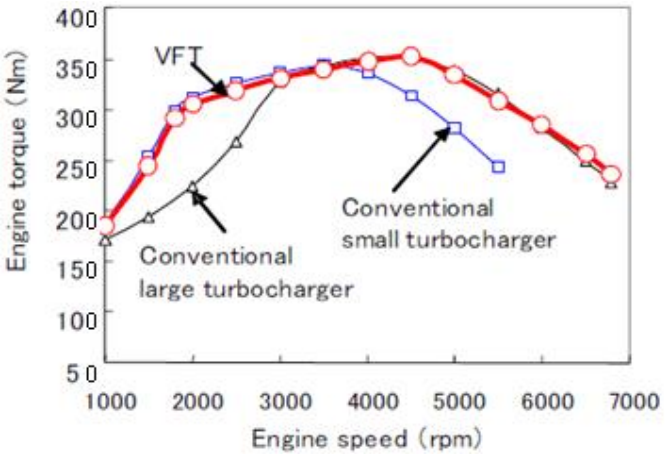

Figure 2.9: Comparison of VGT and FGT turbochargers [37]

Other technologies can facilitate gasoline VGT application. For example, integrated WCEM, which has been used on the Ford 1.0 L Ecoboost, the Audi 1.8T [77], and the 'Sabre' engine [78], can be beneficial in terms of packaging, engine weight and cold start. However, WCEM can limit the low end engine torque since it reduces the available exhaust gas energy.

External exhaust gas recirculation (EGR), used on the Ultraboost, Hyboost and downsized engines of Mahle, can mitigate knock [79], which is one of the key limiting factors of downsized gasoline engines due to the increased chemical reaction

rates under high charge temperatures, especially at low engine speeds at which the overall combustion time is increased [80]. Therefore, this allows the turbocharger to boost the engine to achieve higher BMEP at low engine speeds.

EGR also enables both advanced spark timing and minimal fuel enrichment. Moreover, Turner *et al*. [81] report that on a tested engine, the required Lambda at 5000 rpm full load is increased from 0.95 to 1 by adding 4% cooled EGR, as shown in Figure 2.10. Further advantages comprise the reductions in exhaust gas temperature and required over-fuelling possible through external EGR [82]. In addition, it has been highlighted on Diesel engines that the VGT turbocharger can provide further opportunities to control the EGR rate [61]. This is a result of the relatively low efficiency of the VGT turbocharger at the near fully closed position. Thus, the EGR flow is driven by the differential pressure between exhaust manifold and inlet manifold.

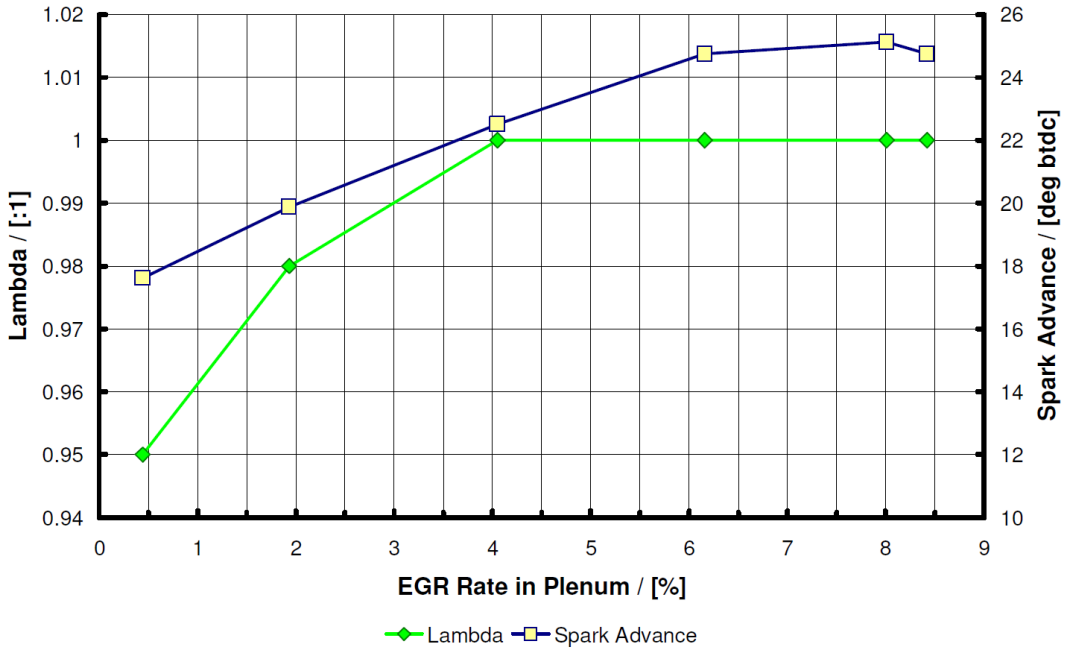

Figure 2.10: Effect of EGR rate on Lambda and spark advance [81]

In fact, this is also a solution for gasoline engines with lean or stratified combustion systems which require the reduction of NOx. Recently, spray guided direct injection (SGDI) enabled stratified combustion systems on both production engines [83, 84] and research prototype engines [85]. A minimum BSFC of 220 g/kWh has been achieved on a SGDI engine thanks to the reduction in cylinder wall heat transfer, lower exhaust gas enthalpy and reduced pumping losses [85]. In general, on these engines, stoichiometric combustion is only required at above approximately 7 to 8 bar BMEP, or above 3500 rpm engine speed [83, 86]. Compared to Diesel engines, SGDI may become a cost effective solution in some applications due to the lower cylinder pressure and fuel rail pressure. The independent control of injection timing and spark timing offers flexibility to optimise the thermodynamic processes. In addition, the potential of operating at compression ratio approximately 1.5 higher than conventional direct injection turbocharged gasoline engine the lower exhaust gas temperature may enable the VGT technologies [87], and the higher mass air flow at low load also improves turbocharger response.

The synergy between several technologies offers great potential on downsized internal combustion engines. And the uses of technologies on combustion system, scavenging system, thermal management system, and air-charging system will diversify depending on the application.

2.4. Gasoline VGT Studies

Gabriel *et al*. [40] presented the first production gasoline engine with an electrically-actuated VGT turbocharger, which came onto the market in 2005; details of the engine performance are listed in table 2.2. The turbine inlet temperature limit of this turbocharger is 1000°C [59], achieved through more costly material and a turbine housing design with a coolant circuit which can reduce the peak temperature of the piston ring by up to 150°C [40]. Additionally, an elastic heat shield behind the turbine is used to prevent the exhaust gas from flowing into the bearing housing and

overheating the piston ring. It has been claimed that the next iteration of this turbocharger will be designed for a turbine inlet temperature of 1050°C.

Wieske *et al*. [64] tested a 1.4 L two-stage boosted (supercharger and turbocharger) production gasoline engine with various exhaust systems. The full load BMEP at 1000 – 2500 rpm is reduced by up to approximately 6 bar by adding a WCEM upstream of the original turbocharger (Figure 2.11). The original turbocharger was then replaced with a Diesel VGT turbocharger, and at engine speeds above 2000 rpm, the Diesel VGT and WCEM can reach the same BMEP as the original supercharger and turbocharger configuration. However, at engine speeds of 1000 – 1750 rpm, the achievable BMEP is only up to 1 bar higher than that of the original configuration without the supercharger. Therefore, although the drop in BMEP due to the WCEM can be compensated by the VGT turbocharger, the improvement at low engine speeds is modest [64], possibly because the heat rejection capability of the WCEM is designed for the Diesel type VGT turbocharger. This could be improved if the turbine inlet temperature limit was higher and the heat WCEM rejection reduced. The full load BMEP at 5000 rpm is increased by approximately 1 bar by replacing the original turbocharger with the Diesel VGT, whilst the full load BSFC at 2500-4500 rpm is reduced by up to approximately 15 g/kWh at 2500 rpm (Figure 2.12), though is larger at higher engine speeds.

From tests with a VFT engine, Ito *et al*. [37] report that the fuel consumption at 1500 rpm at a power output of 12.5 kW is 12% lower than a 3.5 L naturally aspired gasoline engine of similar engine output and that it is also comparable to a 2.5 L naturally aspired gasoline engine. The transient boost pressure response of the engine with and without operating the VFT valve is shown in Figure 2.13. With the flow control valve open, the turbocharger characteristics are similar to those of a large conventional turbocharger. At 2000 rpm, approximately 40 kPa higher boost pressure is achieved in a shorter time by controlling the VFT valve, and at 4000 rpm, the time

to achieve the required intake manifold pressure is reduced from 1.7 to 0.4 s.

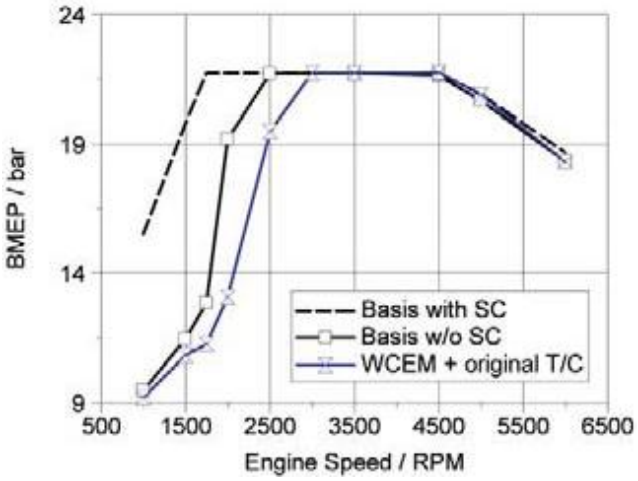

Figure 2.11: Effect of WCEM on BMEP [64]

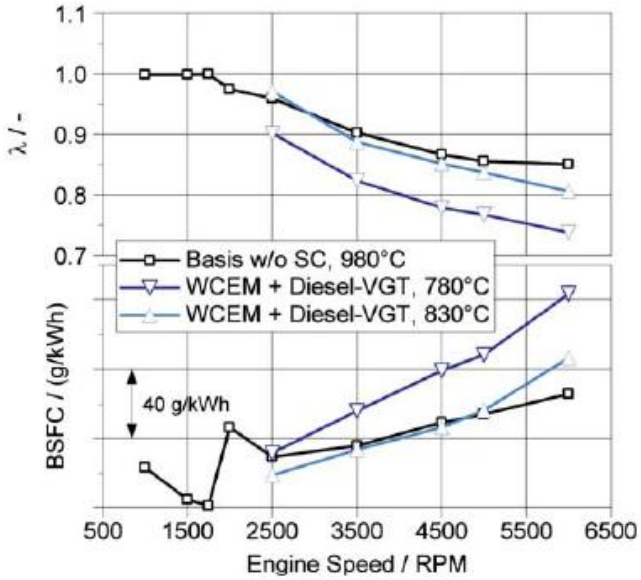

Figure 2.12: Over-fuelling requirements and BSFC comparison [64]

Yang and Wang [15, 88] have presented simulation results of a Turbo-Cool Turbocharging System in which a VGT turbocharger is used. It is claimed that using a VNT turbocharger may result in high knock intensity due to the high mixture temperature at the start of combustion and high peak in-cylinder temperatures found in the simulation.

Gabriel *et al*. [40] tested a Diesel VGT turbocharger on a 2.2 L DI gasoline engine, finding that the maximum power of the engine is increased by 6% compared to the FGT configuration. The achievable BMEP at engine speeds above 3000 rpm is increased by up to 2 bar whilst it is decreased by up to 0.5 bar at engine speeds below 3000 rpm. It is shown that the pressure drop across the engine is largely affected by the back pressure at BMEP above 12 bar. In fact, the pressure drop is increased by approximately 250 mbar at engine speeds above 2500 rpm at full load, indicating a reduction in pumping losses, which depend on the turbine efficiencies (Figure 2.14). However, the pressure drop is reduced by 20 mbar at 1000 rpm at full load, and at low levels of BMEP (12 bar), the pressure drop is reduced by up to 50 mbar. Although VGT efficiency is significantly higher than the FGT at engine speeds above 2000 rpm at full load when the waste-gate is open, it is lower than the FGT at certain low levels of engine speed. In spite of the low efficiency at low vane openings, improvements in fuel were demonstrated (Figure 2.15). Although the BSFC at full load is increased by up to 18 g/kWh at some engine speeds below 3000 rpm, it is decreased by approximately 10 to 23 g/kWh at engine speeds in excess of 3000 rpm. Moreover, the optimum BSFC was reduced from 235 g/kWh to 230 g/kWh. Therefore, the VGT can improve both the both engine output and fuel consumption at high engine speeds.

Serrano *et al.* [89] carried out simulation studies on the use of VGT on a modern 2.0 L gasoline engine using a calibrated one-dimensional engine model. The characteristics of the FGT in the model were scaled to predict the effects of the VGT turbocharger. The VGT turbine size and intake valve timing were varied in order to optimise the engine steady state operation. The data showed that the full load torque was improved by approximately 2% to 10% at engine speeds between 500 and 5500 rpm. The torque increase at speeds 2000 - 4000 rpm was generally in the range of 2% to 3%, while the improvements at 1500 rpm and 5000 rpm were 10% and 6%, respectively, owing to the fact that turbocharger matching of the original FGT

turbocharger represented a trade-off between the performances at low and high speeds. The study verified that the VGT is equivalent to the use of multiple FGT turbochargers targeting different engine operating regions. Engine part load operation at 7 bar BMEP 2500 rpm was also optimised and the specific fuel consumption was reduced by 3%. Regarding the transient response, the time required to achieve 1.6 bar intake manifold pressure (from 0.2 bar) was reduced from 3 s to 1.6 s.

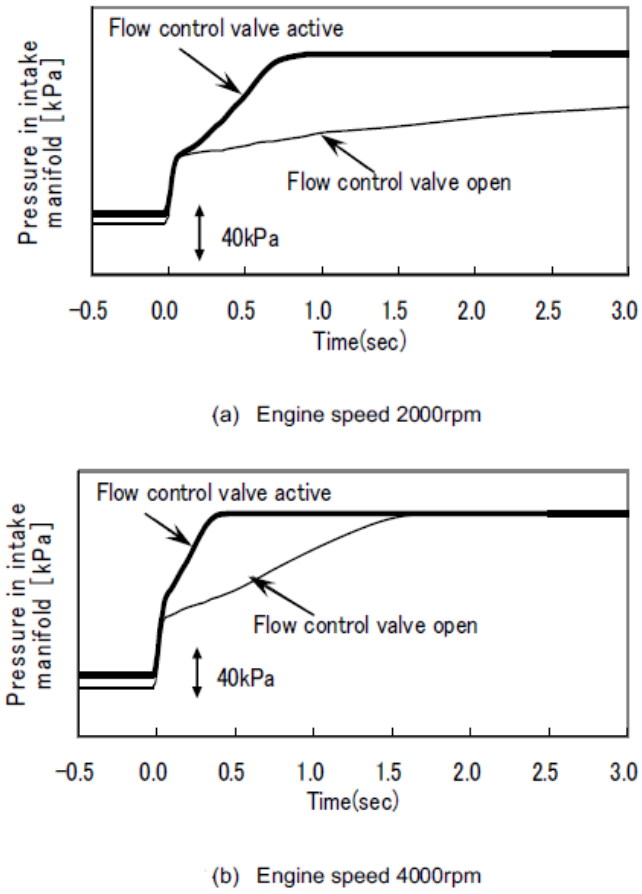

Figure 2.13: Transient response comparison [37]

Andersen *et al*. [57] tested five different VNT turbochargers, one VFT turbocharger and one FGT turbocharger on a 2.0 L gasoline engine. Although the matching between the turbocharger and the engine and that between the compressor and turbine was not optimised, the benefits of using the VGT turbocharger were, nevertheless, evident from the study (Table 2.3). All five VNTs and the VFT

produced higher peak BMEP at both low and high engine speeds. However, there was a 0.5% drop at 1500 rpm for VGT (D). The maximum improvement in low speed BMEP was 22% while the same VNT (C) turbocharger improved the BMEP at high speed by 3 - 5%. In the transient test, VNT (C) increased the IMEP 2 s after tip-in by 0.6 bar at 1500 rpm. It is shown that not all the VGT turbochargers can improve the transient response, possibly due to the test setup, in which the VGT positions were held constant while an additional waste-gate was used to control the boost, limiting the potential to improve the transient response.

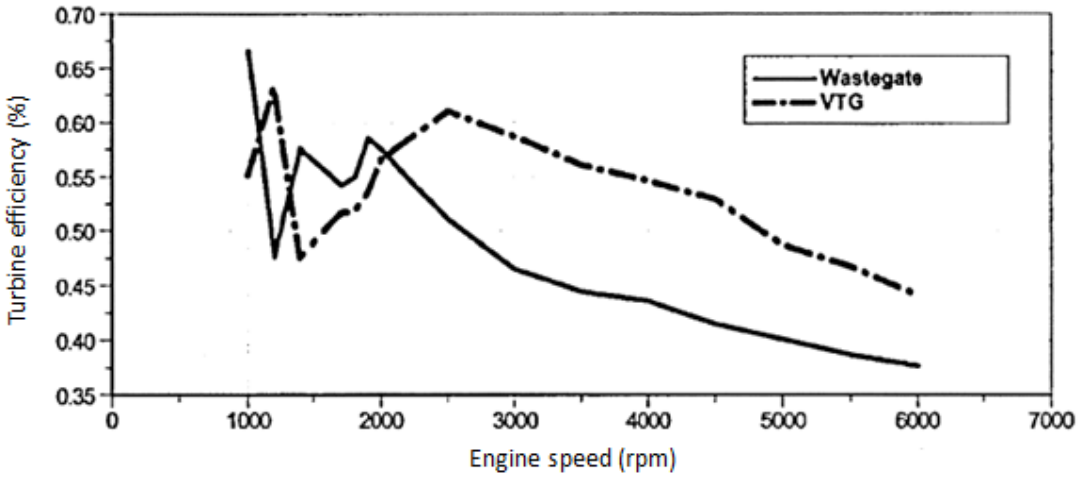

Figure 2.14: Full load turbine system efficiency comparison between FGT and VNT [40]

While several studies have investigated VGT turbocharging application on actual engines, few on-vehicle tests have been carried out. Nevertheless, Lundstrom and Gall [24] tested a VAT turbocharger (Aerodyne Dallas Aerocharger) and a FGT (Garrett T03) on a 1979 Ford Mustang with a 2.3 L gasoline engine, stating that the compressor map for the VAT is comparable to that of the FGT. The boost gauge pressure targets for the FGT and VAT were 1.655 bar and 1.621 bar, respectively. The test results (Table 2.4) revealed reductions in acceleration times and distances of 9.7 - 28.8% and 9 - 29.1%, respectively. The required time to reach a boost gauge pressure of 0.586 bar is lowered by over 49% in test 5, again demonstrating that the VGT can

significantly improve the transient response.

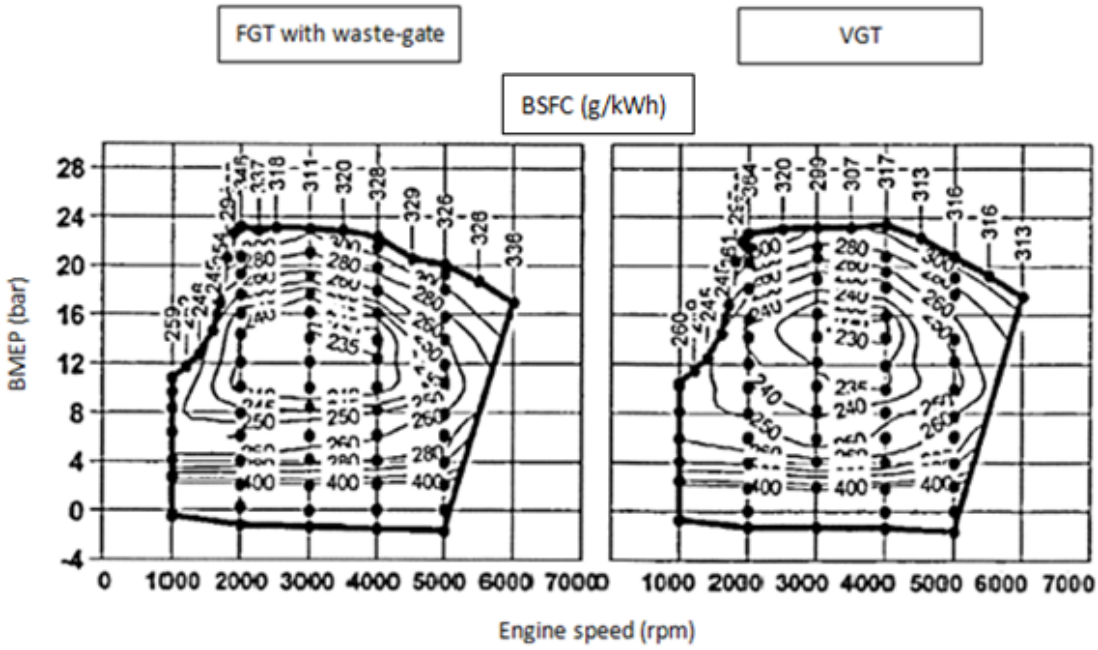

Figure 2.15: Comparison of BSFC between VFT and VGT [40]

Table 2.3 :Comparison between VGT and FGT on a 2.0 L gasoline engine (approximation) [57]

	Full load BMEP (bar) improvement at 1500rpm	Full load BMEP (bar) improvement at 5500rpm	Full load BMEP (bar) improvement at 6000rpm	Transient IMEP (bar), 1s after tip-in (1500rpm)	Transient IMEP (bar), 2s after tip-in (1500rpm)
VNT (A)	+5%	+13%	+12%	13.4	14.7
VNT (B)	+20%	+11%	+12%	11.5	13.5
VNT (C)	+22%	+5%	+3%	13.0	15.5
VNT (D)	-0.5%	+11%	+12%	12.8	14.3
VNT (E)	+20%	+11%	+13%	12.9	15.2
VFT	+12%	+10%	+8%	11.7	13.2
FGT	-	-	-	13.3	14.9

Test	Gear	Speed Range (mph)	Acceleration time (FGT) (s)	Acceleration time (VGT) (s)	Reduction in acceleration time (%)	Acceleration distance (FGT) (meters)	Acceleration distance (VGT) (meters)	Reduction in acceleration distance (%)
1	3	30-60	9.99	8.75	12.4	194.8	173.0	11.2
2	3	40-60	6.37	5.75	9.7	140.3	127.7	9.0
3	4	30-50	16.44	13.48	18.0	292.9	237.9	18.8
4	4	30-60	21.93	17.46	20.4	429.7	340.1	20.9
5	4	40-60	13.75	10.56	23.2	300.9	232.1	22.9
6	4	50-70	12.74	9.81	23.0	342.7	263.2	23.2
7	4	60-80	12.09	9.86	18.4	388.5	312.2	19.6
8	5	40-60	23.03	16.40	28.8	509.3	361.2	19.1
9	5	50-70	19.28	13.83	28.3	509.0	369.0	27.5

Table 2.4: Vehicle acceleration performance comparison: FGT vs. VAT [24]

The potential of the VGT turbocharger to improve downsized gasoline engines has, therefore, been demonstrated in numerous studies. In spite of the difficulties involved in developing a robust and efficient control strategy for the VGT turbocharger, it has been successfully applied on production gasoline engines and has improved the steady state and transient responses of various engines.

2.5. Control Strategy

The VGT turbocharger can provide a higher degree of freedom in air flow rate than FGT turbochargers largely due to the flexibility of varying the turbine characteristics. The control strategy is thus crucial to effective application of the VGT turbocharger on gasoline engines.

Kaiadi *et al*. [90] show that on a spark-ignited natural gas engine, the load of the tested gasoline engine can be controlled in 60% of the whole engine operating region by varying the vane position of the VGT turbocharger, as illustrated in Figure 2.16. The pumping losses are reduced, and hence the strategy is shown to be beneficial with regard to low load fuel consumption. However, the transient response is affected due to the lower turbocharger speed at low engine load - the transient response at 1000 rpm is 20% slower under this control strategy.

Ericsson *et al*. [91] discuss the potential for improving the transient response by using optimised VNT and a variable valve timing (VVT) control strategy. VVT settings (0, 39 and 78° of valve overlap) were simulated at 1750 rpm starting from an initial IMEP of 3 bar (Figure 2.17). The transient IMEP response is largely affected by the control strategies from approximately 0.2 s to the end of tip-in (1.5 s after tip-in), with up to approximately 5 bar IMEP difference being apparent. A fully closed strategy results in an IMEP drop at approximately 0.3 s after tip-in, which is undesirable in terms of drivability and is caused by the high back pressure developed when the compressor power is insufficient to build up the boost pressure, and a large

portion of turbine work is thus used to accelerate the turbocharger. Although the IMEP at 1.5 s post tip-in is higher, the IMEP integral is still lower, which may result in a longer vehicle acceleration time. With this in mind, a new parameter (the product of volumetric efficiency and the turbine pressure ratio) was proposed as a target to optimise the transient control strategy. The authors state that the engine breathing process, important during the first 0.3 s in the tip-in, can be represented by the volumetric efficiency element of the parameter, while the turbocharger acceleration process, dominant during the second phase of tip-in, can be represented by the turbine pressure ratio part in the parameter. It is shown that the optimised control strategy using this parameter delivers the same initial IMEP response, whilst the IMEP at 1.5 s after tip-in is increased by approximately 1.5 bar.

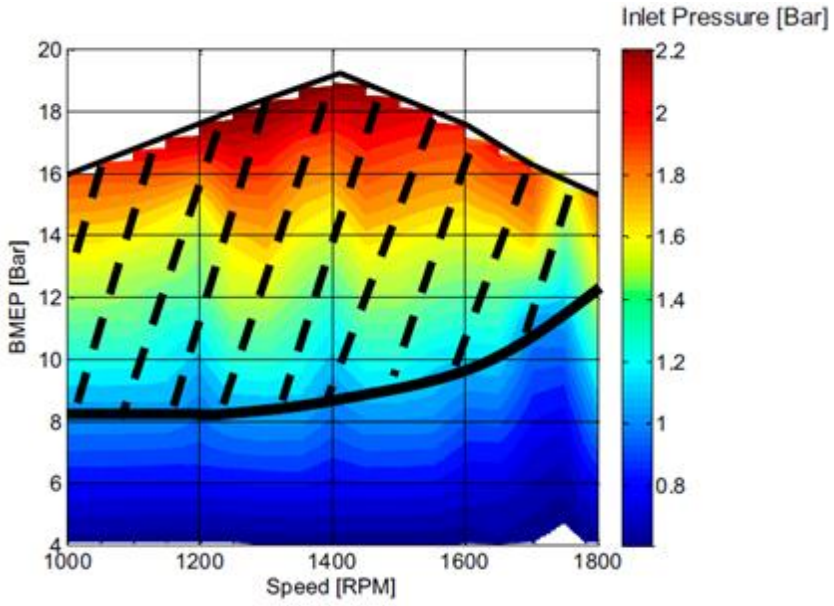

Figure 2.16: The operating range (specified with dashed lines) in which the load can be controlled by the vane position [90]

Lezhew *et al*. [34] have also investigated various control algorithms for throttle and VGT control on the gasoline engine, evaluating the time taken from the maximum response to reach a set proportion of the reference pressure along with the degree of overshoot. The best solution was found to controlling the throttle position by a feed

forward plus proportional-integral controller on the intake manifold pressure, while the VGT position is controlled by a second feed-forward plus proportional-integral controller on a weighted sum of intake and exhaust manifold pressure.

Flärdh [92] carried out simulation studies and optimised the VGT position and valve timing settings to achieve high torque integral in the first 1.5 s of the transient response. The optimum valve position trajectories has a relatively constant pressure ratio across the engine (the ratio of exhaust manifold to intake manifold pressure) at approximately 1.15. Therefore, a feedback control strategy was implemented in experimental work; compared to the base calibration, the IMEP integral was improved by 2%, 4.1% and 5.5% at 1500, 1750 and 2000 rpm, respectively.

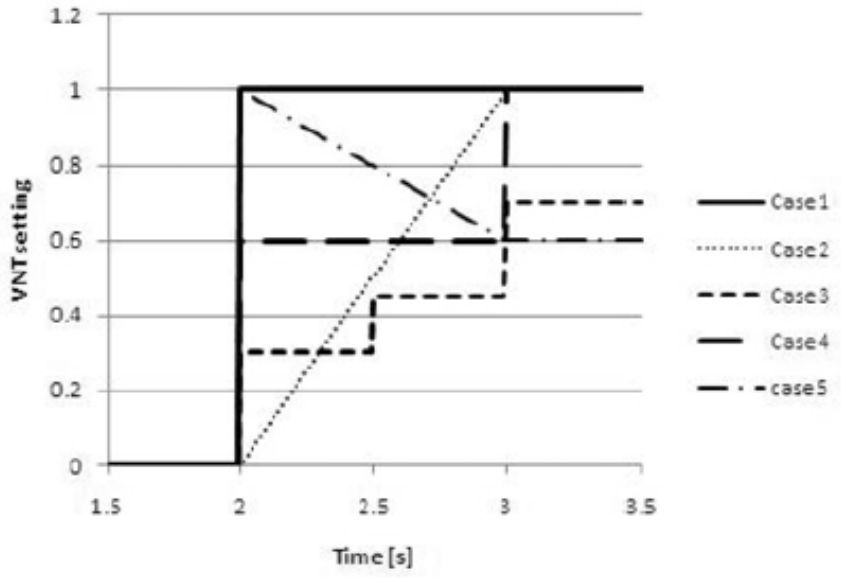

Figure 2.17: Transient vane position control strategies [91]

2.6. Summary

The various comparisons between FGT and VGT turbocharging from the experimental and simulation studies in the literature are summarised in table 2.5, with the stated values being averages taken from each study. It is clear that there have been reported improvements in many key aspects including full load

performance, part load fuel efficiency, transient response and load control range. The full load performance improvement has reached levels of up to approximately 15%, which was also due to turbocharger matching and may differ at different engine speeds. The part load fuel consumption was improved by 2 – 7% and the transient response improvement occurred over a wide range owing to differences in testing methodology, for instance, in terms of vane control.

Table 2.5: Summary of VGT and FGT comparisons

Author	Average of reported improvement			
	Full load torque	Part load fuel consumption	Transient response (time to reach target torque)	Comments
Wieske *et al*. [64]	Up to + 10%			The use of a Diesel VGT may require excessive WCEM cooling
Gabriel *et al*. [40]	Up to +12% at above 3000 rpm, -4% bar at below 3000 rpm	2 – 7%		Turbocharger matching may have affected low speed performance
Serrano *et al*. [89]	2 – 10%	3%	+46.7%	VGT fully closed at low load point in transient test
Andersen *et al*. [57]	+11%		-8%	VGT position held constant in transient test
Lundstrom and Gall [24]			+20%	Tested on vehicle

2.7. Conclusions

This chapter reviewed the fundamentals, research and studies of the application of VGT on downsized gasoline engines. The following points can be drawn from the

literature to provide an overview of the potential of VGT and future technologies on downsized gasoline engines:

1. Although the peak efficiency of VGT is slightly lower than that of FGT, the turbine system efficiency of VGT may be significantly higher due to the by-passed exhaust flow on FGT. Therefore, the engine pumping work can be reduced.

2. Five types of VGT which vary the turbine flow area either radially or axially were compared. While the variable flow type and sliding wall type have higher reliability and lower cost, the variable nozzle type has superior peak efficiency and flow rate range. The selection of the type is dependent on the trade-off between peak efficiency, flow range, reliability and cost.

3. The challenges of applying VGT on gasoline engines are mainly the harsh exhaust environment, complex mechanism and transient control. In spite of the challenges, two of the five types have been used on production gasoline engines.

4. The reported benefit in engine fuel consumption was around 5%, and improvements in the full load torque and transient response of up to 12% and 50% respectively were seen. Therefore, the results of experiments and simulations in this project will be expected to be of similar range.

5. The latest gasoline engine technologies that have been used on production and prototype engines were reviewed. The synergy between the technologies on combustion system, scavenging system, thermal management system, and air-charging system will facilitate VGT application on these engines, and hence further improve the efficiency of the gasoline engine.

Chapter 3 - *Experimental facilities and testing procedures*

In this chapter, the experimental facilities and approaches used in this project are presented. This chapter is formed of three sections. In the first section, the necessary changes and setups required in the test cell are described. The requirements of the experimental work are summarised according to the project objectives in the second section. In the third section, the test system, data acquisition system and testing procedure that were specifically designed to meet the requirements of the experimental work are described.

3.1. Engine hardware

The engine used in this project was a 2.0L gasoline engine equipped with turbocharger system, direct injection, and continuously variable valve timing. The maximum torque and rated power from the production calibration was 300Nm and 150kW. This was a modern downsized gasoline engine, therefore, it was chosen to be used as a platform to investigate the potential of advanced turbocharging systems for further downsizing gasoline engines. This baseline engine was instrumented and tested on a transient test bed at the Powertrain and Vehicle Research Centre at the University of Bath.

The gearbox was removed and replaced with a direct drive, which was connected to the dynamometer. In order to have wide operating range and precise control of the engine boundary conditions, the external cooling circuit for the engine coolant was replaced with a water-to-coolant heat exchanger. In addition, the intercooler was replaced by a water-to-air heat exchanger. Therefore, the temperatures of the engine coolant and the engine intake air could be controlled by varying the water flow rate in each heat exchanger.

Since the engine was used as a platform for investigation of the turbocharging system, including the production unit and prototype hardware, custom-made exhaust manifold and adaptors were used for the prototype hardware. The length of the exhaust runner and the volume of the collector were maintained at the same level as for the production unit. A photograph of the tested engine is shown in Figure 3.1.

Figure 3.1: Photograph of experimental facility

3.2. Purposes and requirements for the experimental campaign

In general, the experimental work was carried out for two purposes. The first was to identify experimentally the improvements from using a VGT turbocharger compared with a FGT turbocharger on a downsized gasoline engine. This allowed the investigation of the differences between the two systems explicitly, without the concerns about the assumptions and uncertainties in the simulation.

Nevertheless, limitations exist in experiments. For example, only a limited number of items of hardware can be tested in experiments. Besides, a number of parameters are difficult to measure. For instance, it was difficult to measure the instantaneous temperature and mass flow rate of exhaust gas under pulses. Therefore, the experimental results were also used for the second purpose: calibration of a high fidelity 1-D engine model for tests that cannot be carried out in experiments, for example, the scaling of the size of turbochargers. To investigate the full potential of the system, the response of the actuators can be assumed to be instant.

Therefore, the requirements of the experiments can be defined as follows:

1. In order to carry out back-to-back comparison and to have flexibility in controlling the engine operating point, ECU parameters need to be monitored and controlled. Actuators on prototype hardware also need to be controlled precisely. In order to carry out repeatable experiments, test systems that allow flexible and automated experiments are required.

2. For the investigation of the turbocharger behaviour, the pressures at the inlet/outlet of the compressor and turbine need to be measured at high frequency (at 1 degree engine crank angle or higher frequency). In addition, in order to calibrate the combustion model for the high fidelity engine model, the cylinder pressure data is required for each cylinder. To eliminate the uncertainties about the resident gas fraction and trapping ratio at each

cylinder, Three Pressure Analysis (TPA) was used for the calibration. This requires instantaneous pressure at each inlet port and exhaust port. The details of the TPA study will be discussed in Chapter 5.

3. In order to eliminate the uncertainties about the boundary conditions and the thermal conditions of the engine, these parameters need to be monitored and maintained for reliable test results.

3.3. Test cell setup

To fulfil these requirements of the test system, the measurement system and the test procedure were defined as follows:

3.3.1 Test control system

The test cell was controlled using the CP Cadet host system. It controlled the dynamometer, test cell facilities and engine pedal box, and it had interfaces with ECU communication software, data acquisition system, and prototype system control software, as shown in Figure 3.2. Customised control functions and programmes were allowed using Visual Basic. This offered sufficient flexibilities in monitoring, processing and controlling the tests. Digital output channels were set up to control the other interfaced system. Therefore, the engine, test facilities, and measurement system could be controlled automatically to perform fully automated tests.

An ASAP3 link was used for the communication between the host system and ECU calibration software ATI Vision, which was operated on an independent computer. ATI Vision also communicated with the ECU via CAN Calibration Protocol (CCP). Back-to-back comparison can be made by controlling and monitoring the ECU parameters and engine actuators on ATI Vision. In addition, selected channels can be transferred to CP Cadet and recorded.

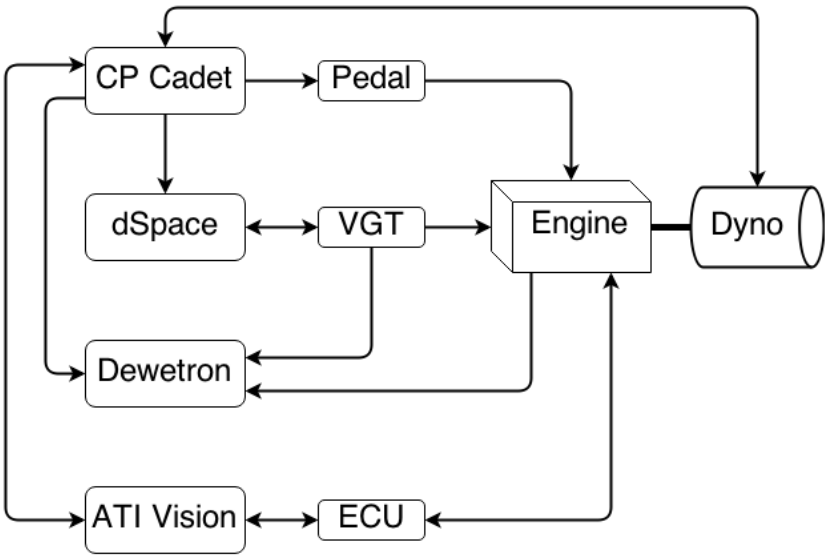

Figure 3.2: Test control systems

In order to control the VGT actuator on prototype hardware, dSpace Micro Auto Box was used. The actuator was cooled using the engine coolant, and the temperature was monitored in dSpace. In transient tests, the user-defined VGT trajectory can be automatically triggered using the pedal position voltage signal from CP Cadet.

Since transient response was to be measured in the experiments, the response of the communication between each system and the response of actuators were important for repeatable and reliable test results. Figure 3.3 shows a group of VGT trajectories recorded in automated transient tests. The dotted lines represent the target VGT trajectories and the solid lines represent the actual VGT trajectories recorded from the actuator. In general, the response time of the VGT actuator was approximately 0.1 to 0.15 seconds. This was sufficient for conducting precisely controlled automated transient experiments.

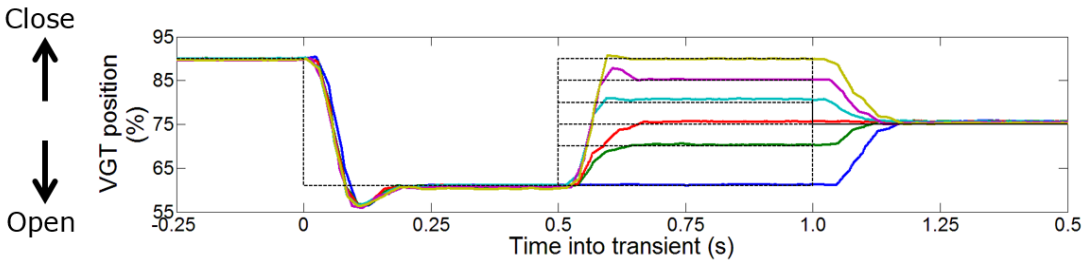

Figure 3.3: Target and actual VGT trajectories

3.3.2 Measurement system

Data were logged in three systems: Dewetron, ATI Vision, and CP Cadet. The resolution of the high frequency data recorded in Dewetron was 0.5 degree crank angle, which was equivalent to a maximum sampling frequency of 78kHz at 6500rpm. These data were used for the investigation of the behaviours of the engine combustion system and the turbocharging system.

Kistler and Dewetron amplifiers were used to amplify the voltage signals from the transducers to measureable voltages. An engine crankshaft encoder was required to provide the engine crank angle position signal to Dewetron. A digital output channel from CP Cadet was used as the triggering signal for the Dewetron logging system.

In addition, low frequency data were also recorded in ATI Vision and CP Cadet. Selected ECU parameters can be recorded in ATI Vision at 100Hz. This was used to investigate the behaviours of the engine control strategy and to calibrate the control strategy. In addition, in CP Cadet, all the output control signals and input sensed channels were recorded at 80Hz. The key sensors in the experiments are listed and shown in Table 3.1 and Figure 3.4.

3.3.3. Test procedures

Three types of experiment have been performed: two steady state tests and one transient tip-in test (which represents a sudden increase of engine load demand, usually from low load to full load). In order to obtain reliable test results, detailed procedures were followed and programmed in the automated tests. Therefore, the engine boundary conditions and thermal conditions were maintained at the same level for the same type of tests. It is worth noting that perfect test conditions can never be reached in real world situations, and there is always a trade-off between the reliability of the test results, and the testing time and complexity. As a result, a procedure based on assumptions and experience needs to be followed to achieve the best reliability within constraints.

Table 3.1: Key measurement channels

Channel	Number of measurements	Sampling resolution	Sensor type	Logging system
In-cylinder pressure	4	0.5 degree crank angle	Piezoelectric (integrated into spark plug)	Dewetron
Intake port pressure	4	0.5 degree crank angle	Piezoelectric	Dewetron
Fuel pressure at injectors	4	0.5 degree crank angle	Piezoresistive	Dewetron
Exhaust port pressure	4	0.5 degree crank angle	Piezoelectric (water-cooled)	Dewetron
Pressures at inlet/outlet of turbine	2	0.5 degree crank angle	Piezoelectric (water-cooled)	Dewetron
Pressures at inlet/outlet of compressor	2	0.5 degree crank angle	Piezoelectric	Dewetron
Turbocharger speed	1	0.5 degree crank angle	Eddy current	Dewetron
Exhaust port Lambda	4	0.5 degree crank angle	Wideband	Dewetron
Engine ECU control parameters	-	100 Hz	-	ATI Vision
Pressures along the air path	-	80 Hz	Piezoresistive	CP Cadet
Temperatures along the air path (intake side)	-	80 Hz	K type 1.5mm	CP Cadet
Temperatures along the air path (exhaust side)	-	80 Hz	K type 3mm	CP Cadet

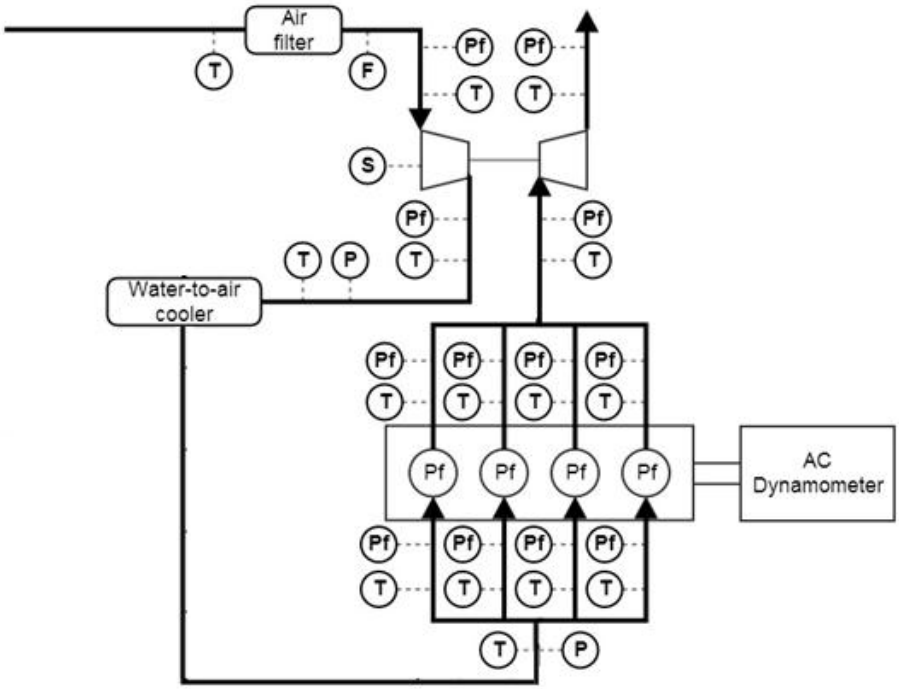

F: Flow measurements; T: Temperature measurements; P: Pressure measurements; Pf: Fast pressure measurements; S: Turbocharger speed measurement

Figure 3.4: Layout of the test facility

3.3.3.1. Steady state tests

Steady state tests were performed to understand the engine behaviours at various engine speeds and load operating points. Since the calibration of the high fidelity 1-D engine model was largely dependent on the steady state test results, a large number of engine operating points were tested to map the engine with production setting, and to cover a wide engine operating range. In total, 46 engine operating points were tested. The tested engine operating points are shown in Figure 3.5. The test campaign consisted of engine load level 20%, 40%, 60%, 80% and 100%. In addition, the engine idle condition is also included. It is worth noting that the full load torque curve at lower engine speeds was slightly reduced due to knock protection.

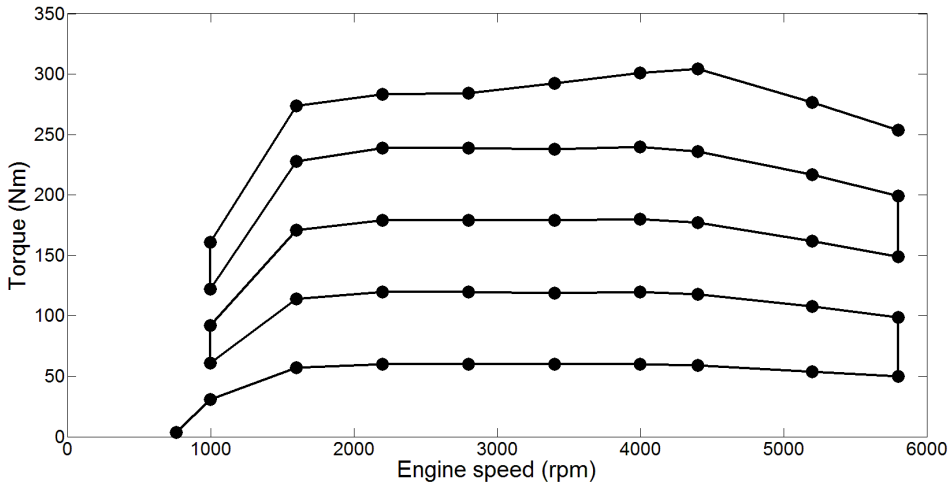

Figure 3.5: Engine operating points for steady state

The test procedure for the engine mapping test was as follows:

1. Safety inspections
2. Engine start and idling
3. Engine warm-up at mid load
4. Ramping up to test point of maximum speed and maximum load
5. Stabilise at target operating point for 5 minutes, followed by recording
6. Ramp to next test point and repeat step 5
7. Back to idling
8. Switch off engine
9. Safety inspection

It is worth noting that the sequence of the test points was defined so that the engine load decreased from 100% to 20%, following the line shown in Figure 3.4. Therefore, the engine thermal condition was maintained at a relatively similar level between each test point. This helped to simplify the calibration of the engine model, since the uncertainties of the thermal condition were minimised. In addition, the operation procedure for recording at each test point was programmed, so that the beaker in the fuel consumption measurement system was always full before triggering the logging systems at each point.

In addition to the engine mapping tests, engine actuator sweep tests were also performed to investigate the potential of using VGT on a downsized gasoline engine. Sufficient time for engine warm-up and stabilising was given to provide reliable test results.

At each steady state test point, the data in CP Cadet and ATI Vision were recorded for 100 seconds. The high frequency data in Dewetron was recorded for 300 consecutive engine cycles, which was equivalent to approximately 36 seconds and 6.2 seconds at 1000rpm and 5800rpm, respectively. Matlab was used to process the data and to calculate averaged data for each channel. For low frequency data, the averaged data were condensed to 1 data point per channel per test point, while for high frequency data averaged cycle data were obtained by averaging the data at each crank angle.

3.3.3.2. Transient tests

Transient tip-in tests were performed to investigate the transient response of the engine system. In these tests, the pedal position was set in close loop control to maintain target engine load before tip-in, typically 2bar BMEP. The pedal position was set to 100% at tip-in. At the same time, the VGT position control was set to transient mode in which the pre-defined trajectory was used.

In order to reach a similar thermal condition to that of the steady state tests, the same warm-up procedure was used at the start of each test campaign. In addition, five minutes were allowed for stabilisation before each tip-in. Although the engine coolant and oil temperature were maintained by the close control of the fluid circuits, variations in the metal temperature of the engine block were expected. However, the metal temperature was not monitored and it was difficult to control. Therefore, the duration of each tip-in test was designed to be as short as possible. In each tip-in test, the target engine load was lowered to settling point within 10 seconds after tip-in. Both the low frequency data and high frequency data were recorded for fixed periods of time covering 5 seconds before tip-in and 10 seconds after tip-in.

3.4. Conclusions

The engine hardware and testing facilities have been presented in this chapter. The purpose of the experiments in this project was also described. This has led to the requirements for the design and setup of the experimental facilities, data acquisition system and test procedures. The following conclusions can be drawn:

1. Necessary changes have been made on the engine cooling system and gearbox to install the engine in the test cell. In order to use the engine as platform to investigate candidate turbocharging system, custom-made exhaust manifold and adaptors were used.

2. The purposes of the experiments are:

   a) Assess novel turbocharging systems
   b) Provide experimental data for engine model calibration

3. According to the purpose of the experiments, the following requirements for the experiment setup have been considered:

   a) Automated test control systems for repeatable experiments

   b) High frequency data acquisition system for investigation of turbochargers and calibration of engine combustion model

   c) Detailed test procedures for reliable test results

4. The test control systems, data acquisition system and test procedure have been designed to meet the requirements of the experiments

   a) Communication between the test host system, ECU calibration tool, prototype hardware control system and the data acquisition system has been setup for precise control and repeatable automated testing. The VGT actuator response

time was approximately 0.1-0.15 second.

b) Experimental data has been recorded in the host system, the ECU calibration tool and in the high frequency data acquisition system. The key measurement channels were summarised in this chapter.

c) In order to achieve reliable test results, detailed test procedures have been designed and conducted for automated steady state and transient tests. A 46 test point engine mapping experiment has carried out to provide data for engine model calibration. Actuator sweep tests have been performed to investigate the comparison between VGT and FGT. In addition, transient tests have been performed.

Chapter 4 - *Turbocharger On-Engine Mapping Facility*

In order to investigate the behaviours of turbocharging systems under on-engine operating conditions and to improve the turbocharger modelling techniques, an on-engine turbocharger mapping facility has been developed at the University of Bath. Details on this facility are presented in this chapter.

Firstly, the challenges in using the turbocharger maps collected from conventional gas-stand and their countermeasures are discussed, which leads on to the requirements for novel mapping facilities to investigate the turbocharger behaviours in more detail. In the second section, the layout of the facility, the measurement system and the test procedure are presented.

A VGT turbocharger has been mapped using this facility, and the test results are discussed in section 3. The test repeatability and the effect of pulsating and thermal conditions are presented in this section. In addition, necessary future improvements are recommended in section 4.

4.1. Introduction

4.1.1. Challenges in using conventional turbocharger performance maps in engine simulation

Engine simulation is widely used in the automotive industry, thanks to the fast simulation speed and good accuracy. This is particularly useful in design optimisation, new technology assessment, turbocharger matching and understanding engine behaviours. Nevertheless, prediction and simulation of internal combustion engines with increasing levels of downsizing and turbocharging have currently become more challenging [93]. Many authors have shown the lack of accuracy in the turbocharger sub-model in 1-D engine models that resulted in the discrepancy between simulation and measurement [94]. The main reasons for this include the effects of exhaust gas pulsation and heat transfer, and the small operating range tested on a conventional gas-stand.

On downsized internal combustion engines, the number of cylinders may be reduced, causing a longer interval between the blow-down process of each cylinder, and hence stronger pulses at the inlet of the turbine housing. The use of twin-entry or multi-entry turbines may also result in higher exhaust pulse magnitudes. In the conventional turbocharger mapping process, measurements are conducted under steady flow, and quasi-steady operation of the turbocharger is assumed in engine simulation. However, Chen *et al*. [95, 96] studied the effect of unsteadiness at turbine volute and rotor by calculating the Strouhal number: unsteady effects dominated if it was above unity, and steady effects dominated if it was less than unity. The results showed that the rotor could be considered as quasi-steady while the unsteadiness in volute was dominant. Fajardo [97] carried out CFD simulations in which pulsating pressure boundary conditions were induced: the same suggestion was given. To

investigate and model the pulsating effects, analytical and empirical methods have been used to incorporate the dynamic responses of the turbine stage within a 1-D engine simulation environment.

Reyes-Belmonte [94] modelled the volute, nozzle, rotor and diffuser, using separate elements in 1-D environments, and achieved capture of the overall pressure waves in the turbocharger. On the other hand, Luján *et al*. [98] correlated the pulsating factor, which took into account both the pulse frequency and amplitude with the turbine efficiency losses under pulsating flow. It was found that the efficiency losses were up to 30% of the steady flow turbine efficiency at high pulsating factor operating points.

The heat transfer effects in turbocharger mapping are generally ignored. However, the differences between the temperatures of the gases in the air path and the boundary conditions result in inevitable heat fluxes [99]. The actual turbocharger operating condition on engine differs from that in the mapping test, causing variations in estimated turbocharger performance [100]. This becomes more significant at low load where the heat transfer rate is comparable to the turbocharger power. Reyes-Belmonte [101] reported that, at turbocharger speed lower than 70krpm, up to 70% of the enthalpy drop at the turbine stage was heat transfer from the exhaust gas to the turbine housing when the turbocharger was insulated. In addition, due to the increasing level of downsizing and turbocharging to reduce fuel consumption of the internal combustion engine, the level of turbine inlet temperature rises [102]. This may also increase the heat transfer from the exhaust gas to the turbocharger. It was found that the apparent compressor efficiency dropped up to 15% when turbine inlet temperature increased from 50ºC to 500ºC [103]. This was because the heat transferred into the compressed air was accounted as part of the aerodynamic work done by the compressor wheel in the compressor efficiency measurement and calculation.

One-dimensional heat transfer models have been used to predict the heat fluxes. The heat transfer at the rotor wheel has been ignored, and it is assumed that the heat addition and dissipation happened before and/or after the compression and expansion processes [99]. Burke [104] performed a turbocharger heat transfer study and stated that the accuracy of gas temperature at turbine outlet was improved by over 50% by incorporating the heat transfer effects.

Besides the pulsating flow and heat transfer effects, the small operating range tested on the gas-stand also introduces uncertainties to the estimation of turbocharger performance when extrapolating outside the tested region, especially for turbines. In the conventional turbocharger mapping approach, the compressor traditionally acts as load control in turbine mapping. Thus, the achievable operating range on the turbine is restricted by the compressor surge limit and choke limit. This is particularly critical for turbines. As a result, only a small operating range can be achieved on the turbine. In addition, a high expansion ratio can only be achieved at high speed, and a low expansion ratio at low speed. The compressor power can be determined by the turbocharger speed and the mass flow, whereas the turbine power experiences large variations as a result of the acceleration and the deceleration of the turbocharger shaft on top of the compressor power and mechanical losses. Therefore, extrapolation of the turbine map into the region where no measurement data is available is necessary for 1-D engine simulation.

4.1.2. Measures to investigate and overcome the challenges

To mitigate the challenges listed above, many techniques have been used. Pulsation sources are required to generate the varying pressure boundary conditions to the turbocharger. Two approaches have been used: rotating plate and piston engine. The

rotating plate acts as a varying restriction between the air supply and the turbine inlet. A group of plates with different opening areas are used to simulate the varying magnitude of the pulses. The rotational speed of the plate can be varied to achieve different pulse frequencies. Since only a finite number of plates can be used, the pulsation characteristics generated from the rotating plate cannot be varied continuously.

A piston engine can also be used as a pulse generator. The pulsation can be varied by changing the engine speed and valve timing. However, the pulse shape cannot be varied with a large degree of freedom because it is also determined by the geometry of the exhaust manifold and number of cylinders. The required lubrication system and cooling system for the piston engine are also more complicated than the rotating plate configuration. Nevertheless, using a piston engine offers the operating condition closest to the actual blow-down processes.

Variable and controllable thermal conditions of the gases are necessary for the investigation of heat transfer effects on the turbocharger. An electric heater or combustion engine can be used as a heat generator. The control complexity on electric heaters is lower than that on combustion engines. However, in general, combustion engines are more cost effective. Higher temperature can be achieved with combustion engines.

To extend the achievable range in turbine mapping, Bellis *et al*. [105] summarised the benefits of a number of alternative mapping techniques. To increase the compressor power range, a recirculation loop was added to feed the compressed air back to the compressor inlet via a cooler and a back pressure valve. By opening and closing the back pressure valve, the inlet condition of the compressor is varied, such that the compressor power can be adjusted. A blow-off valve and an inflation valve

were also added to extend further the achievable range of the compressor flow. It was stated that maximum turbine expansion ratio comparable to on-engine conditions could be achieved while the minimum turbine expansion ratio was still limited. To extend the minimum turbine expansion ratio, the compressor could be replaced with a bladeless disc, so that low expansion ratio could be achieved when the turbine only overcame the friction losses. Besides, a dynamometer can be used to drive or absorb the turbine power. Therefore, lower expansion ratio can be tested by motoring the turbocharger to overcome the friction losses.

With these points in mind, research has been carried out to compare a number of existing novel turbocharger mapping facilities (listed in Table 4.1). This includes two facilities at the University of Bath, one of which was developed in this project.

In general, turbocharger mapping facilities are based on either conventional gas-stand or the internal combustion engine. The internal combustion engine can be used as both heat source and pulsation source. The maximum temperature limit is higher on engine-based facilities. Therefore, most engine-based mapping facilities use the internal combustion engine as the heat generator. A cylinder head has been used on gas stands to provide the cylinder blow-down pulses. The operating conditions can be manipulated in a large window by controlling the inlet pressure and valve events.

However, the internal air supply provided by the charging system on a combustion engine might not be sufficient. This is because the operating range of the air-charging on the engine is restricted by the corresponding engine operating points. Therefore, most on-engine mapping facilities use external air supply systems to extend the achievable operating range.

	University of Bath on-engine gas stand (new facility)	University of Bath gas stand	Imperial College gas stand (for turbine) [113, 114,115]	Imperial College gas stand (for turbine and compressor) [112]	Universidad Politecnica de Valencia on-engine gas stand [110, 111]	Universidad Politecnica de Valencia gas stand [109]	University of Genoa gas stand [106-108]
Air supply	External	External	External	External	Internal	External	External
Flow capability (kg/s)	0.7	0.7	-	0.4	0.6	-	0.6
Heat supply	Internal combustion engine	Electric	Electric	Electric	Internal combustion engine	Electric	Electric
Temperature range (K)	1223	1023	400	923	1100	673	400
Pulse generator	Internal combustion engine	Cylinder head	Rotating plate	Rotating plate	Internal combustion engine	Rotating plate	Rotating plate / cylinder head
Turbine loading	Compressor	Compressor	EC dyno	Compressor	Compressor	Compressor	Compressor
Speed range (krpm)	-	-	60	98	Limited by the power of screw compressor coupled to engine	-	-

Table 4.1: Turbocharger mapping facilities

It is worth noting that Szymko *et al.* has developed an electric turbine dynamometer to map turbines in a wide turbine load range [115]. This has enhanced the understanding and capability of extrapolating the turbine characteristics.

To improve the understanding of turbocharger performance, to operate turbocharger under different conditions and to compare results collected from different facilities, it was decided that a new mapping facility is needed. Having had a novel gas-stand at the University of Bath, an on-engine mapping facility was developed in order to achieve different operating conditions. The next sections will describe the hardware of the new facility and some test results.

4.2. Facility description

4.2.1. Objectives of the test facility

The aim of developing an on-engine turbocharger mapping facility was to be able to evaluate turbocharger performance under the on-engine pulsating condition and blow-down process. It was also desired to be able to raise the turbine inlet air temperature to a high level in a cost-effective manner.

It is necessary to control the combustion system and the air supply system separately to avoid interactions. In addition, the capability to conduct a load changes transient test is required. Thus, the boundary conditions of either of the two systems need to be controlled precisely with a large degree of freedom and transient capability.

Because of the requirements stated above, it was decided to use a reciprocating piston internal combustion engine to generate heat and pulsation. Use of an independent air supply system enables the precise control and separation of the interactions.

4.2.2. Layout of the facility

The test facility consisted of two sub-systems: the internal combustion engine system and the air supply system. Figure 4.1 shows the layout of the turbocharger on-engine mapping facility. The engine system was similar to a conventional engine test cell configuration. The main difference was that the compressor and the turbine air paths were separated in order to use the compressor as a load on the turbocharger shaft. An AC dynamometer was connected to the engine crankshaft to control the engine speed, so that the exhaust pulse frequency could be varied by changing the engine speed. The turbocharger was connected to an adaptor, which was custom made for each turbocharger to be tested, and a custom-made exhaust manifold.

The external air supply system was capable of delivering dried air of up to 7 bar and 0.7 kg/s. The air flow through this device was controlled by a valve downstream of an air filter. A pre-heater was used to heat the air to up to approximately 90ºC, and it was also equipped with a bypass valve. The bypass valve was controlled in closed loop so that the target engine intake air temperature could be achieved.

A dump flow path was integrated so that the total flow would always be sufficient. Therefore, transient manoeuvres can be emulated by closing or opening the valve in the dump flow path. Under steady state operation, the valve in the dump flow path was controlled in closed loop so that the target intake air pressure could be achieved. In addition, another valve was located upstream of the engine intake manifold, so that intake air pressure lower than atmosphere pressure could be achieved if the engine was equipped with no throttle.

A differential pressure air flow sensor was located upstream of the pre-heater to measure total air flow going through the device. In addition, in order to measure the

flow being dumped into the test cell, a hot wire air flow sensor was located downstream of a water-to-air cooler in the dump flow path. Therefore, the mass air flow supplied to the engine was the difference between the total air flow and the dump air flow. Care needs to be taken when the total air supply is not sufficient, since the flow direction in the dump flow path might be changed: thus, the calculated air flow to the engine could be incorrect. In addition, another hot wire air flow sensor was located upstream of the compressor to measure the compressor flow.

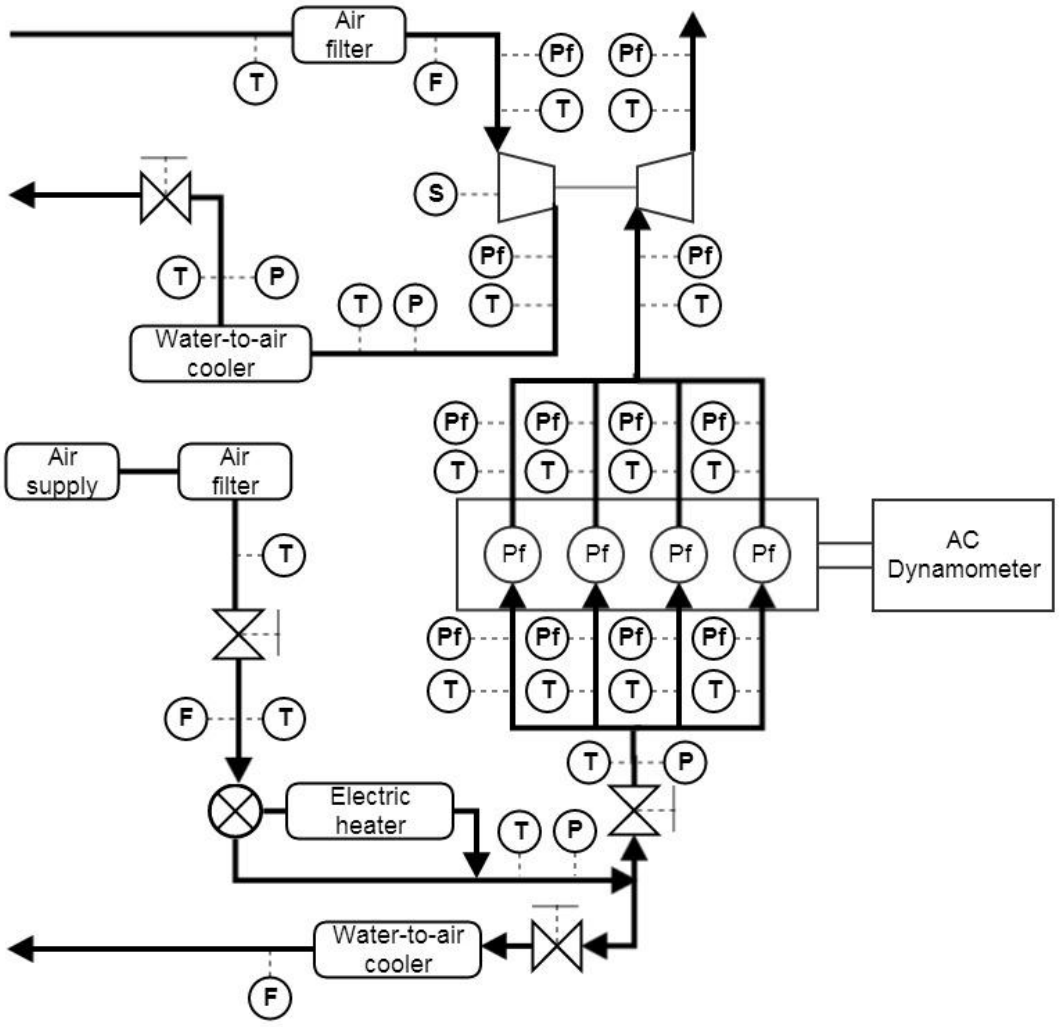

F: Flow measurements; T: Temperature measurements; P: Pressure measurements; Pf: Fast pressure measurements; S: Turbocharger speed measurement

Figure 4.1: Layout of the on-engine turbocharger mapping facility

In order to vary the compressor back pressure, a butterfly valve was located downstream of the intercooler in the compressor air path. The location of the valve was flexible, and the turbocharger could be replaced with the back pressure valve to emulate the back pressure on the engine.

Therefore, two different functions can be realised. Turbocharger mapping can be performed by feeding the external air supply to the engine working as a pulse and heat generator, and by controlling the compressor load using the compressor back pressure valve. In addition, combustion system testing can be carried out by controlling engine intake and exhaust boundary conditions using the air supply and back pressure valve.

The bypass path parallel to the pre-heater and the dump flow path enable the validation of either the combustion system or the boosting system in transient operations. By closing or opening the pre-heater bypass valve and the dump flow valve, step changes in engine intake air pressure and temperature can be achieved. The rate of the pressure and temperature changes can be much faster than typical turbocharging systems, in the order of approximately 0.1 seconds, thanks to the capability of having excessive flow and heating capacity.

4.2.3. Measurement system

The turbine and compressor flow data were recorded in both the slow measurement system and the fast measurement system. Besides the flow measurements, the pressure temperature and turbocharger speed measurements were also logged in both systems. Therefore, the corrected turbocharger flow and speed, as well as the pressure ratio, could be calculated in real time. Thus, with the capability of mathematical operations such as averaging and Fast Fourier Transfer, the

instantaneous compressor and turbine operating points could be plotted in real time on the fast measurement systems. Although the measurements (especially the flow measurements) were not located close to the turbocharger, the real time calculated instantaneous operating points on the compressor and turbine map were still useful information for the test operator.

4.2.4. Test procedure

In order to understand the functionality of the facility, the main control actuators and the effects of changing those parameters are listed in Table 4.2.

Table 4.2: Control actuators and the primary functions

Control parameters	Main control targets affected
VGT position	Compressor corrected speed, turbine operating point
Engine speed	Turbine inlet pulse frequency and pulse shape, turbine flow, compressor corrected speed
Valve timings	Turbine inlet pulse shape
Throttle position	Turbine corrected flow, compressor corrected speed
Air supply pressure	Turbine corrected flow, compressor corrected speed
Compressor back pressure valve	Turbocharger corrected speeds, compressor corrected flow
Engine coolant temperature	Turbine inlet temperature, turbine corrected flow
Air supply temperature	Turbine inlet temperature, turbine corrected flow
Spark timing	Turbine inlet temperature, turbine corrected flow
Lambda	Turbine inlet temperature, turbine corrected flow

It is worth noting that the control parameters do not only affect the listed control targets. For example, the change in throttle position and air supply pressure also

affected the exhaust pulse shape. Not all the effects are listed because some were second order effects. However, they need to be considered by the test operator, so that accurate and efficient testing can be performed.

The frequency and the shape of exhaust pulses were largely affected by the engine speed. In addition, the pressure, temperature and flow of exhaust gas were also affected, due to the changes in the operating condition of the fixed displacement engine and the correspondent variations in the combustion and scavenging processes. Therefore, the engine speed can be varied if the target turbocharger speed cannot be reached, although this also changes the exhaust pulse characteristics. The exhaust pulse shape can also be varied by controlling the valve timings. However, this was not investigated in this study. Further work needs to be carried out to investigate the measures to maintain the exhaust pulse shape when pulse frequency is changed.

The throttle position can be varied to achieve target exhaust flow, and hence turbocharger speed. However, it was preferred to use the external air supply pressure as an actuator of the exhaust flow since supplied pressure was controlled in closed loop.

Tests can be carried out with or without firing the engine. In cold turbine mapping, the turbine inlet temperature was largely affected by the engine coolant temperature, which was a result of the friction in the engine, the compression work, and the temperature of the air supply. The engine thermostat was removed so that the engine coolant temperature could be controlled by the flow in the heat exchanger that cools the engine coolant. The typical engine coolant temperature control range was between 30ºC and 80ºC in cold tests. The air supply temperature can be varied between ambient temperature and approximately 80ºC. When the engine speed was varied to change the exhaust pulse frequency and shape, the flow characteristics also

changed. Therefore, the gas was effectively compressed or expanded through the engine. Thus, the turbine inlet temperature was affected. As a result, the engine coolant temperature and air supply temperature need to be changed to achieve the same turbine inlet temperature. The coolant temperature was the main actuator, since the effect of changing coolant temperature on the turbine inlet temperature was larger than that of air supply temperature.

In hot tests, the spark timing can be used as actuator to control the turbine inlet temperature. Exhaust gas temperature can also be varied by controlling the air-to-fuel ratio. However, as this will affect the exhaust gas properties, its use as a control actuator is not preferred.

The test procedure for cold and hot mappings is described below:

A.1 VGT position – fixed at target turbocharger operating point.

A.2 Engine speed – fixed at target exhaust pulse frequency by varying dynamometer load.

A.3 Throttle position – fixed at wide open for cold test, and fixed at partly open first for hot test before firing.

B.1 Air supply pressure – adjust to achieve target turbine/compressor corrected speed, back to step A if target cannot be achieved.

B.2 Compressor back pressure valve – adjust to achieve target turbine/compressor pressure ratio, then back to step B.1 to adjust air supply pressure to maintain the target turbine/compressor corrected speed.

C.1 Engine coolant temperature – in cold test, fixed at temperature level where target turbine inlet temperature can be achieved. In hot test, fixed at safety temperature.

C.2 Air supply temperature – in cold test, adjust to achieve target turbine inlet

temperature, back to step C.1 if target temperature cannot be achieved. Then, back to step B to adjust turbocharger operating points. In hot test, fixed at safety temperature.

C.3 Spark timing/injection timing – in hot test, adjust to achieve target turbine inlet temperature, back to step B.1 or A.3 if target cannot be achieved. Then back to step B.

The operations are grouped into three categories. Group A defines the basic operating point of the engine. Group B changes the turbine and compressor load, and hence the turbocharger operating point. Group C adjusts the turbine inlet temperature. Group A can be maintained at constant level for the measurement of one speed line. Group C changes turbine inlet temperature, and therefore affects the turbocharger operating condition. Thus, iterations between group B and C may be necessary.

In fact, when the compressor is being mapped, step A.1 becomes part of step B. The VGT (or waste-gate) position is used to control the turbine load, and hence the turbocharger speed. Therefore, the engine can be operated at constant operating point, provided the exhaust pulse condition and exhaust gas energy are adequate. This is under the assumption that the compressor operating point is steady.

Care needs to be taken to ensure that the engine, especially the combustion system, which is largely affected by the spark/injection timing and intake air temperature, operates within the safety limits.

4.3. Test results

4.3.1. Repeatability

First of all, to verify the repeatability of the measurements, one speed line has been repeated three times on different days. The calculated turbine and compressor efficiency of the three tests are compared. The efficiencies are calculated using equations 4.1, 4.2 and 4.3:

$$\eta_{comp} = \frac{\sum\left(\frac{T_{total,\ comp\ inlet} \times \left(PR_{total-to-total,\ comp}^{\left(\frac{\gamma_{air}-1}{\gamma_{air}}\right)} - 1\right)}{T_{total,\ comp\ outlet} - T_{total,\ comp\ inlet}}\right)}{number\ of\ samples}$$

4.1

where γ_{air} is 1.4 for air that goes through the compressor.

$$\eta_{turb,\ using\ compressor\ power} = \frac{\sum\left(\frac{T_{total,\ turb\ inlet} - T_{total,\ turb\ outlet}}{T_{total,\ turb\ inlet} \times \left(1 - \left(\frac{1}{ER_{total-to-static,\ turb}}\right)^{\left(\frac{\gamma-1}{\gamma}\right)}\right)}\right)}{number\ of\ samples}$$

4.2

$$\eta_{turb,\ using\ turbine\ enthalpy\ drop} = \frac{\sum\left(\frac{C_{p\ air} \times MAF_{comp} \times (T_{total,\ comp\ outlet} - T_{total,\ comp\ inlet})}{C_p \times MAF_{turb} \times (T_{total,\ turb\ inlet} \times \left(1 - \left(\frac{1}{ER_{total-to-static,\ turb}}\right)^{\left(\frac{\gamma-1}{\gamma}\right)}\right)}\right)}{number\ of\ samples}$$

4.3

where MAF_{turb} is the flow through the turbine. In cold tests, it is the air flow to the

engine, and in hot tests it is the air flow plus the fuel flow.

The compressor and turbine efficiencies were instantaneously calculated and plotted on-line, and the averaged values were taken from 300 engine cycles (600 rotations) with a sample rate of 720 samples per crankshaft rotation.

It is worth noting that the turbine efficiency can be calculated either using the compressor power calculated from compressor enthalpy or using the enthalpy drop across the turbine. The former was based on the assumption of turbocharger balance, ignoring the mechanical losses at the turbocharger bearing. The latter method was based on the assumption of adiabatic expansion at the turbine, ignoring the heat transfer at the turbine housing and the compressor housing. The two methods will be compared in this study.

Figure 4.2 and Figure 4.3 show the calculated turbine and compressor efficiencies at one speed line repeated three times. It is shown that the error in the calculated efficiency was within ±0.5%.

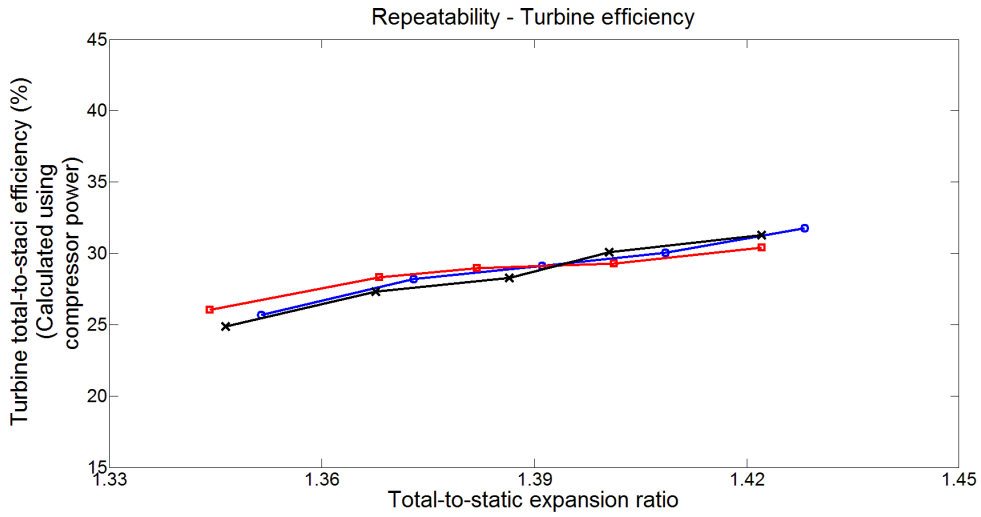

Figure 4.2: Repeatability of turbine efficiency

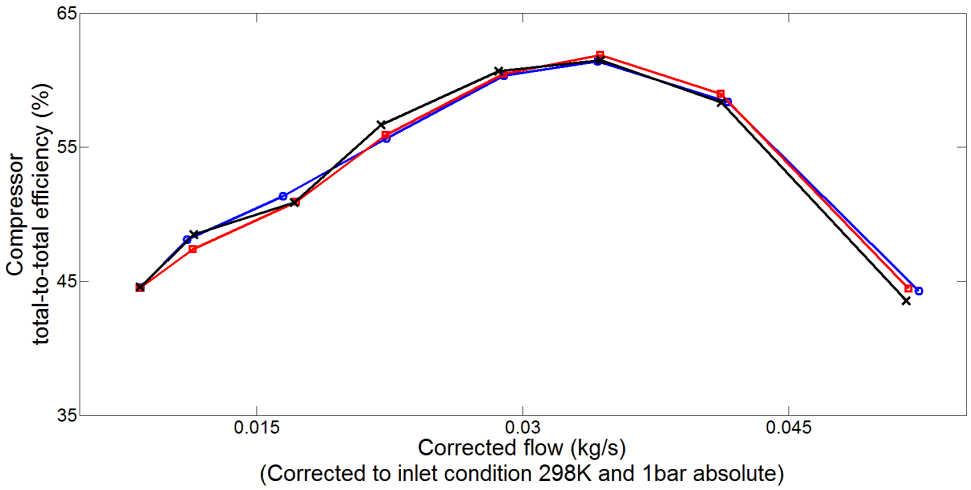

Figure 4.3: Repeatability of compressor efficiency

4.3.2. Turbine mapping

Figure 4.4 shows the VGT turbine flow characteristics obtained from a cold test. The data shown on the turbine map were time-averaged values over 300 engine cycles (600 rotations). Since the air flow at the turbine was dependent on the engine speed, operating conditions with large turbine flow can only be achievable at high engine speed. Therefore, the flow range at a certain exhaust pulse frequency was limited by the maximum pressure level in the intake manifold, which was set to 2 bar absolute in this test (although this was still lower than the safety limit). The dotted line shows the maximum flow and expansion ratio that can be reached at engine speed 3000rpm under unfired conditions. This was also dependent on the matching between the turbocharger and the engine used in the current configuration. The engine platform could be changed whilst the air supply system was maintained. A larger engine could be used if a larger turbocharger were to be mapped.

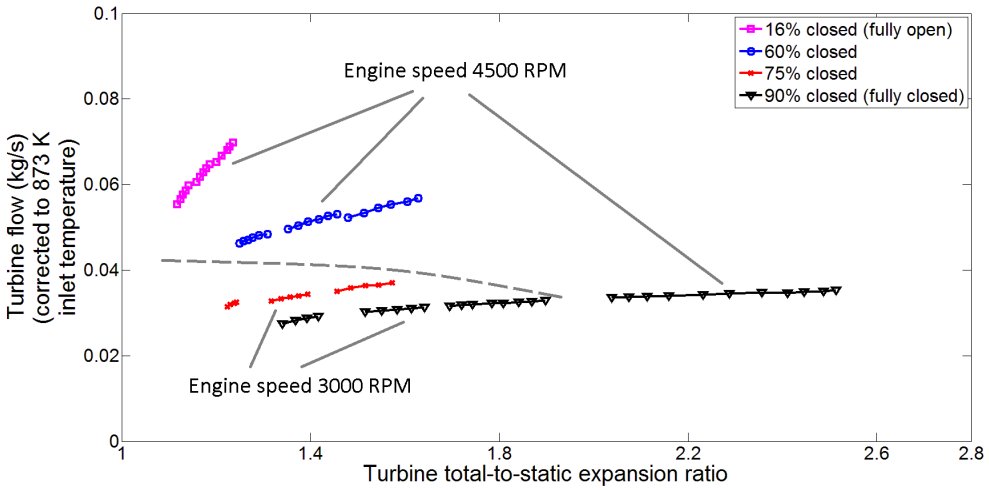

Figure 4.4: Turbine flow characteristics at different VGT positions

To investigate the effect of exhaust pulsation on turbine performance, the turbine corrected speed line 80krpm was tested at three different engine speeds, 2000rpm, 2500rpm and 3000rpm (Figure 4.5). The 95% confidence interval was within 1.5 percentage points. The confidence interval at the last operating point is not at the exact measured expansion ratio. This is because the flow range achieved in the three repeats were slightly different, shown in Figure 4.2, and the measurements were interpolated to calculate the confidence interval.

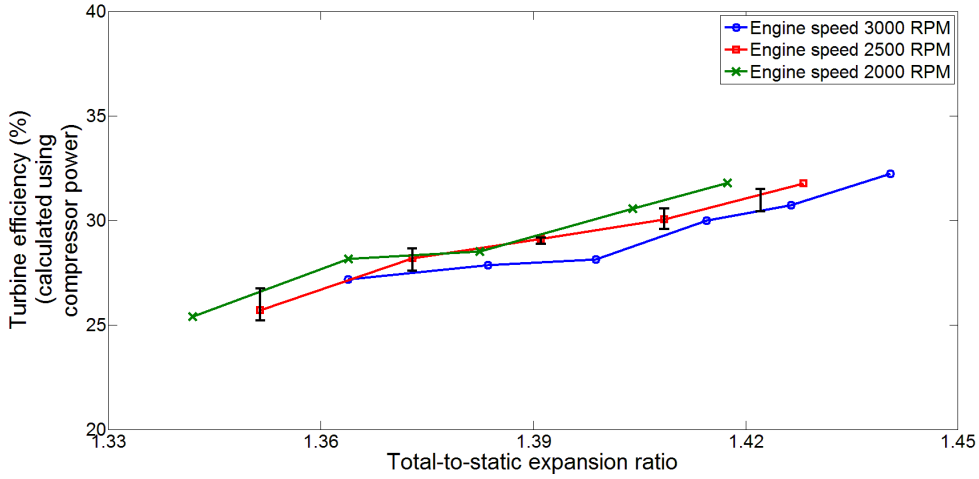

Figure 4.5: Turbine efficiency measured at three different engine speeds

It is shown that, despite the relatively small difference compared to the confidence interval, the turbine efficiency calculated using the compressor power was increased by approximately 1-2% as the engine speed decreased from 3000rpm to 2000rpm. However, this was not only a result of the changes in the exhaust pulse frequency. The amplitude of the pulse was also affected when the frequency was varied, shown in Figure 4.6. The amplitude was approximately 0.3 bar at 3000rpm, compared with approximately 0.15 bar at 2000rpm. The lower turbine efficiency may be a result of the larger variation in the instantaneous turbine blade speed ratio, which caused efficiency drops at extreme blade speed ratio conditions.

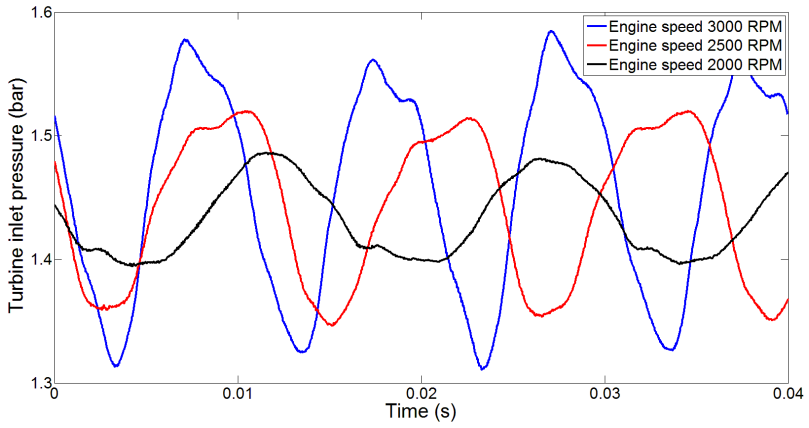

Figure 4.6: Instantaneous turbine inlet pressures at three engine speeds

In addition, the temperature measurement at the turbine inlet was operating under pulsating flow condition, therefore, the thermocouple readings might have been affected. The coolant and oil flow rate at the bearing housing were not controlled. Therefore, the heat fluxes to the compressor may have been changed, resulting in variations in the calculated enthalpy change across the compressor.

The calculated efficiency was time-averaged value. It would be ideal if the power-weighted efficiency could be calculated. However, the instantaneous mass flow was difficult to measure. A hot-wire type flow sensor could be used to measure

the instantaneous mass flow. This may require temperature measurements to compensate the mass flow measurement. The temperature of the gases between the exhaust port and turbine inlet was high and variable, with consequent challenges in measuring the temperature to compensate the mass flow measurements correctly. Gas velocity may change direction transiently, causing difficulties in using the flow sensor under some engine operating conditions. Care also needs to be taken when using hot-wire type flow sensor in exhaust gas environment with particles.

In addition to the uncertainties in efficiency calculation, although the turbine reduced speed was maintained, the absolute inlet conditions at the turbine inlet varied. The flow density and velocity, thus, the Reynolds number and wall friction losses were affected. To study this effect, mean-line turbocharger modelling may be required to separate the flow effects at the rotor, gap, and volute. Nevertheless, this was not in the scope of this project and was neglected.

As a result of these effects, the efficiency variations were not only caused by the frequency and magnitude variations. However, the confidence interval is small and it is capable of detecting small changes. With the planned modifications of the configuration of the facility in the future, the variations in the efficiencies can be understood and explained.

To investigate the differences between the two methods of calculating the turbine efficiency, tests were performed under fired and unfired conditions, and the turbine efficiencies were calculated, shown in Figure 4.7. The speed line 80krpm was tested under both fired and unfired conditions. The turbine expansion ratio was larger in the fired test (1073 K turbine inlet temperature), since the same turbine corrected speed was targeted.

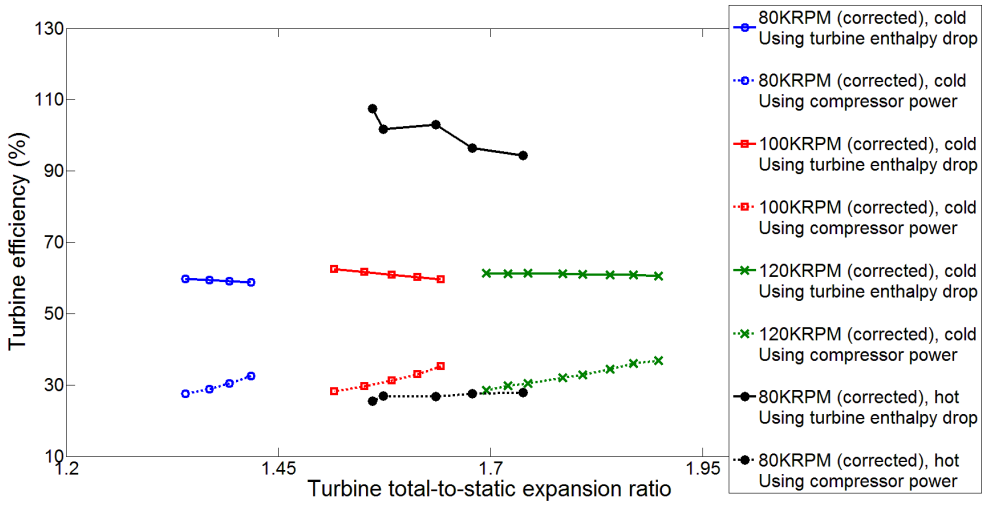

Figure 4.7: Calculated turbine efficiency at VGT fully closed

Under fired conditions, the turbine efficiency calculated using the turbine enthalpy drop was above 100%, which was unrealistic. This was mainly because of the heat transfer effects, which were considered to be turbine power in this method. From the calculation using compressor power, the heat transfer effect on the compressor was ignored. Besides, the oil flow and temperature was not controlled in these tests. This may have affected the heat flux between turbine housing and compressor housing, and thus, the calculated turbine efficiency. However, this was smaller than that on the turbine, due to the different temperature level. It is shown that the turbine efficiency calculated using the compressor power was slightly lower in the fired test. This was also affected by the higher turbocharger rotational speed and mechanical losses in the fired test with high turbine inlet temperature, because turbine inlet temperature was used in the speed correction calculation.

In addition, the turbine expansion ratio was changed, since the corrected speed was maintained in both the fired and unfired tests. Thus, the turbine blade speed ratio was also changed, which affected the turbine efficiency.

As a result, the two methods should be differentiated to avoid confusion. At low turbine inlet temperature level, the difference between the two methods was around 15%. This increased to up to 80% in the hot tests. At high turbine inlet temperature level, the apparent turbine power was unrealistic. The comparison showed that the effects of heat transfer on the turbine efficiency calculated using compressor enthalpy change was small. To investigate the effect of heat transfer in more detail, bearing losses also need to be considered.

In the present investigation, compressor power was used for turbine efficiency calculation because of the reliability and the smaller discrepancies between fired and unfired tests. Cold tests were performed to obtain the turbine map. This was because control freedom was restricted under fired conditions on the gasoline engine, which is expected to be improved in the future when the gasoline engine is replaced with a Diesel engine.

4.3.3. Compressor mapping

Figure 4.8 shows the compressor map obtained from the on-engine mapping facility. The turbocharger speed can be varied by changing the engine intake pressure, engine speed and the VGT position or, if a waste-gated turbocharger is tested, the waste-gate opening. The turbocharger speed range in this cold test was 40krpm to 100krpm. The maximum engine speed and intake pressure defined in the test were 4500rpm and 2 bar absolute, respectively. These were below the limits of this engine. Therefore, it was expected that the achievable speed range could reach over 150krpm in cold tests, if higher engine speed and intake pressure were tested.

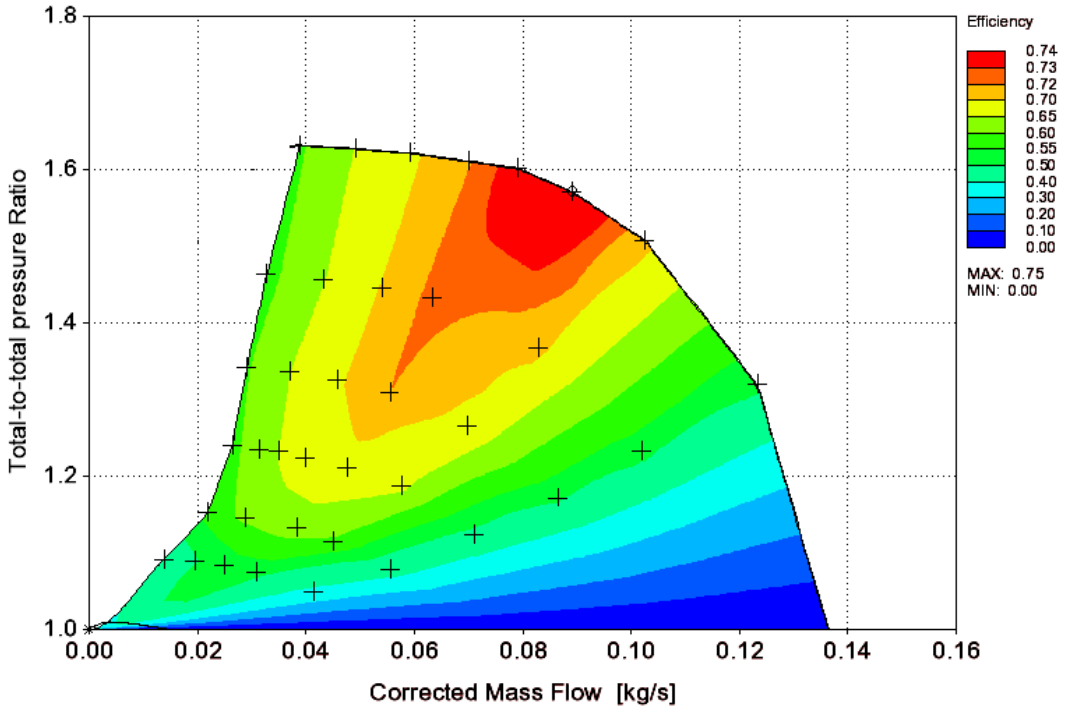

(Compressor mass flow corrected to inlet condition 298 K and 1 bar absolute)

Figure 4.8: Compressor efficiency contour map generated from cold test

Since compressor surge detection was not in the scope of this study, surge was simply defined as compressor inlet temperature shoot up. Operating points beyond the surge line were also recorded for future investigations. The turbocharger speed, temperature and fast pressure measurements will be used in future studies on surge definition. In general, surge limit can be reached on this facility. The compressor efficiency when the compressor back pressure valve was opened was around 40%. Therefore, choke limit on the compressor map was also reached.

To investigate the effect of turbine inlet temperature and heat transfer on the calculated compressor efficiency, two of the compressor speed lines have been tested under fired conditions. Figure 4.9 shows the two compressor corrected speed lines tested under fired and unfired conditions. The different mass flow range on the speed line was because of the spark timing limits due to combustion misfire. The compressor efficiency calculated from fired conditions was considerably lower than

that calculated from the unfired conditions where the turbine inlet temperature was 340 K. This was because of the heat fluxes from the turbine housing to compressor housing, causing high air temperature at the compressor outlet which was counted as enthalpy arising from the compression process. It is also shown that the discrepancy between fired and unfired conditions at 40krpm compressor corrected speed was larger than that at 75krpm. The difference increased from 3-5 percentage points out of 70% to 5-8 percentage points out of 50%. This was due to the lower compressor power at low speed. Therefore, the proportion of heat transfer was larger. In addition, the turbine inlet temperature at low speed was lower, due to the restrictions on the combustion and spark timing window. Therefore, the discrepancy at low speed was expected to be larger if the turbine inlet temperature reached 1073 K.

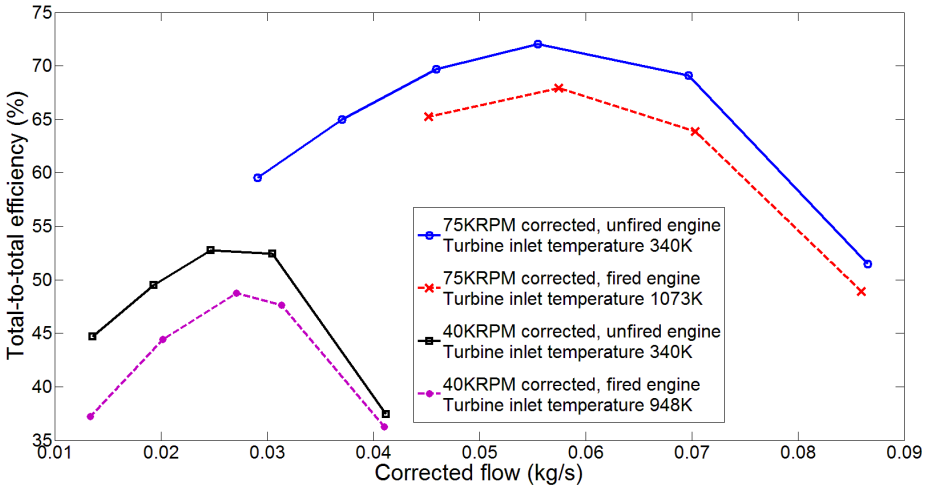

Figure 4.9: Comparison of compressor efficiency under fired and unfired conditions

4.4. Future improvement of the facility

From the turbine and compressor test results shown above, there were a number of areas that still need improvement in order to improve the reliability of the test results and to investigate in more detail.

In order to carry out heat transfer studies, the flow and temperature of coolant and oil should be controlled, independent of the engine operating points. The oil flow and temperature at the turbocharger bearing housing need to be measured and recorded. The metal temperature on the turbocharger may be required. In addition, thermal insulation on the turbocharger may be required to avoid heat transfer between housing and ambient.

It will be necessary to modify the layout of the facility so that wider turbine operating range can be reached. This can be achieved by adding compressor recirculation. It has also been planned that the engine platform will be changed from gasoline engine to Diesel engine to extend the achievable operating range. With Diesel engines, the fuelling amount and the intake air pressure can be controlled independently, whereas they were linked on the gasoline engines, which restricted the operating range.

To calculate the instantaneous turbine power, the instantaneous turbine flow is required. However, it is difficult to measure the instantaneous gas temperature for flow compensation. Thus, simulation may be needed to estimate the gas temperature and flow. Calibrated 1-D or 3-D models of the turbine housing will be useful for the prediction of the instantaneous expansion ratio and flow at the rotor.

To mitigate the uncertainty about the gas pressure and temperature distributions at cross sections, and to improve measurement accuracy, more pressure and temperature measurements should be installed at cross sections at compressor and turbine inlet/outlet. Flush-mounted pressure measurements and different thermocouple depths should also be employed.

4.5. Conclusions

An on-engine turbocharger mapping facility that was developed to improve the understanding and modelling techniques of turbocharging systems was presented in this chapter. The result of a turbocharger mapping test was demonstrated and investigated. The following points can be drawn to conclude this chapter:

1. The challenges in using turbocharger maps collected on conventional gas-stand under steady flow have been discussed. The challenges include the pulsating effects, heat transfer effects and map extrapolation. Research has been carried out to investigate the countermeasures and to compare existing novel turbocharger mapping facilities.

2. In order to evaluate turbochargers under the on-engine blow-down pulses and high temperature conditions, a gasoline engine has been converted into a pulse and heat generator assisted with an external boosting system. The engine and the turbocharger have been heavily instrumented with high and low frequency measurements.

3. Detailed test procedure has been presented. This was applied to the mapping of a VGT turbocharger using this facility. One speed line was repeated three times. The 95% confident region of the measured compressor and turbine efficiency was within ±1.5%.

4. Experiments were performed in the engine speed range of 2000rpm to 4500rpm (exhaust pulse frequency 67Hz to 150Hz). A decrease in turbine efficiency of 2% was found as the engine speed was increased from 2000rpm to 3000rpm. Further improvements in the measurement system and the control of boundary conditions

will be necessary for further investigation.

5. Tests have also been performed in the turbine inlet temperature range of 340K to 1073K. Between hot and cold tests, approximately 5-10% difference was observed in the turbine efficiency calculated using compressor power. However, the effect on the turbine efficiency calculated using turbine enthalpy drop was above 40%. The calculated compressor efficiency was affected by 3-8% due to heat transfer. The effect was more significant at lower compressor power. Thermal condition control and bearing housing friction model will be required for further investigation.

6. Recommendations were provided for the continuation of the development and improvement of the on-engine turbocharger mapping facility. To improve the reliability of the test results, more accurate control of engine thermal boundary conditions will be necessary. Turbine operating range needs to be extended through modifications on compressor loading. Modelling techniques may be used to estimate instantaneous turbine operating point. In addition, multi-point measurements at cross sections of interest will be required to improve measurement accuracy.

Chapter 5 - *Simulation Methodology*

A high fidelity engine model which was supplied to the project has been further calibrated for the investigations of steady state and transient performance of advanced turbocharging systems.

This chapter presents the calibration of the combustion model, the flow element and the turbocharger model at steady state. For each of these sub-systems, the model description, the calibration methodologies and the validation results will be discussed.

In the last section of this chapter, the validation of transient simulation will also be presented. Recommendations will be provided to further enhance the modelling techniques of each sub-system, as future work.

5.1. Introduction

5.1.1. Engine modelling

Engine modelling is extensively used in the engine design process. It is useful in predicting engine performance and simulating parameters that are difficult to measure in experiments. Several types of engine model are used in simulations, for example, the black box model, mean value model, 1-D model and multi-dimensional model. These available tools form a spectrum of computational time and prediction accuracy. Therefore, they are used for different objectives.

In general, models with less insight into the internal processes of the system have lower complexity and, therefore, require a shorter run time. Complex models are used in detailed analysis of particular systems. For example, with regard to dynamics in the fuel injection system, mixture formation process and air motion at the compressor wheel are likely to require multi-dimensional modelling if more details are to be investigated and predicted. The results of the multi-dimensional predictions and experiments can be used in models of lower complexity, such as the 1-D model.

The behaviours of the entire system can be predicted and analysed as long as the operating conditions of the individual systems are within reasonable range and with appropriate assumptions. For example, the empirical combustion model may be sufficient for turbocharger matching at target full load operating points. However, if the engine compression ratio is changed to enable Miller cycle operation, the original combustion model may not be valid, due to the considerable changes in the in-cylinder air motion and thermodynamic processes [116].

In this study, the 1-D modelling approach was selected to simulate and analyse the entire engine system, because of its accuracy, limited run time, and the capability of integrating the whole system. The flow is treated as 1-D, and hence the distributions of gas composition and energies at any cross-section are homogenous. However, the dynamics of pressure propagation along the air path can be captured. This is sufficient in engine behaviour simulations provided that each of the sub-models is

validated. Care needs to be taken to make sure that the operating range of each sub-system is within reasonable range from the points at which the model is calibrated.

The data collected in the experiments in this project have been used to calibrate the engine model. The procedure of calibration of a downsized turbocharged gasoline engine will be described in this chapter. The aim is to calibrate an existing high fidelity engine model, which was provided for this study, to extend the validated steady state operating range, and to calibrate the model for transient simulations.

5.1.2. GT-Power

GT-Power, one of the typical 1-D engine simulation codes, is widely used in engine performance prediction and analysis. It is used in this analysis because of the following advantages. The version of the software used in this project is 7.4.1 [117].

- Crank angle based calculation of gas properties for the analyses of gas dynamics in the ducts, valves and flow element.
- Combustion model calibration tool using experimental data.
- Capability of conducting both steady state and transient simulation.
- Flexibility of building control systems in the engine model, and the availability of built-in model-based control elements.
- Interface to other simulation programs such as Matlab/Simulink for design of more complex control systems and integrated simulation.
- Capability of carrying out Design of Experiments (DOE), empirical model generation and optimisation.

It is worth noting that other 1-D engine simulation programs exist. Ricardo Wave is also capable of carrying out similar studies. However, the lack of flexibility in building control systems in Wave results in the unnecessary co-simulation with Matlab/Simulink, which increases computational time.

5.2. Modelling techniques and simulation validation at steady state operating points

5.2.1. Combustion modelling

5.2.1.1. Available models in GT-Power

To carry out engine simulation, an appropriate combustion model is necessary. An inaccurate combustion model may result in unreliable predictions of engine thermodynamic processes, and hence engine output. Predictive, semi-predictive, and non-predictive combustion models are available in GT-Power. Links to other CFD combustion analysis software are also possible for predicting details of the combustion system. However, long simulation time is required due to the complexity of the CFD model. This can be used in the design stage before the hardware is available.

The quasi-dimensional combustion model based on turbulent flame is available in GT-Power as a predictive combustion model. The heat release prediction is based on the in-cylinder turbulence intensity and scale, which are then used in the calculation of fuel burn rate [118]. In addition, knock intensity can be simulated based on in-cylinder pressure and temperature. Simulation time is faster than for complete three-dimensional tools, and it is comparable to non-predictive combustion models [119]. However, extensive calibration work is required. Nevertheless, once the model is calibrated based on measurement data, the effects of variation (including fuel properties, cylinder geometry and spark timing) on combustion behaviours can be analysed.

Several non-predictive combustion models are available in GT-Power: the Wiebe model, Multi-Wiebe model, and user profile input. Combustion 10%-90% burn duration, Wiebe exponent, combustion efficiency and 50% burn angle (which can be further controlled by spark timing actuator) are defined in the Wiebe model to determine the combustion cumulative heat release profile, by assuming an S-curve profile. The four parameters can be mapped based on engine operating range.

Therefore, the advantage of using the Wiebe model is that the parameters can be interpolated and extrapolated so that a semi-predictive combustion model can be generated. To be able to define a profile using four parameters, this simplification requires curve fitting for the actual heat release profile, which can be either calculated from measured cylinder pressure trace or predicted using other combustion analysis software. Therefore, this results in errors in the curve fitting process.

The Multi-Wiebe model is an extension of the ordinary Wiebe Model. The cumulative heat release profile is represented by the combination of several single Wiebe profiles with different parameters. This results in better fitting at the calibrated operating point.

Another non-predictive combustion model is the user profile input, which uses the input profile as the heat release curve. The heat release profile can be calculated from measured cylinder pressure data. Therefore, the error introduced by curve fitting can be eliminated. Similar to the Wiebe model, a semi-predictive combustion model can also be generated by interpolating between the profiles to predict the heat release within the calibrated operating range.

Since the engine hardware was available for this project, experiments could be conducted to measure and calculate the combustion heat release. Therefore, extensive predictability was not required. In addition, the engine block geometries were not to be changed. The control parameters were not to be varied in a wide range in simulation studies. Therefore, the user profile input method was chosen to build a semi-predictive combustion model in this study, because it provides accuracy, fast computational time and reasonable accuracy in the calibrated range.

5.2.1.2. Three pressure analysis

To calculate the combustion heat release profiles, three pressure analysis (TPA) has been performed at each engine operating point tested in the experiments. The model used in this TPA is shown in Figure 5.1. The elements of intake port, exhaust port

and one cylinder were used. The instantaneous pressure measurements at intake port, cylinder and exhaust port was used to determine the residual gas fraction and trapping ratio, and net and gross heat release. Therefore, the uncertainties caused by making assumptions about volumetric efficiency could be avoided.

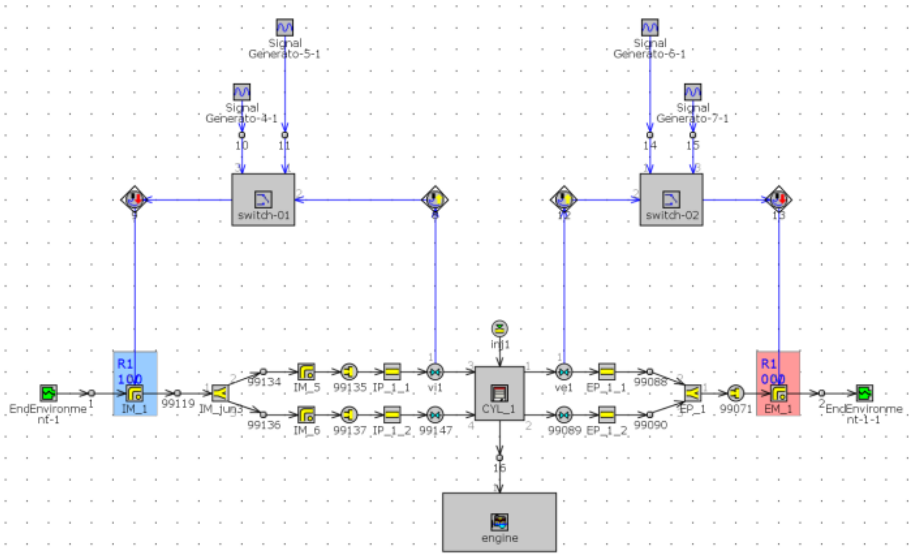

Figure 5.1: Three pressure analysis

The measured cylinder pressure was pegged to the instantaneous intake port pressure at bottom dead centre (BDC) in the compression stroke. In order to avoid spurious pressure fluctuation between an imposed instantaneous static pressure boundary condition and a simulated pressure wave, the friction multiplier at the two pipe elements connected to the boundaries were switched to a very high value, 100, when the valves were closed.

The experimental engine control parameters for the scavenging system and fuelling system were imposed. The combustion chamber wall temperature was modelled using a finite element model, and the measured oil and coolant temperature were used as boundary conditions. The wall temperature was then used for the calculation of heat transfer from gas to combustion chamber.

The cylinder was treated as a varying volume between the intake valves and exhaust valves. A two-zone combustion model was employed. The burned and unburned air-fuel mixtures were trapped in the burned and unburned zones respectively. The

pressure distribution in the whole combustion chamber was homogeneous, whereas the temperatures in the two zones were modelled separately. At the start of combustion, all the gases in the cylinder were in the unburned zone. After the start of combustion, the unburned mixture was moved to the burned zone at the rate determined by the burn rate at each time step. Therefore, the volumes of the two zones changed at each time step. At the same time, the chemical equilibrium calculation was carried out in the burned zone. In addition, the conservation of energy was calculated in the two zones.

In the unburned zone:

$$\frac{d(m_u e_u)}{dt} = -p * \frac{dV_u}{dt} - Q_u - \left(\frac{dm_f}{dt} * h_f + \frac{dm_a}{dt} * h_a\right) + \frac{dm_{fi}}{dt} * h_{fi} \quad \textbf{5.1}$$

where m is mass of denoted gases

e_u is the unburned zone energy

p is the cylinder pressure

V_u is the unburned zone volume

Q_u is the unburned zone heat transfer

h is the enthalpy of the denoted gases

subscript u, f, a, and fi denote unburned zone, fuel, air and fuel injected, respectively

In the burned zone:

$$\frac{d(m_b e_b)}{dt} = -p * \frac{dV_b}{dt} - Q_b - \left(\frac{dm_f}{dt} * h_f + \frac{dm_a}{dt} * h_a\right) \quad \textbf{5.2}$$

where subscript b denotes burned zone

The terms on the right-hand side of the equations represent the useful work, heat transfer to combustion chamber, the energy flow as a result of fuel flow, air flow and fuel injection, respectively. The advantage of the two-zone combustion model is that the thermodynamic processes in the two zones are simulated separately with different

temperatures. This allows more accurate simulation of useful work, since the work done is largely dependent on the temperature of expanding gases [120].

When the TPA was performed, a dummy heat release profile was used in the first cycle. From the second cycle onwards, the simulation was paused at the start of the cycle and a reverse simulation was conducted. In the reverse simulation, the heat release was calculated using the trapped conditions and the cylinder heat transfer model. This was achieved by iterating the amount of fuel transferred from the unburned to the burned zone at each time step until the measured cylinder pressure was matched. Then the forward simulation started again, and the cylinder pressure was simulated using the calculated heat release profile. The cycle was repeated until the steady state convergence tolerance was achieved.

5.2.1.3. Combustion model validation

An engine model was provided for this study. The combustion model was calibrated using the measured data that covered engine speed range of 1000rpm to 5800rpm and load range of 20% to 100% (approximately 60Nm to up to 300Nm). The combustion heat release profiles were normalised to fuel fraction burnt profiles, and the profiles were stored in XY tables in GT-Power for interpolation within the tested operating range.

The original combustion model was calibrated using the experimental data collected from the production configuration with the original production FGT turbocharger. Therefore, the simulation with the VGT turbocharger needed to be validated. In addition, the maximum torque achieved with VGT and the required load range in transient simulation (from 2 bar BMEP, 32Nm) were outside the original calibration range. Since the transient experiments were carried out at 2000rpm, the steady state engine operating points listed in Table 5.1 were selected in order to cover the engine operating range experienced in the transient tests.

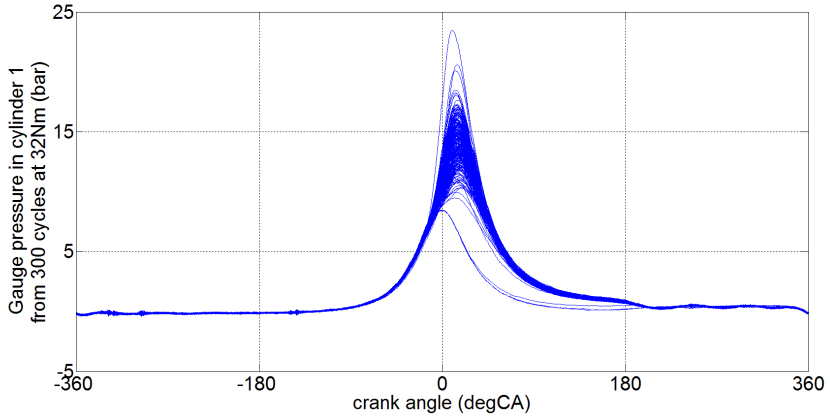

Figure 5.2 shows pressure in cylinder 1 measured in 300 consecutive cycles at 32Nm 2000rpm. Large cyclic variation can be observed at low engine load and small mass air flow. In addition, the test cell control system was maintaining the engine torque, whilst the ECU was also aiming to maintain a target torque determined by the pedal position. It is worth noting that three misfire cycles occurred at cylinder 1 during the test. This also caused cyclic variation due to the changes in mixture property, local air fuel ratio and residual gas, and hence flame speed. An empirical Wiebe combustion model can be built based on the air fuel ratio and residual gas to model the cyclic variation [121]. Nevertheless, the cyclic variation was not in the scope of this project, since the project was focused on the turbocharging system. Averaged cylinder pressure and heat release profile were analysed.

Table 5.1: Operating points for combustion model validation

	Test point 1	Test point 2	Test point 3
Operating condition	2000rpm, 32Nm	2000rpm, 229Nm	2000rpm, 319Nm
Validation objective	For low load operation in transient simulations. This was outside the original calibration range.	To validate part load operation with VGT, moderate boost pressure. (boost pressure approximately 1.3 bar absolute)	To extend full load range outside original calibration region. (boost pressure approximately 1.9 bar absolute)

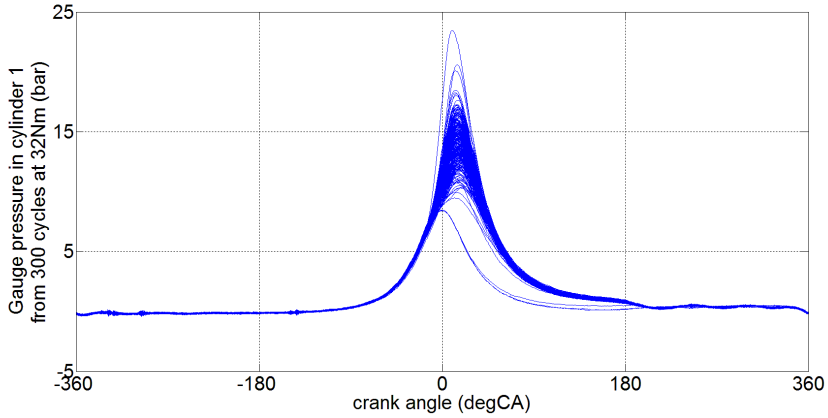

Figure 5.2: Cyclic variation in cylinder 1 at 32Nm

Figure 5.3 and Table 5.2 demonstrate the comparison between measurements and simulation results at 32Nm. Cylinder-to-cylinder variation can be observed in the measured data. This may be a result of several factors: for example, 3-D flow behaviours, different thermal conditions and blow-by. The 3-D air and gas motion in the intake manifold, exhaust manifold and cylinders might cause variations in the air flow into and out of each cylinder. This was difficult to capture in 1-D simulation. The blow-by in each cylinder may be affected by the variations in thermal condition, the actual geometry of each combustion chamber and aging.

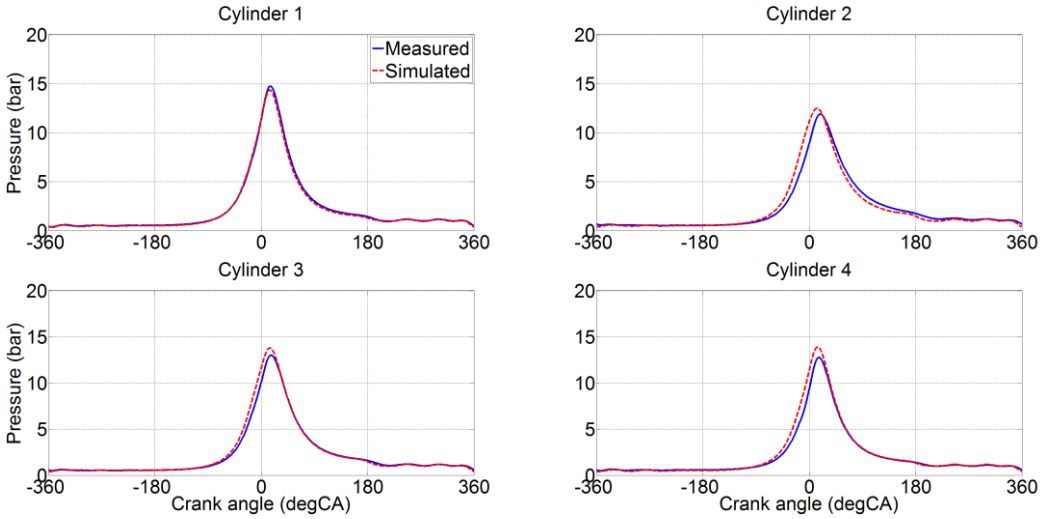

Figure 5.3: Simulated cylinder pressure from TPA and measured pressure at 32Nm

The discrepancy between measured and simulated mass air flow was 0.01%. Despite the 9.37% error in the averaged indicated mean effective pressure (IMEP), the

averaged absolute error in net IMEP was below 0.3 bar. Therefore, the modelling of the scavenging system and combustion system at low engine load is satisfactory.

At 229Nm, the operating point was within the original combustion model region, calibrated using the FGT experimental data. With the VGT, the scavenging process may have been affected by the changes in the exhaust manifold geometry and instantaneous turbine operating points. The averaged pressure differential across the engine (exhaust manifold pressure – intake manifold pressure) decreased by approximately 5kPa by replacing the FGT with VGT. In addition, the spark timing at knock limit was advanced by 2.25 degrees crank angle. (Detailed studies will be presented in Chapter 6.) As a result of these changes, it was necessary to validate the original combustion model for use in part load and transient simulation for the VGT turbocharger.

Table 5.2: TPA simulation results at 2000rpm 32Nm

	Cylinder 1	Cylinder 2	Cylinder 3	Cylinder 4
Measured total mass air flow (kg/hr)	34.95			
Simulated total mass air flow (kg/hr)	34.71			
Error in total mass air flow (%)	0.57			
Simulated mass air flow (kg/hr)	8.14	8.96	9.26	8.35
Measured net IMEP (bar)	2.51	3.04	2.68	2.44
Simulated net IMEP (bar)	2.33	2.37	2.58	2.34
Absolute error in net IMEP prediction (bar)	0.19	0.68	0.10	0.10
Error in net IMEP prediction (%)	7.39	22.24	3.61	4.25
Averaged absolute error in net IMEP (bar)	0.26			
Averaged error in net IMEP (%)	9.37			

The measured inlet and exhaust port pressure data from the VGT experiment were used as the boundary conditions, and the valve timing and spark timing were changed according to the experiment setups. The heat release profile was defined by the original combustion model, instead of the TPA calculation based on measured cylinder pressure data. Despite the changes in the scavenging process, good matches between prediction and measured data can be observed (Figure 5.4). The measured

and predicted net IMEP are listed in Table 5.3. The effect of changing the turbocharger and manifold on the heat release profile was small. It was found that the measured IMEP of cylinder 4 was approximately 15% lower than the other three cylinders. Since cylinder-to-cylinder variation is not studied in this project and the prediction of the other three cylinders was within 5% error, the accuracy of the prediction at 229Nm is satisfactory. Therefore, the original combustion model can be used for VGT simulations at engine operating points within the original calibrated region.

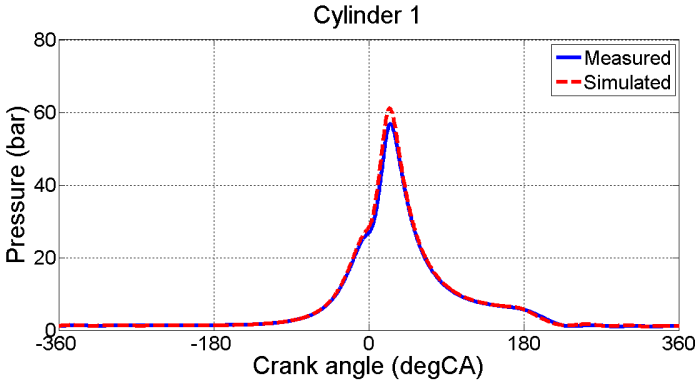

Figure 5.4: Measured and simulated cylinder pressure at 229Nm with VGT turbocharger

Table 5.3: Measured data and simulation results at 229Nm

	Cylinder 1	Cylinder 2	Cylinder 3	Cylinder 4
Measured total mass air flow (kg/hr)	170.37			
Simulated total mass air flow (kg/hr)	175.91			
Error in total mass air flow (%)	3.26			
Measured net IMEP (bar)	15.03	14.86	15.24	12.76
Simulated net IMEP (bar)	15.41	15.39	15.40	15.40
Absolute error in net IMEP prediction (bar)	0.39	0.53	0.17	2.65
Error in net IMEP prediction (%)	2.56	3.59	1.10	20.76
Averaged absolute error in net IMEP (bar)	0.93			
Averaged error in net IMEP (%)	7.00			

The cylinder-to-cylinder variation was also observed at 319Nm. The comparison between simulation and measured data is listed in Table 5.4. The net IMEP of

cylinder 4 was approximately 13% lower than that of the other cylinders. Nevertheless, the cylinder-to-cylinder variation is not analysed in this study. The combustion model in cylinder 1 will also be used for cylinder 4 in the simulation studies.

To summarise the combustion model validation, the correlations at the three operating points are listed in Table 5.5. It is shown that the total mass air flow prediction is satisfactory. The net IMEP prediction is accurate, despite the relatively large percentage error at very low load due to the small absolute values.

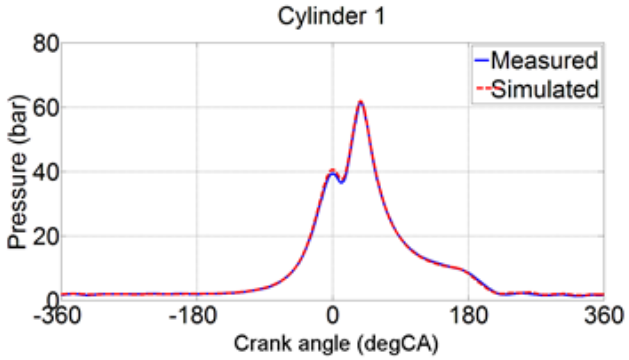

Figure 5.5: Measured and simulated cylinder pressure at 319Nm with VGT turbocharger

Table 5.4: Measured data and simulation results at 319Nm

	Cylinder 1	Cylinder 2	Cylinder 3	Cylinder 4
Measured total mass air flow (kg/hr)	258.69			
Simulated total mass air flow (kg/hr)	263.65			
Error in total mass air flow (%)	1.92			
Measured net IMEP (bar)	20.71	21.19	20.75	18.29
Simulated net IMEP (bar)	20.44	20.76	20.30	18.02
Absolute error in net IMEP prediction (bar)	0.39	0.43	0.45	0.27
Error in net IMEP prediction (%)	1.87	2.05	2.15	1.47

Averaged absolute error in net IMEP (bar)	0.36
Averaged error in net IMEP (%)	1.89

Table 5.5: Summary of combustion model validation at 2000rpm

	32Nm	229Nm	319Nm
Error in total mass air flow prediction (%)	0.69	3.26	1.92
Averaged error in net IMEP prediction (bar) (cylinder 1)	0.19	0.39	0.39
Averaged error in net IMEP prediction (%) (cylinder 1)	7.39	2.56	1.87

For steady state simulations with target engine torque set in the closed-loop boost pressure controller, the combustion heat release profiles were interpolated based on engine speed and percentage load for faster simulation and convergence. For transient simulations, the heat release profiles were interpolated based on the engine speed and mass air flow to avoid simulation convergence to unrealistic conditions.

Therefore, the combustion heat release profiles were interpolated with a pre-lookup table which converted from mass flow interpolation to engine percentage load interpolation. This was based on the measured mass flow data at each calibrated operating point.

5.2.1.4. Critiques on combustion model calibration

It is worth noting that a number of assumptions had been made when the combustion model was calibrated and used. Uncertainties were introduced because of these assumptions. The measured cylinder pressure was pegged to instantaneous port pressure at BDC in the compression stroke. This was based on the assumption that

the cylinder pressure and port pressure are equal at BDC, due to the low gas velocity at zero piston speed. In fact, cylinder pressure can also be pegged by matching pressure rise in the compression stroke based on polytropic coefficient. The uncertainties about the pressure difference at BDC can be avoided. Nevertheless, assumptions need to be made for the effective compression ratio (which is affected by timing of intake valve closing) and the gas property gamma (which is affected by residual gas fraction and temperature). Additional uncertainties may be introduced due to the variations of intake and exhaust valve phasing on modern downsized gasoline engines.

The prediction of wall temperature was not calibrated in this project. Nevertheless, this can be carried out in future work if detailed heat transfer study is required. The metal temperature at cylinder wall and the coolant temperature at various locations in the engine block can be measured for model calibration [122].

The blow-by was ignored in this study, introducing uncertainties in the mass air flow and trapped mass in cylinder. If the blow-by were to be studied, the ventilation flow from the crankcase could be measured and used to calibrate the blow-by model in the simulation.

The calculation of the scavenging process, and hence the residual gas fraction and trapping ratio, was based on the assumption of homogeneous mixture in the cylinder. The accuracy can be improved by carrying out multi-dimensional simulation. However, the computational time will be increased significantly. Nonetheless, the accuracy was satisfactory, considering that the TPA study was carried out so that assumptions on volumetric efficiencies were not necessary.

Since the combustion model was calibrated based on the boundary conditions at each test point, the accuracy of the estimation of the heat release process would decrease if the simulated operating points were outside the calibrated region. Therefore, more experimental data will be required to calibrate an empirical model that covers wider operating range or a predictive combustion model.

5.2.2. Gas dynamics modelling

5.2.2.1. Flow modelling in GT-Power

The combustion behaviours and the thermodynamic processes can be simulated only if the flow in to and out of the cylinder is accurate. In GT-Power, this is achieved by modelling the gas dynamics in the flow elements: for example, duct, junction, orifice, valve, and compressor and turbine. The pressure wave propagation is modelled by treating the gases as 1-D flow with even radial distribution. The friction losses and heat transfer at each element are modelled, and the flow discharge behaviours between elements are also simulated.

The length of ducts is further discretised to improve the fidelity and accuracy. The discretisation length can be defined by the user, and different values should be used in ducts in intake and exhaust systems, due to the different temperature, and hence the variations in sound speed. The following equations for conservation of mass (5.3), energy (5.4) and momentum (5.5) are solved by using in each discretised volume in the crank angle domain.

Mass conservation:

$$\frac{dm}{dt} = \sum_{boundaries} \dot{m} \qquad \textbf{5.3}$$

where $\dot{m}$ is the boundary mass flux into the volume

m is the mass of the volume

Energy conservation:

$$\frac{d(m * e)}{dt} = P * \frac{dV}{dt} + \sum_{boundaries} (\dot{m} * H) - h * A_s * (T_{fluid} - T_{wall}) \qquad \textbf{5.4}$$

where e is the total internal energy per unit mass

P is the pressure

V is the volume

H is the total enthalpy

A_s is the heat transfer surface area

h is the heat transfer coefficient

T_{fluid} is the fluid temperature

T_{wall} is the wall temperature

The groups of terms in the energy conservation equation represent the useful work, mass flow, and heat transfer, respectively.

Momentum conservation:

$$\frac{d\dot{m}}{dt} = \frac{dp * A + \sum_{boundaries}(\dot{m} * \mu) - 4 * C_f * \frac{\rho * \mu * |\mu|}{2} * \frac{dx * A}{D} - C_p * \left(\frac{1}{2} * \rho * \mu * |\mu|\right) * A}{dx} \quad \textbf{5.5}$$

where dp is the pressure differential across dx

A is the flow area

μ is the velocity at boundary

C_f is the skin friction coefficient

ρ is the density

dx is the length of mass element in flow direction

D is the equivalent diameter

C_p is the pressure loss coefficient

The groups of terms in the momentum conservation equation represent impulse, momentum of flow, friction losses, and pressure losses, respectively.

5.2.2.2. Flowsplit element

In GT-Power, flowsplit elements are used to model the conservation of momentum in three dimensions. The flowsplit element is treated as a single volume, and the mass flow vector is solved at the boundaries. Therefore, the angles of each opening are required for the calculation of transfer of momentum. In addition, another two parameters, expansion diameter and characteristic length, are also required. The expansion diameter is the maximum diameter to which the flow can expand after entering the flowsplit element. It is used in the calculation of the flow velocity, pressure loss and discharge coefficient of the orifice. Therefore, the kinetic energy losses due to the expansion and the discharge from the port to the volume are modelled.

These two parameters are dependent on the geometry and the flow pattern, which may not be obvious in some cases. For example, in Figure 5.6, gas flow enters the volume from sections 2 and 3 and exits the volume from section 1. The expansion area can be solved using the following equation:

$$\mathrm{EA}_1 = \mathrm{A}_1$$
$$\mathrm{EA}_2 = \mathrm{F}_2 * \mathrm{A}_1$$
$$\mathrm{EA}_3 = \mathrm{F}_3 * \mathrm{A}_1 \qquad \textbf{5.6}$$

where EA is the expansion area of each port

A is the area of each port

F is the fraction of the total area A_1 into which the flow from the port can expand

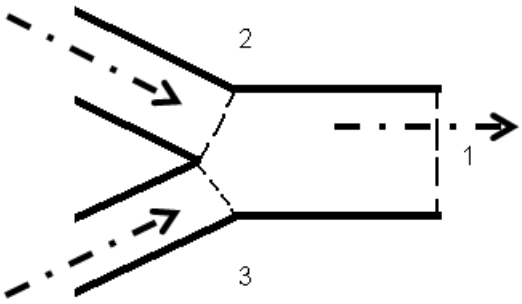

Figure 5.6: Example of a flowsplit element

It is recommended that the fraction F should be set to 0.5 if the flows from port 2 and 3 are completely in-phase, since the flow entering the flowsplit can only expand into half of the large pipe. If the flows from ports 2 and 3 are out-of-phase, the fraction F should be set to 1, since the flow is free to expand to the entire diameter.

The characteristic length needs to be adjusted according to the fluid behaviours in the manifold. In the example shown in Figure 5.6, the gas flow from sections 2 and 3 enters the volume and curves slightly in the volume before it exits from section 1. It is recommended that the characteristic length is set to the distance between the inlet section and the outlet section.

5.2.2.3. Model set up

Since a custom-made exhaust manifold was used to fit the VGT turbocharger, the 1-D elements that represent the exhaust manifold need to be built accordingly. The geometry of the manifold was taken from a CAD model and specifications. They were converted into pipe and flowsplit elements in GT-Power. A number of elements were used to represent the straight pipes and bends. The collector where the four ports jointed was represented by a flowsplit element. Figure 5.7 shows the CAD model of the exhaust manifold.

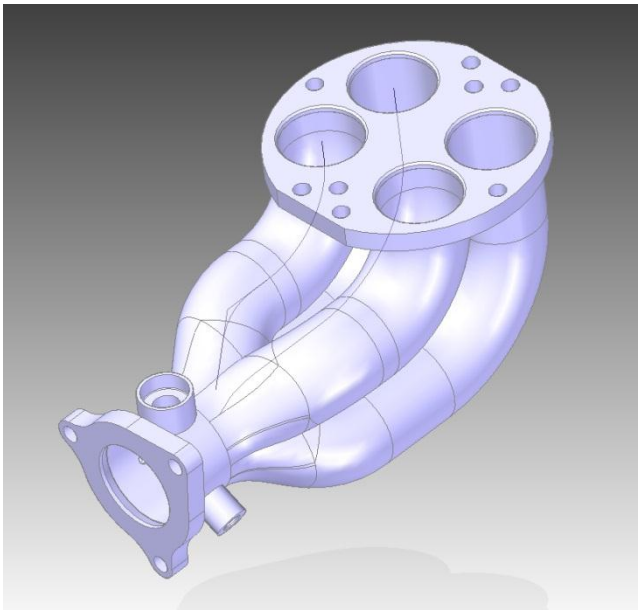

Figure 5.7: Exhaust manifold for VGT

In order to define the expansion diameter for the flowsplit element, the flow behaviour in the manifold was considered. Since the volume and the shape of the FGT exhaust manifold was maintained at the same level, the flow pattern in the FGT manifold was referred to for the selection of the expansion diameter of the VGT manifold.

Figure 5.8 shows the simulated flow rate from the four exhaust runner boundaries to the collector. It can be observed that the blow-down from each cylinder was separated. Therefore, the exhaust gas flow from each runner can expand to approximately the full area at the inlet planes of the flowsplit element. Thus, the area of the inlet plane was used to calculate the effective expansion diameter. The characteristic length was set to the distance between the inlet plane and the outlet plane, because of the flow behaviour and the geometry.

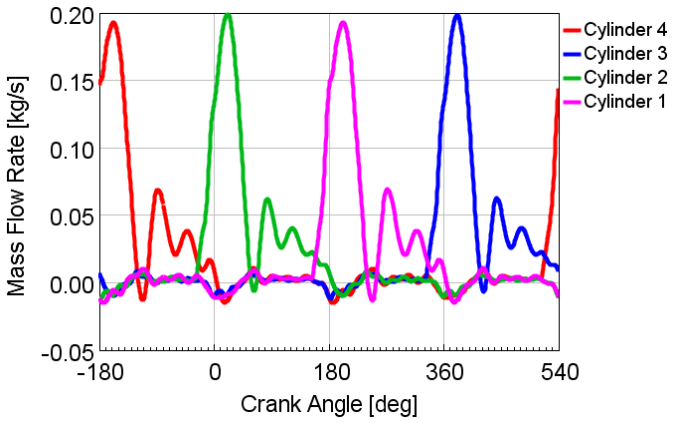

Figure 5.8: Mass flow entering flowsplit element (FGT turbocharger, 2200rpm full load)

5.2.2.4. Model validation

To validate the exhaust manifold model, the engine system was simulated without the turbocharger (Figure 5.9). The calibrated combustion model was used in this simulation. Since the instantaneous pressure was not measured at the inlet of the intake manifold, the measured averaged pressure and temperature downstream of the intercooler were used as boundary conditions in the simulation to avoid spurious pressure fluctuation in the intake manifold. On the exhaust side, the measured instantaneous pressure at turbine inlet was used as a boundary condition. The engine control actuators were set according to the experiments.

A PI controller was used to control the throttle position in order to achieve the target manifold pressure and to create a restriction in the inlet air path. This was because the throttle was not fully opened at 32Nm in the experiments.

The measured and simulated instantaneous pressures at the exhaust port of cylinder 1 are compared in Figures 5. 10 - 5. 12. The overall shape of the port pressures at three operating points was captured. The magnitude of the blow-down pulses and the pressure wave reflections was well predicted. Therefore, the pressure propagation between the port and turbine inlet, and the damping effect at the manifold, were preserved.

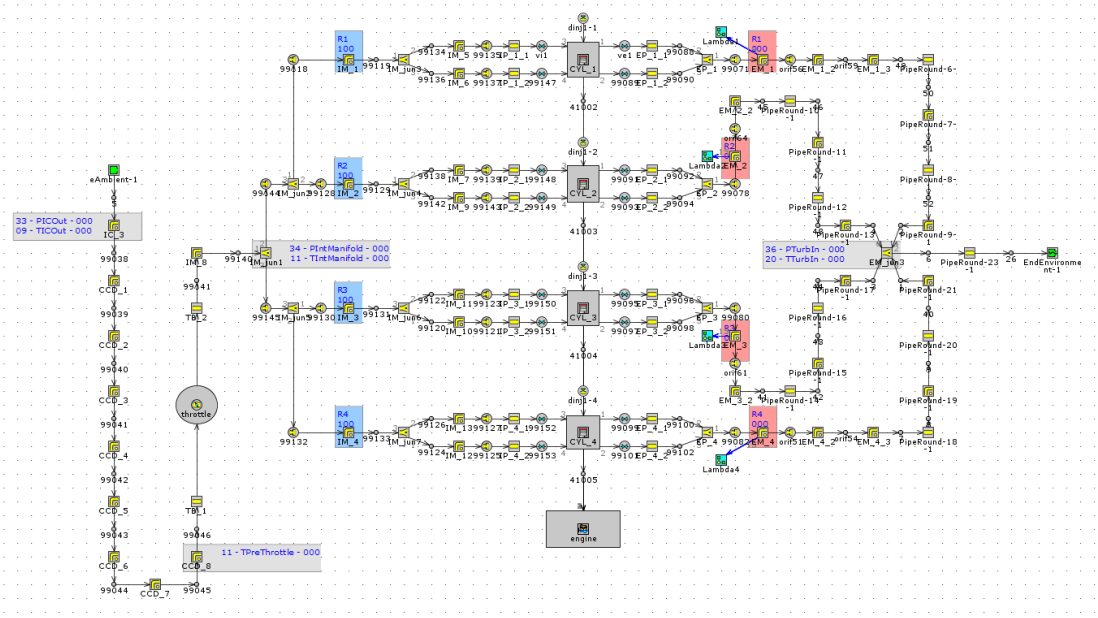

Figure 5.9: Engine model without turbocharger

A shift of approximately 10 degrees crank angle (about 0.001 seconds at 2000rpm) can be observed at all three operating points. This could be caused by several effects: for example, the dynamics of the valve system, turbine volute volume which was not represented in the model, pressure wave propagation in complex volume. However, these were difficult to measure, and they cannot be simulated in a 1-D environment.

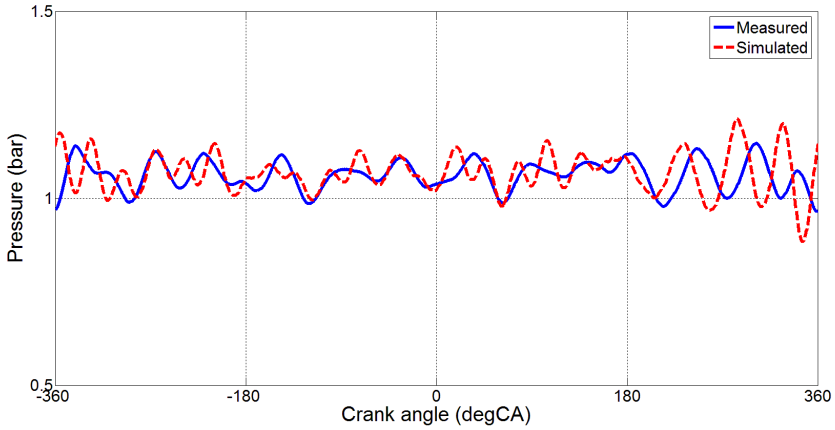

Figure 5.10: Instantaneous pressure at exhaust port of cylinder 1, 2000rpm 32Nm

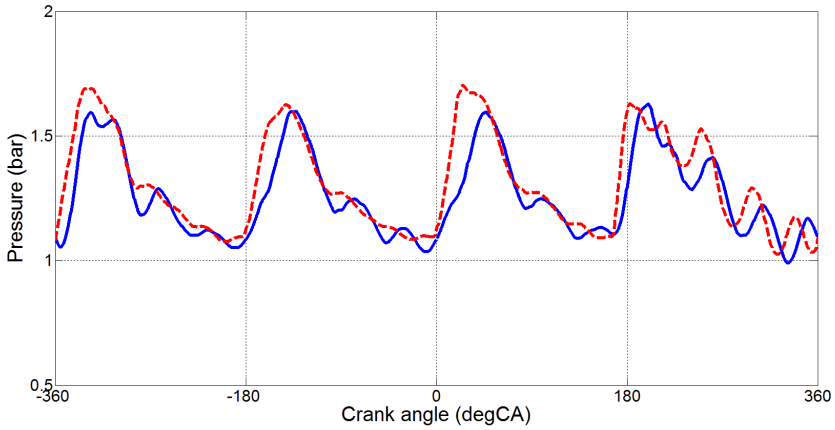

Figure 5.11: Instantaneous pressure at exhaust port of cylinder 1, 2000rpm 229Nm

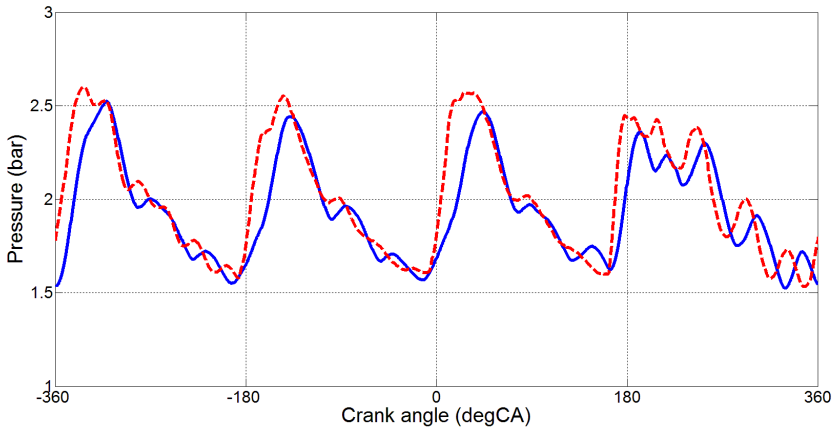

Figure 5.12: Instantaneous pressure at exhaust port of cylinder 1, 2000rpm 319Nm

Table 5.6 lists the comparison between measured data and simulation results of the mass air flow and engine net IMEP. Similar to the combustion model validation results, the discrepancies in the exhaust manifold model validation was due to overestimation of air flow. Nevertheless, the absolute errors in mass flow and net IMEP were small.

In addition to the comparison with experimental data, a sensitivity study of expansion diameter and characteristic length at flowsplit was carried out. A 9-point factorial DOE was conducted with the variation range of ±10mm for both the two parameters. The effect was small (Figure 5.13). The variation of the pulse magnitude was below 0.02 bar. The shape of the pulse and the pressure wave were not affected.

Thus, it was not necessary to further adjust the two parameters. The exhaust manifold model was validated.

Table 5.6: Comparison between measured data and simulated results of the engine model without turbocharging system

	32Nm	229Nm	319Nm
Measured mass air flow (kg/hr)	34.9500	170.3663	258.6886
Simulated mass air flow (kg/hr)	38.2431	175.9130	262.4910
Error in mass air flow prediction (%)	9.42	3.26	1.47
Measured net IMEP (bar)	2.6691	14.4690	20.2350
Simulated net IMEP (bar)	2.6677	15.4029	20.8295
Error in net IMEP prediction (%)	0.05	6.45	2.94

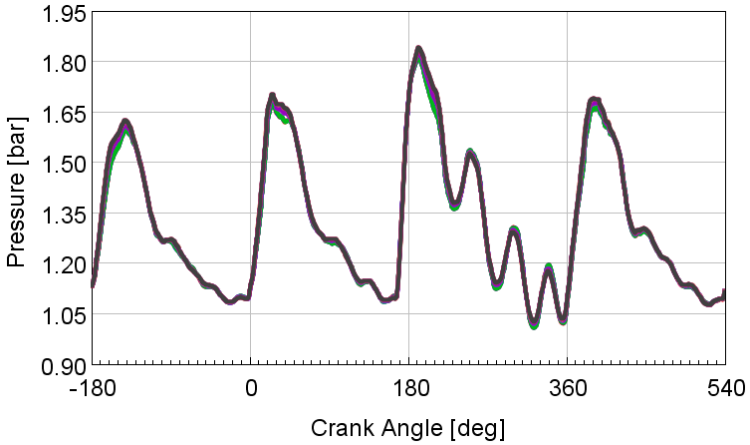

Figure 5.13: Effects of expansion diameter and characteristic length on exhaust port instantaneous pressure

5.2.3. Turbocharger modelling

5.2.3.1. Representation of turbocharger elements

Turbocharger simulations with various complexities are available, including 0-D, 1-D and 3-D. The 0-D mean-value models are based on experimental data collected from gas-stand. This is widely used in 1-D engine simulation because of the

simplicity and the reasonable accuracy in the measured operating range. Extrapolation is needed for turbocharger operation outside the measured range.

In 1-D turbocharger models, the turbomachinery geometry is simplified and modelled using 1-D elements. Therefore, the pressure propagation and dynamics can be captured in 1-D models. However, a large amount of data is required for calibration of 1-D models [94]. In 3-D models, the full geometry information is used to model the performance of the turbocharger. While more details, such as the surge line prediction and air velocity, can be studied in a 3-D environment, the model complexity is significantly larger than for the 0-D and 1-D models.

These three types are used at different stages of engine development. Since the geometry of the turbocharger was not available, 0-D turbocharger models are used in this study. Nevertheless, 1-D turbocharger models should be considered in future work when the necessary data becomes available.

In GT-Power, the compressor and turbine are treated as 0-D elements in which the flow and efficiency are calculated based on the turbocharger speed and gas properties upstream and downstream of the element. The moment of inertia of the turbocharger was represented at the turbocharger shaft element. The power balance across the shaft is calculated instantaneously for the simulation of power imbalance at the turbocharger shaft, hence the speed variations during the simulation. The reduced speed, reduced mass flow, pressure ratio and efficiency measured on gas-stand are stored in turbocharger maps. These dimensionless reduced parameters are used to avoid the effects of the variations in the measurement conditions and applications.

$$\widetilde{N} = \frac{N}{\sqrt{T_{o,in}}} \tag{5.7}$$

where $\widetilde{N}$ is the reduced turbocharger speed of compressor or turbine

N is the physical turbocharger speed

$T_{o,in}$ is the absolute total temperature at inlet of compressor or turbine

$$\widetilde{m} = \frac{\dot{m} * \sqrt{T_{o,in}}}{P_{o,in}}$$

5.8

Where $\widetilde{m}$ is the non-dimensional mass flow of compressor or turbine

m is the physical mass flow of compressor or turbine

$P_{o,in}$ is the total pressure at inlet of compressor or turbine

Besides temperature and pressure corrections, the reduced speed and reduced mass flow also need to be corrected based on gas constant and specific heat ratio. This is based on the following two multipliers:

$$M_s = \sqrt{\frac{\gamma_R R_R}{\gamma_a R_a}}$$

5.9

$$M_m = \sqrt{\frac{\gamma_a R_R}{\gamma_R R_a}}$$

5.10

where M_s and M_m are multipliers for reduced speed and reduced flow respectively

γ_R and γ_a are reference specific heat ratio and actual specific heat ratio respectively

R_R and R_a are reference gas constant and actual gas constant respectively

The pressure ratio and efficiency of the compressor are usually total-to-total values which are directly linked to compressor power, while total-to-static values are typical for turbines, due to the wasted exhaust gas kinetic energy at the turbine outlet. Nevertheless, standards vary among the turbocharger manufacturers. Care must be taken when comparing and using the turbocharger performance maps, since the flow characteristics and efficiency might be changed when different methods are used. In this study, total-to-total values are used for compressors (equation 5.11) and total-to-static values are used for turbines (equation 5.12).

$$\eta_{comp} = \frac{T_{o,comp\ in} * (PR_c^{\left(\frac{\gamma-1}{\gamma}\right)} - 1)}{T_{o,comp\ out} - T_{o,comp\ in}}$$

5.11

where η_{comp} is the compressor efficiency

PR_c is compressor total-to-total pressure ratio

γ is the ratio of specific heat

$$\eta_{turb,comp\ power} = \frac{C_{p,air} \times m_{comp} \times (T_{o,comp\ out} - T_{o,comp\ in})}{C_{p,turb} \times m_{turb} \times (T_{o,turb\ in} \times \left(1 - \left(\frac{1}{ER_t}\right)^{\left(\frac{\gamma-1}{\gamma}\right)}\right))}$$

5.12

where $\eta_{turb,comp\ power}$ is the turbine efficiency calculated using compressor power

C_p is the specific heat

m_{comp} is the compressor mass flow

m_{turb} is the turbine mass flow

ER_t is turbine total-to-static expansion ratio

The calculation of turbine efficiency is based on the assumption of turbocharger power balance, because the temperature measurement downstream of the turbine is subject to the heat transfer effects at the turbine. Therefore, the calculated enthalpy drop across the turbine is not representative of the aerodynamic work. Most turbocharger manufacturers use the compressor as load when a turbine is mapped on a conventional gas-stand. Therefore, the turbocharger bearing mechanical losses are included in the turbine efficiency. It is worth noting that some turbocharger manufacturers map turbines on electrical dynamometers. As a result, the mechanical losses are not included in the turbine efficiency and a mechanical losses model is required.

5.2.3.2. Compressor model in GT-Power

To cover the entire operating range in engine simulations, turbocharger maps need to be extrapolated.

The compressor performance data is used to interpolate the flow characteristics and efficiency at each tested speed line. Linear interpolation is employed on speed lines within the region where experimental data is given. In GT-Power, extrapolation of speed line to the low speed region is achieved by interpolating between the lowest tested speed line and an artificial speed line at 0rpm at pressure ratio 1 and mass flow 0kg/s. The efficiency at the added line is set to a minimum efficiency of 20% by default. The mass flow rate is interpolated proportional to speed, and the pressure ratio is interpolated proportional to the square of speed. Therefore, the surge line is also extended to the low speed region. In addition, the efficiency in the low speed region is interpolated linearly between the added speed line and the lowest speed line from the provided data.

In GT-Power, the flow characteristic of each speed line in the surge region is linearly extrapolated from the data point at lowest reduced flow to zero flow by assuming a slope slightly below zero. The efficiency in the surge region of each speed line is set to the efficiency at end points by default. Linear or quadratic interpolation between end point efficiency and minimum efficiency can also be selected. This is a simplified model. If the compressor surge is to be investigated and the compressor is meant to operate in the surge region, the reverse flow in the compressor can be modelled in GT-Power. Nevertheless, this is outside the scope of this study. The FGT compressor was matched to the test engine, and surge was not observed in the experiments with production level control strategy.

The two points with highest flow rate on each speed line are used to extrapolate to the choke region. The efficiency at pressure ratio 1 is also set to 20% in the default setting, and the efficiency in the choke region is interpolated.

5.2.3.3. Turbine model in GT-Power

The turbine model in GT-Power interpolates and extrapolates the turbine reduced mass flow and efficiency, based on blade speed ratio at each constant expansion ratio line. The flow and efficiency are normalised to the values at the point where the peak

efficiency at each expansion ratio line is found. Then the normalised mass flow and normalised efficiency are fitted, using the following equations:

$$\dot{m}_{norm} = cm + BSR_{norm}^{m} * (1 - cm)$$

5.13

where $\dot{m}_{norm}$ is the normalised mass flow

BSR_{norm} is the normalised blade speed ratio

cm is fitting exponent

m is fitting coefficient

$$\eta_{norm} = 1 - (1 - BSR_{norm})^{b} \qquad BSR_{norm} \leq 1$$

5.14

where η_{norm} is the normalised efficiency

b is fitting shape factor

$$\eta_{norm} = 1 - c * (BSR_{norm} - 1)^{2} \qquad BSR_{norm} > 1$$

5.15

where c is fitting coefficient

VGT turbochargers are represented by a group of turbine maps at different VGT positions. Thus, the turbine characteristics at any VGT opening can be interpolated within the tested range of vane positions.

5.2.3.4. Scaling of turbocharger performance map

The scaling of compressor and turbine performance data is based on non-dimensional representation of compressor and turbine characteristics. The non-dimensional groups are represented as [38]:

For mass flow: $\dfrac{m\sqrt{RT_{o,in}}}{P_{o,in}D^{2}}$

5.16

For rotational speed: $\frac{ND}{\sqrt{RT_{o,in}}}$

5.17

Therefore, the non-dimensional groups become a function of the wheel diameter, provided that the other parameters are unchanged. The reduced mass flow and reduced rotational speed can be scaled using the following equations:

$$(\frac{m\sqrt{T_{o,in}}}{P_{o,in}})_{scaled} = (\frac{m\sqrt{T_{o,in}}}{P_{o,in}})_{ref}(\frac{D_{scaled}}{D_{ref}})^2$$

5.18

$$(\frac{N}{\sqrt{T_{o,in}}})_{scaled} = (\frac{N}{\sqrt{T_{o,in}}})_{ref}\frac{D_{ref}}{D_{scaled}}$$

5.19

As a result, the pressure ratio in the map data is not affected. If the wheel diameter is enlarged, the mass flow at the same pressure ratio will be increased and the speed required to achieve the same pressure ratio is reduced.

In addition to the map data, the mass, and hence the moment of inertia of the compressor and turbine, are also affected by the size. Therefore, the moment of inertia is also scaled, based on the mass and the diameter of the wheel.

$$m_{scaled} = m_{ref}(\frac{D_{scaled}}{D_{ref}})^3$$

5.20

The moment of inertia can be calculated using:

$$I = mr^2$$

5.21

where I is the moment of inertia

r is the effective radius of a ring of mass to represent the wheel

Assuming the effective radius is proportional to the outside diameter of the wheel, then:

$$I_{scaled} = I_{ref}(\frac{D_{scaled}}{D_{ref}})^5$$

5.22

As a result, the reduced flow, reduced speed and moment of inertia of the compressor and turbine can be scaled in the simulation for investigation of the matching of the turbocharger and the effect of the size of the turbocharger on engine performance.

Although this is a simplified approach for turbocharge map scaling which cannot capture all the variations in reality, such as the losses at the tip gap, this is reliable to investigate the trade-offs in engine development [123]. Nonetheless, CFD study can be performed to predict turbocharger performance if the compressor geometry data is available.

5.2.3.5. Turbocharger model validation

The compressor and turbine maps that were obtained using the test facility described in the previous chapter were used in the engine model to carry out full engine simulation.

Turbine maps were collected at four different vane positions. Due to the non-linear characteristics of the VGT turbocharger, the VGT position in steady state simulations was set in closed-loop control for comparison between measured data and simulated results. Measured turbocharger speed was used as the target for the controller.

Table 5.7 shows the comparison between the measured data and the simulated results at 2000rpm 229Nm. The prediction of the compressor pressure ratio was accurate. The discrepancies in the mass air flow and the IMEP were within 3%. Therefore, the compressor model, scavenging model and combustion model were accurate. The

VGT position in simulation was 48.9% closed, compared with 57% closed in the experiments. This may be due to the nonlinearity in the effects of the vane position on turbine characteristics and accumulative errors in the entire engine system.

Table 5.7: Comparison between measured data and simulated results of full engine model with turbocharging system at 2000rpm 229 Nm

	Experimental data	Simulation with turbocharger	
		Results	Error (%)
Compressor pressure ratio	1.322	1.323	0.07%
Inlet manifold pressure (bar)	1.291	1.289	0.15%
Total mass air flow (kg/h)	170.4	174.5	2.4%
Gross IMEP (bar)	14.84	15.27	2.9%

Figure 5.14 shows the measured and simulated turbine expansion ratio. The prediction of maximum and minimum expansion ratio was accurate. The overall shape of the pulses was captured. However, discrepancies can be found at around 65 to 85 degrees crank angle in the blow-down process of each cylinder. This may be a result of the 3-D effects in the exhaust system. Nonetheless, the accuracy of the overall steady state simulation is satisfactory. Errors in the simulation of engine air flow and IMEP were within 5%.

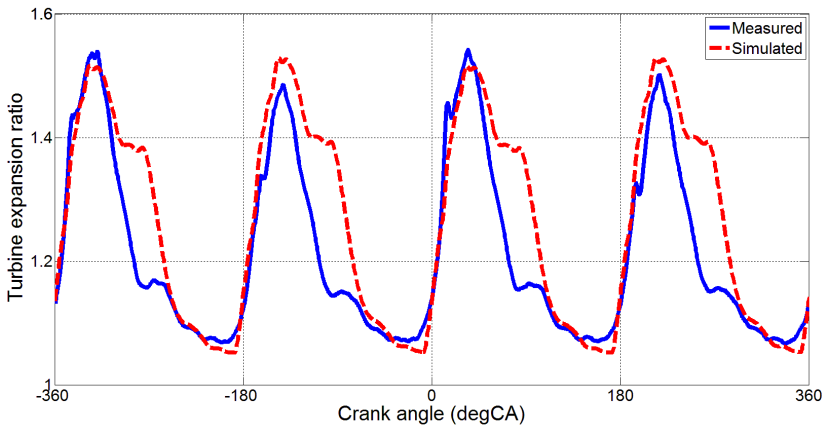

Figure 5.14: Measured and simulated turbine expansion ratio

5.2.3.6. Critique of turbocharger simulation

Conventional compressor and turbine 0-D model maps cannot fully represent the complex flow and thermal dynamic behaviours within a turbocharger. The maps were obtained under non-adiabatic conditions, since the heat transfer between the gas and turbocharger housings was included when the enthalpy changes across the compressor or turbine were calculated using experimental data. Nevertheless, in this study, the turbine was mapped on the engine under low inlet temperature conditions (below 100ºC) without firing. Therefore, the heat transfer between turbine housing and compressor housing was minimised. In order to capture the thermal responses of the turbocharger in the future, the heat transfer model for the turbocharger with measured or estimated heat transfer coefficients is required.

The bearing mechanical losses were included when the compressor power was used to calculate the turbine efficiency. Thus, the calculated turbine efficiency might differ from the actual isentropic efficiency. This may be improved if the bearing friction is modelled and added to the turbine power. Accurate prediction of friction losses may require further instrumentations, for example, oil temperature at the bearing housing.

It is worth noting that no volume is represented in the 0-D turbocharger model, whereas lag can be found between the pressure waves measured at turbine inlet and outlet (Figure 5.15). A phase lag of approximately 15 degrees crank angle can be found between the two pressure traces measured at 2200rpm. Several studies have shown that the gas dynamics can be captured using 1-D turbocharger models to represent the flow behaviours inside turbine housing [124, 125]. This should be considered in the improvement of the engine model in the future.

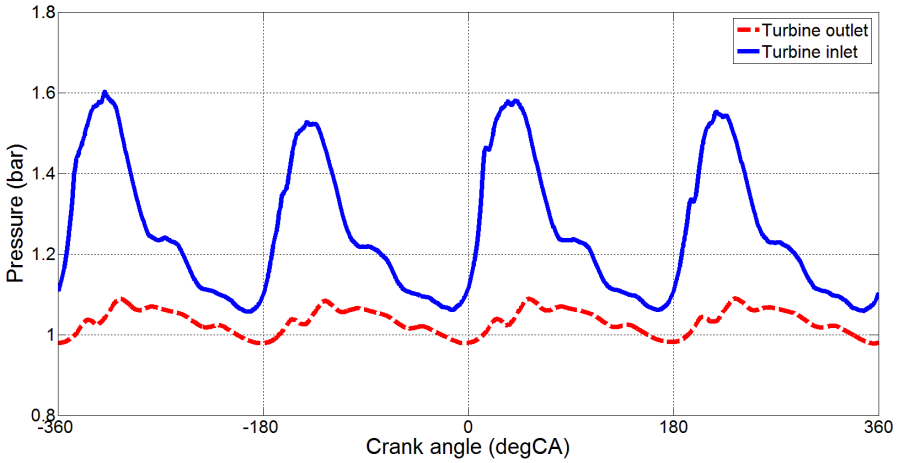

Figure 5.15: Instantaneous pressure at turbine inlet and outlet measured at 2200rpm

5.3. Validation of transient simulation

5.3.1. Overall performance

After the engine model had been validated for steady state simulation, it was also validated against experimental data collected from transient tests performed with the VGT turbocharger. To avoid accumulative errors and interactions between combustion system and turbocharging system, the validation simulations were first run with imposed turbocharger speed measured from transient experiments. The experimental valve timing settings were used in this simulation. The combustion model that was calibrated under steady state operation was employed. The throttle controller was in closed-loop control mode targeting 2 bar BMEP before tip-in, and it was switched to fully open after tip-in.

Three VGT settings were simulated. The VGT was fully closed (90% closed) before tip-in, and it was set to 60% closed, 75% closed and 90% closed after tip-in. The turbine maps at these three openings were collected from the on-engine mapping facility, therefore, no interpolation was required in this simulation. Since the moment of inertia of the test VGT turbocharger was unknown, it was estimated using the scaling factor and data of a turbocharger of similar size.

Figure 5.16 shows the comparison between measured and simulated mass air flow. The flow characteristics of the entire system were captured. In the simulation with VGT 60% closed after tip-in, the flow was underestimated by up to approximately 10% in the first 1.2 seconds. Further, it was overestimated by approximately 5% between 3 and 5 seconds after tip-in in the simulation with 90% closed VGT position.

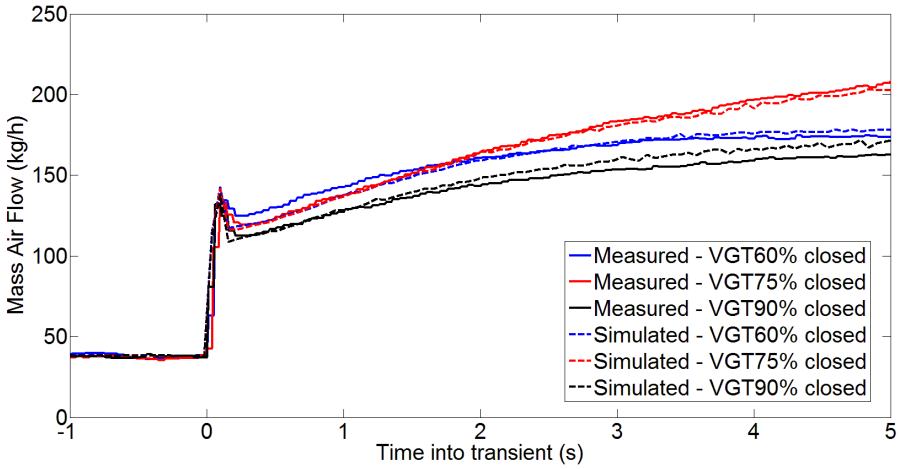

Figure 5.16: Comparison between measurements and simulation results of transient performance with imposed turbocharger rotational speed

This might be the result of the scavenging model in 1-D engine simulation. Figure 5.17 shows the predicted residual gas fraction. Since the residual gas fraction is difficult to measure, no experimental data were available for comparison. However, significant variation in the residual gas fraction is shown. In 1-D simulation, air flow into a cylinder is assumed to be homogeneously mixed immediately after it enters the cylinder volume. Therefore, the composition of any flow out of the cylinder is the same as the averaged composition in the cylinder.

However, this may not be true, especially during transient, since the air motion at the ports and in the cylinders is complex. The valve timings were set to achieve maximum overlap in this test. In addition, the engine back pressure might be higher than intake pressure, due to the response of turbocharger acceleration. In these tests the minimum back pressure during tip-in occurred at the start of the tip-in with 60% closed VGT, and the maximum back pressure occurred at the end of the tip-in with 90% closed VGT. This was one of the most difficult operating conditions to simulate

in a 1-D environment. As a result, uncertainties could exist in these cases. Nevertheless, the maximum discrepancy was within 10% and it was in a short period of time. This is satisfactory for transient simulation.

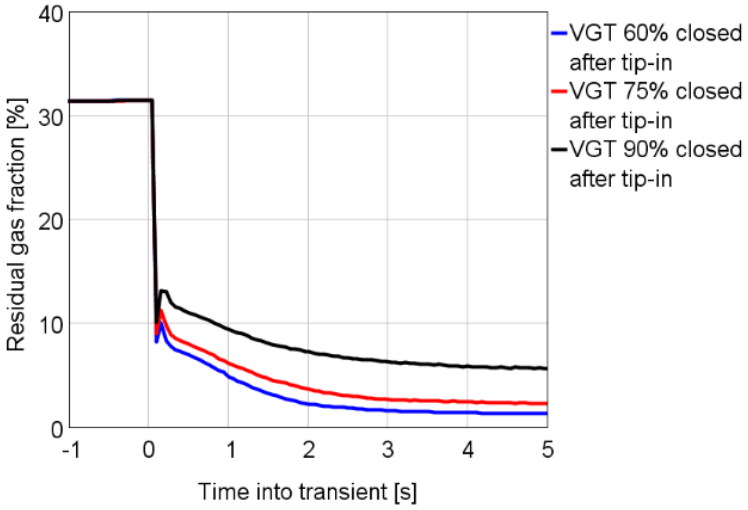

Figure 5.17: Predictions of residual gas fraction during transient

To improve the scavenging model, information predicted from multi-dimensional tools may be provided for the 1-D environment in either separated simulation or co-simulation.

5.3.2. Combustion system

In Figures 5. 18 – 5. 20, the simulated and measured combustion behaviours are compared. The measured data was processed so that each of the steps represents an engine cycle. At 2 bar BMEP before tip-in, a good match can be found, since the combustion model was calibrated using the experimental data collected at 2 bar BMEP. After tip-in, the estimated 10-90% combustion apparent burn duration was shorter than the measured data. This was because the boundary conditions varied from steady state operating conditions, where the combustion model was calibrated, to transient operating conditions. The variations in the intake and exhaust pressure, residual gas fraction, air motion in cylinder and engine thermal conditions might have affected the heat release process. Nonetheless, the estimated peak cylinder pressure and net IMEP are satisfactory for transient simulation. The trends in the IMEP were captured.

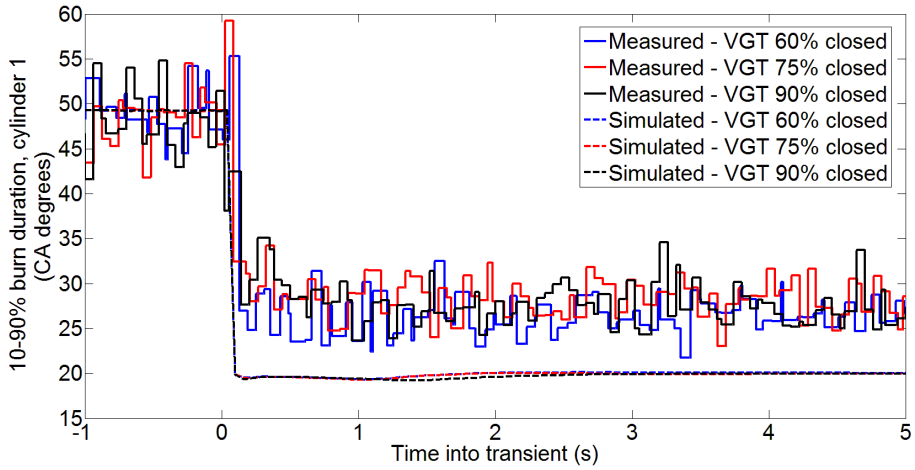

Figure 5.18: Measured and simulated 10-90% burn duration during transient

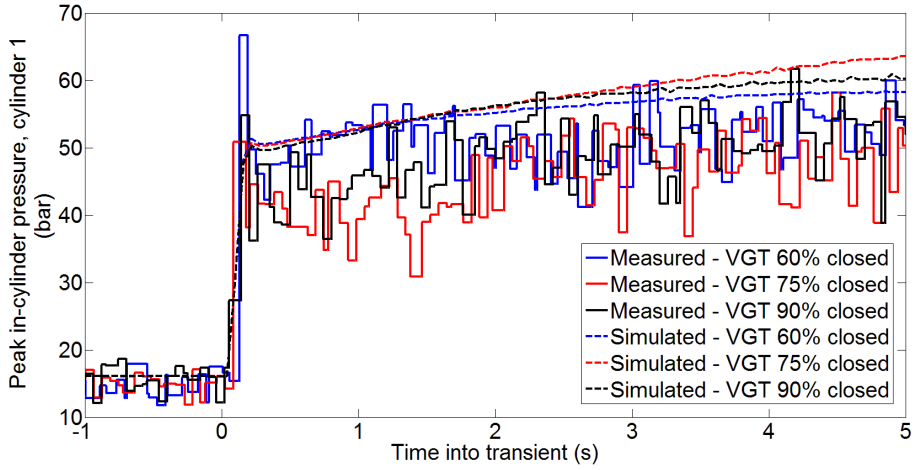

Figure 5.19: Measured and simulated peak pressure in cylinder 1 during transient

It is worth noting that the engine IMEP dropped in the first cycle after tip-in in the experiments. Similarly, the peak cylinder pressures in the first cycle after tip-in were also lower than the following cycles. This was a result of the manual control of the target Lambda in the fuelling system in the experiments. The target Lambda was set to 1, and therefore the transient fuelling compensation was disabled, resulting in the mixture being too lean to be ignitable.

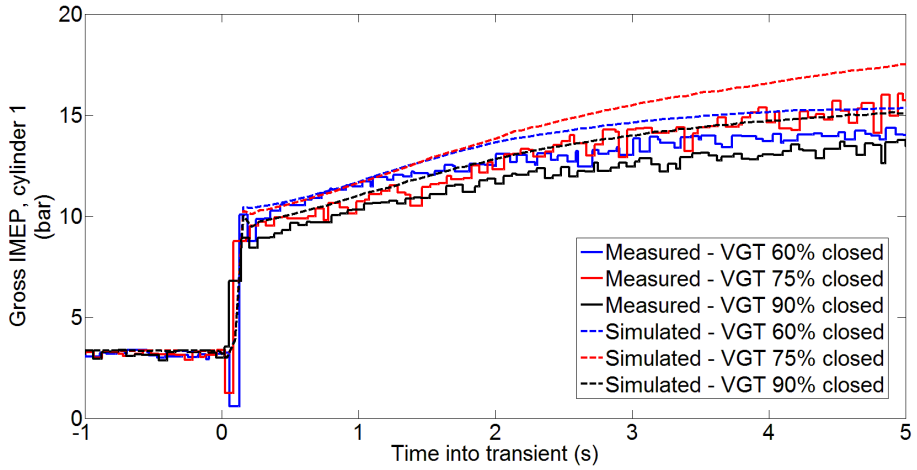

Figure 5.20: Measured and simulated gross IMEP at cylinder 1 during transient

5.3.3. Turbocharging system

Figure 5.21 shows the instantaneous turbine expansion ratio at 0.1, 1, 2.5 and 5 seconds after tip-in with VGT 60% closed. The maximum and minimum expansion ratios were captured in the whole transient simulation. Similar to the results at steady state, discrepancies in the pressure waves can be found.

So far, the estimations of the mass air flow and turbine expansion ratio have been validated against measured results. Since the measured turbocharger speed was used as input data in this simulation, the only parameter left for the validation of turbine power was the turbine efficiency. During transient, the acceleration of the turbocharger requires higher power output of the turbine than the compressor power. The engine back pressure is likely to be higher than the intake pressure to drive the turbine. Therefore, the turbine may operate with high expansion ratio and low corrected speed conditions, resulting in a low blade speed ratio that is usually outside the mapped region.

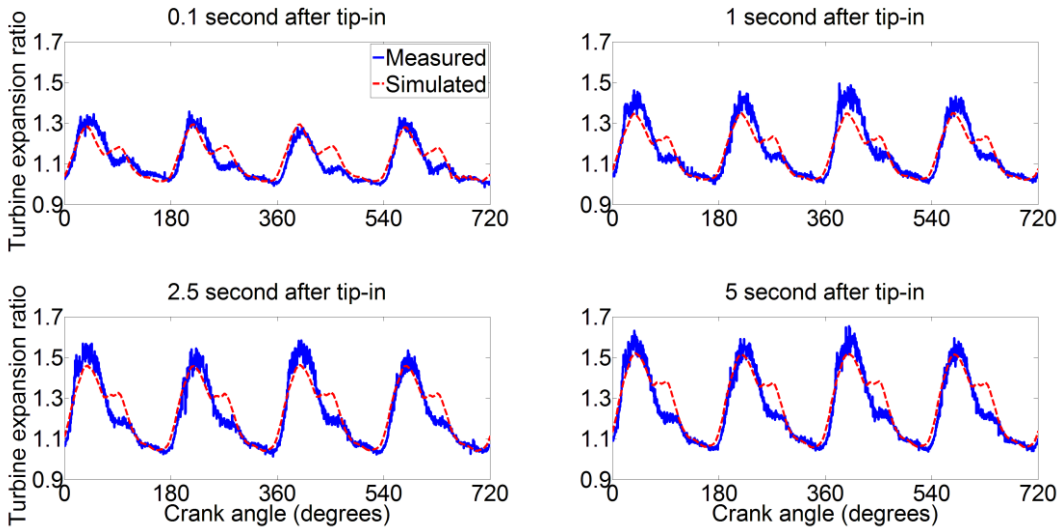

Figure 5.21: Instantaneous turbine expansion ratio during transient, VGT 60% closed

As described in the turbine modelling section in this chapter, the turbine efficiency was extrapolated from the optimum blade speed ratio, where the peak efficiency of each expansion ratio was reached, to higher and lower blade speed ratio. The major difficulty in extrapolating the turbine map using the experimental data collected in this project was that the maximum measured turbine efficiency was always at the maximum expansion ratio achieved at each speed line. Therefore, it was not clear whether the actual maximum efficiency at each speed line had been reached. This could be due to the limitations on the compressor loading. The air cooler and the pipes downstream of the compressor might have caused excessive pressure drop, which restricted the compressor flow. In addition, no data were available for fitting the normalised efficiency curve in the low blade speed ratio region.

To overcome these difficulties, the turbine efficiency low blade speed ratio fitting shape factor was selected initially. This initial selection was based on estimation of optimum blade speed ratio and optimum efficiency. These estimations were only used for initial selection. Calibration of this factor might still be required.

Calculated from the measured data and the turbine diameter, the blade speed ratio at the peak efficiency achieved in the mapping test was between approximately 0.62 and 0.75 for the four VGT positions mapped. Unlike the case for a nozzle-less

turbine, the optimum blade speed ratio may be affected by the vane position on the VGT turbocharger. Reyes-Belmonte [94] showed that the optimum blade speed ratio was between approximately 0.6 and 0.85 for different vane positions on a VGT turbocharger. Therefore, despite the lack of data for the low blade speed ratio, the actual peak efficiency points may be close to the points achieved in the experiments, even if the actual peak efficiency was not achieved.

As a result, two possible conditions were compared: 1. the achieved peak efficiency points were the actual optimum efficiency points. 2. The actual optimum efficiency point was at a blade speed ratio 5% lower than the measured data, and the actual peak efficiency was 5% higher than the measured peak efficiency.

In GT-Power, the recommended typical range for the shape factor was between 1.4 and 2.2. Therefore, fitted curves with a shape factor of 1.6 and 2.0 were compared (Figure 5.22). They were considered to represent the range of possible fittings for an actual efficiency curve if measured data points in this region could be reached. It is shown that the fitted curve extrapolated from the original peak efficiency point with shape factor 2.0 was within the possible efficiency range. Therefore, with the available data, the initial shape factor for calibration was chosen as 2.0.

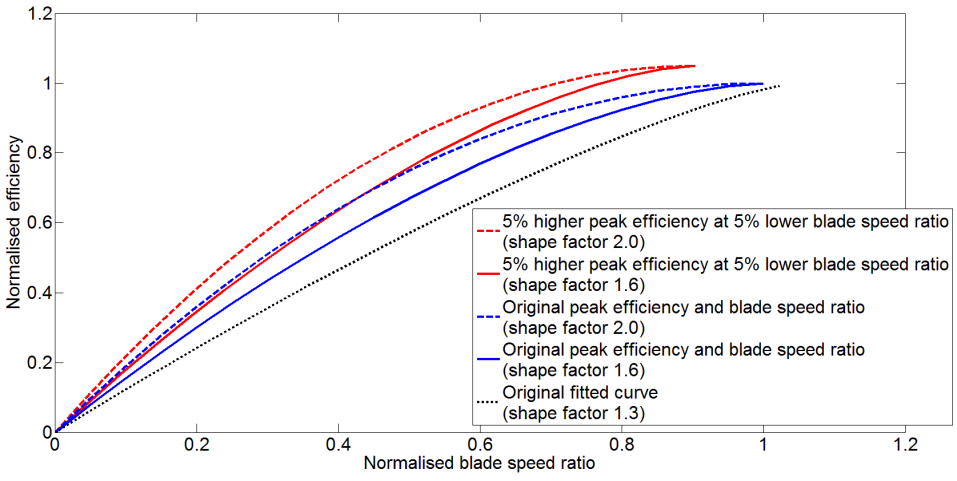

Figure 5.22: Fitted curves of normalised turbine efficiency against normalised blade speed ratio

In Figure 5.22, the original fitted efficiency curve for VGT 90% closed (shape factor 1.3) is also plotted. This was fitted using the raw data and the default settings in GT-Power. For comparison, the blade speed ratios for all the curves were normalised to the operating point where the measured peak efficiency occurred. It is shown that, using the raw data and default settings, the estimated optimum blade speed ratio was larger than the measured data. This was because the default setting in GT-Power was to fit a curve of optimum expansion ratio against reduced speed for all speed lines measured. This resulted in errors in the fitted optimum blade speed ratio. Because of the shift in the optimum blade speed ratio, some of the data points on the high blade speed ratio side were shifted and used in the fitting for the low blade speed ratio region. As a result, the shape factor (and hence the turbine efficiency) were likely to be underestimated. Therefore, it was decided to use the raw data at measured maximum efficiency points to avoid the shift in optimum blade speed ratio.

To summarise, two settings in the turbine map extrapolation were adjusted. The measured maximum efficiency points were imposed to be the actual optimum efficiency points to disable the default fitting, which shifted the optimum blade speed ratio in an unrealistic direction, due to the small number of data points available for fitting. In addition, the shape factor for efficiency fitting in the low blade speed ratio region was set to 2 as an initial value for calibration.

With shape factor 2, the turbocharger shaft rotational acceleration was calculated using the simulated turbine and compressor power (Figure 5.23). The experimental data are also plotted for comparison. In general, good correlation can be found between measurements and simulated results after 2 seconds into transient. The rotational acceleration was overestimated before around 0.5 seconds, and it was underestimated between 0.5 and 1.5 seconds.

The turbocharger rotational acceleration is proportional to the power imbalance on the turbocharger shaft. Hence, the accuracy of the predictions of compressor power and turbine power are crucial to the estimation of turbocharger acceleration. In the first approximately 0.8 seconds into the tip-in, the compressor operating points were outside the region where measured data were available.

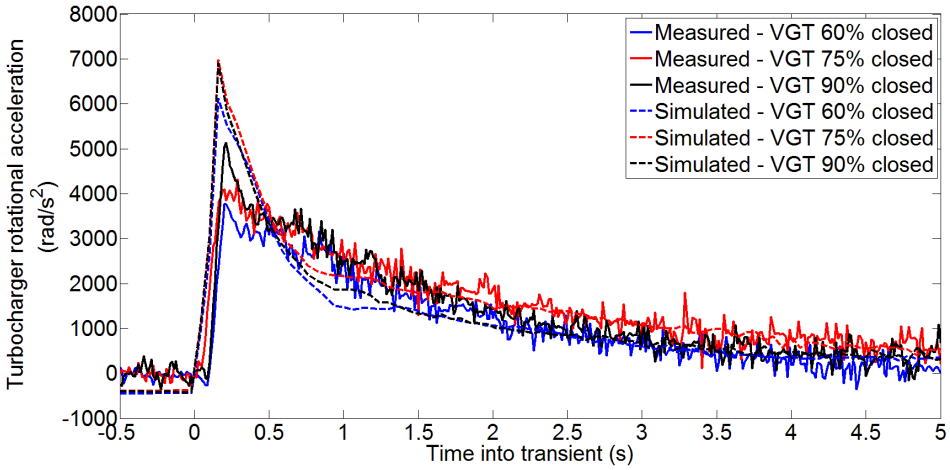

Figure 5.23: Comparison between measured and simulated turbocharger rotational acceleration

Figure 5.24 shows the fast measurement data and predicted compressor pressure ratio during the transient. Good correlation can be found in the region where map data were available. This confirmed the compressor map collected from the on-engine mapping facility used in this project.

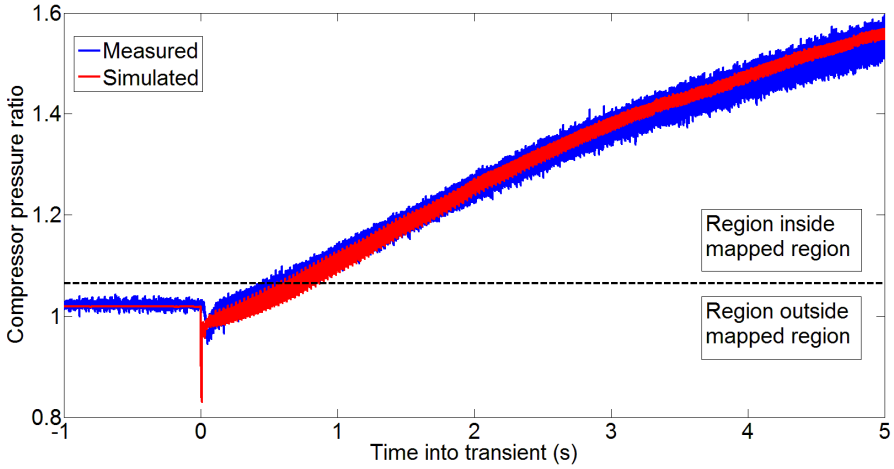

Figure 5.24: Compressor pressure ratio during transient (VGT 75% closed after tip-in)

However, discrepancies were found in the region where no measurement data were available. The differences in the initial drop in pressure ratio may be relevant to the actuator response time. In the experiments, the time lag between the VGT actuator response and the pedal position signal response was up to approximately 0.05 seconds. In addition, the response time for the output voltage of the test cell control

system to increase from minimum to maximum voltage was approximately 0.05 to 0.1 seconds. This was inevitable for experimental facilities.

The discrepancy was also relevant to the prediction of compressor performance at an extremely low pressure ratio – below 1, outside the data window. Compressor map extrapolation was employed in simulations for the estimations of compressor performance in the low speed and low pressure ratio region. This resulted in uncertainties in this region. Nevertheless, both the measured data and the simulated data in Figure 5.24 show that the compressor pressure ratio recovered to approximately 0.95 bar after the initial drop. The errors diminished after the compressor operating point entered the measured map data region.

As a result of the uncertainties in the compressor performance at low pressure ratios, the errors in the averaged compressor pressure ratio were up to 5% in the first 0.5 seconds. As shown in Figure 5.25, the predicted compressor power was below 0.1 kW in the first 0.4 seconds. Since the absolute value of the compressor power was small, relatively large errors in the turbocharger acceleration might have been introduced.

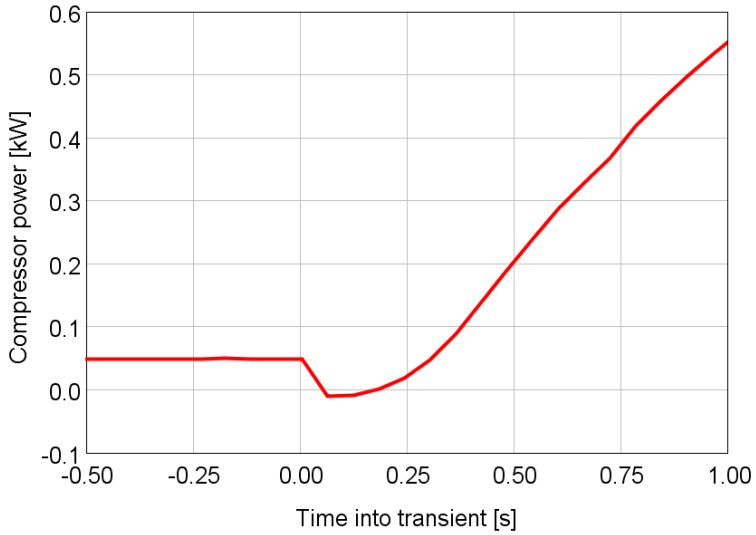

Figure 5.25: Predicted compressor power during transient (VGT 75% closed after tip-in)

To investigate the compressor behaviours at low pressure ratio and speed, compressor performance data in this region needs to be measured and modelled. This is more important for transient simulation, since the opening of the throttle requires a large amount of air to be drawn into the manifold volume. This results in an extremely low pressure ratio at compressor, where the compressor may operate as an expander transiently. Nevertheless, due to the availability of the data, the results shown in Figure 5.24 and Figure 5.25 are satisfactory.

Besides the challenges in simulating compressor power in the low pressure ratio region, the turbocharger shaft friction was also difficult to estimate. The bearing friction is normally integrated into the turbine efficiency, since the compressor power is used to calculate turbine efficiency when generating the turbine performance map. However, the operating speed during transient might have been different from the speed points where map data were collected. The oil temperature at the turbocharger bearing housing, which also affected the shaft friction, was difficult to measure and estimate during transient. As a result, this is ignored in this study. It has been planned to control and measure the oil temperature in future tests.

Figure 5.26 shows the maximum and minimum values of predicted instantaneous normalised blade speed ratio during the transient. The normalised blade speed ratio before tip-in was high because the turbine expansion ratio instantaneously dropped below 1 at low engine load. After tip-in, the normalised blade speed ratio dropped to below 1, and gradually increased and stabilised after approximately 1 to 1.5 seconds into the transient as the turbocharger acceleration reduced. Since low blade speed ratio represented high available energy to the turbine, the turbine efficiency at low blade speed ratios was more important to the turbine power calculation. However, the minimum normalised blade speed ratio during the transient, especially in the first 1.5 seconds, was below approximately 0.5: this was in the region where no data were available and the uncertainties were relatively large.

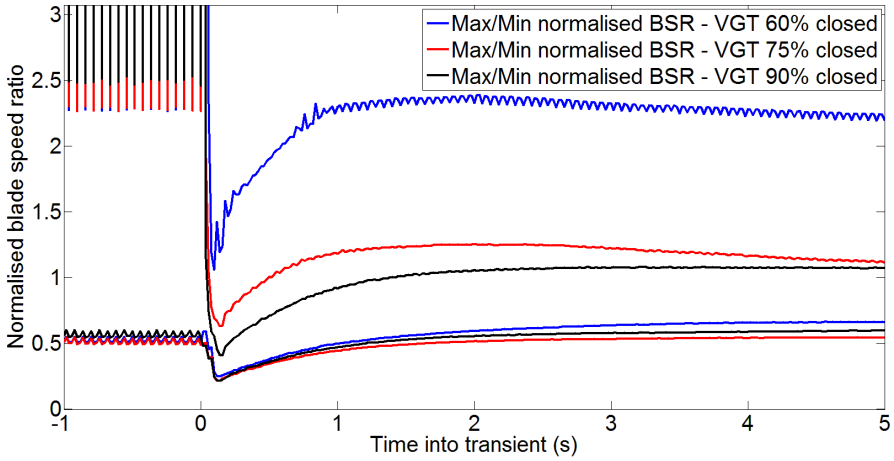

Figure 5.26: Predicted normalised blade speed ratio

Figure 5.27 shows the cycle-averaged turbine operating points on the turbine map in the transient simulation with 60% closed VGT after tip-in. It was found that the turbine operating points moved into a low efficiency region immediately after tip-in. This was a result of the low blade speed ratio shown in Figure 5.26.

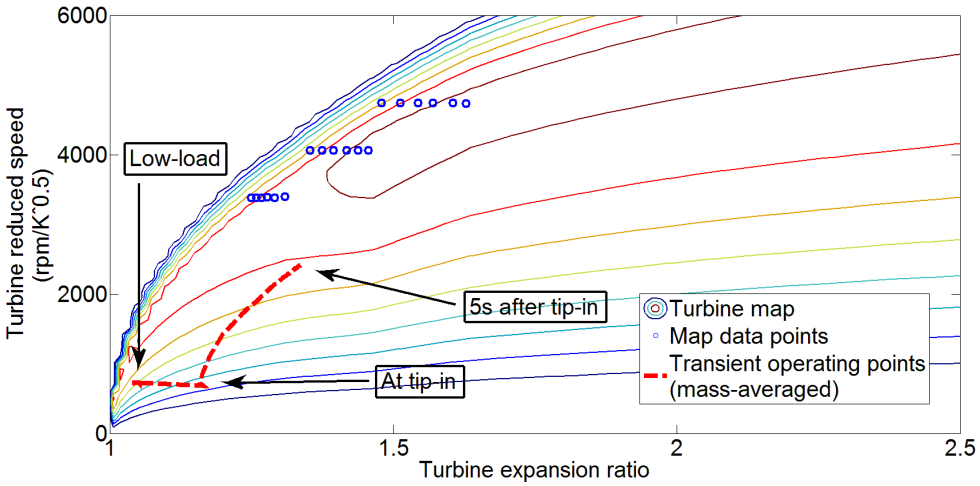

Figure 5.27: Turbine operating points during transient, VGT 60% closed after tip-in

In addition to the variations in the blade speed ratio during the transient, the uncertainty in the low turbine expansion ratio region where no turbine map data were available, also affected the accuracy of the transient simulation. The minimum turbine expansion ratio in the available turbine map data shown in Figure 5.27 was approximately 1.25, and the mass-averaged turbine expansion ratio did not enter the

measured expansion ratio region until 1.5 seconds after tip-in. The same trends can be found in simulations with VGT 75% closed and 90% closed after tip-in. The 60% closed VGT was the worst scenario among these three simulations, because the time required to move the turbine operating point into the available expansion ratio region was longer for VGT 60% closed.

Figure 5.28 shows the effects of the efficiency fitting shape factor at low blade speed ratio on the calculated turbocharger rotational acceleration. In general, the shape factor 2.0 provided the best overall fitting. Therefore, this shape factor was used in transient simulations.

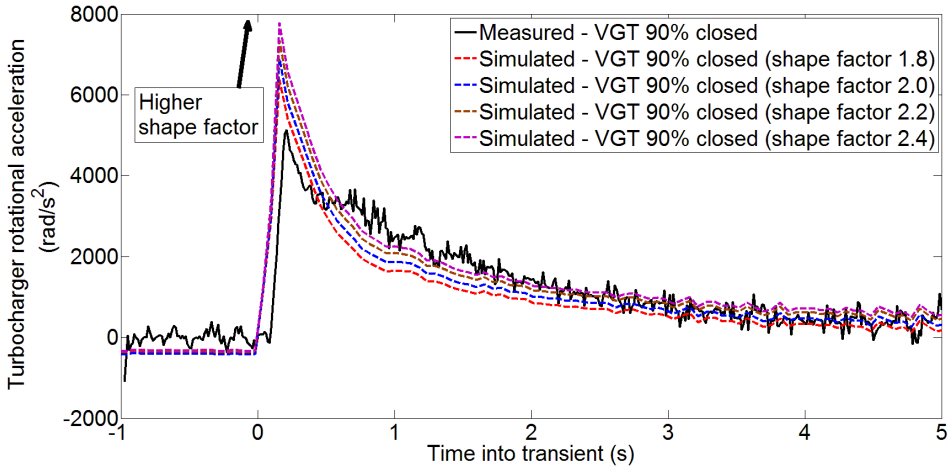

Figure 5.28: Effects of changing turbine efficiency shape factor at low blade speed ratio on the simulated turbocharger rotational acceleration

To overcome the challenges in estimating the compressor and turbine behaviours during transient, accurate measurements in wider operating range and effective modelling will be necessary. This requires better control of boundary conditions and testing procedures, since the accuracy becomes more sensitive to the precision of measurements at low power [126, 127]. The conventional gas stand layout may need modification, such as a compressor recirculation loop for wider turbine operating range. The use of turbocharger 1-D models will also benefit from the accuracy of the extrapolation. The on-engine turbocharger mapping facility presented in Chapter 4 will be a useful platform for the investigation of turbocharger behaviours in more detail.

5.3.4. Final validation

The responses in the combustion system, air path, and air charging system with the imposed turbocharger speed trajectory have been validated. Thus, the final validation was with the turbocharger shaft connected between the compressor and turbine. Figure 5.29 and Figure 5.30 show the simulated mass air flow and turbocharger speed. Despite the errors in the estimated turbocharger rotational acceleration, the error in the turbocharger speed was within 5krpm, 7.5% after tip-in.

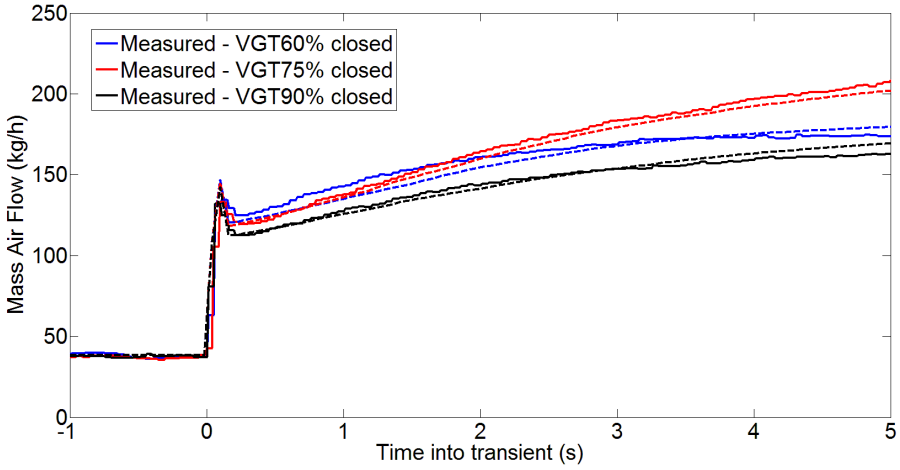

Figure 5.29: Mass air flow during transient (simulations with connected turbocharger shaft)

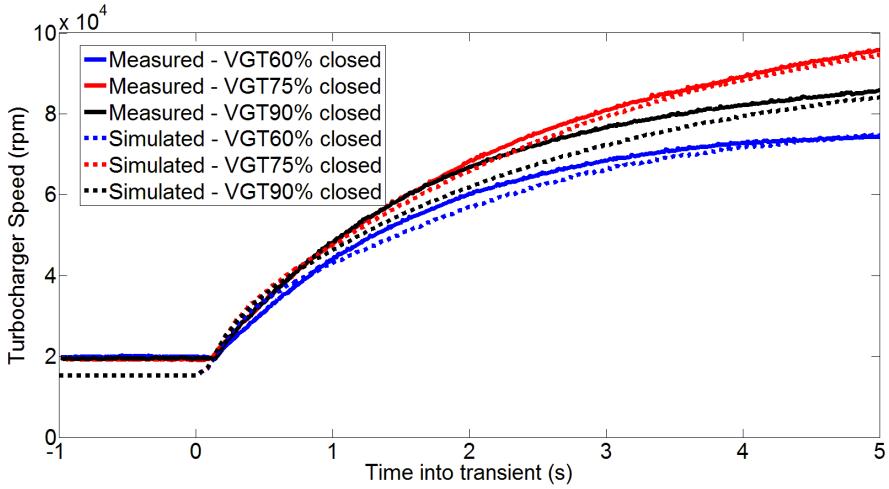

Figure 5.30: Turbocharger speed during transient (simulations with connected turbocharger shaft)

Thanks to the precise modelling of the combustion system and the air path, accurate boundary conditions were provided for the turbocharger model. Thus the cumulative errors in the engine and the turbocharging systems were minimised during transient. The accumulative error was also minimised.

Table 5.8 shows the comparison between the original turbine fitting shape factor and the modified shape factor. The shape factor 2 was used for all four VGT maps. Although this was only an estimated value, unrealistic fittings shown in Figure 5.22 can be avoided. In addition, the comparisons shown in Figure 5.24 were satisfactory.

Since the turbine extrapolation has been modified in the transient calibration process, the modified map needs to be validated at steady state again. As in the previous calibration, a PI controller was used to control the VGT position to achieve the measured turbocharger speed in the simulation at 2000rpm 229Nm. Figure 5.31 shows the comparison of the turbine expansion ratio for the steady state simulations with original map and with modified map. The VGT position was changed from 48.9% closed to 50.3% closed. No significant variation was found. As a result, the full engine model was validated for both steady state and transient simulation.

Table 5.8: Comparison between turbine efficiency fitting factors with default settings and modified settings

	VGT position			
	16% closed	60% closed	75% closed	90% closed
Original efficiency fitting shape factor for low blade speed ratio	1.5	2	1.5	1.3
Modified efficiency fitting shape factor for low blade speed ratio	2			

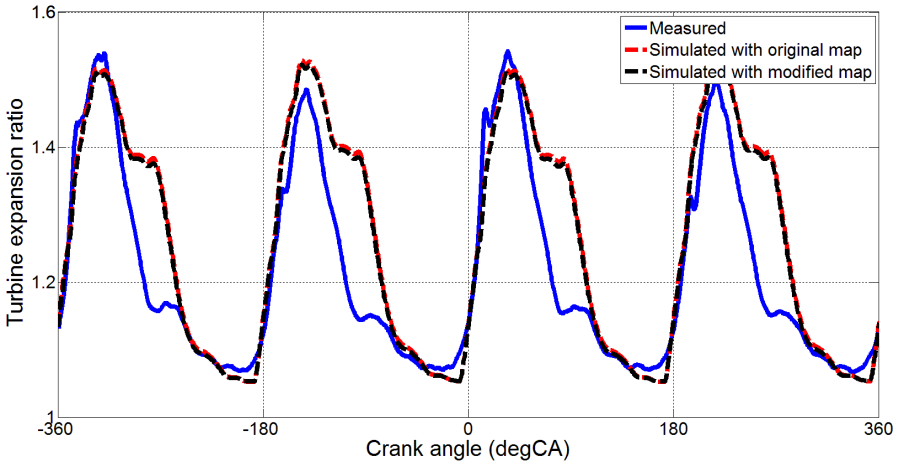

Figure 5.31: Comparison between simulations with original map and modified map

5.4. Conclusions

In this chapter, the engine modelling techniques and the details of the calibration process were presented and discussed. The engine model used in this project was validated at both steady state and transients. The principle points to conclude this chapter are listed below:

1. A procedure was followed to calibrate the combustion model, flow elements and turbocharger model in the engine model in 1-D environment. Experimental data was used to calibrate the engine model in the operating range of 1000rpm-5800rpm, at 10%-100% load.

2. Semi-predictive combustion model was generated using the experimental data to cover the entire engine operating range. The exhaust manifold elements were created using actual exhaust geometry data. The turbine efficiency fitting coefficients were estimated to extrapolate into the low blade speed ratio region.

3. In general, the accuracy of the estimation of mass air flow, net IMEP and turbocharger speed was within 5% at both steady state and transient operation. In addition, the instantaneous pressure in cylinders, intake and exhaust ports, and the inlet/outlet of compressor and turbine were also captured with excellent

accuracy. The predictions of the pressure wave and pulse magnitudes were accurate.

4. In order to further enhance the accuracy and predictability of engine modelling, the following improvements may be carried out in future work:

   a) Combustion model - More experimental data will be required to calibrate an empirical model that covers wider operating range of boundary condition (for example intake and exhaust pressures) or a predictive combustion model.

   b) Turbocharger model – 1-D turbocharger model may be used to capture the effects of heat transfer and gas dynamics. In addition, a wider range of turbocharger operating points need to be covered in the mapping process. Turbocharger mapping facilities such as the one presented in chapter 4 may be useful to improve the understanding and modelling techniques of turbocharging systems.

Chapter 6 - *Steady state behaviour*

In this chapter, a series of scoping investigations of the engine steady state behaviour will be presented. The chapter is split into three sections. In the first section, an experimental investigation of the overall effect of fuel enrichment and the trade-off between engine fuel consumption and turbine inlet temperature limit will be discussed.

In the second section, the experimental results of steady state comparison between FGT and VGT will be shown. This will be followed by a simulation analysis to understand the findings from the experiments.

Finally, the simulation of turbine matching will be presented to demonstrate the full potential of VGT in improving the steady state performance of gasoline engines. In addition, the trade-offs between steady state performances will be investigated.

The work presented in this chapter formed part of the research paper presented at the IAV International Congress on Engine Processes in Berlin, 2013 [128], and was also presented at the conference of The Spark Ignition Engine of the Future in Strasbourg, 2013 [129].

6.1. Trade-off between fuel consumption and turbine inlet temperature

Fuel enrichment is a common measure to reduce exhaust gas temperature on turbocharged gasoline engines. This causes effects on the mixing process, and hence the combustion process. In addition, the evaporation process of the fuel reduces the mixture temperature and exhaust gas temperature. Lambda value is a parameter that indicates the level of fuel enrichment. Lambda above 1 indicates lean mixture, while Lambda below 1 indicates rich mixture.

$$Lambda = \frac{AFR}{AFR_{stoi}}$$

where AFR is air-to-fuel ratio

AFR_{stoi} is stoichiometric air-to-fuel ratio

In order to investigate the overall effects, spark timing and Lambda sweeps were performed in experiments. Two engine operating points were selected: 1600rpm 200Nm and 2800rpm 150Nm. These two operating points were within the stoichiometric operating region. Thus, the Lambda can be varied in a wide window at these operating points. In addition, turbine inlet temperature (TIT) was close to the limits. Thus, these two operating points were models likely to be affected if the TIT was lowered.

The pre-catalyst Lambda target varied between 1.08 and 0.9 (Lambda 1.08 was not tested at 1600rpm 200Nm due to knock limits). For each Lambda setting, a spark timing sweep was performed from the most advanced knock-limited setting to the most retarded TIT-limited setting. For simplification, the knock sensor on the engine was used as knock indicator. At each test point, the engine was stabilised for 5 minutes before recording. If knock occurred before recording was finished, the spark timing was retarded and the data point was deleted.

The valve timing and pedal position were maintained at constant level. The production ECU strategies for throttle position and boost pressure control were

applied to achieve a stable torque level, while the Lambda and spark timing settings were varied. The engine torque variation was within ±3.5% and ±2.5% at the two test points, respectively. The mass air flow variation was within ±0.5% and ±0.2% at the two test points.

The recorded test points at the two engine operating points are presented in Figure 6.1. It is shown that the knock-limited spark timing was advanced when fuel enrichment was applied. At the two engine operating points, the spark timing can be advanced by 2.25 and 3 degrees crank angle by enriching from Lambda 1 to Lambda 0.9, respectively.

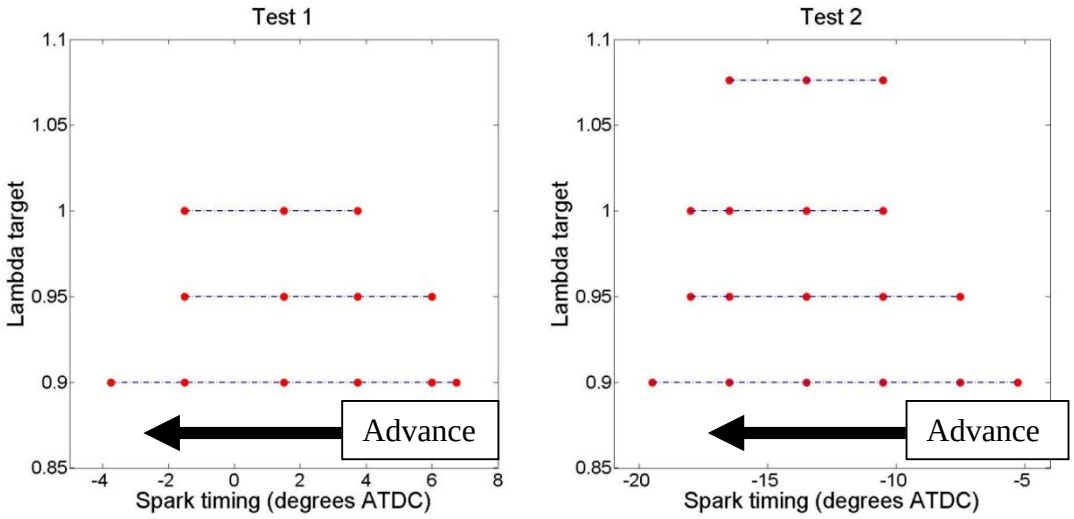

Figure 6.1: Spark timing and Lambda test points

In Figure 6.2, the Brake Specific Fuel Consumption (BSFC) at different spark timings and settings of pre-catalyst Lambda is plotted against the equivalence ratio, which is proportional to the fuelling amount, provided that the mass air flow is maintained at constant level. The relationship between BSFC and equivalence ratio at the same spark timing was linear in the rich combustion region. The optimum BSFC occurred close to Lambda 1. Either richer or leaner mixture causes increased the fuel consumption.

In order to investigate the effect of fuel enrichment on fuel consumption, the average impact on the engine fuel consumption was calculated using the data in the fuel

enrichment region highlighted in Figure 6.2. At the corresponding spark timing, the average BSFC impact at two test points was 25.9 g/kWh and 28.4 g/kWh for a 0.1 increase in equivalence ratio, which was equivalent to 28.8 g/kWh and 33.1 g/kWh for a 0.1 decrease in Lambda.

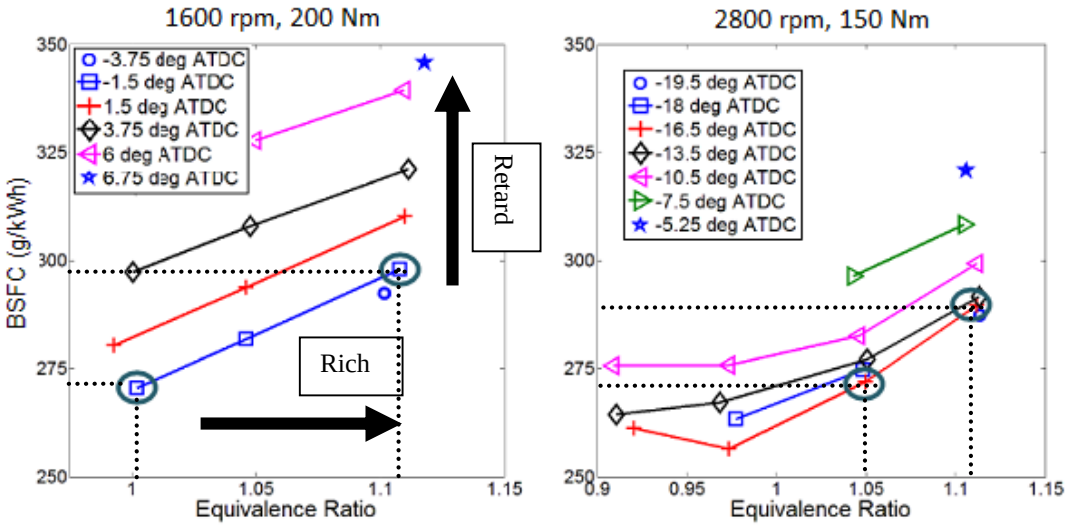

Figure 6.2: BSFC at various equivalence ratios

In Figure 6.3, the BSFC is plotted against the TIT. For the same operating points as those in Figure 6.2, the average BSFC impact was 33.7 g/kWh and 38.9 g/kWh respectively, for a 50°C decrease in TIT.

It is worth noting that, compared with fuel enrichment, lean air-fuel mixture offered a smaller BSFC penalty for a unit decrease in TIT. This was because as much fuel as possible was burned with the weak mixture, and this offered both excellent combustion efficiency and low TIT. However, lean mixture is not a preferred method to reduce TIT at high load, as the engine torque is also reduced significantly. In this experiment, the reduced torque was compensated for by opening the throttle and increasing mass air flow. This cannot be achieved at full load. Therefore, only fuel enrichment is analysed in this study.

By enriching the mixture from Lambda 1 to Lambda 0.9, the knock-limited spark timing can be advanced by 2.25 and 1.5 degrees crank angle at the two test points respectively. Advancing the spark timing was beneficial because the reduction in

both fuel consumption and TIT could be achieved. As shown in Figure 6.2, the engine fuel consumption deteriorated as the spark timing was retarded.

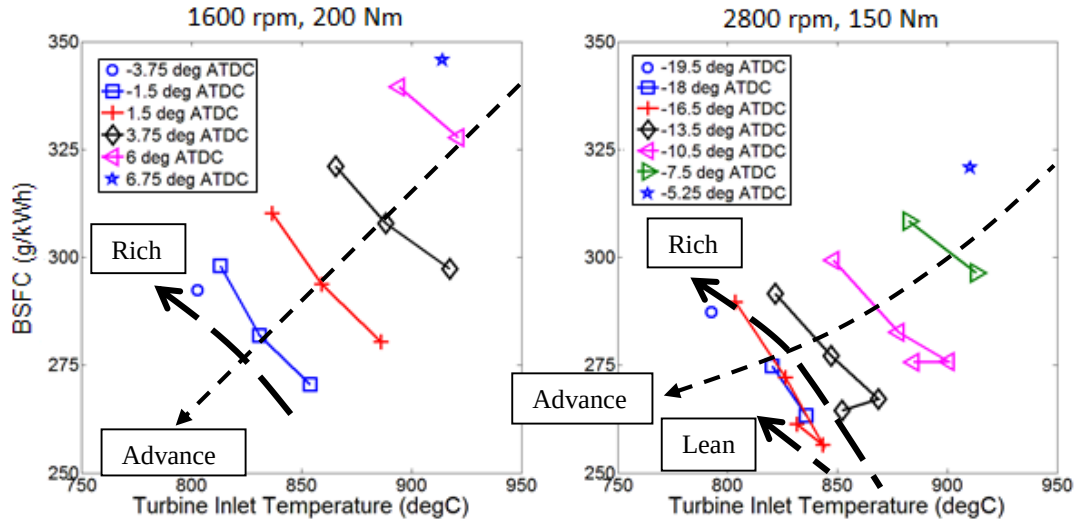

Figure 6.3: BSFC and TIT at various operating conditions

The combustion thermal efficiency can be improved by advancing the spark timing (Figure 6.4). Therefore, advancing spark timing offered the opportunity to reduce the fuel consumption impact due to fuel enrichment.

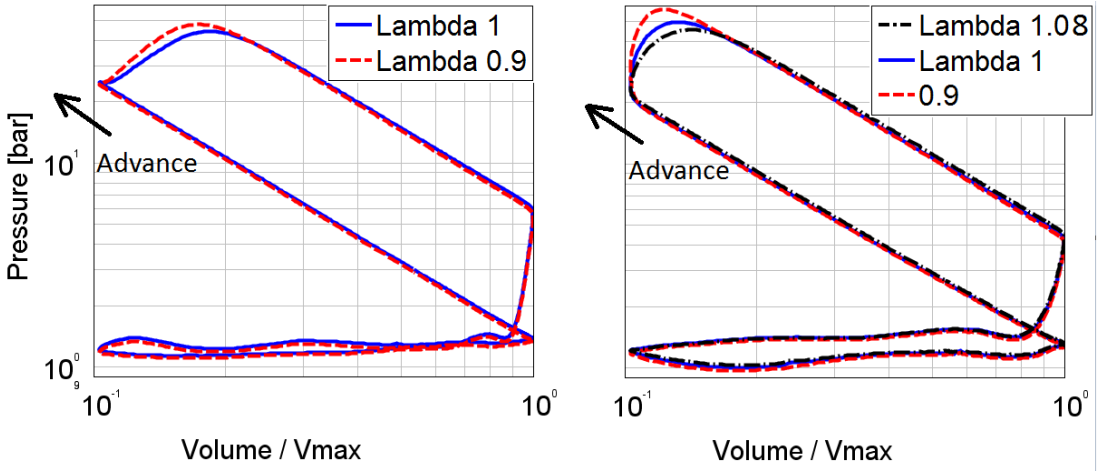

Figure 6.4: P-V diagram of the most advanced spark timing settings at each Lambda target

Thus, taking into account the extended window for spark timing, the trade-offs between BSFC and TIT at the two tests points were 21.5 g/kWh and 22.6 g/kWh (7.9%

and 8.6%) increase in BSFC respectively, for a 50°C decrease in TIT. This was a result of a BSFC deficit of 36.2% and 41.9% being offset by advancing the spark timing.

Nevertheless, the engine operating points at lower load will not be affected by the variations in the TIT. Therefore, it is also necessary to understand the operating region where the fuel consumption will be affected if the TIT is varied.

Measurement data from the engine mapping test was used to investigate the effect of varying the TIT limit on the requirement for fuel enrichment. A quadratic response polynomial model of TIT was generated, based on the inputs of engine speed and torque at 23 operating points, at which the pre-catalyst Lambda target was 1. Another three stoichiometric operating points were used for validation of the response.

The fitted response is :

TIT = 227 + 0.1581 * Speed + 2.13 * Torque - 8.862e-06 * Speed ^ 2
-2.28e-04 * Speed * Torque - 8.548e-04 * Torque ^ 2

where TIT is turbine inlet temperature (°C)
Speed is the engine speed (rpm)
Torque is the engine torque (Nm)

The summary statistics for the response model are listed in Table 6.1. The R^2 and Root Mean Square Error (RMSE) were both excellent, and the Predicted Residual Error Sum of Squares (PRESS) statistics were very close to their non-PRESS equivalents. The validation RMSE was also close to RMSE. Therefore, the accuracy and the predictive ability of the model were both excellent, and the model was not over-fitted.

Table 6.1: Summary statistics for the TIT response model

RMSE (°C)	Press RMSE (°C)	R^2	Press R^2	Validation RMSE (°C)	Normalised validation RMSE
6.847	8.543	0.998	0.996	10.208	5.32%

The model was then used to predict the TIT-limited engine load above which a fuel enrichment strategy was required (Figure 6.5). The change in achievable engine load with stoichiometric combustion was relatively linear in this operating region. The average increase in the constrained engine load for a 50°C rise in TIT limit was 2.44 bar BMEP.

In Figure 6.6, measured engine speed and torque from a New European Driving Cycle (NEDC) test in which the data was recorded at 10Hz is also plotted. It is shown that the entire NEDC test can be operated with Lambda target 1, if the TIT limit is above 850°C. It should be noted that this response model was generated from the steady state test data, while the NEDC test points were mostly under transient conditions. Thus, the thermal inertia of the exhaust system and the thermal couple were not considered. As a result, peak TIT in the NEDC test predicted by the fitted response model was 45.3°C higher than that measured in the NEDC test. In addition, the ECU transient load control strategy was not taken into account in this prediction. Therefore, the Lambda target may be lower than 1 when the torque target in ECU is higher than the measured torque.

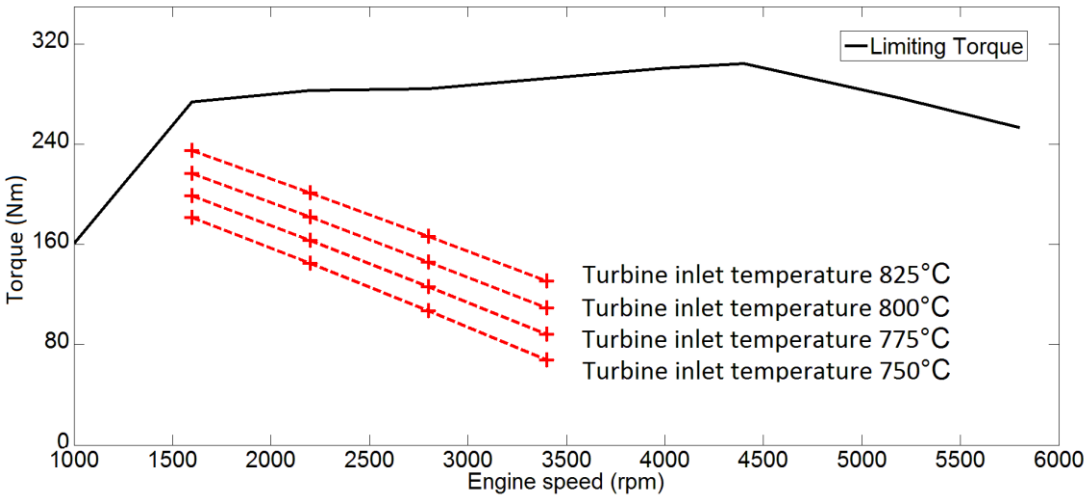

Figure 6.5: Constrained engine load with stoichiometric combustion for different TIT limits

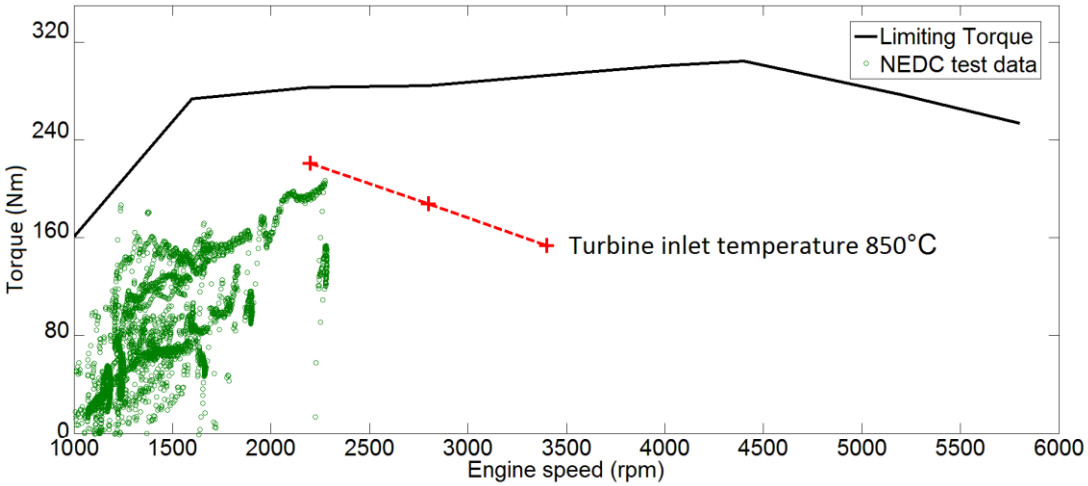

Figure 6.6: Engine operating points in NEDC test

It is shown that, with the same level of ICE technology, the exhaust gas temperature increased with the increasing engine load. Thus, the fuel enrichment may still be required in real world driving, where the engine speed and load can exceed the NEDC operating region. Therefore, to reduce the real world emissions, stoichiometric combustion is required in a larger engine operating region.

In order to optimise the required level of fuel enrichment on highly downsized gasoline engines, the turbocharger design (as well as other ICE technologies on the fuelling system, scavenging system, exhaust gas recirculation system and water-cooled exhaust manifold, etc.) needs to be considered in a systematic way. As a wider operating range will be covered by the new legislation drive cycles, the fuel enrichment should be kept at minimum level. Fuel enrichment may still be required in the region not covered, for example, peak power operating points which may only be needed in rare occasions. Thus, optimisation of fuel enrichment and systematic design of the engine are required to avoid over engineering and to improve the cost-effectiveness of the product. Nevertheless, real-world driving emission should be set as the ultimate target, so that the vehicle emissions in drive cycle tests and real driving conditions are on the level. The industry is moving in this direction as lower level of fuel enrichment can be seen on latest gasoline engines.

The use of VGT on gasoline engines has a more stringent requirement for low TIT, and hence fuel enrichment. More efforts may be necessary to fulfil the TIT requirements on gasoline engines with VGT. Nevertheless, part load operation where fuel enrichment is not required may also be improved by using VGT. Thus, both part load and full load operation need to be optimised for the comparison of overall fuel consumption for VGT and FGT.

6.2. Comparison of FGT and VGT

6.2.1. Experimental results

In order to compare FGT and VGT, the original FGT turbocharger and the VGT turbocharger were tested on the 2.0L gasoline engine. The tests were performed at 2000rpm since the low-end torque is crucial to downsized engines. This engine speed was chosen because the available boost pressure of the FGT turbocharger at 2000rpm was representative of the full load capability of this engine.

The throttle was kept at wide open for back-to-back comparison. The valve phasing was kept at maximum overlap, and the Lambda target was set to 1. The control parameter of the turbocharger actuators (FGT: Pulse Width Modulation (PWM) duty cycle of solenoid valve on the pneumatic actuator driven by engine inlet manifold pressure; VGT: electric actuator position) were varied from the minimum turbine load to the maximum within knock limits. Thus, the full wide-open-throttle (WOT) region was covered in the experiments.

At each VGT actuator setting, the spark timing was varied from the knock limits to the TIT limits at several engine load levels. The achieved knock-limited spark timing settings are presented in Figure 6.7. In addition, the maximum and minimum engine torque are also demonstrated.

As the engine load increased, the knock-limited spark timing was retarded. The maximum engine load achieved with the VGT turbocharger was 319Nm, which was limited by the knock limit and the TIT limit (917°C at this test point). With the FGT

turbocharger, the maximum engine torque was 260Nm (TIT 888°C at this test point), 59Nm lower than that achieved with the VGT turbocharger. This was because of the knock limit, which, with the VGT turbocharger, can be advanced by up to around 3 degrees crank angle compared with the FGT turbocharger.

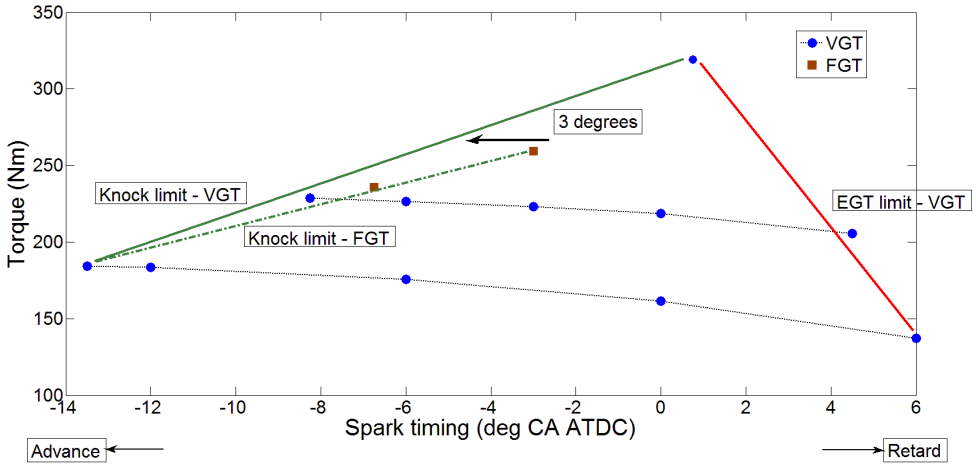

Figure 6.7: Comparison of engine operating window at 2000rpm WOT

It should be noted that TIT difference was observed (917°C at 319Nm on the VGT, 888°C at 260Nm on the FGT). To compensate for this variation (which is inevitable in experiments), the trade-off between maximum engine torque and TIT limit discovered in the previous section was applied. Therefore, the estimated peak torque achieved on the FGT became 271Nm if the TIT limit could be controlled at 917°C precisely. As a result, the maximum engine torque at 2000rpm was improved by 48Nm (17.7%) by replacing the production FGT turbocharger with the VGT turbocharger.

The minimum engine torque achieved with the FGT and VGT turbochargers was 236Nm and 184Nm respectively. The variation was because of the different types of actuator used on the two turbochargers. On the VGT, the electric actuator was flexible to reach any target position within the hard-stop limits. However, on the FGT, the opening was dependent on the intake manifold pressure, dynamic exhaust gas pressure and the physical properties of the waste-gate mechanism. In addition, the minimum engine load at WOT was also affected by the flow capacity of the waste-gate. A detailed model of the waste-gate mechanism is required; however, this

is outside the scope of this project. Future work will need to be carried out to investigate the response of the waste-gate and the minimum engine load achieved with the FGT without the limitation of the actuator.

Figure 6.8 shows the comparison of BSFC for the FGT turbocharger and the VGT turbocharger. At WOT, the fuel consumption was reduced by approximately 4% by replacing the FGT turbocharger with the VGT turbocharger. Because of the differences in the achievable minimum load, the throttle was closed to achieve 184Nm on FGT. This was achieved at the cost of increased pumping work, due to the excessive compressor power and throttling. On the VGT, the compressor outlet pressure was 1.07 bar at 184Nm. However, on the FGT, the air pressure at compressor outlet pressure was 1.31 bar, which was throttled to 1.15 bar at inlet manifold.

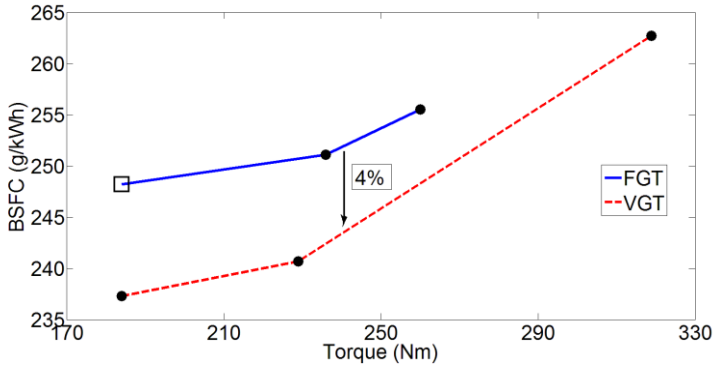

Figure 6.8: Comparison of engine fuel consumption

6.2.2. Simulation results

In order to investigate the fuel consumption improvement in more detail, simulations at medium boost level (engine torque 229Nm at 2000rpm) were carried out. Tests that cannot be performed in experiments were simulated using the validated high fidelity 1-D engine model.

The waste-gate was assumed to be flexible to control the engine torque with fully opened throttle at this operating point. Friction Mean Effective Pressure (FMEP) measured in VGT tests at 229Nm was imposed for both FGT and VGT simulation.

The start of combustion used in the FGT simulation was interpolated from the knock-limited spark timing measured in the FGT experiments: 1.5 degrees crank angle later than the most advanced setting at 229Nm in the VGT experiments.

The simulated BSFC for FGT and VGT was 251.7 g/kWh and 245.9 g/kWh, equivalent to 2.3% difference. Although a variation smaller than 2% was found between the experimental data and simulation results, this was an excellent level of accuracy for investigation of improvements.

6.2.3.1. Effect of changes in exhaust manifold

It was found that the exhaust gas pulses were affected due to the change of exhaust manifold (Figure 6.9). The manifold damping effect and the reflected pressure wave were affected by the changes in the exhaust manifold volume and additional cavity.

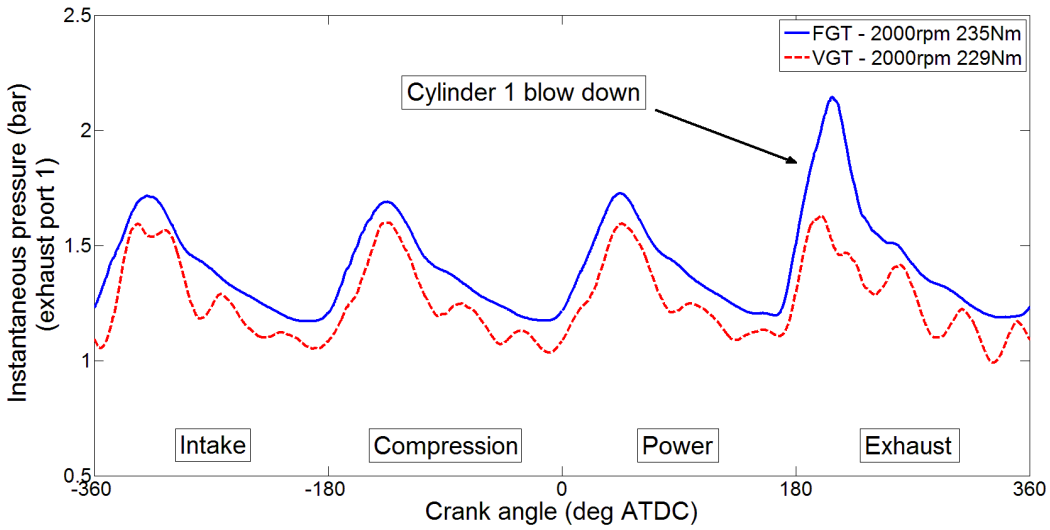

Figure 6.9: Measured instantaneous pressures at exhaust port of cylinder 1

The original exhaust manifold for the production FGT turbocharger had a twin-skin structure. In the 1-D engine model, the cavity between the two layers was represented by an additional volume, and the gap between the two layers was represented by an orifice (Figure 6.10). Compared with this structure, the custom-made exhaust manifold used for the VGT turbocharger had the following changes:

1). Single layer structure. Therefore, no gap and cavity.

2). Volume of the exhaust manifold is affected due to the different shape.

3). No waste-gate required for the VGT turbocharger.

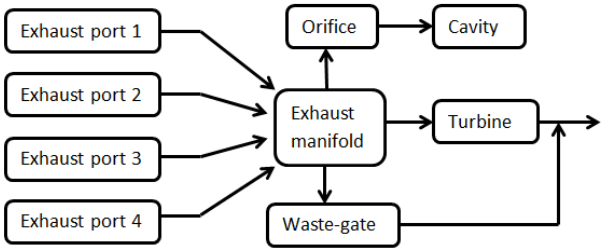

Figure 6.10: Layout of exhaust system in 1-D engine model

Thus, to investigate the effect of the change to the exhaust manifold, the FGT engine system was simulated with custom-made exhaust manifold elements. The turbine internal waste-gate was used in this simulation. Figure 6.11 shows the simulated exhaust port pressures. The effect of changes to the exhaust manifold on the pressure wave in the exhaust manifold was captured in 1-D simulation.

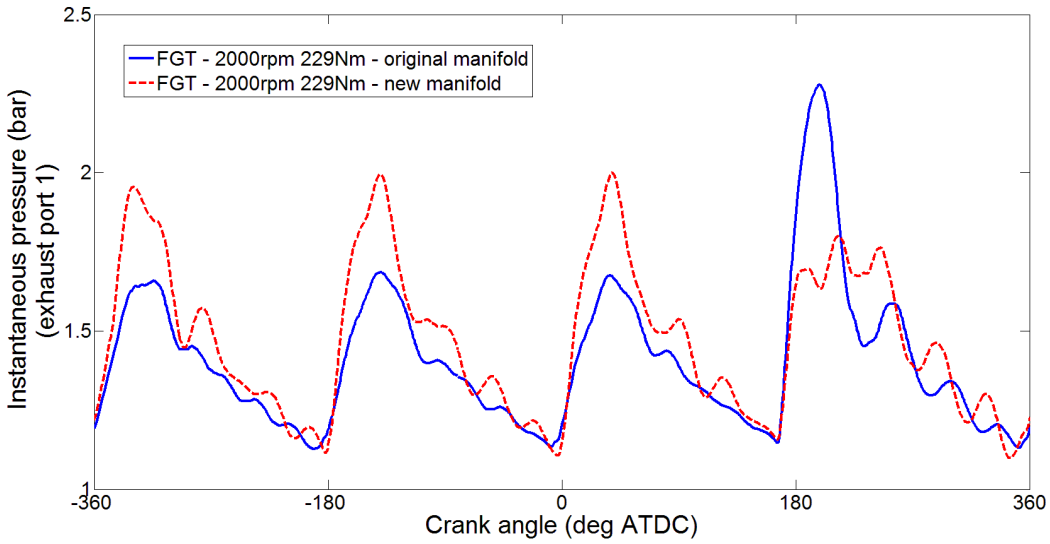

Figure 6.11: Simulated instantaneous pressures at exhaust port of cylinder 1

It was found that the BSFC and gross IMEP variations between simulations using the original manifold and the custom made manifold were smaller than 0.1%. Therefore, the effect of the change of exhaust manifold on the engine fuel consumption at

229Nm can be ignored. Nevertheless, the effect of the exhaust pulses on the gas motion in the cylinder, and hence the scavenging and combustion process, cannot be captured unless CFD study is performed.

6.2.3.2. Effect of changes in knock-limited spark timing

Since the knock-limited spark timing was advanced by up to 3 degrees crank angle by replacing the FGT with the VGT, the effect of this variation on the combustion thermal efficiency needed to be studied. To separate different effects, engine simulation was run at constant engine torque 229Nm, with the 1-D model of the custom-made exhaust manifold and the FGT turbocharger. Two spark timing settings were compared: 8.25 degrees crank angle (VGT) and 6.75 degrees crank angle (FGT) before Top Dead Centre (TDC). These were the most advanced knock-limited spark timing settings at this engine load level for the VGT and FGT. Therefore, tests that cannot be conducted in experiments were simulated to demonstrate the benefits in the fuel consumption, provided that the spark timing with FGT could be further advanced.

According to simulation results, by advancing the spark timing from 6.75 to 8.25 degrees crank angle before TDC, the in-cylinder peak pressure was increased from 58 bar to 60 bar. The BSFC was lowered from 251.7 g/kWh to 248.0 g/kWh, equivalent to a 1.5% improvement of fuel consumption.

6.2.3.3. Effect of changes of turbine

The potential for advancing the knock-limited spark timing was likely to be a result of better scavenging due to the lower exhaust manifold pressure from replacing the FGT turbine with the VGT turbine. Both systems were simulated in a 1-D environment. The same spark timing (6.75 degrees BTDC) and the model of the custom-made exhaust manifold were used in the simulation.

By using the VGT turbine, the engine delta pressure (average pressure in exhaust manifold – average pressure in intake manifold) was reduced by 0.1 bar. The pumping loss was reduced from 0.25 bar Pumping Mean Effective Pressure (PMEP) to 0.16 bar PMEP (0.6% gross IMEP reduction). This was because of the waste-gate on the FGT, which bypassed some of the exhaust gas. Thus, the turbine system efficiency, which takes into account the by-passed flow, dropped and this required a higher turbine expansion ratio to produce the required turbine power.

The power-weighted turbine efficiencies of the FGT and the VGT were 48.7% and 39.1% respectively. However, 30.5% of the exhaust flow was bypassed on the FGT, which reduced the VGT system efficiency to 33.8%. Since no exhaust flow was bypassed on the VGT, the VGT system efficiency was the same as the turbine efficiency. Therefore, the system efficiency of the VGT was 5.3% higher than that of the FGT. Although the VGT turbine isentropic efficiency was lower than that of FGT at this engine operating point (which might be due to the vane aerodynamic losses and the turbocharger matching), the system efficiency of the turbine stage was improved by replacing the FGT with the VGT. The potential of reduction in bypassed flow is one of the key benefits of using VGT, as was discovered in the literature review. As a result of the lower pumping work, the engine BSFC was reduced from 248.0 to 246.4 g/kWh, equivalent to a 0.6% improvement.

It is worth noting that the residual gas fraction in cylinder was reduced from 1.34% to 1.20%. Despite the difficulties in predicting the magnitude of the reduction of the residual gas fraction using 1-D simulation, this proved the trend that the scavenging process was improved, which was likely to be the cause for the extended knock-limited spark timing window.

6.2.3.4. Effect of changes of compressor

It should be noted that the compressor efficiency in the simulation of the FGT and VGT systems varied, due to the change of compressor. The efficiencies for the FGT and VGT in the simulation at 229Nm were 60.0% and 70.1% respectively. Therefore, the compressor in the VGT turbocharger was replaced with the FGT

compressor in the simulation, in order to analyse the effect of the change of compressor.

By replacing the compressor performance map, the engine BSFC was increased from 245.9 g/kWh to 246.4 g/kWh (0.2%). This was due to the increase in compressor power from 1.59 kW to 1.9 kW. As a result, the waste-gate opening was reduced to provide the additional load required by the compressor. The engine pumping work was increased from 0.13 bar PMEP to 0.16 bar PMEP (0.2% increase in gross IMEP).

Therefore, 0.2% out of the 2.3% predicted BSFC improvement was due to the change of the compressor. If the same compressor was used on both the FGT turbocharger and the VGT turbocharger, the estimated BSFC improvement became 2.1%.

6.2.3.5. Distribution of fuel consumption improvement

By investigating the engine behaviour in a simulation environment, the effects can be separated and studied, which cannot be achieved in experiments. Out of the 2.3% BSFC improvement achieved by replacing the FGT with the VGT turbocharger, 1.5 percentage points was from the combustion thermal efficiency due to the extended knock-limited operating window (Figure 6.12). A 0.6% improvement was from the use of VGT turbine technology, due to the elimination of bypassed exhaust flow, which improved the system efficiency of the turbine stage and reduced pumping work. A 0.2% improvement was due to the change of compressor, irrelevant to VGT technology. Figure 6.12 illustrates the distribution of the benefit.

It is worth noting that both the experimental data and simulation results from this study represented the benefit of using the specific hardware available in this project, which is also subjected to turbocharger matching. Therefore, it is necessary to

demonstrate the full potential of using the VGT by performing the matching for the VGT.

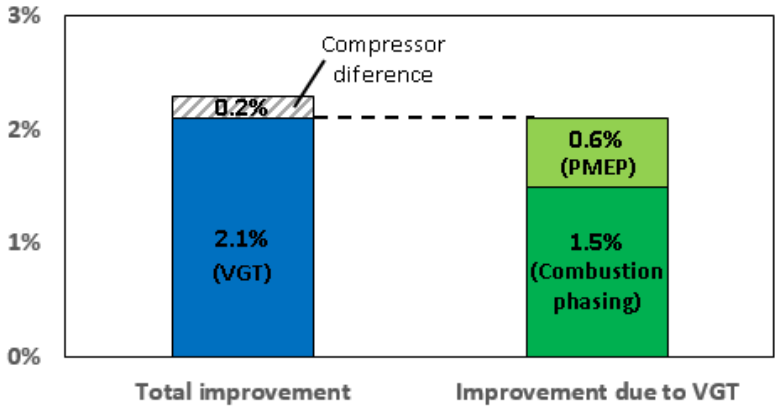

Figure 6.12: Distribution of fuel consumption improvement

6.3. Turbine matching for steady state performance and comparison between FGT and VGT

6.3.1. Turbine matching criteria

In order to determine the full potential of the application of VGTs on gasoline engines, turbine matching was performed in simulations using scaled turbine maps, while the compressor was kept the same for back-to-back comparison. Several variable nozzle-type VGT maps were supplied by the turbocharger manufacturer for scaling and matching, they were from the same turbine family for comparison. The scaling of turbine maps was based on the algorithms described in Chapter 5. Several turbine sizes were selected and compared to investigate any potential trade-offs in matching VGT to gasoline engines.

Thus, the optimum size of the turbine wheel can be selected for the prediction of the full potential of the use of VGT on gasoline engines. By using a turbine with smaller swallowing capacity, the maximum engine torque achievable at low engine speed may be improved, due to the higher turbine expansion ratio. However, at high engine speeds, the turbine efficiency may be lowered and the flow range of the turbine may not be sufficient, resulting in higher exhaust manifold pressure and fuel consumption.

Thus, the selection of the turbine size depends on the target performance at high speed and low speed.

With the intention of avoiding the use of large scaling factors, and to improve simulation accuracy, 0-D turbine matching was performed to select base turbine maps for preliminary simulations and scaling. This was followed by the 1-D engine simulations for the fine scaling and selection of the turbine sizes.

In accordance with the preliminary simulation results, three turbine sizes were chosen for comparison in this study. Table 6.2 lists the matching criteria for candidate turbines. The large turbine was selected to represent the system solution with the lowest cost and simplest packaging, because the flow range was large, the waste-gate was not required at full load peak power WOT operating point. The small turbine was selected to represent the turbocharger with low moment of inertia for fast transient response. In addition, this was likely to improve the low-end torque. As these two turbines could actually be too big or too small for the best turbine efficiency, a medium sized turbine might provide the best turbine efficiency, and hence full load capability. The selection of a medium VGT would be dependent on the matching of the large VGT and small VGT. According to the preliminary simulation results, three VGT maps with the potential to meet the matching criteria were chosen. In the following section, the process of scaling and selecting the size of the three turbines will be presented.

Firstly, the engine peak power operating point was simulated in a 1-D environment. The extrapolation of the combustion model was not enabled. Therefore, in this study, the combustion heat release profiles at the end points were used if the engine load was above the calibrated region of the combustion model. Knock prediction was not used for simplification. Therefore, the actual maximum engine torque on a real engine may be limited due to knock. In addition, the effect of the scavenging process on the knock-limited spark timing window cannot be captured in this simulation. The resultant simulated fuel consumption variation was from the changes in pumping work.

Table 6.2: Turbine matching criteria for investigation

	Large VGT	Medium VGT	Small VGT
Size	Large	Medium	Small
Flow capacity	High	Medium	Low
Waste-gate requirement for full load operation	No	Yes	Yes
Potential advantages	Lower cost and easier packaging	Better fuel consumption	Low-end torque and transient response
Normalised turbine outside diameter of the base VGT maps for scaling studies	1	0.94	0.86

In order to verify the flow capacity, the throttle and vane position were kept at fully open. Since the flow capacity may not be sufficient, an additional waste-gate was used to control the engine load to reach the original engine torque target. The size of large VGT was selected so that it was the smallest size to reach target engine torque at WOT without the need for a waste-gate. The size of small VGT was selected so that the exhaust manifold pressure and, hence, fuel consumption achieved with the aid of additional waste-gate were not worse than those achieved with the original FGT turbocharger.

Figure 6.13 shows the simulated exhaust manifold pressure with various turbine sizes. For the large VGT (VGT A), a waste-gate was required at peak power WOT if the normalised diameter was smaller than 1.03. For the small VGT (VGT C) with normalised diameter 0.78, the exhaust manifold pressure matched the level of the FGT. Therefore, these two normalised diameters were chosen for the large and the small VGTs. The two selected sizes are also highlighted in the figure.

It is worth noting that, although the two VGT turbine maps used in the scaling simulation were in the same family, an approximately 0.1 bar exhaust manifold pressure discrepancy can be found when they were scaled to the same diameter level. This was because the effects of the turbine size on the performance cannot be fully captured by a simple scaling algorithm. Therefore, in order to maximise the accuracy

of the simulation results, the scaling of the turbine diameter should be as close to unity as possible by using the closest performance map available. For the large VGT and the medium VGT, the diameter scaling factors were 1.03 and 0.91 from the base VGT maps respectively. Thanks to the iteration of the turbine matching process, these were the minimum scaling factors that could be achieved.

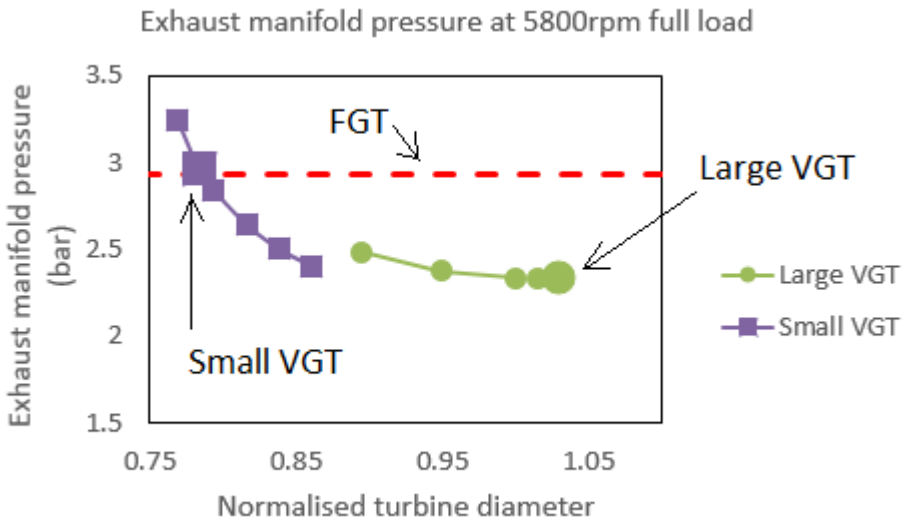

Figure 6.13: Effect of turbine size on exhaust manifold pressure

It was found that the turbine operating points were not in the optimum efficiency region for either the large or the small VGT. They were either too large or too small. Figure 6.14 shows the turbine operating point (averaged expansion ratio and reduced speed). Therefore, turbine matching was also performed to find the size of the medium VGT for optimum turbine efficiency, and hence engine fuel consumption, at full load.

The matching of the medium VGT was scaled and optimised to achieve the best engine fuel consumption. Figure 6.15 shows the averaged turbine operating points for the medium VGT with optimised scaling factor. It is shown that the turbine operating points were close to the optimum efficiency islands, and the VGT position was close to medium opening. The resultant normalised turbine diameter was 0.96, corresponding to a scaling factor of 1.025 from the base map used for the medium

VGT. Therefore, the sizes for the three turbine matching strategies are listed in Table 6.3.

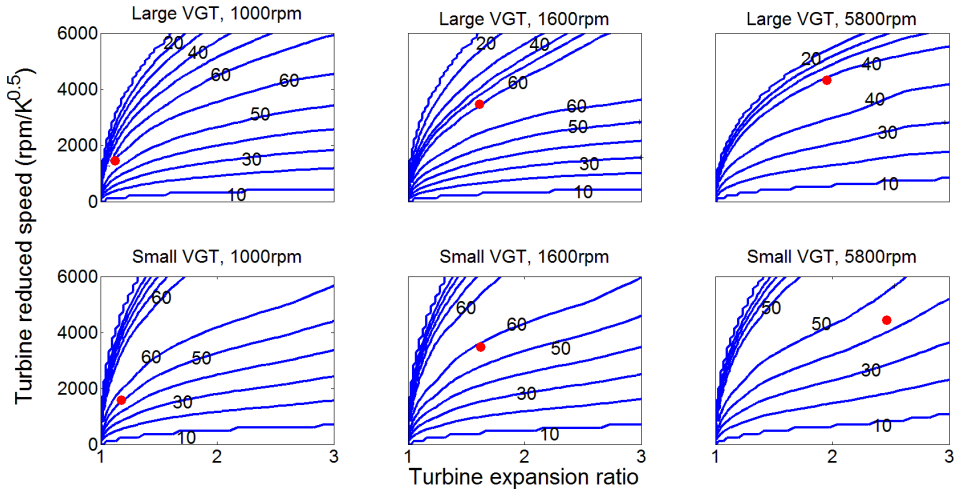

Figure 6.14: Contour plot of turbine efficiency (%) and full load turbine operating points on the large and small VGTs

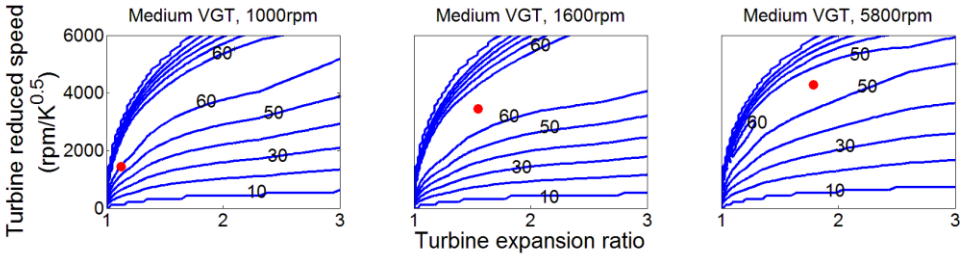

Figure 6.15: Contour plot of turbine efficiency (%) and full load turbine operating points for the medium VGT

Table 6.3: Turbine scaling factors

	Large VGT	Medium VGT	Small VGT
Normalised turbine outside diameter of the base VGT maps for scaling studies	1	0.94	0.86
Additional scaling factor for turbine outside diameter	1.03	1.025	0.91

This was in fact a better matching than the original FGT turbine, shown in Figure 6.16. This was because the size of the FGT was also dependent on the required flow range to achieve the target exhaust manifold pressure. This was a trade-off between low speed performance and high speed performance. If the selected flow range were optimised for turbine efficiency at low-end, more exhaust flow might need to be bypassed at high speeds, reducing VGT system efficiency and increasing engine fuel consumption. However, with a VGT the turbine matching can be optimised with minimum exhaust flow being bypassed. Thus, the two configurations of variable nozzle type VGT, with and without an additional waste-gate, were investigated and compared in this project, as they represented different levels of system cost.

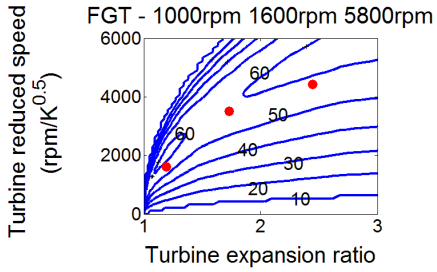

Figure 6.16: Contour plot of turbine efficiency (%) and full load turbine operating points for the original FGT

6.3.2. Comparison of engine steady state performance

6.3.2.1. Engine fuel consumption

Engine full load performance was simulated in a 1-D environment using the three scaled VGT turbines. The original FGT full load curve was used as target engine torque level in this simulation. The Lambda was maintained at the same level as for the FGT, assuming that the exhaust gas temperature limit was kept the same. Since the flow range of the medium and small VGTs was not sufficient for full load operation, both throttling and waste-gate bypassing were used as measures to control engine load. These two measures will be studied and compared.

Figure 6.17 shows the fuel consumption saving over the original FGT at full load. The engine fuel consumption with all three VGTs with waste-gate was better than for the original FGT. It was found that the fuel efficiency of the large VGT at high speeds was lower than that of the medium VGT, although the large VGT did not require an additional waste-gate. This was because of the differences in the aerodynamic design of the two turbines. The peak turbine efficiency at fully open position was approximately 45% for the large VGT and 60% for the medium VGT. Nevertheless, the peak efficiencies of the three turbines are similar at closed vane position and medium vane openings.

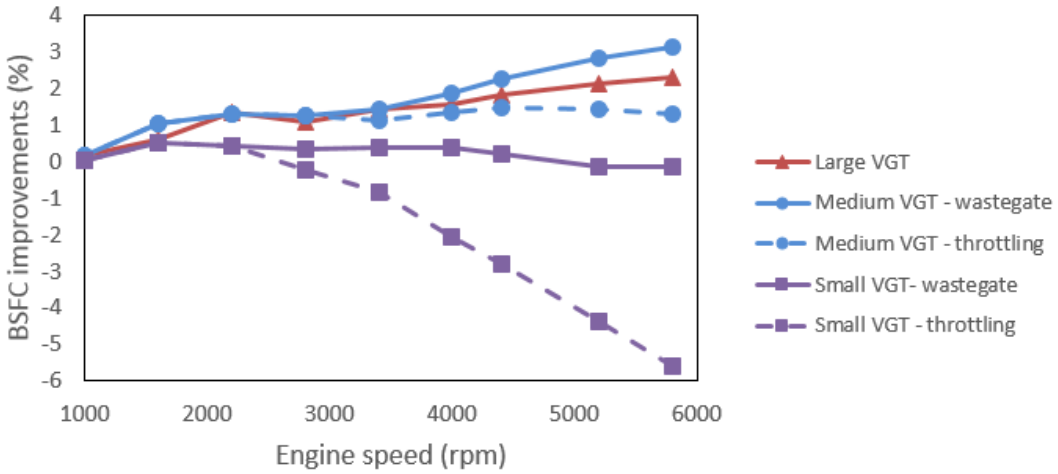

Figure 6.17: Fuel consumption benefits compared to FGT – full load

Figure 6.18 shows the comparison of the turbine apparent efficiencies. Despite the high turbine efficiency of the FGT, the system efficiency of FGT was lower than all the VGTs due to the bypassed exhaust gas flow. The system efficiency of the medium VGT was the highest, because of the better matching. The system efficiency of the small VGT was very close to that of the FGT. This is the same trend as for the BSFC comparisons shown in Figure 6.17.

For the medium and large VGTs, the largest fuel consumption benefit occurred at high engine power operating points. This is the region where more exhaust gas flow needed to be bypassed.

It is also shown in Figure 6.17 that the engine fuel efficiency dropped significantly when throttling was used instead of the waste-gate. A fuel consumption deficit of up

to 5.5% was found on the small VGT if the waste-gate was not used. For the medium VGT, the engine fuel consumption dropped below that for the large VGT if throttling was used instead of waste-gate bypassing. Therefore, the waste-gate was always preferred to throttling in the cases where the VGT flow capacity was not sufficient.

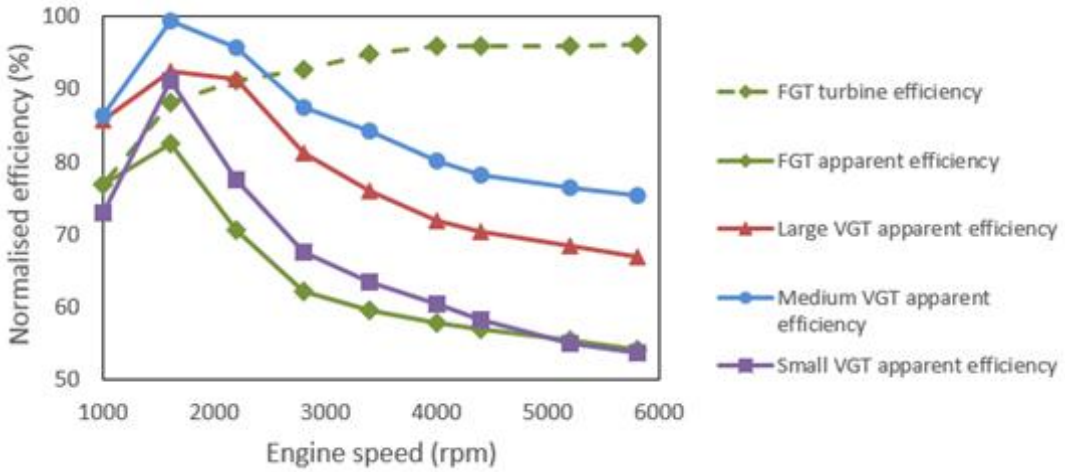

Figure 6.18: Turbine efficiency comparison at full load (VGT turbines with waste-gate if necessary)

Although the flow range of the large VGT was sufficient for full load operation, a waste-gate might still be required at part load operation when lower boost pressure is needed. Figure 6.19 shows the fuel consumption comparison at moderate boost level, approximately 1.3 bar boost pressure across the engine speed range, apart from 1000rpm, where the maximum boost pressure was 1.1 bar.

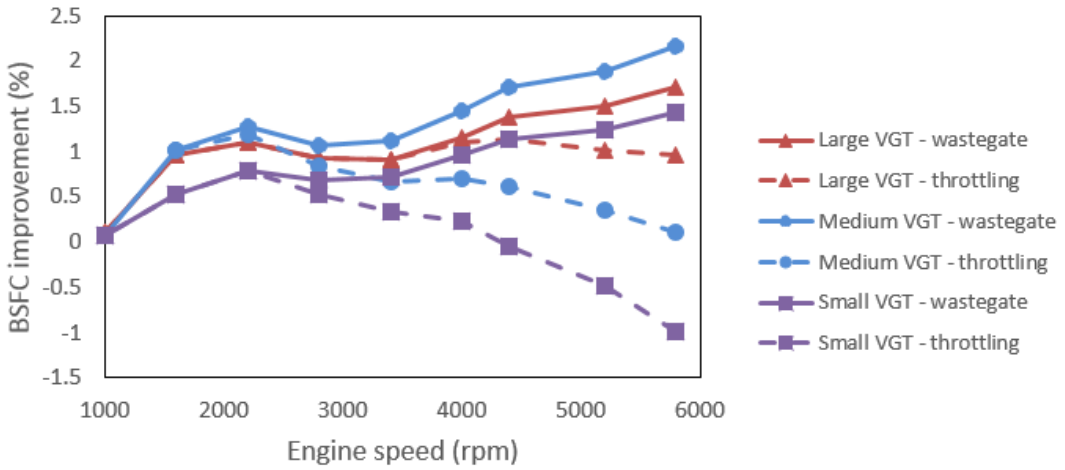

Figure 6.19: Fuel consumption benefits compared to FGT – part load

It is shown in Figure 6.19 that the trends are similar to that shown in the full load comparison. The maximum improvements were still in the high speed and high power region. The medium VGT was still the best matching if a waste-gate was equipped. However, if it was not equipped with a waste-gate and throttling was used to control the engine load, the large VGT, which had large flow range, could still offer 1% fuel consumption benefits over the FGT, whereas the benefits of the medium VGT diminished. Similar to the full load results, the fuel consumption of the small VGT was worse than that of the FGT at high speed, if it was not equipped with a waste-gate.

At engine speed above 3500rpm, all three turbines required a waste-gate to control the boost pressure at part load. In addition, 3500rpm was higher than the maximum speed covered by most of the current drive cycles. Therefore, the fuel consumption at low speeds (3500rpm and below) and high speeds (above 3500rpm) were investigated separately. Table 6.4 lists the averaged BSFC improvements for each VGT configuration at high speeds and low speeds. For simplification, this was a mathematical average of the data at full load and part load (Figure 6.17 and Figure 6.19), each point had the same weighting factor. To obtain more accurate predictions for individual vehicle applications, mini-map points can be selected with weighting factors dependent on the importance of each point.

Table 6.4: Fuel consumption improvement comparison at high speeds and low speeds

	Large VGT		Medium VGT		Small VGT	
	Low speeds (at 3500rpm and below)	High speeds (above 3500rpm)	Low speeds	High speeds	Low speeds	High speeds
Averaged BSFC benefit over FGT (waste-gate)	0.87 %	1.70 %	0.98 %	2.17 %	0.46 %	0.65 %
Averaged BSFC benefit over FGT (throttling)	0.87 %	1.51 %	0.86 %	0.92 %	0.22 %	-2.01 %

In general, the fuel consumption improvements over FGT were around 0.5% to 2%, depending on the selection of the VGT and configuration. It is shown that the flow range of the VGT was important. This was because, if the flow range was insufficient, an additional waste-gate was necessary to prevent significant fuel consumption deficit at high speeds.

6.3.2.2. Maximum torque at low engine speeds

Although the fuel consumption improvements offered by the small turbine were lower than for the other turbines, the engine low-end torque might be improved. Therefore, simulation was carried out to investigate the maximum engine torque that could be achieved using the original FGT and the three VGTs at low engine speeds.

VGT vane position sweep was carried out to predict the maximum engine torque achieved within the compressor surge limit, in-cylinder pressure limit and exhaust gas temperature limit. Since the combustion model was calibrated using experimental data collected from the tests with the FGT, the torque prediction was likely to be unreliable if the engine operating point was too far away from the measured engine operating points. Therefore, torque level above 300Nm was not of interest in this study, and the torque knee-point was investigated.

Figure 6.20 shows the simulation maximum engine torque in the low speed region. The FGT can reach 90% of the maximum torque from around 1500rpm, whereas the three VGTs can reach 90% of the peak torque between 1250rpm and 1400rpm. Down-speeding of the torque knee-point was up to 250rpm compared with the FGT. Therefore, the drivability of the vehicle could be improved. Larger gear ratios may be selected for better powertrain optimisation and vehicle fuel consumption. In addition, further downsizing may be enabled. Engines with small displacements may be able to drive a heavier vehicle.

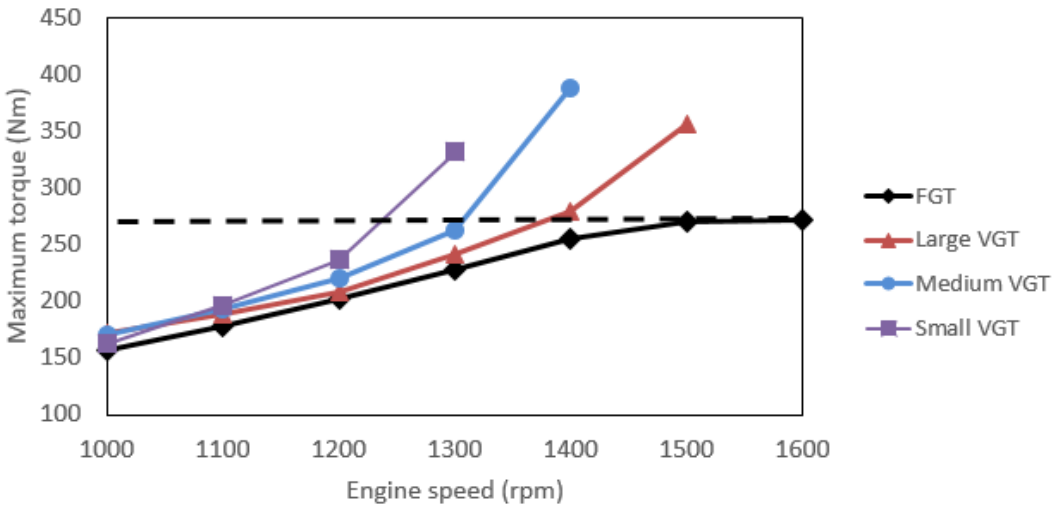

Figure 6.20: Predicted engine low-end torque

It is worth noting that the maximum engine torque achieved with VGTs at low speeds was limited by the compressor surge limit, rather than turbine power. Figure 6.21 shows the simulated compressor operating points of the three VGTs with a series of vane positions. The green point in the plot was the compressor operating point with the FGT and fully closed waste-gate. The FGT turbine power was not sufficient to drive the compressor to the surge limit defined by the compressor performance map data. The engine running line at this engine speed is also plotted. This was based on the assumption of constant engine volumetric efficiency. The maximum compressor pressure ratio was approximately 1.7 with constant engine volumetric efficiency, provided that the turbine was able to deliver sufficient power.

All three VGTs were able to provide sufficient turbine power to drive the compressor to the surge line. However, the maximum level of compressor pressure ratio, and hence the engine torque that could be achieved, varied. As the size of the VGT became smaller, the engine volumetric efficiency increased. Therefore, more air flow could be displaced at the same boost pressure level. Thus, the compressor operating point was shifted to the higher flow region (which could allow a higher pressure ratio). This was because the smaller turbine was operating in a more efficient region (Figure 6.22). This was a result of the turbine vane position being closer to the medium opening position where the VGT optimum efficiency is always found (Figure 6.23).

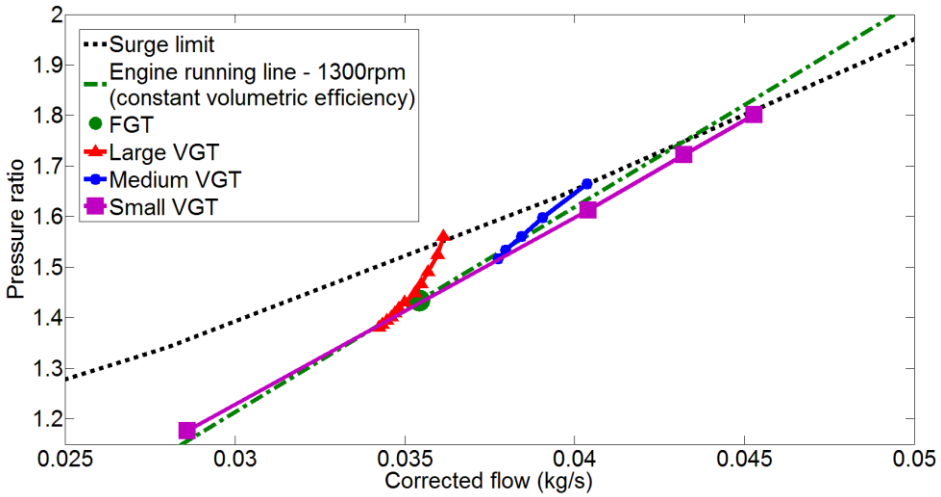

Figure 6.21: Simulated compressor operating points at 1300rpm engine speed

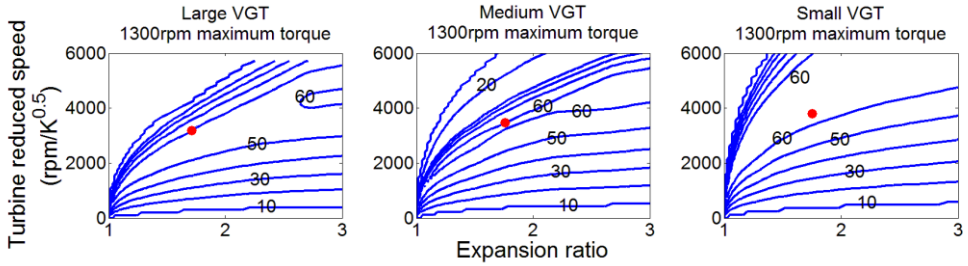

Figure 6.22: Contour plot of turbine efficiency (%) and 1300rpm maximum load

As the vane was closed to increase boost pressure, the vane position of the large VGT and the medium VGT was almost fully closed, whereas the vane position of the small VGT was close to medium opening position where the VGT optimum efficiency is always found. Therefore, the low turbine efficiency of the medium and large VGTs resulted in low engine volumetric efficiency.

Therefore, when VGT matching is performed in the engine design process, the vane position at target engine operating point needs to be close to medium opening position. Nevertheless, turbine scaling might be required when the maximum engine torque level is investigated without the target operating point being known.

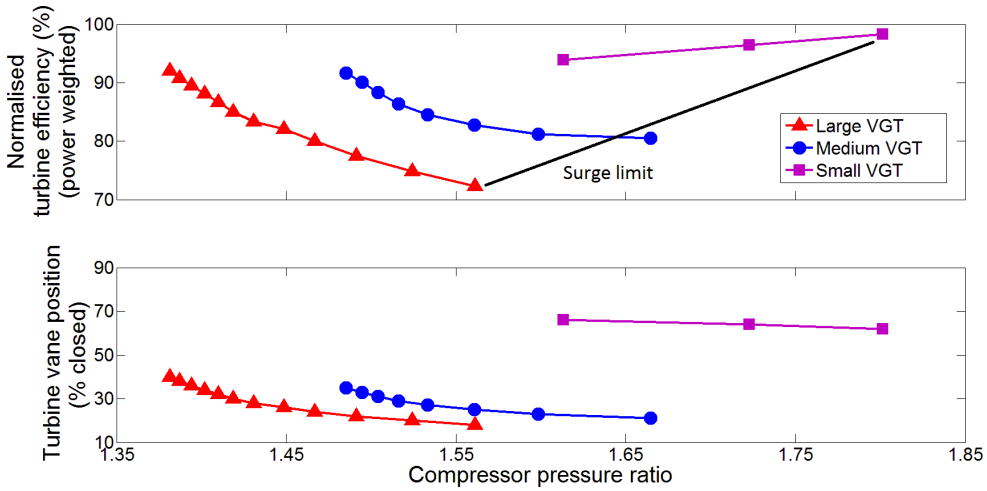

Figure 6.23: Normalised power weighted turbine efficiency and vane position

It is worth noting that the actual compressor surge line may be affected by the measurement condition and the layout of the entire intake air path. Therefore, the actual surge line may be shifted to a higher flow region or a lower flow region. If it were shifted to the original FGT operating point, the potential for using the VGT to drive the compressor to a higher pressure ratio region would be diminished. Nevertheless, this will be dependent on the characteristics of the individual system. In addition, with the technology improvements in compressor map width enhancement, the benefit of using VGT may be extended.

6.3.2.3. Trade-off between low-end torque and fuel consumption

It has been shown that the three VGTs had different characteristics of steady state operation. Thus, they may be used on applications with different targets of fuel consumption and full load profile. In this section, the trade-offs between the attributes will be studied.

Figure 6.24 and Figure 6.25 demonstrate the trade-offs between the engine torque knee point and the engine fuel consumption at high speeds and low speeds. Three levels of cost and packaging challenges are plotted:

1. FGT – Low cost and packaging challenge
2. VGT without waste-gate – Medium cost challenge because of the material requirement of the use of VGT on gasoline engines
3. VGT with waste-gate – High cost and packaging challenges because of the requirement of the use of the additional waste-gate

In Figure 6.24 and Figure 6.25, the optimum system is in the top left corner where the fuel consumption is low and the maximum engine torque can be reached at low speeds. By replacing the FGT with VGT, the torque knee-point and the fuel consumption can be improved at the same time.

The engine torque knee-point can be lowered by 100–250rpm, compared to the FGT: the smaller the VGT used, the lower the torque knee-point. If the VGTs were not assisted by an additional waste-gate, the large VGT offered the optimum fuel consumption at both high speeds and low speeds. However, if the VGTs were assisted with an additional waste-gate, the medium VGT provided the most fuel consumption benefits, because of the optimum turbine matching at full load.

At high speeds, the fuel consumption of the small VGT was worse than the original FGT, due to the insufficient flow range. However, this can be recovered by using an additional waste-gate. The additional waste-gate offered another 0.15-0.25% fuel consumption benefit at low speeds and 1% to 2.5% fuel consumption benefit at high speeds.

Trade-offs are shown in this comparison. The knee-point of the small VGT was the lowest. This was achieved at a cost of a fuel consumption deficit, compared to the medium VGT. The selection criteria for the engine system are summarised in table 6.5. The predicted fuel consumption benefit was a result of the reduction in engine pumping work. According to the results presented in previous sections, the benefit due to the changes in combustion phasing, which was not taken into account in the turbine matching, was likely to offer additional fuel consumption benefits.

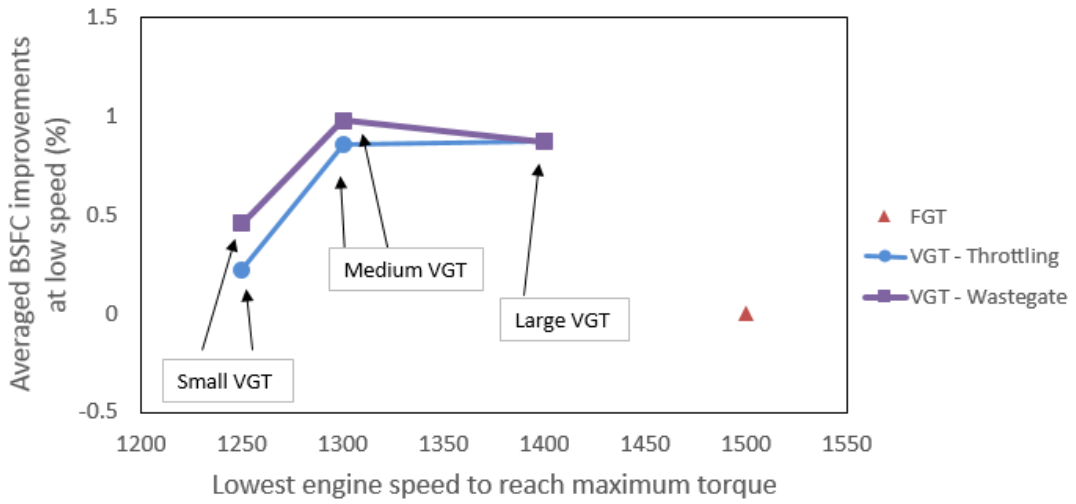

Figure 6.24: Trade-off between torque knee-point and fuel consumption at high speeds

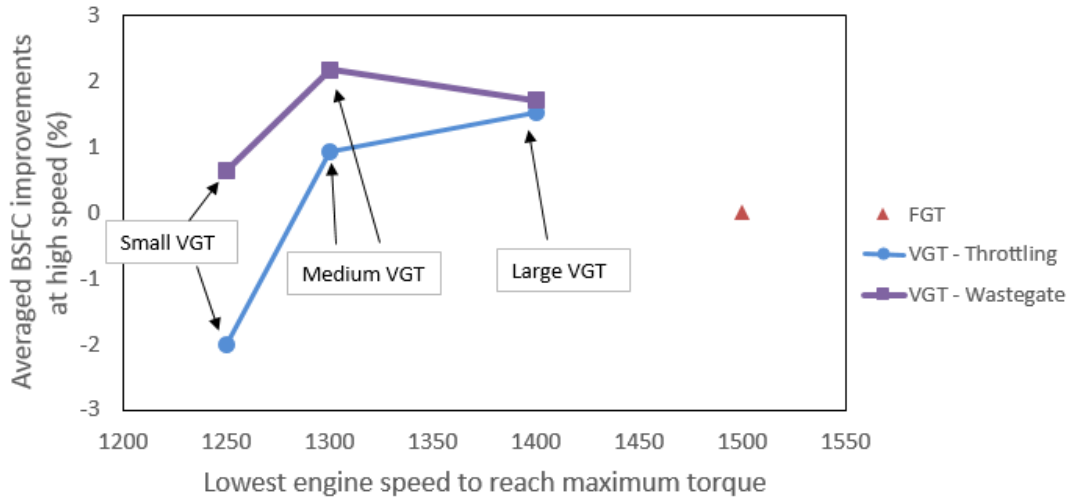

Figure 6.25: Trade-off between torque knee-point and fuel consumption at high speeds

In addition, the optimisation of the transmission and the entire powertrain was not considered in this study. The improvement of torque knee-point and drivability can provide additional benefits from further downsizing and down-speeding the system. When the entire powertrain is designed, this should also be taken into account.

It is shown that, if the large VGT is used, both low-end torque and fuel consumption can be improved at the same time. If low-end performance is prioritised for the application, the matching can be shifted to the smaller turbine to improve the knee-

point, by sacrificing some of the benefits at the top-end, while it can still be more efficient than the FGT. Therefore, matching the VGT was more flexible than matching the FGT. This was because of the flexibilities in the flow range and characteristics of the VGT. Besides the trade-off between fuel consumption improvement and the level of engine down-speeding, another potential of using a small VGT is the transient response due to the low inertia and better turbine efficiency at low flow region. This will be investigated in the next chapter.

Table 6.5: VGT selection criteria based on steady state performance

	VGT selection – cost level 1 (not equipped with waste-gate)	VGT selection – cost level 2 (equipped with waste-gate)
Best fuel consumption at all speeds	Large VGT	Medium VGT
Best fuel consumption at low speeds (for drive cycles)	Medium VGT	Medium VGT
Best low-end torque (fuel consumption not worse than FGT)	Medium VGT	Small VGT
Best low-end torque	Small VGT	Small VGT

6.4. Conclusions

In this chapter the steady state behaviour of the FGT and the VGT turbochargers were investigated and compared. While the experiments provided a fundamental understanding of the comparison, simulations were carried out to obtain results that cannot be achieved in experimental testing. Therefore, the use of both experimental and simulation data improved a thorough understanding of the system. The key findings of this chapter are listed below:

1. By using fuel enrichment, the gas temperature at turbine inlet at the two engine operating points tested (1600rpm, 200Nm and 2800rpm, 150Nm) can be reduced by 50°C, at a cost of 7.9% and 8.6% of engine fuel consumption. This was a result of 36.2% and 41.9% of the fuel consumption deficit being offset by advancing the spark timing in the extra operating window. For a 50°C rise in TIT limit, the achievable engine load limit can be extended by 2.44bar BMEP.

2. In addition to the fuel consumption deficit, exhaust emissions are also affected under over-fuelling conditions. On the engine tested in this project, fuel enrichment was not required in the engine operating range of the NEDC. Nevertheless, a wider operating range will be covered in future drive cycles which means that the level of fuel enrichment should be minimised. The fuel enrichment should only be used in limited window, such as the peak power operating region.

3. From experimental data, the maximum engine torque at 2000rpm achieved with the VGT was 317Nm, 48Nm (17.7%) higher than that achieved with the FGT. The knock-limited spark timing can be advanced by up to 3 degrees crank angle, due to the lowered exhaust manifold pressure and improved engine scavenging process.

4. According to experimental results at 2000rpm, the engine fuel consumption was improved by 4% by replacing the FGT turbocharger with the VGT turbocharger. A 2.3% fuel consumption improvement was estimated in the simulation, of which 0.6% was from the reduction of pumping work. This was a result of higher VGT system efficiency due to the elimination of waste-gate. 1.5% of the improvement was from the changes in combustion phasing due to extended spark timing window, while the remaining 0.2% improvement was because of the change in the compressor hardware which was irrelevant to VGT technologies.

5. A matching criteria was developed to investigate the full potential of VGT over FGT. Three VNTs with different sizes were selected and used in engine

simulation. It was found that both the low-end torque and the fuel consumption can be improved when compared to the FGT.

6. According to simulation results, a maximum fuel consumption improvement of over 3.1% was seen due to reduction in engine pumping work. This was found at the peak power operating point where a large amount of exhaust gas flow was by-passed on the FGT. The engine torque knee-point can be advanced by up to 250rpm.

7. Trade-off between improvements in fuel consumption and the knee point of the engine torque was found. A criteria was summarised for the selection of VGT turbine size and configuration based on steady state performance.

8. A novel configuration of variable nozzle type VGT turbocharger assisted by an additional waste-gate was proposed. The use of the additional waste-gate improved the average fuel consumption by up to 2.5% at high speeds, whilst the improvement in low-end torque was maintained.

9. The use of VGT enabled further downsizing of gasoline engines. Additional fuel consumption benefits can be achieved by optimising the driveline.

10. In order to further improve the use of VGT on gasoline engines and to utilise its full potential, larger maximum flow capacity will be required. This will improve the optimisation of the VGT turbocharger on gasoline engines.

Chapter 7 - *Transient behaviour*

In parallel to the work presented in chapter 6, the transient behaviour of the engine are shown in this chapter. The optimisation of the transient response of VGT has been performed in both experiments and simulations. The results of the experiments and simulations are presented in the first and second sections, respectively.

A thorough investigation of the transient behaviour of VGT demonstrating the fundamentals of the responses are discussed in the third section. The VGT behaviour at three different stages during transients has been analysed.

In the last section, the effects of the size of VGT on performance are shown. This leads to the conclusions of the comparison between FGT and VGT, and the trade-off between steady state performance and transient response.

The work presented in this chapter was in part presented at the 11th International Conference on Turbochargers and Turbocharging in London, 2014 [130].

7.1. Optimisation of transient response in experiments

7.1.1. Experimental approach

The same VGT turbochargers used in the steady state experiments were also tested in transient experiments. The experiments were performed at one engine speed, 2000rpm, which was close to the engine torque knee-point.

In order to study the effect on transient engine operation unconstrained by possible deficiencies in the feedback controller, a series of open loop VGT actuator trajectories generated in dSpace were used to control the VGT position. The blow-off valve on the compressor housing was deactivated to avoid variations in the compressor operating point before tip-in.

To eliminate the interaction between the turbocharger and the valve timing, the intake and exhaust valve timings were kept at the maximum overlap positions in the transient test. The Lambda target was maintained at 1, and the original production level spark timing control strategy was used. Before the start of each transient test, the engine was settled at 2 bar BMEP for five minutes. At tip-in, the throttle was fully opened and the open-loop VGT transient trajectory was also triggered at the same time. The coolant temperature at engine outlet and the air temperature at intercooler outlet were maintained at approximately 90˚C and 30˚C, respectively.

To determine the VGT position before tip-in, the steady state fuel consumption and turbocharger speed at three VGT positions, 16% closed (fully open), 60% closed and 90% closed (fully closed), were tested at 2 bar BMEP 2000rpm. The averaged fuel consumptions at the three operating points were the same, considering that the accuracy of the measurements is ±0.05% [131]. However, the averaged turbocharger speeds at the three VGT positions were 7.7krpm, 12.9krpm and 19.3krpm, respectively. Therefore, the VGT position that provided the highest turbocharger speed at low load was chosen for the VGT before transient trajectory was triggered.

The aim of this experiment was to analyse the transient behaviour of the engine in the first 1.5 seconds, which is crucial to the engine transient response. Therefore, the time required to reach 50% of maximum torque rise (T_{50}) and the turbocharger acceleration were the two key measurements for the comparison. As it was necessary to have more than two stages in the transient to optimise the dynamic response of the system, the limit of the number of tests, and the VGT actuator response time, it was decided that the 1.5 second period would be divided into three 0.5 second stages, each of which had a number of optional VGT positions. In order to define the boundaries for the VGT positions in the transient operation, a range of VGT actuator trajectories with single step change from fully opened to fully closed have been tested:16% fully open, 40% closed, 60% closed, 70% closed, 75% closed, 80% closed, 85% closed and 90% fully closed (Figure 7.1).

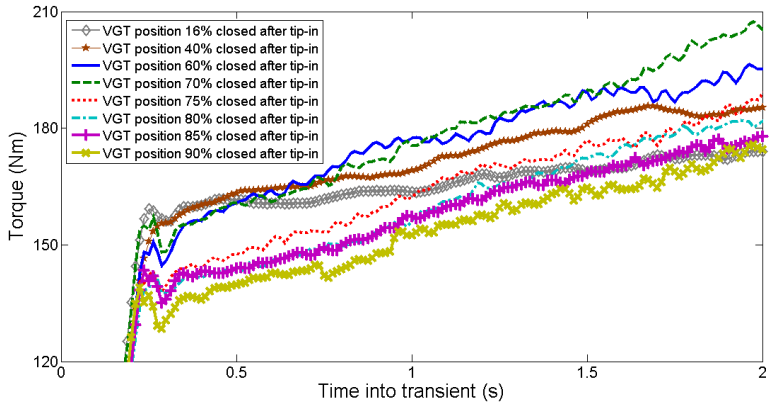

Figure 7.1: Torque responses of single step change VGT actuator trajectories

It was found that with the VGT position between 60% and fully closed after tip-in, 1.1 bar boost pressure downstream of the compressor can be achieved at 1.5 seconds into transient. In addition, although T_{50} (178Nm) cannot be achieved within 1.5 seconds with the VGT position 80%, 85% and 90% closed, these three VGT positions were still selected as options because of the potential for increasing the acceleration of the turbocharger. Therefore, six different VGT positions (from 60% to 90% closed) were selected as optional openings at each one of the three transient stages after tip-in. Thus, a full factorial DOE of 216 transient tests was carried out in the experiments.

7.1.2. Experimental results

7.1.2.1. Response of engine brake torque

The engine brake torque response for six tests with different VGT positions at the second stage (0.5–1.0 seconds) are compared in Figure 7.2. The VGT position described in Figure 7.2 and the following figures in this chapter as, for example, 90-60-60-75, is defined as follows: the VGT setting before tip-in, VGT setting at first stage (0.0–0.5 s), VGT setting at second stage (0.5–1.0 s), and VGT setting at third stage (1.0–1.5 s). The comparison of torque response at the second stage is also shown in Figure 7.3. The VGT positions in the first stage and third stage in the six tests were not varied. The torque and turbocharger speed variations at the end of the first stage were within ±0.6% and ±2.1%, respectively. However, the maximum difference in torque at the second stage was up to 17.8Nm (14.1%).

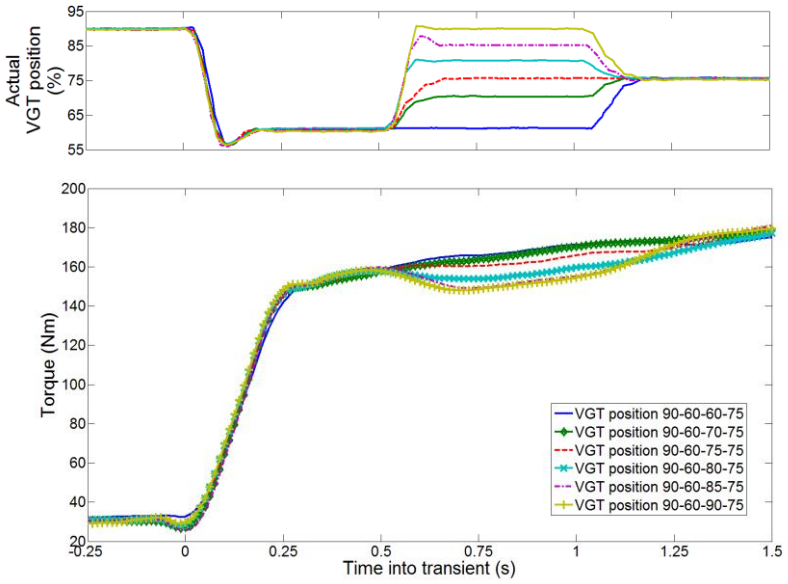

Figure 7.2: Torque responses of the six tests with different VGT settings; the measured torque has been smoothed using 10-points smoothing

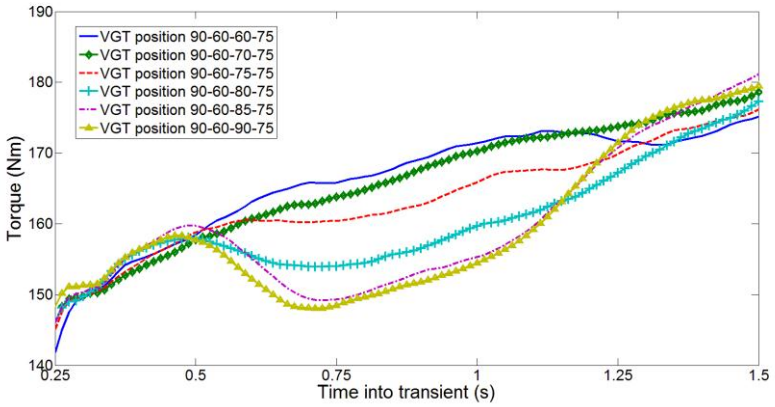

Figure 7.3: Torque responses at the second stage (0.5 – 1.0 s); the measured torque has been smoothed using 10-points smoothing

With the VGT 90% closed in the second stage, the torque dropped immediately after the vane was closed and resulted in restriction in the exhaust system. The instantaneous turbine inlet pressures are shown in Figure 7.4. With 60% closed VGT, the turbine inlet pressure was approximately 0.2 bar lower than that with fully closed VGT. This resulted in a lower turbine total-to-static pressure ratio and higher engine volumetric efficiency (Figure 7.5). The calculated volumetric efficiency was approximately 0.2 seconds delayed compared with the turbine pressure ratio, due to the damping effect of the air-path between the cylinder and the flow sensor.

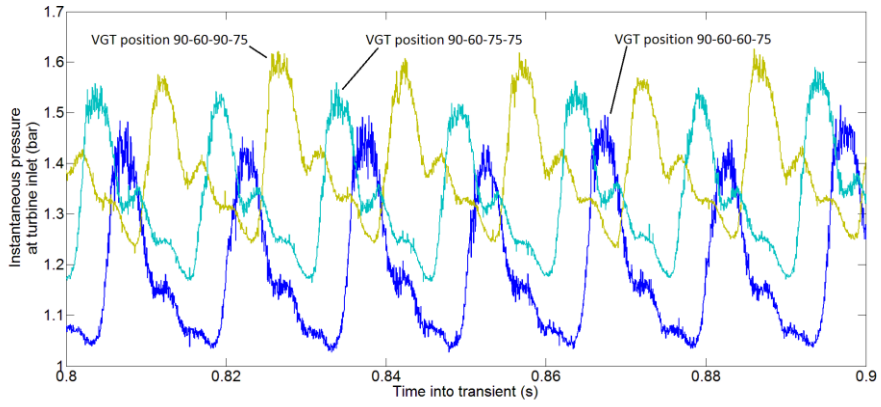

Figure 7.4: Instantaneous turbine inlet pressures at the second stage of three tests

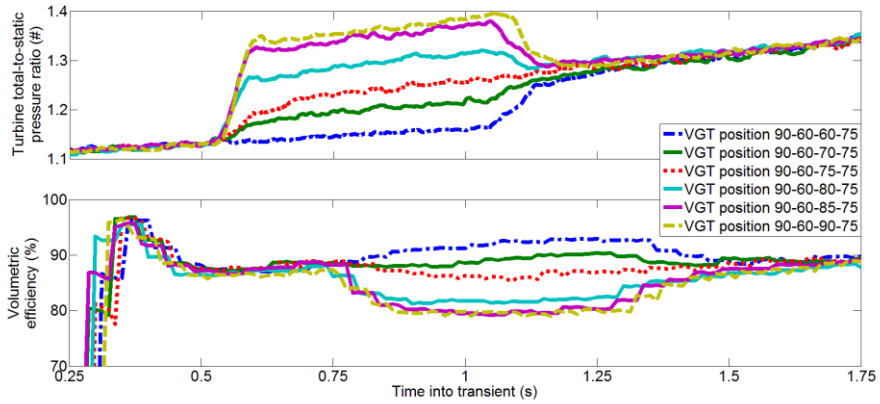

Figure 7.5: Turbine total-to-static pressure ratio and engine volumetric efficiency

However, the turbocharger acceleration rate was 8.8%, lower than that with fully closed VGT. In addition, a torque drop can be observed when the VGT was returned to 75% closed at the third stage, and approximately 0.35 seconds was required to recover this torque drop. This was not acceptable in terms of drivability. Compared with other trajectories, the slow torque rise at the third stage was also a result of the low turbocharger acceleration at the second stage. This delay was approximately 0.2 seconds at 1.5 seconds after tip-in.

Therefore, a clear trade-off between the torque rise and turbocharger acceleration is seen, which affects the torque response at the next stages in the transient event. The optimised trajectory is also constrained by the drivability requirements.

7.1.2.2. Response of turbocharger speed

On turbocharged gasoline engines, the engine torque response is largely affected by the acceleration of the turbocharger. Therefore, the turbocharger acceleration rate was investigated.

At each of the three stages in the transient tests, for the tests with the same VGT setting, first order and second order curves were fitted to the turbocharger speed entering the stage and the turbocharger speed at the end of the stage. A typical fitting at the third stage with the VGT 75% closed is shown in Figure 7.6: the R^2 of the first

order fitting and second order fitting are 0.9476 and 0.9478, respectively. No significant difference between the first order and the second order fitting was observed. The fittings at other stages with different VGT settings show similar trends, and they are not presented.

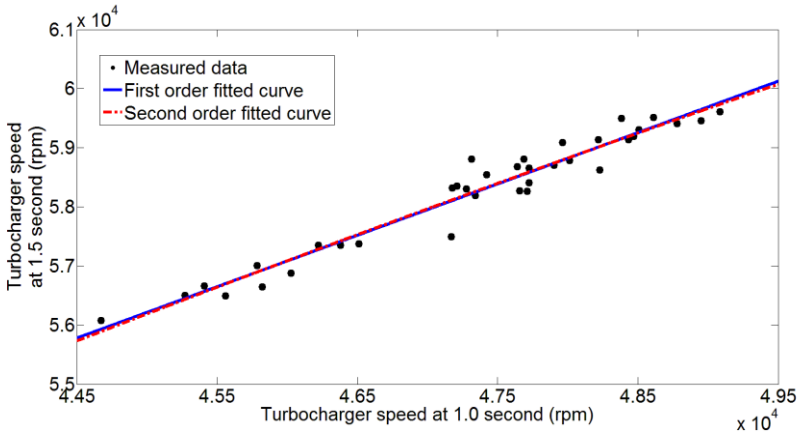

Figure 7.6: Fitted responses of the turbocharger speed at 1.5 s and turbocharger speed at 1.0 s with VGT 75% closed

Therefore, the rise in turbocharger speed at each 0.5-second stage in the first 1.5 seconds was dependent on the turbocharger speed at the time of entering the stage and the VGT position at the stage: this relationship was relatively linear. Therefore, the turbocharger acceleration could be split into linear stages, provided that the duration of each stage was short. The chosen stage duration, 0.5 seconds, was small enough to optimise the transient operation.

This was a demonstration of the fact that the turbocharger acceleration at each stage during transient needs to be optimised in order to achieve the fastest overall turbocharger response of the transient.

7.1.2.3. Optimisation of the transient operation

Two parameters were chosen for the optimisation of the transient operation: engine torque rise and turbocharger acceleration. The engine torque rise was selected because this was the output of the engine. The turbocharger acceleration was also selected because time to reach 90% of maximum torque rise (T_{90}) cannot be reached within 1.5 seconds, and the turbocharger acceleration during the first 1.5 seconds

needs to be optimised to provide high turbocharger speed when entering the next transient stage.

Firstly, the response in the first 0.5 seconds was analysed. The elliptical 50% probability regions of torque and turbocharger speed rises in the first 0.5 seconds have been plotted in Figure 7.7. The shape of the ellipse was calculated assuming bivariate normal distribution. This was achieved by solving the eigenvalue of the covariance, which represents the length of the two axes of the ellipse, and the eigenvector of the covariance, which represents the direction of the two axes.

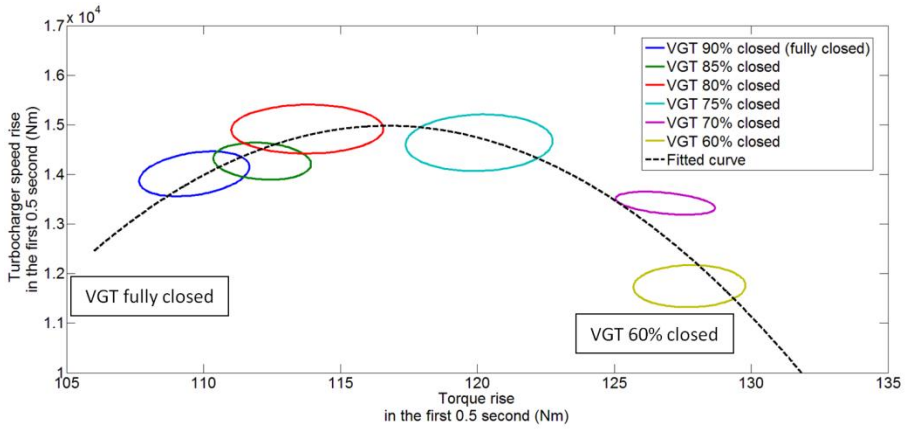

Figure 7.7: Response curve between the turbocharger speed at the end of the first stage and the torque rise in the first stage. The ellipses shown in the figure represent the 50% probability region of the distribution of the data having the same VGT position at the first stage

Each one of the six groups of data represents the test result of 36 different VGT actuator trajectories that had the same VGT position in the first 0.5 seconds. Therefore, the size of the circles represents the level of the experimental error. Overlap between the groups can be observed because the VGTs were close to fully closed position. Nevertheless, only four test points in total were outside the 75% probability regions. Therefore, the repeatability of the test was acceptable.

A second order polynomial curve has been fitted to the mean values of torque and turbocharger speed rises of the six data groups. The non-linear response of the VGT turbocharger has been illustrated. Fully closing the VGT was not beneficial to either the torque rise or the turbocharger speed rise. Therefore, although the VGT

turbocharger is flexible in reducing the effective area and accelerating the exhaust gas velocity, fully closed was not an optimum VGT position for the first 0.5 seconds of the transient. This may be a result of low turbine efficiency at fully closed VGT position. However, it was difficult to calculate the turbine efficiency in a transient test due to the response time of the thermocouples and the heat transfer effect on the turbocharger. This will be further investigated in simulations in the next sections.

It is also shown that, because of the non-linearity of the VGT turbocharger, overshoot in VGT position feedback control may result in both slow turbocharger acceleration and slow torque response. In addition, the controller output may converge to unwanted values, for example, fully closed. Thus, to enable the use of the VGT turbocharger on gasoline engines, advanced control strategies may be necessary.

On the other hand, opening up the VGT position to below 60% closed only gave marginal benefit on the torque rise at the first stage, and the turbocharger speed rise significantly deteriorated. Therefore, the calibration of the strategy depends on the requirement of the transient operation, which can be either a fast torque rise or fast turbocharger acceleration at the first stage.

Secondly, the VGT positions at the second and third stage were investigated. In Figure 7.8, the turbocharger speed at 1.5 seconds is plotted against T_{50}. Tests in which 50% of the maximum torque rise cannot be reached within 1.5 seconds are not shown. A Pareto optimal front was drawn. It was found that the highest Pareto efficiency could not be achieved with a VGT position of 60% (yellow rectangular) or 90% (blue dot) closed at the first stage. With the VGT 60% closed at the first stage, the Pareto optimal front cannot be reached because the rise of turbocharger speed, and hence boost pressure, was slow. With the VGT 90% closed at the first stage, the turbocharger acceleration was delayed due to too much VGT closure (Figure 7.7). As the turbocharger speed at 1.5 seconds strongly affects the time required to reach higher torque (for example, 90% of maximum torque rise), it is likely to cause a slow torque response at a later stage in the transient, if the VGT position is fully closed or lower than 60% closed.

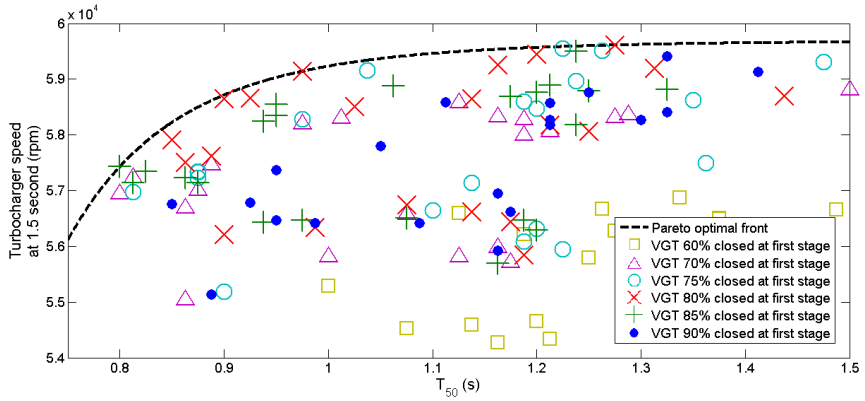

Figure 7.8: Trade-off between the turbocharger speed at 1.5 s and T_{50}

The Pareto optimal curve was divided into three regions (Figure 7.9). In region 1, the turbocharger speed at 1.5 seconds was relatively low but the T_{50} was fast. The fast T_{50} was achieved by opening the VGT to 60% closed at the second stage to release the restriction in the exhaust system and to allow the 50% of maximum torque rise to be reached within 1 second. A significant torque drop can be observed in the torque responses of the majority of trajectories in region 1 (Figure 7.10), due to the closing of the VGT to accelerate the turbocharger after T_{50} was reached. With all the possible VGT settings at the third stage, the turbocharger speed cannot recover from the losses due to the opening of the VGT at the second stage.

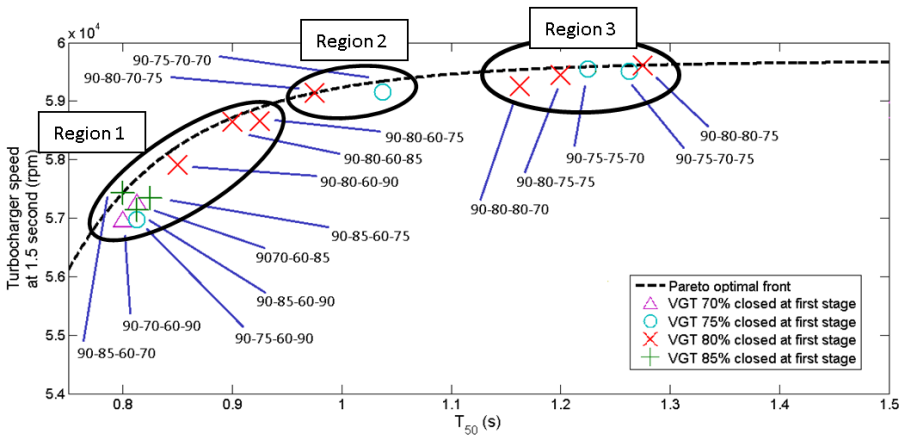

Figure 7.9: Pareto optimal front of the trade-off between turbocharger speed at 1.5 s and T_{50}

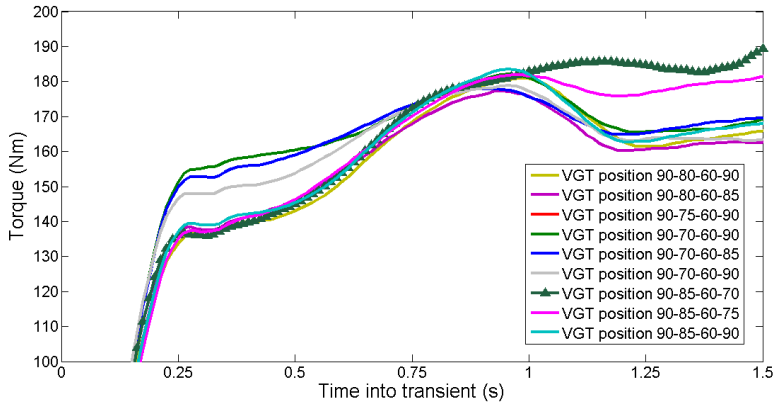

Figure 7.10: Torque responses of trajectories in Pareto optimal curve region 1

In region 2, the two trajectories were with intermediate VGT position (80% and 75% closed) at the first stage. The VGT was opened to 70% after T_{50} was reached. No torque drop was observed.

In the third region of the Pareto optimal curve, the turbocharger acceleration was maximised. Therefore, the VGT was kept between 80% and 75% closed in most of the trajectories in region 3. This matched the trends demonstrated in Figure 7.7. The highest turbocharger speed at 1.5 seconds was achieved in this region, although the torque rise was slower.

Thus, the trade-off between the turbocharger speed at 1.5 seconds and T_{50} has been shown. It was possible to optimise the transient VGT control strategy such that:

a. The minimum T_{50} was achieved by opening up the VGT and releasing the restriction in the exhaust system. However, the turbocharger acceleration was deteriorated and this cannot be offset at later stages.

b. The VGT was set to the opening optimised for turbocharger acceleration at the first stage, and it was then opened slightly to allow both acceptable turbocharger acceleration and torque build up.

c. The VGT position was kept at the opening optimised for turbocharger acceleration until the target turbocharger speed was reached. This resulted in

slower response of engine brake torque at early stages during transient.

Table 7.1 presents the optimisation criteria for the VGT actuator trajectories, targeting different requirements of the transient operation. It was found that, despite the flexibility of fully closing the VGT and reducing the effective area to accelerate the exhaust gas and increase the kinetic energy, the turbocharger acceleration and torque response cannot be benefitted by fully closing the VGT at all three stages. In order to achieve fast transient response, the VGT position at all stages needs to be optimised.

The torque responses of optimised VGT actuator trajectories are compared with a single-step-change VGT actuator trajectory (fully closed before tip-in and 75% closed after tip-in), as shown in Figure 7.11. The T_{50} was reduced by up to 47.1%, although the torque rise in the first 0.5 seconds and the turbocharger speed at 1.5 seconds were slower. If the turbocharger speed at 1.5 seconds was not prioritised, the T_{50} could be improved by 35.5%. The turbocharger speed at 1.5 seconds could be improved by up to 0.5krpm, while the T_{50} could still be improved by 16.5%. By pursuing the fastest torque build-up in the first 0.5 seconds, the T_{50} improvement was limited to 33.9% and the turbocharger speed at 1.5 seconds was also lowered by 6.4%.

This highlighted the necessity of implementing an appropriate transient control strategy that prioritised the turbocharger acceleration only when it was required: for example, when the turbocharger speed corresponding to the target engine brake torque was higher than the current turbocharger speed. Therefore, if the demanded engine torque was within the naturally aspirated region, the engine torque response should be prioritised.

From the experimental results, it seems that the VGT position of 75%-85% closed was the optimum for turbocharger acceleration at all three stages. In order to investigate the transient response in more detail, simulation investigation was necessary because the repeatability of the experimental results is never perfect. In addition, the reliability of the test results may result in challenges in interpreting the

data due to, for example, the response time of the thermocouple.

Table 7.1: Comparison of the optimised strategies

	Requirements of transient response			
	Fast torque response in the first 0.5 seconds	Fastest T_{50}	Fast T_{50} and high turbocharger speed at 1.5 seconds	Highest turbocharger speed at 1.5 seconds
VGT position at first stage	60% closed	75% - 85% closed	75% - 85% closed	75% - 85% closed
VGT position at second and third stage	60% closed before T_{50} is reached	60% closed before T_{50} is reached	70% closed before T_{50} is reached	75% - 80% closed
Improvement of torque rise in the first 0.5 seconds	14.4 Nm (10.6%)	-2.5 Nm (-1.8%)	-	-
T_{50} improvement	0.51 s (33.9%)	0.71 s (47.1%)	0.54 s (35.5%)	0.25 s (16.5%)
Improvement of turbocharger speed at 1.5 seconds	-3.8 krpm (-6.4%)	-1.7 krpm (-3.8%)	-	0.5 krpm (0.9%)

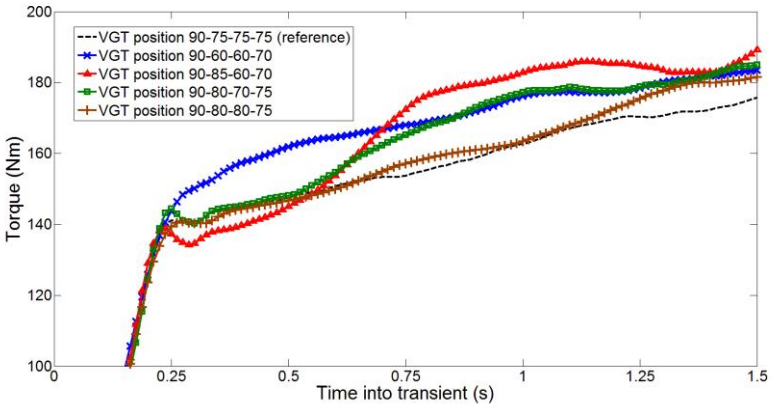

Figure 7.11: Comparison of the optimised trajectories and the reference trajectory

It should be noted that the duration of the three stages in the transient was 0.5 seconds, and the intervals between the optional VGT positions were 5-10%. Therefore, larger improvement might be achievable if a smaller time step and VGT position interval were used.

7.2. Optimisation of transient response in simulations

Using the calibrated 1-D engine model, simulations were carried out to understand the experimental data by investigating the parameters that cannot be measured easily. The same full factorial DOE for VGT open-loop trajectories was performed. The turbine maps collected from the on-engine mapping facility were used in this simulation.

The simulation result has been validated against experimental data, and it has been discussed in Chapter 5. In transient simulations, 5 seconds were given for the engine to settle down before tip-in. The engine speed was kept at 2000rpm constant, and the initial engine torque was set to 2 bar BMEP. A throttle controller was used to maintain the engine load. After tip-in, the throttle was fully opened.

To perform transient simulation, the maps of the combustion heat release profile and the Lambda setting (which were mapped based on engine speed and torque) were re-mapped based on engine mass air flow and engine speed. For the calculation of the valve timing, the engine volumetric efficiency was used to convert the engine air flow into relative air charge, which was then used to look up the valve timings during transient.

Figure 7.12 shows the key parameters of the turbine and the engine during the transient simulation at 2000rpm. Among the three transients shown in the graph, the VGT position 75% closed offered the fastest turbocharger acceleration. This was because of the high turbocharger shaft power imbalance due to the high turbine power. Since the turbine power was a function of turbine expansion ratio, mass flow and efficiency, the high turbine power was not a result of a single parameter, but a result of the optimisation of these parameters. Due to the effect of engine volumetric

efficiency, the high turbine expansion ratio resulted in low mass flow, assuming that the compressor pressure ratio remained the same. In addition, the turbine efficiency is also dependent on the VGT position. The turbine efficiency is always low at extreme opening or closing positions. Therefore, the optimum VGT trajectory was dependent on the optimisation of the turbine expansion ratio, the engine volumetric efficiency and the turbine efficiency.

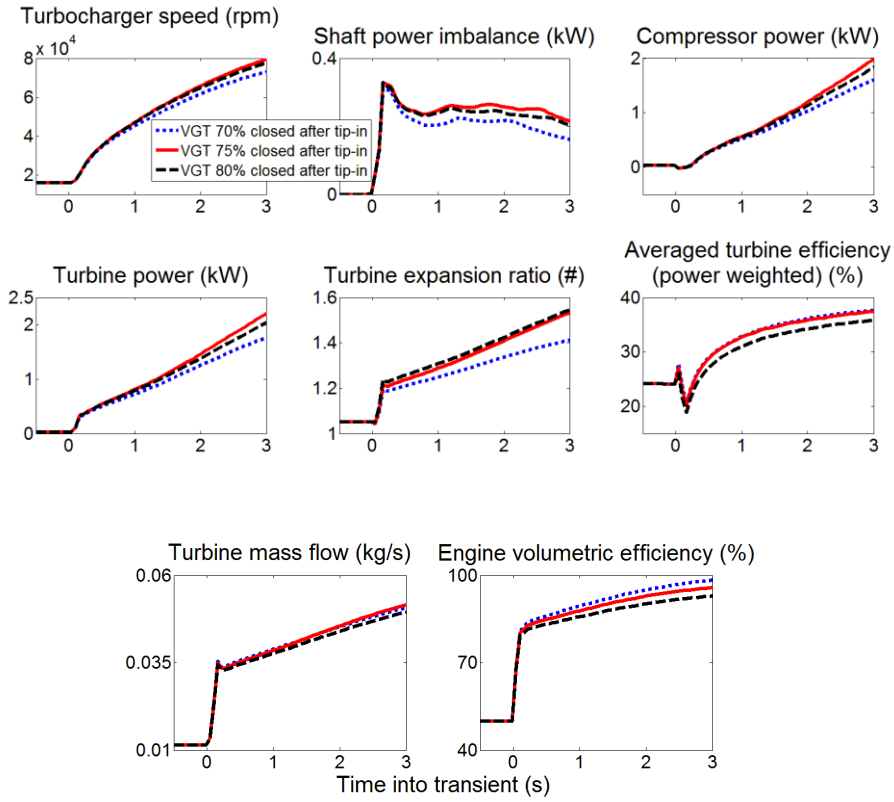

Figure 7.12: Simulated responses of the turbocharger and engine during transient

The trade-off between the turbocharger speed rise and engine torque rise are plotted in Figure 7.13 and Figure 7.14. Figure 7.13 shows the simulated results of all the VGT trajectories with 70% closed in the first 0.5 seconds after tip-in. It is shown that the effect of increasing the VGT closing percentage on the turbocharger acceleration rate was non-monotonic. In order to achieve the highest turbocharger speed at 1.5 seconds, the optimum VGT position at second and third stage during the transient was 75% closed. Closing the VGT too much resulted in low engine volumetric efficiency and low turbine efficiency, which offset the benefits offered by the high

turbine expansion ratio.

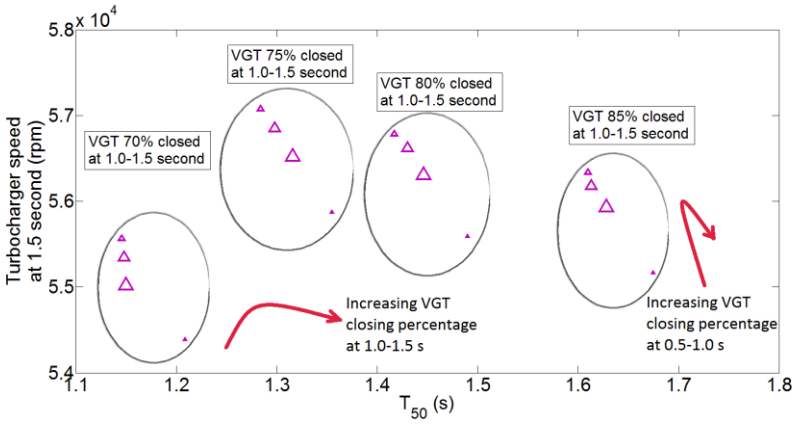

Figure 7.13: Simulated turbocharger acceleration against T_{50} (VGT 70% closed at first stage in transient)

Figure 7.14 shows the simulation results of all the VGT trajectories with different VGT settings at the first stage. The shape of the marker in the graph represents this additional dimension: the VGT setting at the first stage. It is shown that the trends are the same as those shown in Figure 7.13. The optimum turbocharger acceleration was achieved with the VGT 75% closed at the first stage. Further closing the VGT did not provide faster acceleration.

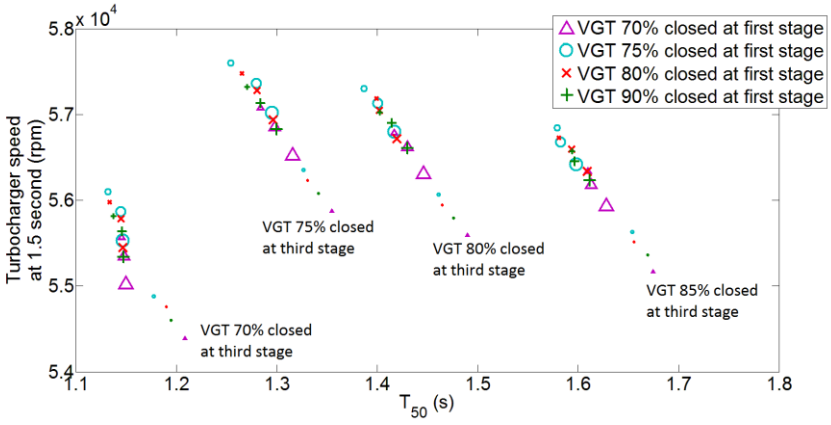

Figure 7.14: Simulated turbocharger acceleration against T_{50} (all VGT openings at first stage in transient)

Varying the VGT position at the first stage in the transient seems to have added a shift in both the x axis and the y axis. The shift was a result of the variation of the initial condition at the second stage. A higher turbocharger speed entering the second stage was beneficial to both further turbocharger acceleration and torque rise, due to

the larger air flow to the engine at higher turbocharger speed.

Figure 7.15 shows a comparison between the simulated results and the experimental data. There was an offset between the two data sets. In addition, the experimental data covered a wider range. The offset was a result of the simulation accuracy, and the wider range that the experimental data covered was because of experimental error. Therefore, in order to obtain thorough understanding of the behaviour, both the simulation and experimental results are necessary.

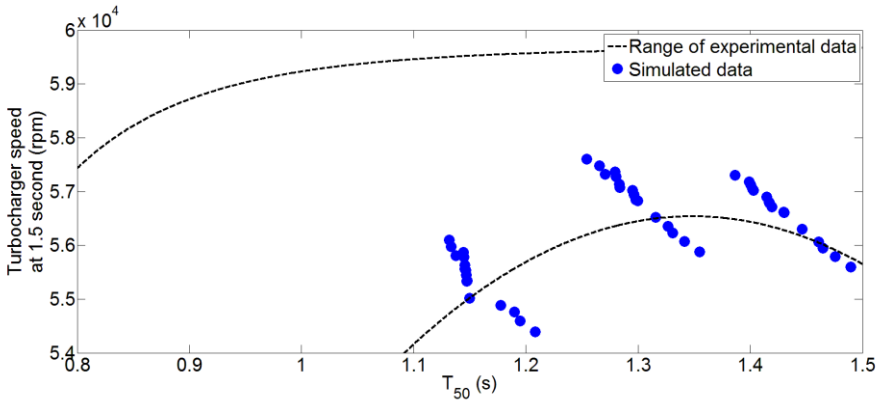

Figure 7.15: Comparison between experimental data and simulation results

Based on the simulation results, the selection of the VGT position during transient should depend on the optimisation of the engine volumetric efficiency and turbine power. Although the VGT positions simulated were discrete, it was clear that the optimum VGT position for the fastest turbocharger acceleration at the first 1.5 seconds at 2000rpm was around 75% closed for this particular turbocharger.

If the fastest T_{50} was pursued, the optimum VGT trajectory needed to be 75% closed for the fastest turbocharger acceleration, until the target turbocharger speed was reached, with the VGT position set to approximately the steady state opening corresponding to the target torque. This was well correlated to the strategy summarised using the experimental data.

It is worth noting that both the turbocharger response and the T_{50} of the original FGT turbocharger were faster than the VGT at 2000rpm. The turbocharger speed at 1.5

seconds and the T_{50} achieved with the FGT were 86.5krpm and 0.82 seconds, respectively. However, the comparison was subject to the matching of the turbine and the available hardware in the experiments. Therefore, detailed understanding of the VGT response during transient and investigation of the effect of the turbine matching on engine response are necessary.

7.3. Investigation of transient response

In this section, transient simulations are analysed to understand the behaviour of three VGTs with different sizes selected and investigated in the last chapter (turbine A – large diameter, turbine B – medium diameter, and turbine C – small diameter). This is to obtain a comprehensive understanding of the effects of turbine matching on engine behaviour.

The settings in the simulation were kept the same as those used in the transient simulation described in the previous section, except that the turbine maps were replaced. In addition, the simulation time was extended from 1.5 seconds to 4.5 seconds, comprising three 1.5-second stages. The vane position for each VGT at the initial operating condition before tip-in was determined as the VGT opening that provided the same fuel consumption rate as FGT at 2 bar BMEP.

Firstly, the small VGT was used and analysed in transient simulation at 1500rpm. In order to determine the optional VGT positions for DOE, a series of single step change VGT trajectories were used in simulation. The VGT position was set to 30% closed at initial condition, and the VGT position after tip-in was varied between 50% and 100% closed, with a step of 5%.

The simulated responses of the engine torque and turbocharger speed are shown in Figure 7.16. It is shown that fully closing the VGT resulted in poor engine torque response due to the negative effect on engine breathing, and it was not beneficial to turbocharger acceleration either, because of the small mass flow through the turbine. Closing the VGT to 50% closed improved the response in the naturally aspirated region, however, this was not beneficial to either the engine torque rise or the

turbocharger acceleration at a later part of the transient. Among the five simulations shown in Figure 7.16, VGT setting 60% closed provided the highest engine torque at the end of transient, and the VGT setting 80% closed provided the highest turbocharger speed at the end of transient.

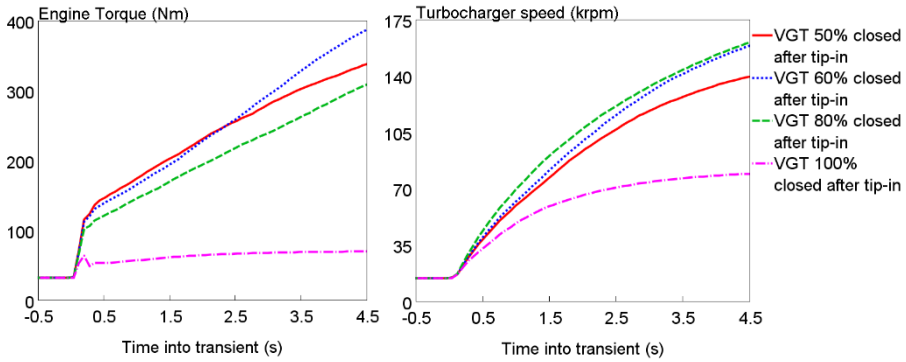

Figure 7.16: Simulated response of engine torque and turbocharger speed (Small VGT, 1500rpm)

Figure 7.17 shows the turbocharger speed rise at each 1.5-second stage. It was found that, unlike the transient simulation results presented in the last section, the optimum VGT position for the fastest turbocharger speed rise at each stage varied between stages. The VGT position marked in black represents the VGT position that provided the highest turbocharger speed rise at each 1.5-second stage. However, since the VGT trajectories used in the simulation were single step changes, the initial condition at the start of a stage was the end condition of the previous stage with the same VGT setting. For example, the highest turbocharger speed rise at the second stage was with the 60% closed VGT position in the entire transient simulation. If the VGT position was 80% at the first stage, the selection of the VGT position at the second stage might not be 60% closed.

Therefore, in order to investigate the transient responses in more detail, a full factorial DOE of the VGT trajectories was also performed for the small VGT at 1500rpm. According to the simulation results of the single step change VGT trajectories, the optional VGT positions for each one of the three stages were chosen as 55% closed, 60% closed, 65% closed, 75% closed, 80% closed and 85% closed. Thus, the DOE of the VGT trajectories was formed of 216 different combinations of

VGT positions. The complex behaviour of the engine system has studied to understand the variations of the optimum VGT position between stages during transient.

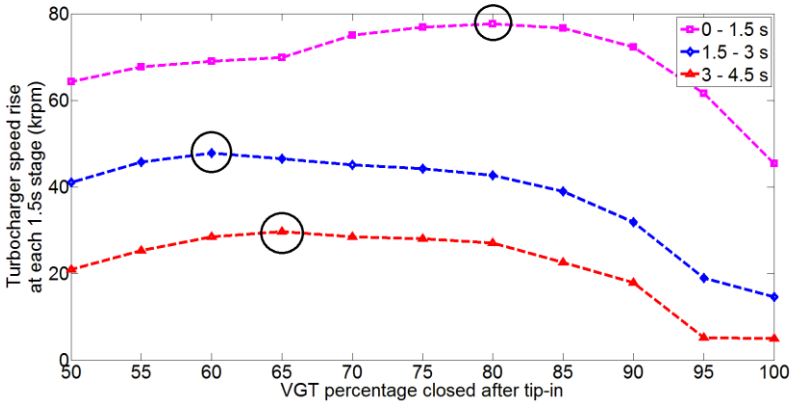

Figure 7.17: Transient simulation results of single step change VGT trajectories (Small VGT, 1500rpm)

Figure 7.18 shows the turbocharger speed rise at each stage in the DOE for the transient simulation. The VGT positions marked by the solid black circle were the optimum VGT positions from the single step change simulations, while the VGT positions marked by the dotted black circle were the optimum positions from the full factorial DOE simulations. Since the initial condition before tip-in was not changed, the results of the first 1.5 seconds from this DOE simulation were identical to the simulation results with the single step change VGT trajectories.

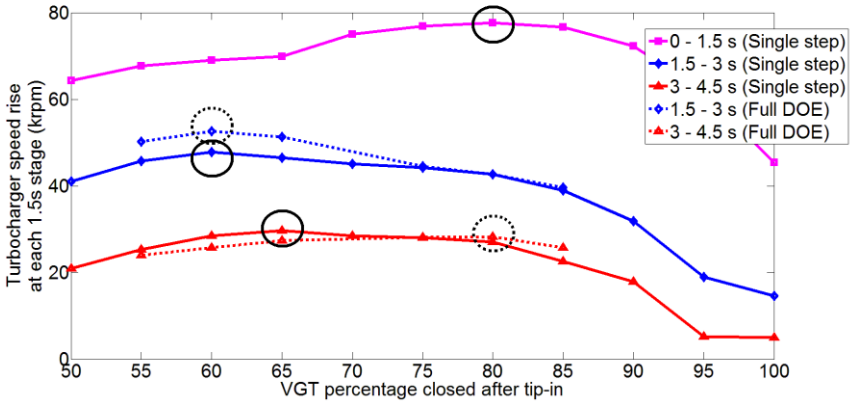

Figure 7.18: Comparison of turbocharger speed rise between single step change simulations and full DOE simulations (Small VGT, 1500rpm)

At second stage, the optimum VGT position was unchanged, however, the maximum turbocharger rise increased by approximately 5krpm. This was because the VGT position in the first stage was chosen as 80% closed for the maximum turbocharger acceleration. For the third stage, the maximum acceleration was not affected greatly, however, the optimum VGT position was moved from 65% closed to 80% closed as a result of the changes in the VGT trajectory at previous stages. Despite the variations in the turbocharger speed rise between the two simulations, the simulations with single step changes were able to capture the trends of the optimum VGT trajectory.

The optimum VGT trajectory found in the DOE simulation for fastest turbocharger acceleration is shown in Figure 7.19. To achieve the highest turbocharger speed at the end of the transient, the VGT position was set to 80% closed in the first 1.5 seconds, and it was opened slightly at the second stage. At the third stage, the VGT position was again set to 75% closed. This trajectory was subject to the resolution of the DOE, the duration of each stage, and the number of stages.

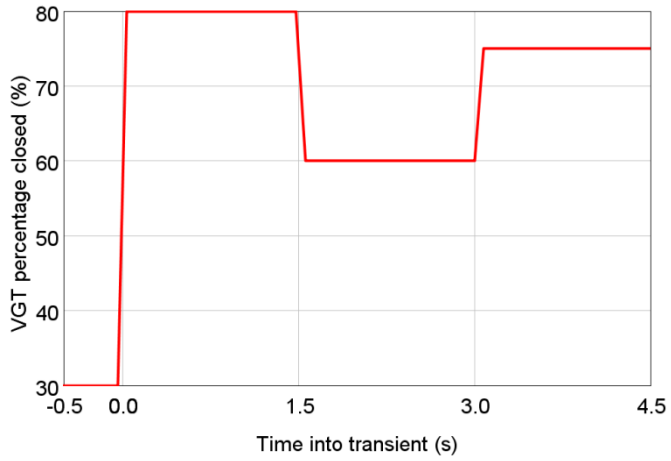

Figure 7.19: Simulated optimum VGT trajectory for small VGT at 1500rpm

Therefore, in order to fully understand the response of the entire system, the simulation results were investigated in more detail. Figure 7.20 shows the simulated responses of the key parameters during the first stage of the transient. Simulations of three VGT trajectories are compared in the figure. Trajectory 2 in the graph (80% closed) provided the fastest turbocharger acceleration at the first stage. The VGT

positions in the other two trajectories are 85% closed and 75% closed respectively.

At the first stage in the transient, the high turbine expansion ratio should be pursued. However, this should not be achieved at the cost of the noticeable drop in turbine efficiency which resulted in low turbine power for trajectory 1, despite the high turbine isentropic power shown in Figure 7.21. This was the same as the trend found in the 2000rpm transient simulation using the VGT map collected from the on-engine mapping facility.

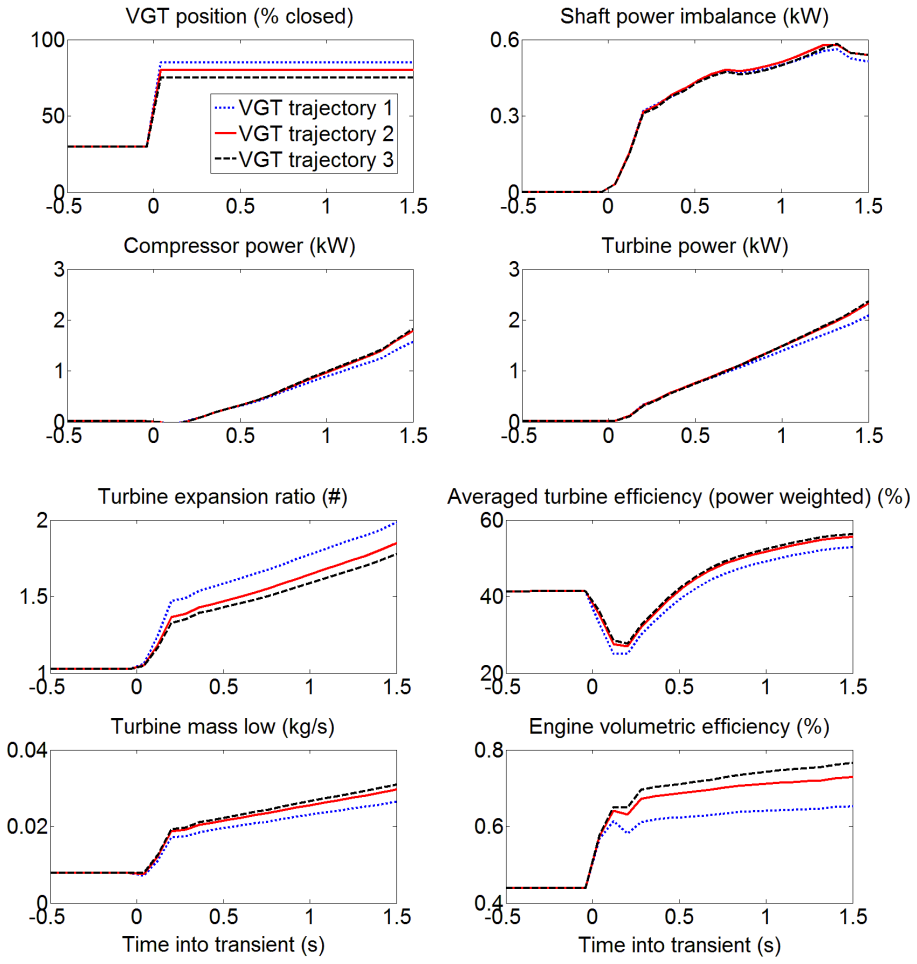

Figure 7.20: Simulated responses of key parameters during the first stage of transient (Small VGT, 1500rpm)

At the second stage of the transient, the VGT position was slightly opened in the optimum trajectory, shown in Figure 7.22. This was because of the significant difference in the engine volumetric efficiency between the two settings (trajectory 2

and trajectory 4). As the air flow built up, the effect of the changes in engine exhaust manifold pressure on the engine volumetric efficiency seemed to become more significant.

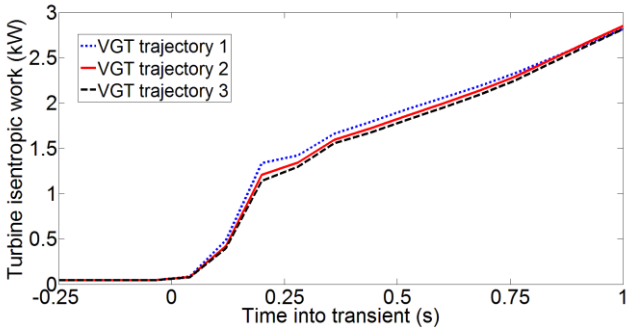

Figure 7.21: Simulated turbine isentropic power at first 1 second after tip-in (Small VGT, 1500rpm)

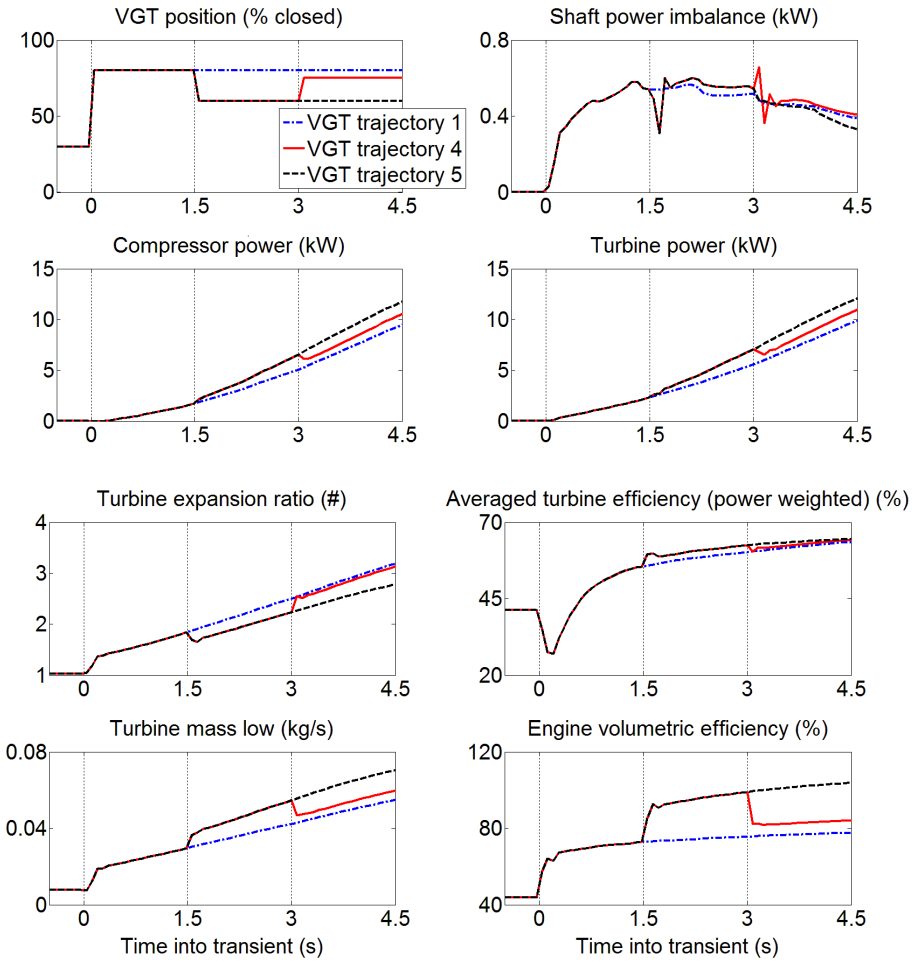

Figure 7.22: Simulated responses of key parameters during entire transient (Small VGT, 1500rpm)

In order to understand the effects on the engine volumetric efficiency, the results of all the transient simulations at 1500rpm were used to create polynomial models of the engine volumetric efficiency. The first input to the model was engine air mass flow. Since the valve timings were kept at constant during the transient for simplicity, the second input to the model was chosen between the delta pressure across engine block (exhaust manifold pressure – intake manifold pressure) and the pressure ratio across engine block (exhaust manifold pressure / intake manifold pressure) to represent the scavenging condition of the engine during the transient.

Second order polynomial models were built. The coefficient of determination of the two models with different input parameters were 0.9888 (model with input of pressure ratio across engine block) and 0.9858 (model with input of delta pressure across engine block). Both models could capture the response accurately. Since the model with the input of pressure ratio across engine block offered slightly higher accuracy, the pressure ratio across engine block was chosen as the second input parameter of the model structure for further investigation. Figure 7.23 shows the accuracy of the prediction of the engine volumetric efficiency.

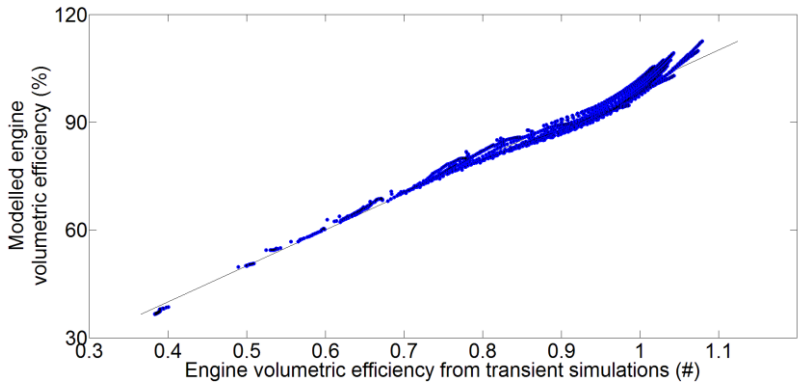

Figure 7.23: Prediction of the engine volumetric efficiency using the input of engine mass air flow and pressure ratio across engine block (1500rpm)

Therefore, this model was used to predict engine volumetric efficiency at two different mass air flow levels (75 kg/h and 200 kg/h), corresponding to the flow levels achieved at the naturally aspirated condition and full load condition at 1500rpm (Figure 7.24). It is shown that, at high flow level, the effect of change in pressure ratio across the engine block on the engine volumetric efficiency was more

significant. This affected the optimisation of the turbine expansion ratio and the engine volumetric efficiency.

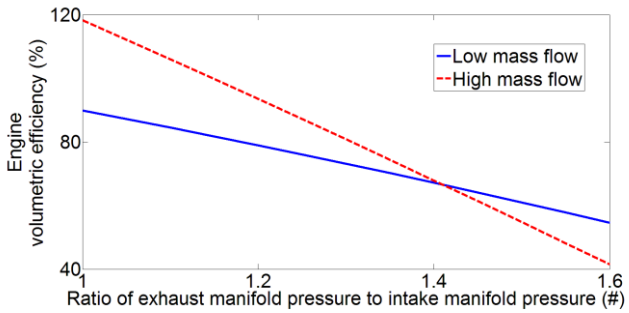

Figure 7.24: Prediction of the engine volumetric efficiency at two engine mass flow levels (1500rpm)

At the third stage in the transient, the VGT setting in the optimum trajectory was closed again. This resulted in a drastic drop in engine volumetric efficiency, and hence turbine mass flow. Both the turbine power and compressor power dropped. However, the turbocharger shaft power imbalance was highest: that is, the acceleration of the turbocharger was maximised during this stage. This was because the drop in turbine power was offset by the drop in compressor load power. While both the compressor power and turbine power were proportional to the mass air flow, the drop in turbine isentropic power was offset by the increase in the turbine expansion ratio as a result of the closing VGT position, shown in Figure 7.22.

The increase in the turbocharger shaft power imbalance due to reduction of mass air flow happened only at a later stage during the transient. This was because of the increase in the ratio of compressor power to turbine power (Figure 7.25). At early stages in the transient, only a small portion of turbine power was used on compressor fluid work. Thus, the drop in compressor power by closing the VGT was not sufficient to offset the drop in turbine power.

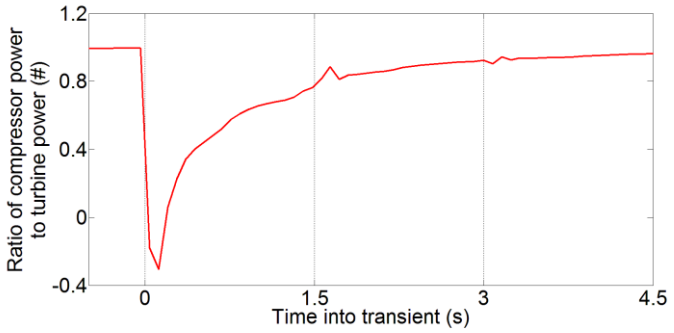

Figure 7.25: Simulated ratio of compressor power to turbine power during transient (Small VGT, 1500rpm)

The three stages during the transient are explained in Figure 7.26. The optimum VGT trajectory for maximising turbocharger acceleration is summarised below:

1. The VGT should be closed at an early stage during transient to achieve high turbine expansion ratio and hence turbine power.
   The selection of VGT position during this stage was dependent on the optimisation of turbine expansion ratio and turbine efficiency.

2. As the engine mass air flow builds up, the VGT should be opened slightly to benefit engine volumetric efficiency which allows more air flow through the turbine.
   The effects of exhaust manifold pressure on engine volumetric efficiency became more significant at this stage. Therefore, the selection of VGT position during this stage was dependent on the optimisation of turbine expansion ratio, turbine efficiency and the engine volumetric efficiency.

3. As the turbocharger power imbalance diminishes, the VGT should be closed again to deliberately reduce the engine volumetric efficiency, which reduces the compressor load. Whilst the compressor power is reduced, the turbine power can be recovered due to the increase in turbine expansion ratio, resulting in faster turbocharger acceleration. As a result, the selection of VGT position during this stage was dependent on the optimisation of turbine power and compressor power.

It is worth noting that the entire transient was discretised into three stages for simplicity. In real engine transient manoeuvres where the transient can be divided into an infinite number of stages, the transition between the stages and the changes in VGT position should happen continually. The transitions are dependent on the changes in the characteristics of the engine volumetric efficiency and the changes in the ratio of compressor power to turbine power, which affects the optimisation of turbine power, compressor power and engine volumetric efficiency.

However, closing the VGT at a later stage in the transient resulted in a drastic drop in engine torque as a result of the variation in mass air flow (Figure 7.27). This was not acceptable in terms of drivability. Thus, the reduction of compressor power by closing the VGT should be avoided during the transient. The optimisation strategy for the second stage should also be used at the third stage of the transient. Nonetheless, an advanced transient control strategy was needed because of the non-monotonic response of the VGT turbocharger. A simple PI controller was unlikely to be able to control the complex system.

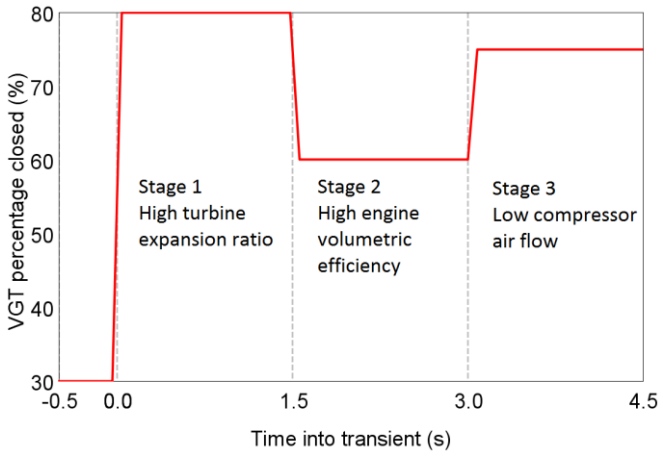

Figure 7.26: Three stages during transient (Small VGT, 1500rpm)

It is worth noting that, at the first and second stage, the turbine power and the turbocharger shaft power imbalance were both maximised in the simulation with the optimum VGT trajectory. This was also found in the simulation of the VGT at 2000rpm in the previous section. Therefore, the VGT trajectory that maximised the

turbine power was chosen as the strategy for optimised turbocharger speed acceleration.

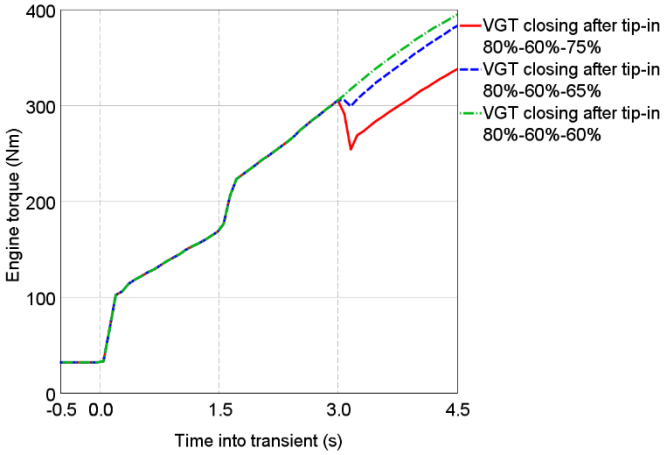

Figure 7.27: Simulated response of engine torque (Small VGT, 1500rpm)

7.4. Turbine matching for transient response and comparison between FGT and VGT

In the previous section, the simulation with single step change VGT trajectories and the simulation with full factorial DOE of trajectories were compared. It was found that the former was able to capture the trend in the optimum trajectories. Therefore, for the investigation of the responses of the VGTs of different sizes, single step change trajectories were used to save computational time. If the optimum trajectory for any case involved large variations in VGT position between stages, the full factorial DOE of trajectories would be performed again to confirm the results.

In these simulations, the same setups as previous transient simulations have been kept. The turbine maps that were studied in the steady state matching were used to investigate the trade-offs between steady state performance and transient responses.

Figure 7.28 shows the simulated turbocharger speed rise at each 1.5-second stage for the three VGTs at two engine speeds. Unlike the small turbine, no significant variation of the optimum VGT position between stages was found on the medium turbine and the large turbine. For the large turbine at 1500rpm, the optimum VGT position was varied from 90% closed to 80% closed during the transient. However,

the difference in the turbocharger speed rise between VGT 80% closed and 90% closed at the first stage was below 1.7krpm out of 46krpm. This was negligible. Therefore, the simulation results of the single step change trajectories are valid for the optimisation of the transient responses at 1500rpm and 2000rpm for the medium and large VGTs.

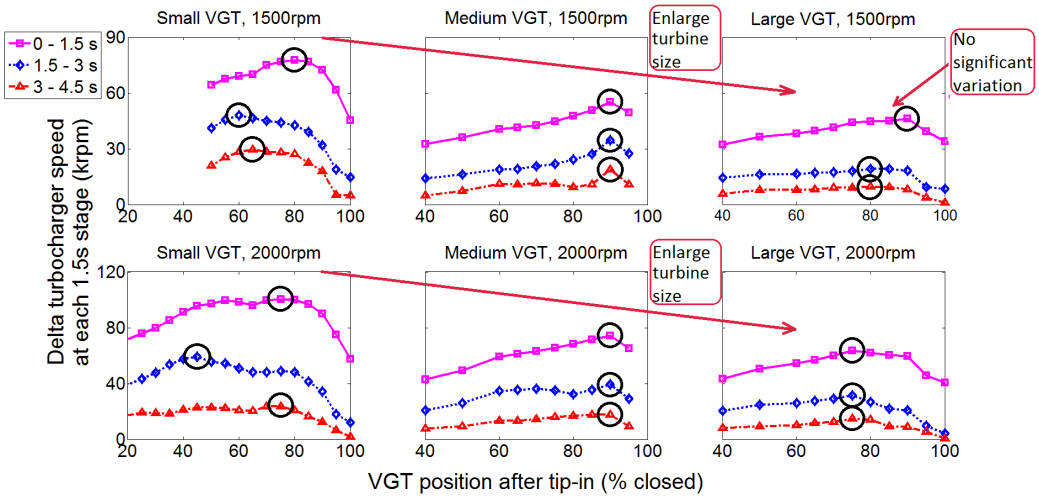

Figure 7.28: Simulated turbocharger speed rise of the three VGTs during transient at 1500rpm and 2000rpm

However, significant variations in the optimum VGT position can be found in the transient response of the small VGT at 2000rpm. Therefore, a full factorial DOE was also performed. Figure 7.29 shows the comparison between single step change simulations and full DOE simulations for the small VGT at 2000rpm. The VGT positions marked by the solid black circle were the optimum VGT positions from the single step change simulations, while the dotted black circle marks the VGT positions that were the optimum positions from the full factorial DOE simulations.

As with the comparison of the small VGT at 1500rpm, the selection of the optimum VGT position for the first two stages was not affected. Both simulations showed that the VGT should be closed slightly for faster turbocharger acceleration at the third stage. Nevertheless, the additional turbocharger speed rise in the third stage that can be achieved by closing the VGT was insignificant. The engine torque already exceeded the full load torque target before the end of the second stage in transient. In addition, torque drop was observed when VGT was closed at the third stage.

Therefore, although closing the VGT at the third stage provided faster turbocharger acceleration at the third stage, this was not a realistic solution. In addition, the optimum VGT setting for the second stage should also be used for the third stage.

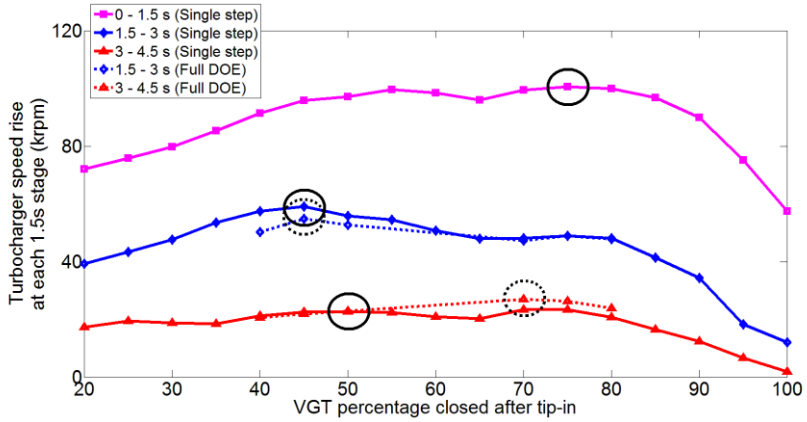

Figure 7.29: Comparison of turbocharger speed rise between single step change simulations and full DOE simulations (Small VGT, 2000rpm)

The optimum VGT trajectory at the three 1.5-second stages can be summarised in Figure 7.30. The dotted line and the solid line represent the optimum VGT trajectories with and without the engine torque drop due to the closing of the VGT during the transient.

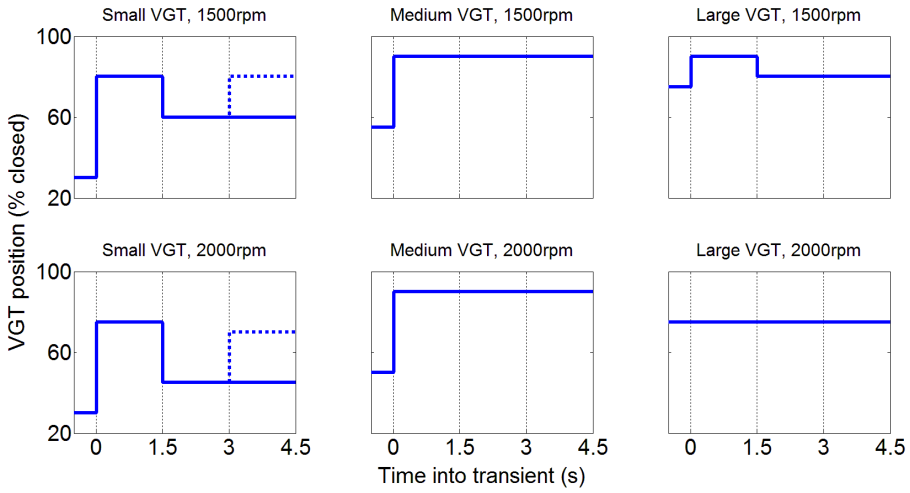

Figure 7.30: Optimum VGT trajectories from simulation results

To compare the behaviour of different VGTs, the flow characteristic of the optimum VGT settings (at the first stage) and the FGT are plotted in Figure 7.31. The flow characteristics of these VGT settings were interpolated from the raw data supplied in the turbine performance map.

As the size of the VGT reduced, the flow capacity of the optimum VGT setting was lowered. Therefore, the turbine expansion ratio, and hence the turbine power during transient, could be improved. This was achieved without a significant drop in turbine efficiency. For all three VGTs, the flow capacity could be further reduced by closing the vanes. However, the flow capacities shown in Figure 7.31 were the optimum setting at the first stage as a result of the optimisation of turbine expansion ratio and turbine efficiency.

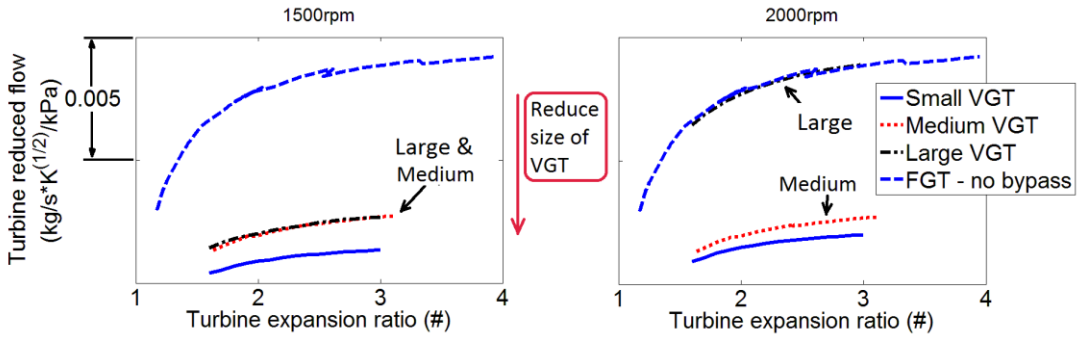

Figure 7.31: Flow characteristics of the optimum VGT settings at first stage during transient simulation

At the first stage in the transient, the optimum flow capacity of the small VGT was lower than that of the larger VGTs. This was because the larger VGTs would have moved into a low efficiency region if they were further closed. However, the small VGT was operated at medium opening setting. At later stages during the transient, the optimum VGT setting for the small VGT was opened slightly when the effect of exhaust manifold pressure on engine volumetric efficiency became more significant. As a result, the use of the smaller VGT offered the opportunity to set the turbine to a lower flow capacity during the early stage of the transient for faster turbocharger acceleration.

Since the flow capacities of the optimum VGT settings were mostly lower than the FGT, the flexibility of varying the flow characteristics of the VGT was beneficial to the optimisation of the turbine power. The only exception was the larger VGT. At 2000rpm, the flow capacity of the optimum VGT setting for the large VGT at the first stage was almost the same as the FGT flow capacity. At 1500rpm, the optimum flow capacity of the large VGT at the first stage was close to that of the medium

VGT. This was because the resolution of the turbine performance data of the large VGT was low in this region.

Thus, for the large VGT, interpolation of the turbine efficiency was necessary for VGT settings between these two flow ranges, which represented a relatively large window. Furthermore, the difference in maximum turbine efficiency at these two turbine settings was over 20 percentage points. Therefore, the simulation result was affected by the resolution of the turbine performance data. Increasing the number of vane positions where the performance data were measured can improve the accuracy of the simulation.

To be able to investigate the trade-off between steady state performance and transient response, the responses of the three VGTs at two engine speeds were measured, using the time required to accelerate the turbocharger to the speed where 80% of the full load torque could be achieved at steady state. Since the original compressor was used in these simulations, the difference in the turbocharger speed required to achieve the torque target for the three VGTs and the FGT was only 2krpm out of approximately 100krpm. The small variation was because engine volumetric efficiency was affected by the turbine matching and the resultant exhaust manifold pressure. Therefore, only one target turbocharger speed was used to measure the turbocharger response time for each engine speed condition.

Steady state simulation was carried out to find out the corresponding target turbocharger speed. It was assumed that once the turbocharger speed reached the target, the response time of the engine torque was affected by the feedback controller. 80% of full load torque was used as the target engine torque, since the later part of the engine response was more dependent on the thermal condition of the engine system. Modelling the details of the thermal system was outside the scope of this project.

The time required to reach target turbocharger speed during transients is summarised in Table 7.2. Compared with the FGT, the response was up to 4 seconds faster at this engine speed. At 2000rpm where the response of the FGT was already fast, the time

required to reach target turbocharger speed was improved by 0.68 seconds. At 1500rpm, the turbocharger response time can be shortened by 3.3 seconds by replacing the large VGT with the small VGT.

Figure 7.32 shows the comparison of the turbocharger response during transient simulations. While in most cases the response of the VGT was faster than that of the FGT, no benefit could be found for the large VGT at 2000rpm. This correlated to the optimum flow capacity shown in Figure 7.30. This may be affected by the resolution of the turbine performance data. In addition, the moment of inertia of the large VGT was larger than that of the FGT, due to the slightly larger turbine diameter. Therefore, replacing the FGT with the VGT did not necessarily improve the transient performance of the engine, if the VGT was not matched to the engine appropriately.

Table 7.2: Simulation results of time required to reach target turbocharger speed

		FGT	Large VGT	Medium VGT	Small VGT
1500rpm	Turbocharger response time (s)	5.45	4.74	2.25	1.45
	Improvement over FGT (s)	-	0.71 (13.0%)	3.20 (58.7%)	4.00 (73.4%)
2000rpm	Turbocharger response time (s)	1.67	1.86	1.49	0.99
	Improvement over FGT (s)	-	-0.19 (-11.4%)	0.18 (10.8%)	0.68 (40.7%)

As the size of the VGT reduced, the improvement in the transient response over the FGT became more significant. The time required to accelerate the turbocharger to the speed where 80% of full load torque could be achieved at steady state was below 1.5 seconds for the small VGT.

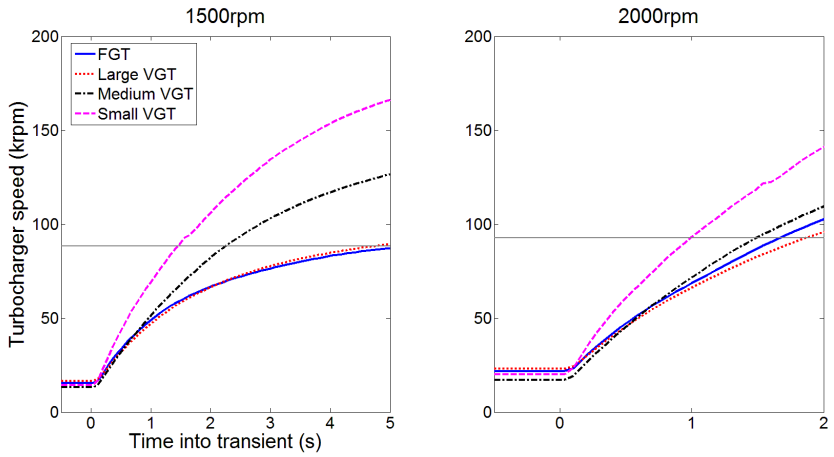

Figure 7.32: Simulated turbocharger response during transient with optimum trajectories

Figure 7.33 demonstrates the engine low-end torque performance at steady state and the turbocharger response time improvement at 1500rpm. Both performances can be improved by replacing the FGT with the VGT, and by reducing the size of the VGT. Therefore, within the turbine diameter range investigated, the engine low-end torque performance was correlated to the transient response of the engine. This was because the two measures were directly correlated to the diameter of the turbine.

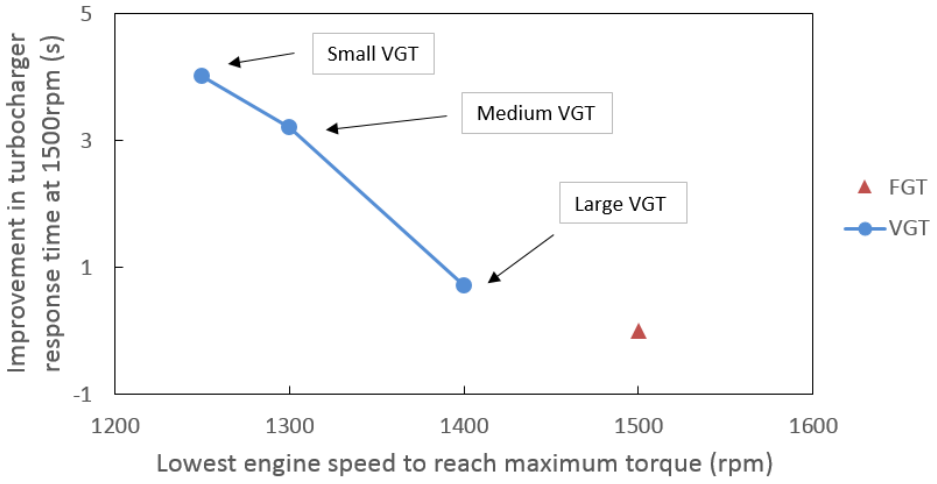

Figure 7.33: Simulated engine torque knee point and improvement in turbocharger response time

Figure 7.34 and Figure 7.35 show the trade-offs between the transient response and the steady state fuel consumption. Since the response time at low engine speeds is more critical to downsized turbocharged engines, the turbocharger response time at

1500rpm was selected to represent the engine transient response.

Without the use of an additional waste-gate for high-speed operation, trade-off needs to be made between the engine fuel consumption and the transient response when selecting the size of the VGT. The smallest VGT offered the most significant improvement in response time, while the largest VGT provided the highest fuel consumption reduction. On the other hand, with the use of an additional waste-gate, the large VGT was no longer an optimum selection, since the medium VGT was the best turbine matching for fuel consumption saving. Nevertheless, the cost of the additional waste-gate, and the effort required to implement and control the waste-gate, need to be considered.

The radar chart in Figure 7.36 demonstrates the comparison of the key performance of downsized engines. The two configurations with and without waste-gate are shown separately, since the system simplicities were different for the two configurations. The engine performances compared in the charts are the normalised improvements of each VGT configuration over the original FGT.

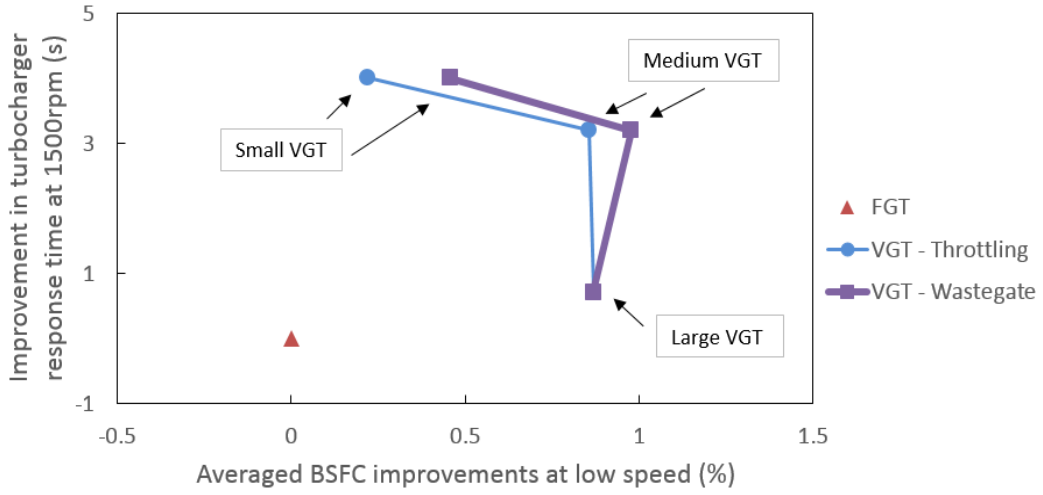

Figure 7.34: Trade-off between turbocharger response time and averaged fuel consumption at low speeds

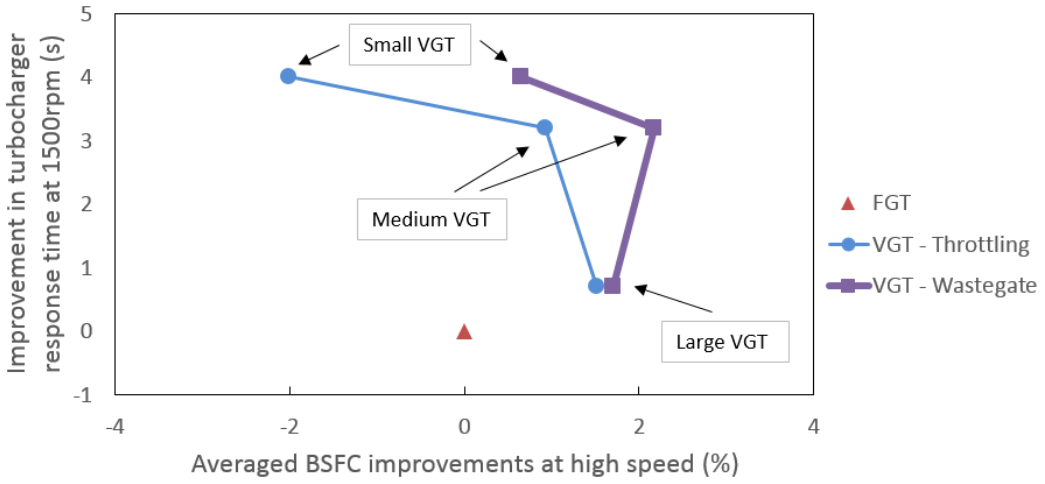

Figure 7.35: Trade-off between turbocharger response time and averaged fuel consumption at high speeds

It is shown that, for both configurations, the small VGT provided the best transient response and low-end torque, whereas the fuel efficiency improvement was minimal. While the transient response and low-end torque of the medium VGT were close to those of the small VGT, the engine fuel consumption could be significantly improved with the medium VGT due to the optimum turbine matching. The configuration of the medium VGT, assisted with an additional waste-gate, provided the highest fuel efficiency. Although implementing and controlling the waste-gate introduced additional cost and complexity, using the additional waste-gate further improved the fuel consumption of all VGTs. Therefore, the configuration of a VGT assisted with an additional waste-gate was proposed for use on gasoline engines. This enabled the use of the full potential of the VGT.

Table 7.3 summarises the selection criteria for the VGT configurations. If the VGT were simply used to replace the FGT with minimum additional cost and effort, the selection of VGT would be dependent on the trade-off between fuel efficiency, and transient response and low-end torque. Without an additional waste-gate, improving the transient response and low-end torque resulted in a deficit for fuel consumption. This was because the maximum flow capacity of the VGT was not sufficient to allow the use of the best match of the turbine.

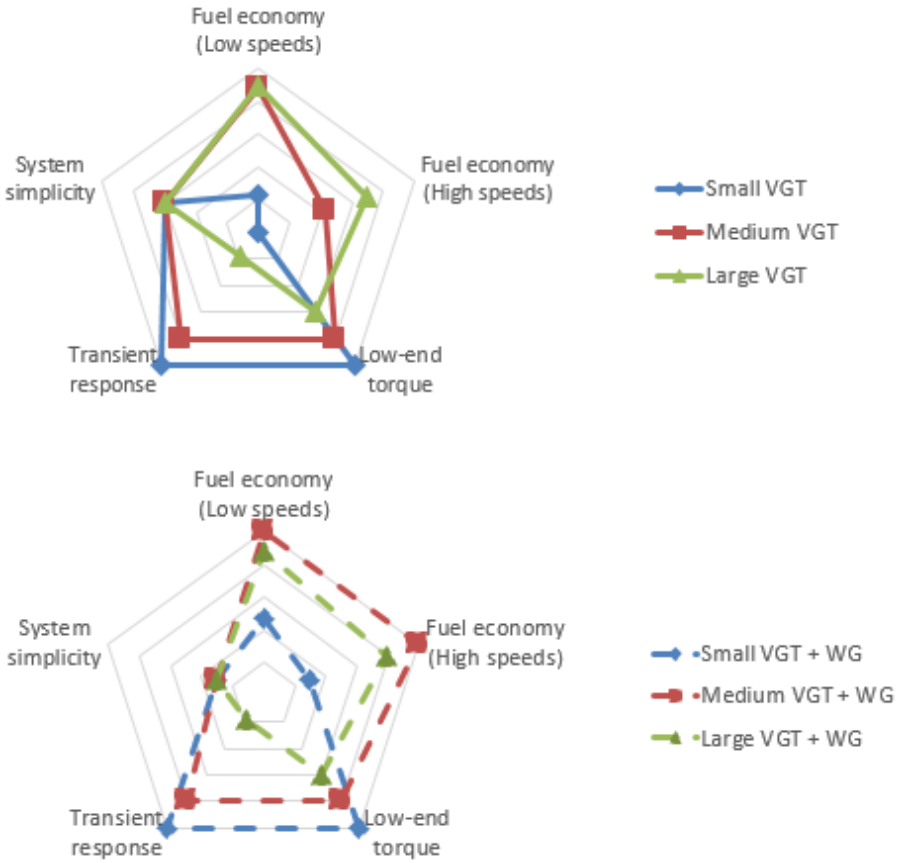

Figure 7.36: Radar charts showing normalised improvements of each VGT system compared with the FGT

In cases where additional effort and cost can be made to further downsize the internal combustion engine and optimise the system, the medium VGT or the small VGT assisted with a waste-gate would be an optimum selection. In addition, further fuel consumption savings can be achieved by increasing the level of downsizing and optimising the powertrain.

Therefore, for the optimisation of the VGT for use on gasoline engines, the maximum flow capacity and the efficiency in the region close to fully closed vane position are the two key parameters. Increasing the maximum flow capacity allows the use of a smaller VGT, while the fuel consumption at high speeds is not compromised. Unlike Diesel engines (which require the exhaust manifold pressure to be higher than intake manifold pressure for the use of EGR systems), production gasoline engines which do not commonly use EGR systems require high turbine

efficiency at all operating conditions. Thus, improving the turbine efficiency at the closed vane position may offer opportunities to close the VGT to maximise turbine power and turbocharger acceleration during transients. If the fully closed vane position is not to be used (provided that the turbine efficiency is significantly lower), the design of the vanes can be improved to increase flow range. Therefore, in addition to the optimisation of turbine efficiency and turbine flow flexibility, the design of the vane and blade can be further optimised for the use of VGTs on gasoline engines. As a result, the design of the VGTs for gasoline engines and Diesel engines might differ for system optimisation.

Table 7.3: Selection criteria for VGT configurations

	VGT selection – cost level 1 (not equipped with waste-gate)	VGT selection – cost level 2 (equipped with waste-gate equipped)
Best fuel consumption at all speeds	Large VGT	Medium VGT + waste-gate
Best fuel consumption at low speeds (for drive cycles)	Medium VGT	Medium VGT + waste-gate
Good capability of further downsizing	Medium VGT	Medium VGT + waste-gate
Best capability of further downsizing	Small VGT	Small VGT + waste-gate

7.5. Conclusions

In this chapter both experimental and simulation investigations of the transient response of FGT and VGT were presented. The matching of VGT has been performed in simulations to compare between the FGT and the VGT and to demonstrate the full potential of the application of VGT on gasoline engines. The conclusions of the comparison are listed below:

1. An open-loop search of the optimum VGT actuator trajectory was carried out in both experiments and simulations. A method was established to investigate and optimise the transient response. The experimental and simulation results of transient operation were well correlated. Therefore, a high fidelity engine model can be used for comparison and optimisation of transient behaviour in simulation environment. To further improve the simulation accuracy, turbine performance maps need to be collected at higher resolution at small openings.

2. It was found that the turbocharger acceleration should be prioritised before the target turbocharger speed was reached during transient operation. Therefore, if the target engine torque during a transient was within naturally aspirated range, the engine volumetric efficiency should be prioritised.

3. A fast transient response consisted of three stages:

    a. Maximising turbine power based on the optimisation of turbine expansion ratio and turbine efficiency.

    b. Maximising turbine power based on the optimisation of turbine expansion ratio, engine volumetric efficiency and turbine efficiency. The effects of exhaust manifold pressure on engine volumetric efficiency became more significant at high engine flow.

    c1. Continuation of second stage if engine torque dip during transient was not acceptable for good drivability.

    c2. Maximising the turbocharger shaft power imbalance based on the optimisation of compressor and turbine power, if engine torque dip during transient was acceptable. This may require the VGT to be further closed to deliberately reduce compressor flow and compressor power, while the reduction in turbine power can be minimised due to the increase in turbine expansion ratio.

4. From the results of the transient simulation, the turbocharger response time at 2000rpm can be improved by up to 4.0 seconds (73.4%) by replacing the FGT

with the VGT. The improvement decreased as the size of the VGT was increased, and the response of the VGT may be slower than that of the FGT if it was not matched to the engine appropriately. The use of a smaller VGT allowed the selection of lower turbine flow capacity at the early stage of transient operation due to the improved matching of the turbine.

5. Both steady state and transient performance can be improved by replacing the FGT with a VGT. Therefore, the VGT was an optimum system which enabled further downsizing of the internal combustion engine, and optimisation of the powertrain at a cost of increasing system complexity and cost.

6. The trade-off between steady state performance and transient response was found. The engine transient response and the steady state low-end torque were correlated so that both can be optimised at the same time. However, the selection of VGT size was based on the trade-off between response time and fuel consumption. A selection criteria was summarised so that the selection of VGT configuration and size were recommended for a number of system requirements.

7. With the proposed configuration of variable nozzle type VGT with an additional waste-gate, the full potential of VGT can be utilised. Despite the complexity and cost of implementing an additional waste-gate, the engine fuel economy can be further improved with no deficit on transient response or low-end torque.

8. Concluded from the experimental and simulation results, suggestions were provided for further optimisation of the VGT for its application on gasoline engines. The maximum flow capacity and the efficiency at small openings are the two key areas to optimise. This resulted in different design requirements than those for applications on Diesel engines.

9. It was challenging to control the VGT efficiently during transient, because the VGT behaviour was non-monotonic and complex. Therefore, an advanced control strategy was necessary for the control of VGT turbochargers on internal combustion engines.

Chapter 8 - *Transient control strategy*

Having investigated the complex behaviour of VGTs during transient operation, this chapter describes the comparison between several possible control strategies that have the potential of controlling the VGT efficiently. Based on the comparison, an advanced semi-physical control strategy was selected to address the challenges in controlling VGT during transients.

The validation of the control strategy for three VGTs at two engine speeds is presented. Using the proposed strategy, the VGT can be controlled efficiently to achieve target engine torque and turbocharger speed, which cannot be reached by a simple PID controller. The optimum open-loop VGT trajectories can be captured by the strategy.

The proposed control strategy is applicable to ECUs on modern internal combustion engines. The required effort for calibration can be significantly reduced by using this strategy. The structure of this strategy is also able to capture the response of the complex turbocharging systems such as two-stage turbocharging systems and Diesel air-path systems.

8.1. Selection of control strategy

The ECU control strategy for internal combustion engines on passenger cars is generally formed of sub-functions with different levels of complexity. The selection of the structure of each sub-function depends on factors that include the accuracy required, the characteristics and complexity of the target sub-system, the computational time, and the effort required to calibrate the model in the control strategy.

For example, the throttle control strategy on gasoline engines, which aims to achieve a target relative air charge, always relies on the modelling of the flow characteristics of the throttle plate and the corrections of the air condition: the physics of this are relatively simple to capture. However, the control of spark timing and valve timing maps are commonly based on a large set of empirical data. Significant calibration effort is necessary, since the complex behaviours of the combustion system and scavenging system are difficult to capture in ECUs. Another example is the transient control of the fuelling system, which is correlated to the variation of engine load. Therefore, the calibration effort required can be reduced by using an intermediate parameter to capture the response of the system.

On modern turbocharged gasoline engines, the turbocharger control strategy is normally formed of two parts: the physical model of the compressor and turbine for feed-forward control, and a close-loop feedback control. FGT turbochargers can be controlled using this structure with a feedback controller, because the waste-gate should be fully closed for fastest turbocharger acceleration before the target is reached. However, the optimum setting for the VGT varied during the transient, due to the non-monotonic and complex behaviours of the VGT. A simple feedback control strategy cannot capture this behaviour.

A number of possible alternative control strategies inspired by the existing strategies and advanced technologies have been studied in this project. These are the possible strategies that could offer the fastest VGT turbocharger response during transient. These strategies are for transient operation, and they can be triggered when a tip-in is

detected. In addition, if the target engine load during the transient is within the naturally aspirated region, engine volumetric efficiency, rather than turbocharger acceleration, should be the aim. Three possible structures of the control strategy for VGT turbochargers are compared below and listed in Table 8.1:

1. Feed-forward VGT position limiter map

This empirical approach sets the VGT opening based on a calibrated map, similar to the control of spark timing and valve timing. Because of the variations in the design of the VGT, each new VGT needed to be tested at a number of engine speeds. Thus, a look-up table can be formed to control the VGT position. The complexity of the look-up table can vary from 1-D (engine speed) to 2-D (engine speed and load), depending on the complexity of the response of the system. For example, the small VGT investigated in Chapter 7 might require complex look-up tables because of the variation of the optimum VGT position between stages.

However, similar to the control of spark timing and valve timing, significant calibration effort was required. In addition, calibration of the VGT setting during transient involved additional dimensions, including time during transient and engine load steps, resulting in an enormous amount of calibration work and considerable controller deficiencies.

2. Feedback control of engine pressure ratio or delta pressure

This semi-empirical approach used intermediate parameters to correlate the VGT position limitation. Either the engine pressure ratio or the engine delta pressure may be used as an intermediate parameter, as the engine volumetric efficiency and the turbocharger load were related to these two parameters. Figure 8.1 and Figure 8.2 show the correlation between the turbocharger speed rise and the two intermediate parameters. The maximum turbocharger speed rise at each stage and the corresponding engine pressure ratio/delta pressure are marked in the plots.

Control strategy	Type	Complexity	Calibration effort	Accuracy	Confidence region
Feed-forward VGT position limiter map	Empirical	Low	Large	Acceptable	Small
Feedback control of engine pressure ratio or delta pressure	Semi-empirical	Medium	Medium	Acceptable	Medium
Feed-forward control based on predictions of possible VGT trajectories	Semi-physical	High	Little	High	Large

Table 8.1: List of three possible structures of control strategy

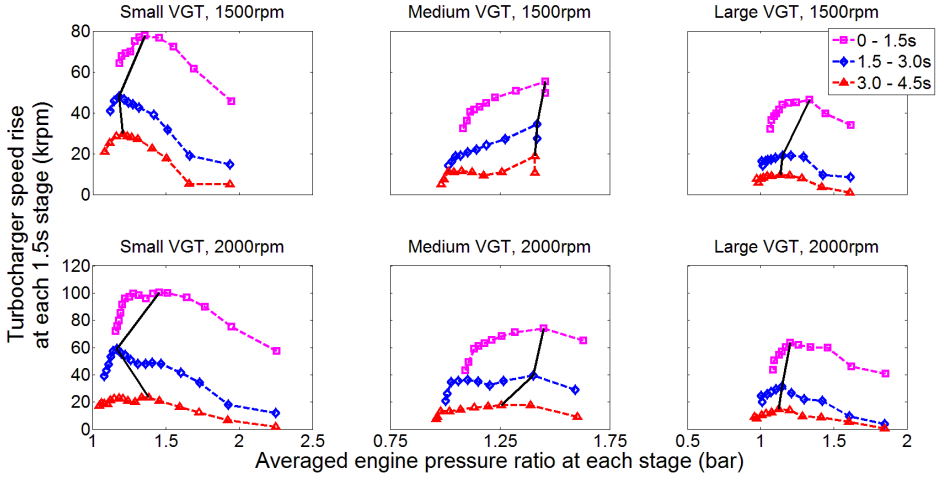

Figure 8.1: Correlation between maximum turbocharger speed rise and the engine pressure ratio

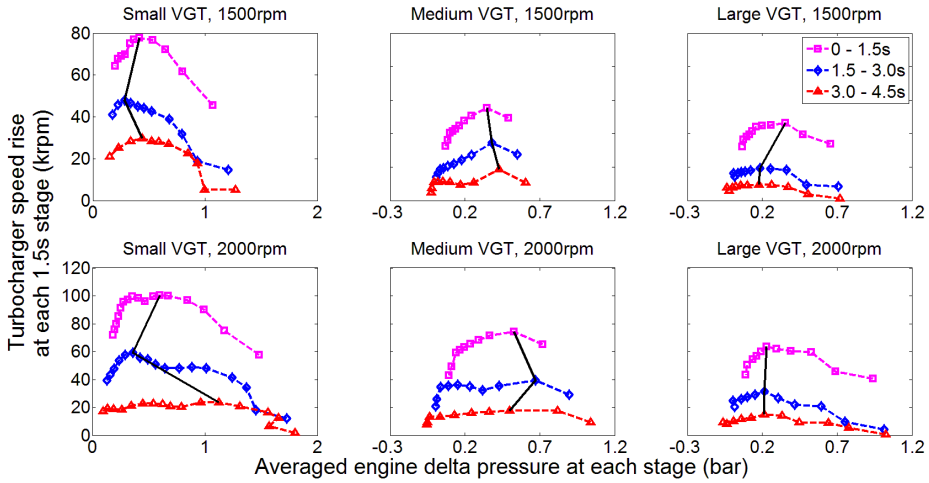

Figure 8.2: Correlation between maximum turbocharger speed rise and the engine delta pressure

However, a large variation in the engine pressure ratio/delta pressure was found at the optimum VGT setting at each stage. Therefore, the turbine response could not be captured by using these two parameters. This was because the turbine behaviour was a function of a number of variables. In addition, since there is no direct control of the engine pressure ratio/delta pressure, a feedback structure was necessary. Thus, additional deficiency was introduced by this feedback controller.

3. Feed-forward control based on the prediction of possible VGT trajectories

Due to the complexity of the VGT behaviour, it could not be represented in a simple model. In addition, calibration of transient control is time consuming. Therefore, a VGT model that represented sufficient physical fundamentals was necessary to improve the accuracy and to simplify the calibration.

This necessitated the use of a turbine mean-value model. This is a semi-physical model as this turbine model does not take into account the pressure and flow pulsations, although this is built based on the physical behaviours of the turbine under steady flow condition. The model assumes that the dynamics in the turbine boundary conditions can be ignored, so that the computational time can be minimised for real-time uses. This can be achieved with sufficient accuracy. The simplicity and the predictability of the model enabled the prediction of possible VGT trajectories in advance in real time. Thus, the optimum VGT trajectory could be selected.

As was demonstrated in Chapter 7, the turbine power was always maximised in the optimum VGT trajectory. Therefore, the VGT setting that could provide the maximum turbine power was sought at any time step and was chosen for the next time step.

Therefore, the semi-physical feed-forward control strategy that is based on the prediction of possible VGT trajectories was selected because of the high level of accuracy, minimum required calibration effort and the fast computational time.

8.2. Development of the semi-physical control strategy

Figure 8.3 demonstrates the proposed structure for the calculation for each VGT opening. The structure was based on the conventional approach for the calculation of turbine power. In order to predict the turbine operating points for all possible VGT

openings, prediction of the engine volumetric efficiency was necessary for the estimation of turbine mass flow and expansion ratio, which also affected the engine boundary conditions and volumetric efficiency. Therefore, an algebraic loop was formed. The estimated turbine power of each VGT opening was averaged every cycle. Further, it was compared to find the VGT opening that provided the highest estimated turbine power every cycle.

Several parameters were measured directly from the engine model while the simulation was running. Therefore, the prediction of the turbine operating condition was dependent on the current measurements, assuming that variation of these parameters between two adjacent engine cycles was negligible. Thus, the compressor behaviour at the current time step was used for the calculation of turbine power at the next time step, and the estimation of engine breathing was conducted using the empirical model of the volumetric efficiency. This simplified the tasks from modelling the behaviours of the entire engine to the modelling of turbine behaviours.

Figure 8.4 shows the integration of the engine model and the strategy. The control strategy was formed of multiple sub-models, each of which has a structure (Figure 8.3). The required measurements were sensed from the engine model and sent to the control strategy. The optimum VGT position estimated by the control strategy was used to actuate the VGT. Because of the use of these measured parameters, the computational effort required to run the mean value models was minimal. Thus, this could run on ECUs in real time. Table 8.2 lists the parameters that were required to measure and model in this control strategy. These parameters have already been used in model-based-calibration in modern ECUs. Therefore, this control strategy can be adopted on modern powertrains without significant modification.

The volumetric efficiency models in modern ECUs are complex, and several inputs are used. In addition, a large number of tests need to be performed to calibrate the model. Therefore, it is out of the scope of this project to build a complex engine volumetric efficiency model. Thus, the polynomial model with the input of engine mass air flow and engine pressure ratio was implemented for the validation of the control strategy in the 1-D simulation environment. The data used to build this model

were from the transient simulations carried out for the three VGTs.

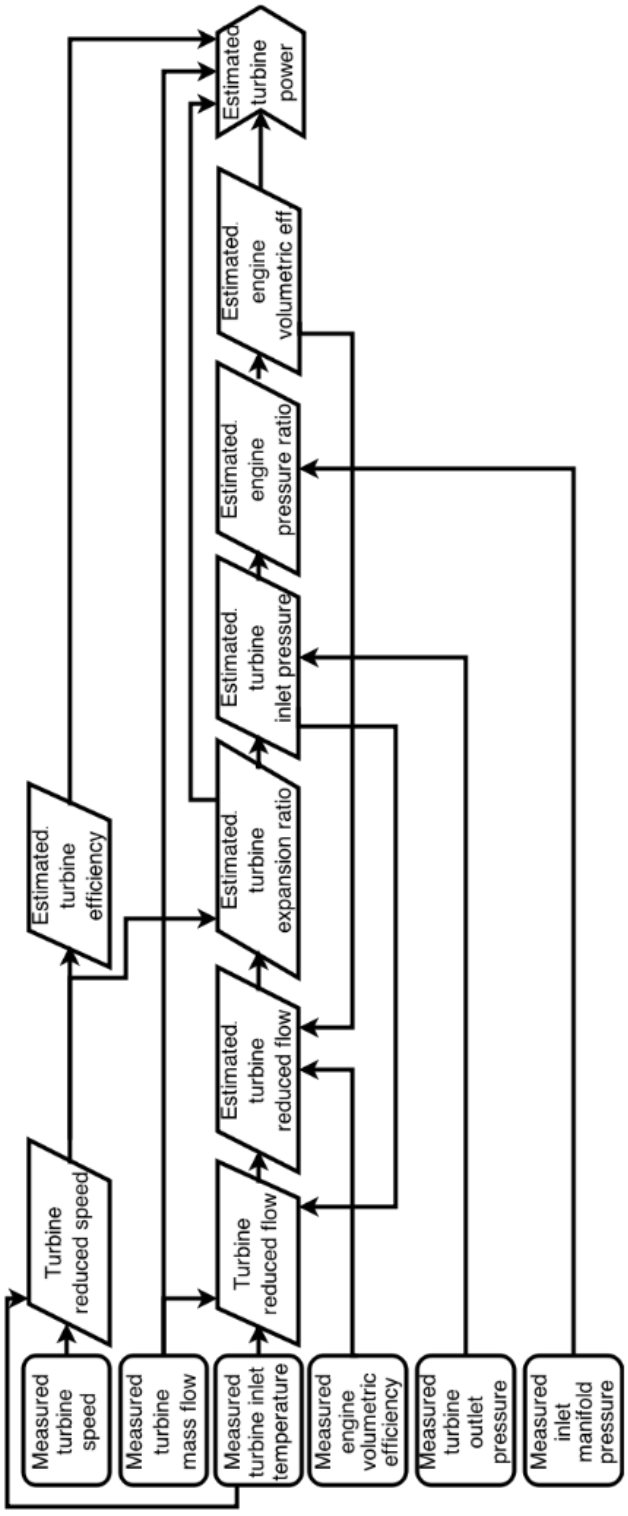

Figure 8.3: Diagram of the estimation of turbine power for each VGT opening

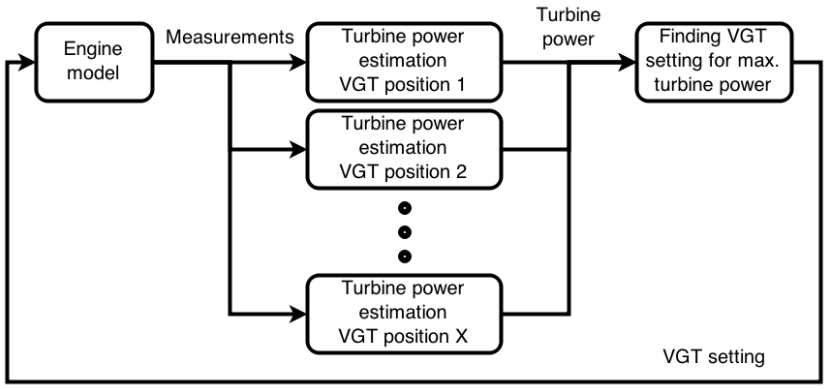

Figure 8.4: Integration of the engine model and the control strategy

Table 8.2: Summary of the parameters required to measure and model for this control strategy

Name of parameter	Source on modern engines
Intake manifold pressure	Measured
Mass air flow	Measured
Engine volumetric efficiency	Modelled
Turbine mass flow	Modelled
Turbine inlet temperature	Modelled
Turbine outlet pressure	Modelled
Turbocharger speed	Modelled

As shown in the previous chapter, the coefficient of determination of the engine volumetric efficiency model was over 0.98. This was sufficient for predicting engine volumetric efficiency. A model was built for each of the two simulated engine speeds. However, when implementing this control strategy for a real ECU, the existing model of engine volumetric efficiency in the ECUs should be used instead.

First order filters were used to enable the calculation of the algebraic loops in GT-Power. To avoid oscillations and to simulate the response of the actuator on VGT

turbochargers, the VGT position target was filtered, using a first order filter with a time constant of 0.1 seconds.

8.3. Validation of the control strategy

Figures 8.5–8.7 demonstrate the comparison of the VGT position and the turbocharger response for the open loop simulation, simulation with the semi-physical control strategy and the simulation with fully closed VGT after tip-in. The target turbocharger speed and engine brake torque (80% of maximum torque rise) are also marked in the plots. The control strategy was enabled after tip-in. It is shown that the optimum VGT trajectories of the three VGTs at the two engine speeds can be captured. The opening of the small VGT at a later stage of the transients was predicted.

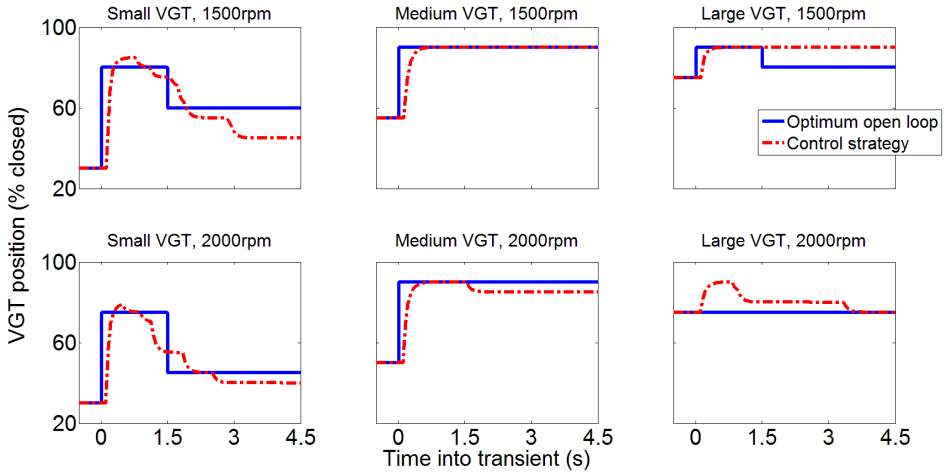

Figure 8.5: Comparison of the VGT trajectories

The turbocharger responses as a result of the control strategy were close to the optimum responses detected from the open loop simulations. It was found that the optimum turbocharger response could not be achieved in some cases, especially for the small VGT at 1500rpm. This was because of the level of accuracy of the engine volumetric efficiency model. Figure 8.8 shows the data points used to fit the polynomial model. In the case of the small VGT at 1500rpm, the engine operating point moved into the high flow/low pressure ratio region where no data were available.

At this region, the engine pressure ratio was around 1. The effect of the engine pressure ratio on the scavenging process and the volumetric efficiency became insignificant. This resulted in inaccuracy in the estimation of the turbine power and hence the optimum VGT position.

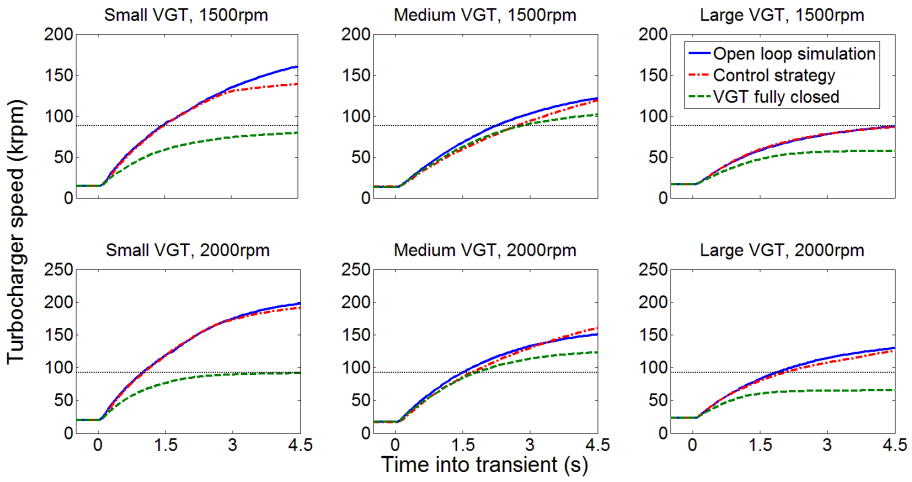

Figure 8.6: Comparison of the turbocharger response

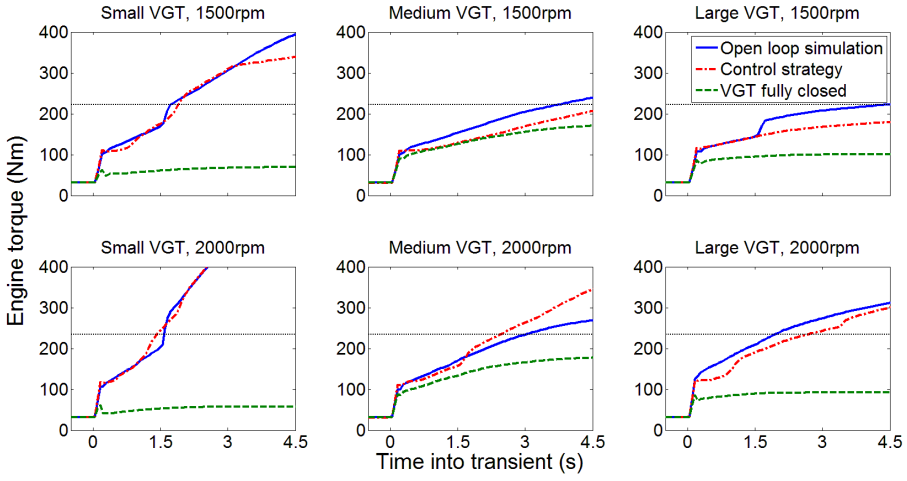

Figure 8.7: Comparison of the engine brake torque response

Additional inputs to the model might be required to predict the volumetric efficiency accurately in this region. This could be improved when the polynomial model is replaced with the model used in the ECUs. Nonetheless, the turbocharger shaft power imbalance was small in this region, meaning that it was close to the end of a transient manoeuvre. The engine torque already exceeded the full load torque curve at the

point where the VGT trajectory started to deviate from the optimum trajectory. Therefore, the transient response was not affected.

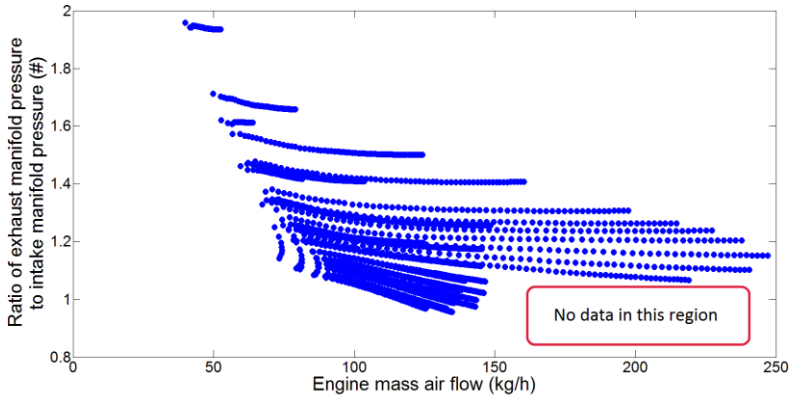

Figure 8.8: Data points used to calibrate the engine volumetric efficiency model at 1500rpm

In fact, when using this control strategy on real engines, the controller should be switched to steady state operating mode when the torque target has been reached. The switching should be triggered either by a negative change in driver's demand or when the engine pressure ratio falls below a certain level, representing the end of a transient.

It is worth noting that, for simulation of the medium VGT at 2000rpm, the turbocharger speed at the end of the transient was even higher than that found in the open loop simulations. This was because of the use of single step change VGT trajectories in the open-loop simulations. Therefore, the strategy was able to detect the optimum VGT trajectory.

The turbocharger responses with fully closed VGT are also plotted in Figure 8.6. This was to represent the likely results if the control strategy was replaced with a conventional PID feedback controller, which would close the vanes to accelerate the turbocharger, since the non-monotonic response cannot be captured. Although using a VGT position limiter to assist the PID controller might improve the response, a large amount of calibration effort would be required.

It is shown that the engine operating condition converged to a different point, and the target turbocharger speed could not be achieved. Table 8.3 summarises the time required to reach the target turbocharger speed corresponding to 80% of the steady state engine torque. With fully closed VGT, the target turbocharger speed can only be achieved with the medium VGT. This was because the optimum VGT position for the medium VGT was only 5% below fully closed vane position.

In four out of the six cases simulated, the target turbocharger speed could not be achieved with simple PID controller. In the two cases where PID controller could achieved the target turbocharger speed, the turbocharger response time was improved by 15-19%.

Table 8.3: Comparison of turbocharger response time between different controllers (-- : target turbocharger speed not achieved)

		Large VGT	Medium VGT	Small VGT
1500rpm	Turbocharger response with open loop trajectory (s)	4.74	2.25	1.45
	Turbocharger response with control strategy (s)	5.08	2.28	1.48
	Turbocharger response with fully closed VGT (s)	--	2.81	--
2000rpm	Turbocharger response with open loop trajectory (s)	1.86	1.49	0.99
	Turbocharger response with control strategy (s)	2.04	1.54	1.01
	Turbocharger response with fully closed VGT (s)	--	1.80	--

When the control strategy was enabled, the deficiency in the turbocharger response time compared with the optimum open loop VGT trajectories was below 0.05 seconds for the medium and small VGTs, and it was up to 0.3 seconds for the large VGT.

As a result, the control strategy was able to capture the non-monotonic behaviours of the VGT turbocharger. Benefits have been shown compared with the conventional

PID feedback controller. It is also expected that the structure of this control strategy can be used for other complex air-charging systems, such as two-stage turbocharging systems and air-path systems with both turbocharger and EGR. For example, two-stage turbocharging systems can be controlled with the behaviours of the two stages being estimated separately. This can be simulated by modelling a number of different positions of the bypass valves and VGT actuators.

8.4. Conclusions

In order to capture the complex behaviours of the VGT and to control it efficiently during transient operation, a semi-physical feed-forward transient control strategy was proposed based on the comparison between three possible strategies. The fundamentals and the capability of this control strategy were discussed in this chapter. The following conclusions can be drawn:

1. Three types of control strategies with different complexity, calibration difficulty and accuracy have been compared in this chapter. Considerable calibration effort will be required if the empirical look-up tables were used for transient condition. In addition, the complex VGT behaviours cannot be correlated to an intermediate parameter. Thus, a semi-physical strategy that was able to predict the turbine performances of possible VGT settings in advance, and also able to select the optimum opening for the next time step was proposed.

2. According to the findings in chapter 7, the optimisation criteria was to maximise the turbine power. Therefore, the proposed control strategy maximised the turbine power for the fastest turbocharger acceleration.

3. The transient control strategy was validated in simulation for the three VGTs at two engine speeds. The non-monotonic behaviours of the VGT were captured, and the optimum VGT trajectories can be achieved. In four out of the six cases simulated, the target turbocharger speed could not be achieved with PID controller. In the other two cases, the proposed control strategy improved the turbocharger response time by 15-19% compared with PID controller.

4. Since the prediction of turbine power was based on mean-value turbine model, real-time operation was allowed. The parameters used as inputs to the strategy were either measured or modelled in current ECUs on modern passenger car engines. Therefore, the challenges in applying this strategy to the current ECU were minimised.

5. The structure of the proposed transient control strategy can also be used to control complex turbocharging systems, such as two-stage turbocharging systems and air-path systems, with both turbocharger and EGR.

Chapter 9 - *Conclusions*

In this final chapter, the contributions and conclusions of the work presented in this thesis are summarised. This will be followed by suggestions and recommendations for future work.

9.1. Summary

The achievements presented in this thesis will be discussed with reference to the project aim and objectives laid out in Chapter 1.

1. *"Review the literature in the field of engine downsizing and turbocharging, especially the use of VGT technologies on gasoline engines."*

A literature review was presented in Chapter 2. The principles of VGT technology were detailed, and several types of VGT were compared against each other. In spite of the challenges in applying VGT technology to gasoline engines due to the harsh exhaust conditions, and it has been used on production gasoline engines. This was achieved through the synergy between several internal combustion engine technologies, such as high knock-tolerance combustion system, water-cooled exhaust manifold and advanced turbocharger material.

The use of the VGT technologies has the potential of facilitating further downsizing the gasoline engines. Fuel consumption saving of around 5% has been demonstrated. Studies also showed benefits in full load torque and transient response of up to 12% and 50% respectively.

2. *"Define and implement required testing and data acquisition systems. Apply test procedures to achieve repeatable and reliable experimental results."*

According to the project aims and objectives, reliable and repeatable experiments need to be performed to evaluate advanced turbocharging systems and to provide experimental data for engine model calibration. Therefore, the required automated test control system, high frequency data acquisition system and detailed test procedures were presented in Chapter 3.

Communication between test host system, ECU calibration tool, prototype hardware control system and data acquisition system was set up. Experimental data was recorded in different systems at various frequencies. In addition, detailed test

procedures for steady state and transient tests were designed and performed.

3. *"Develop advanced turbocharger testing facility to enhance understanding of turbocharger behaviours under complex operating conditions."*

Having reviewed of the challenges and the countermeasures in using turbocharger maps collected from conventional gas-stand, an on-engine turbocharger mapping facility was developed in this project. The design of the facility was presented in Chapter 4. A 95% confident region of 1.5% in measured compressor and turbine efficiencies was demonstrated. A VGT turbocharger was also mapped using this facility.

This facility enabled detailed investigation of turbocharger behaviour under complex operating conditions. Experiments were performed in the engine speed range of 2000rpm to 4500rpm (exhaust pulse frequency 67Hz to 150Hz) and in the turbine inlet temperature range of 340K to 1073K. A variation of up to 10% in compressor and turbine efficiencies were found and investigated. In order to improve the testing capability, recommendations to further improve of the facility were provided.

4. *"Calibrate and use engine model for simulation comparison, and to assist experimental investigation."*

The procedure that was followed in the steady state and transient calibration of the engine model was described in Chapter 5. The combustion model, exhaust manifold model and turbocharger model of the 1-D engine model were calibrated using the experimental data collected in the engine operating region of 1000rpm - 5800rpm and 10 - 100% load. In general, the accuracy of the predictions was within 5% at both steady state and transient. In addition, the dynamic pressures were also captured with excellent accuracy. Suggestions were also recommended for future improvements of the combustion model and turbocharger model.

5. *"Develop thorough understanding of VGT behaviours at steady state. Demonstrate the potential of gasoline VGT technologies for engine steady state*

operation."

According to experiment results at 2000rpm, the maximum engine torque achieved was increased by 48Nm (17.7%) by replacing the FGT with the VGT. Fuel consumption in the boosted region was reduced by around 4%. Simulation demonstrated that the improvement was mainly due to the reduction in pumping work and the extended knock-limited spark timing window.

Three VGTs of different sizes were selected for steady state simulations to demonstrate the potential of the VGT technology. The 3.1% improvement in fuel consumption was a result of the reduction in pumping work. The torque knee-point can be advanced by up to 250rpm. The trade-off between these two aspects was found for the selection of the optimum turbine size. This enabled further downsizing of gasoline engines for fuel economy.

A novel configuration of VGT turbocharger with an additional waste-gate was proposed, to use the full potential of VGT by improving the matching of the turbine.

6. *"Develop thorough understanding of VGT behaviour at transient conditions. Demonstrate the potential of gasoline VGT technologies for engine transient operation, and illustrate trade-off between steady state performance and transient performance."*

The VGT transient trajectories were optimised in both experiments and simulations. The results of the experiments and simulations correlated well, demonstrating the capability of conducting transient optimisation using high fidelity engine model. To further improve the accuracy of the transient simulation in the future, turbine maps need to be collected at higher resolution at small openings.

The engine transient response was divided into three stages and investigated. In order to minimise the time required to reach target engine torque during transient, the turbocharger acceleration should be prioritised before reaching the target turbocharger speed. The turbocharger acceleration was dependent on the optimisation

of turbine expansion ratio, turbine efficiency, engine volumetric efficiency and compressor power. If engine torque drop during transient is to be avoided, turbine power should be maximised.

According to simulation results, the turbocharger response time can be improved by up to 4 seconds (73.4%), by replacing the FGT with the VGT. The smallest VGT offered the largest improvements. Thus, the selection of VGT size was dependent on the trade-off between steady state performance and transient performance.

The requirements for gasoline VGT are different from those for Diesel VGT. In order to further improve gasoline VGT technologies, maximum flow capacity and efficiency at small openings are the two key aspects.

7. *"Propose and develop a transient control strategy to maximise the potential of complex turbocharging systems. "*

A novel semi-physical feed-forward transient control strategy was developed to cope with complex behaviours of VGT. This strategy is based on turbocharger mean-value model. It searches possible VGT positions in advance and selects the optimum setting for next time step in real time.

The optimum VGT trajectories can be achieved. The target turbocharger speed could not be achieved with PID controller in four of the six cases simulated. By using the proposed control strategy, the turbocharger response time was improved by 15-19% compared with PID controller in the other two cases. Therefore, the non-monotonic behaviours of the VGT were captured.

This strategy is applicable to current ECUs, and the calibration effort for transient response can be minimised. The structure of this strategy can also be used on other complex turbocharging systems, such as two-stage systems and Diesel air-path systems.

9.2. Outlook

The work performed in this project has had a number of impacts on the continuation of this project, as well as initiation of projects with different industrial partners.

1. The on-engine turbocharger mapping facility has been further developed for the next phase of the project. More accurate boundary condition control has been implemented. The flow measurements have been upgraded to achieve high accuracy in a wide flow range. In addition, advanced turbocharger modelling techniques are being used to capture and understand the dynamic behaviour of turbochargers.

2. The procedure of the engine model calibration has been used in other projects. The high level of the instrumentation used in this project developed a thorough understanding of calibration requirements. Therefore, the required instrumentation can be designed for each project with different aims and calibration targets.

3. Recommendations for gasoline VGT turbochargers have been suggested. It is clear that the VGT technologies for gasoline engines and Diesel engines have different requirements for the flow and efficiency characteristics. Thus, the two applications are likely to divert in their designs.

4. The structure of the semi-physical feed-forward transient turbocharger control strategy developed in this project can be applied to other complex turbocharging systems. This will enable the use of advance boosting systems and air-path systems to achieve their full potential in the real world.

References

[1] **Jackson, N.**, 2012, "The Cars of Tomorrow."

[2] **Jackson, N.**, 2015, "Energy & Fuels Road Map Technology Group 2015 activities."

[3] **Atkins, P., Cornwell, R., Tebbutt, N., et al.**, 2013, "Preparing a Low CO2 Technology Roadmap for Buses."

[4] **Jackson, N.**, 2013, "Advanced Internal Combustion Engines Workstream Conclusions & Consensus Roadmap."

[5] **E4Tech**, 2013, "A Harmonised Auto-Fuel Biofuel Roadmap for the EU to 2030."

[6] **Owen, N. and Jackson, N.**, "A New Look at the Low Carbon Roadmap," Low-Carbon Vehicles, London, 2009

[7] **Kuhn, M.**, 2012, "Automotive Powertrain Technologies through 2016 and 2025."

[8] **Kasab, J. J., Crossley, R. B. and Jackson, N.**, 2014, "Technology Roadmap for Light-Duty Vehicle CAFE & GHG Emissions."

[9] **Dhand, A. and Pullen, K. R.**, 2015, "Analysis of Continuously Variable Transmission for Flywheel Energy Storage Systems in Vehicular Application. ," Proceedings of the Institution of Mechanical Engineers, Part C: Journal of Mechanical Engineering Science, Vol. 229(2), pp. 273-290

[10] **Dhand, A. and Pullen, K. R.**, 2015, "Review of battery electric vehicle propulsion systems incorporating flywheel energy storage," International Journal of Automotive Technology, Vol. 16(3), pp. 487-500

[11] **Dhand, A. and Pullen, K. R.**, 2013, "Review of Flywheel based Internal Combustion Engine Hybrid Vehicles," International Journal of Automotive Technology, Vol. 14(5), pp. 797-804

[12] **Gannon, M. C.**, 2009, "Hydraulic Hybrids on the Rise," Hydraulics & Pneumatics, Vol. 62(7), pp. 28-31

[13] **Hancock, D., Fraser, N., Jeremy, M., et al.**, 2008, "A New 3 Cylinder 1.2l Advanced Downsizing Technology Demonstrator Engine," SAE Technical Paper 2008-01-0611, 2008, doi:10.4271/2008-01-0611

[14] **Leduc, P., Dubar, B., Ranini, A., et al.**, 2003, "Downsizing of Gasoline Engine: an Efficient Way to Reduce CO2 Emissions," Oil & Gas Science and Technology - Rev. IFP, Vol. 58(1), pp. 115-127

[15] **Wang, L.-S. and Yang, S.**, 2006, "Turbo-Cool Turbocharging System for Spark Ignition Engines," Proceedings of the Institution of Mechanical Engineers, Part D: Journal of Automobile Engineering, Vol. 220(8), pp. 1163-1175

[16] **Turner, J. W. G., Pearson, R. J., Bassett, M. D., et al.**, 2003, "Performance and Fuel Economy Enhancement of Pressure Charged SI Engines through Turboexpansion - An Initial Study," SAE Technical Paper 2003-01-0401, 2003, doi:10.4271/2003-01-0401

[17] **Petitjean, D., Bernardini, L., Middlemass, C., et al.**, 2004, "Advanced

Gasoline Engine Turbocharging Technology for Fuel Economy Improvements," SAE Technical Paper 2004-01-0988, 2004, doi:10.4271/2004-01-0988

[18] **Guzzella, L., Wenger, U. and Martin, G.**, 2000, "IC-Engine Downsizing and Pressure-Wave Supercharging for Fuel Economy," SAE Technical Paper 2000-01-1019, 2000, doi:10.4271/2000-01-1019

[19] **Wallace, F. J., Howard, D. and Roberts, E. W.**, "Variable Geometry Turbocharging - Optimization and Control Under Steady State Conditions " 3rd International Conference on Turbocharging and Turbochargers, London, 1986

[20] **Wallace, F. J., Anderson, K. and Howard, D.**, "Variable Geometry Turbocharging - Control Under Transient Conditions," 3rd International Conference on Turbocharging and Turbochargers, London, 1986

[21] **Wilhelmsson, C., Tunestål, P. and Johansson, B.**, 2007, "Operation strategy of a Dual Fuel HCCI Engine with VGT," SAE Technical Paper 2007-01-1855, 2007, doi:10.4271/2007-01-1855

[22] **Eichhorn, R. H. L., Boot, M. D. and Luijten, C. C. M.**, 2010, "Throttle Loss Recovery using a Variable Geometry Turbine," SAE Technical Paper 2010-01-1441, 2010, doi:10.4271/2010-01-1441

[23] **Bauer, K.-H., Balis, C., Donkin, G., et al.**, "The Next Generation of Gasoline Turbo Technology," 33rd International Vienna Motor Symposium 2012, Vienna 2012

[24] **Lundstrom, R. R. and Gall, J. M.**, 1986, "A Comparison of Transient Vehicle performance Using a Fixed Geometry, Wastegated Turbocharger and a Variable Geometry Turbocharger," SAE Technical Paper 860104, 1986, doi:10.4271/860104

[25] **Singer, D. A.**, 1985, "Comparison of a Supercharger vs. a Turbocharger in a Small Displacement Gasoline Engine Application," SAE Technical Paper 850244, 1985, doi:10.4271/850244

[26] **Fraser, N., Blaxill, H., Lumsden, G., et al.**, 2009, "Challenges for Increased Efficiency through Gasoline Engine Downsizing," SAE Int. J. Engines 2(1):991-1008, 2009, doi:10.4271/2009-01-1053

[27] **Pullen, K. R., Etemad, S. and Cattell, R.**, "Experimental Investigation of the TurboClaw Low Specific Speed Compressor," ASME International Gas Turbine Institute, Copenhagen, 2012

[28] **Pullen, K. R., Etemad, S., Thornton, W. E., et al.**, "The TurboClaw Compressor for Engine Downsizing by Twin-charging," 10th International Conference on Turbochargers and Turbocharging, London, 2012

[29] **Hu, B., Tang, H., Akehurst, S., et al.**, 2015, "Modelling the Performance of the Torotrak V-Charge Variable Drive Supercharger System on a Ford 1.0L GTDI Engine – Preliminary Simulation Results," SAE Technical Paper 2015-01-1971, 2015, doi:10.4271/2015-01-1971

[30] **Uchida, H.**, 2006, "Transient Performance Prediction for Turbocharging Systems Incorporating Variable-geometry Turbochargers," R&D Review of Toyota CRDL, Vol. 41(3), pp. 22-28

[31] **Capobianco, M. and Gambarotta, A.**, 1992, "Variable Geometry and Waste-Gated Automotive Turbochargers - Measurements and Comparison of Turbine Performance," Journal of Engineering for Gas Turbines and Power-Transactions of the ASME, Vol. 114(3), pp. 553-560

[32] **Arnold, S., Groskreutz, M., Shahed, S. M., et al.**, 2002, "Advanced Variable Geometry Turbocharger for Diesel Engine Applications," SAE Technical Paper 2002-01-0161, 2002, doi:10.4271/2002-01-0161

[33] **Shimizu, K., Sato, W., Enomoto, H., et al.**, 2009, "Torque Control of a Small Gasoline Engine with a Variable Nozzle Turbine Turbocharger," SAE Technical Paper 2009-32-0169

[34] **Lezhnev, L., Kolmanovsky, I. and Buckland, J.**, 2002, "Boosted Gasoline Direct Injection Engines: Comparison of Throttle and VGT Controllers for Homogeneous Charge Operation," SAE Technical Paper 2002-01-0709

[35] **Buckland, J., Cook, J., Kolmanovsky, I., et al.**, 2000, "Technology Assessment of Boosted Direct Injection Stratified Charge Gasoline Engines," SAE Technical Paper 2000-01-0249, 2000, doi:10.4271/2000-01-0249

[36] **Tang, H., Pennycott, A., Akehurst, S., et al.**, 2015, "A Review of the Application of Variable Geometry Turbines to the Downsized Gasoline Engine," International Journal of Engine Research, Vol. 16(6), pp. 810-825

[37] **Ito, N., Ohta, T., Kono, R., et al.**, 2007, "Development of a 4-Cylinder Gasoline Engine with a Variable Flow Turbo-charger," SAE Technical Paper 2007-01-0263, 2007, doi:10.4271/2007-01-0263

[38] **Watson, N. and Janota, M. S.**, 1982, "Turbocharging the internal combustion engine", 1st ed. Basingstoke: Macmillan Education Limited.

[39] **Elpern, D.**, 1982, "The Effects of Turbocharger Design and Installation on Gasoline Vehicle Transient Response," SAE Technical Paper 821149, 1982, doi:10.4271/821149

[40] **Gabriel, H., Jacob, S., Munkel, U., et al.**, 2007, "The Turbocharger with Variable Turbine Geometry for Gasoline Engines," MTZ, Vol. 68(2), pp. 96-103

[41] **Corky, B.**, 1997, "Maximum Boost: Designing, Testing, and Installing Turbocharger Systems", 1st ed. Cambridge: Robert Bentley Automotive Publishers.

[42] **O'Connor, G. and Smith, M.**, 1988, "Variable Nozzle Turbochargers for Passenger Car Applications," SAE Technical Paper 880121, 1988, doi:10.4271/880121

[43] **Hishikawa, A., Okazaki, Y. and Busch, P.**, 1988, "Developments of Variable Area Radial Turbine for Small Turbochargers," SAE Technical Paper 880120, 1988, doi:10.4271/880120

[44] **Kawaguchi, J., Adachi, K., Kono, S., et al.**, 1999, "Development of VFT (Variable Flow Turbocharger)," SAE Technical Paper 1999-01-1242, 1999, doi:10.4271/1999-01-1242

[45] **Rogo, C., Hajek, T. and Roelke, R.**, 1983, "Aerodynamic Effects of Movable Sidewall Nozzle Geometry and Rotor Exit Restriction on the Performance of a Radial Turbine," SAE Technical Paper 831517, 1983, doi:10.4271/831517

[46] **Umezaki, E., Ogura, M. and Tomita, T.**, 1989, "Study of Variable Scroll Type Turbocharger (Determination of Shape of Scroll)," SAE Technical Paper 891874, 1989, doi:10.4271/891874

[47] **Ishihara, H., Adachi, K. and Kono, S.**, 2002, "Development of VFT Part 2," 2002-01-2165

[48] **Baines, N. C.**, 2005, "Fundamentals of Turbocharging", 1st ed. White River Junction, Vt.: Concepts NREC.

[49] **Capobianco, M. and Gambarotta, A.**, "Performance of a twin-entry automotive turbocharger turbine," Energy-Sources Technology Conference and Exhibition, Houston, 1993

[50] **Hajilouy, A., Rad, M. and Shahhosseine, M. R.**, 2009, "Flow and performance characteristics of twin-entry radial turbine under full and extreme partial admission conditions," Archive of Applied Mechanics, Vol. 79, pp. 1127-1143

[51] **Flaxington, D. and Szczupak, D. T.**, "Variable Area Radial Inflow Turbine," 2nd International Conference on Turbocharging and Turbochargers, London, 1982

[52] **Wallace, F. J., Baghery, A. and Ziriati, M. R.**, "Variable Geometry Turbocharging for Transport Engines," 2nd International Conference on Turbocharging and Turbochargers, London, 1982

[53] **Watson, N. and Banisoleman, K.**, "Performance of a Highly Rated Vehicle Diesel Engine With a Variable Geometry Turbocharger," 3rd International Conference on Turbocharging and Turbochargers, London, 1986

[54] **Hu, L., Yang, C., Sun, H., et al.**, 2011, "Numerical Analysis of Nozzle Clearance'sEffect on Turbine Performance," Chinese Journal of Mechanical Engineering, Vol. 24, pp. 1-8

[55] **Miller, K.**, 2008, "Turbo: Real World High-Performance Turbocharger Systems: S-A Design", 1st ed. North Branch: CarTech Inc.

[56] **Flardh, O. and Martensson, J.**, "Nonlinear Exhaust Pressure Control of an SI Engine with VGT Using Partial Model Inversion," 49th IEEE Conference on Decision and Control, Atlanta, USA, 2010

[57] **Andersen, J., Karlsson, E. and Gawell, A.**, 2006, "Variable Turbine Geometry on SI Engines," SAE Technical Paper 2006-01-0020, 2006, doi:10.4271/2006-01-0020

[58] **Hawley, J. G., Wallace, F. J., Cox, A., et al.**, 1999, "Variable geometry turbocharging for lower emissions and improved torque characteristics," Proceedings of the Institution of Mechanical Engineers, Part D: Journal of Automobile Engineering, Vol. 213, pp. 145-159

[59] **Bender, W., Gabriel, H., Lingenauber, R., et al.**, 2006, "Turbocharger with Variable Turbine Geometry (VGT) for the New Porsche 911 Turbo - A Milestone in Gasoline Turbocharging," Journal of Beijing Institute of Technology, Vol. 15, pp. 99-107

[60] **Matsumoto, K., Jinnai, Y. and Suzuki, H.**, "Development of Variable Geometry Turbocharger for Diesel Passenger Car," 6th International Conference on Turbocharging and Air Management Systems, London, 1998

[61] **Black, J., Eastwood, P. G., Tufail, K., et al.**, 2007, "The effect of VGT vane control on pumping losses during full-load transient operation of a common-rail diesel engine," SAE Technical Paper 2007-24-0063, 2007, doi:10.4271/2007-24-0063

[62] **Heywood, J. B.**, 1988, "Internal Combustion Engine Fundamentals", 1st ed. Grand Rapids: McGraw-Hill.

[63] **Copeland, C., Martinez-Botas, R., Turner, J., et al.**, "Boost system selection for a heavily downsized spark ignition prototype engine," 10th International Conference on Turbochargers and Turbocharging, London, 2012

[64] **Wieske, P., Lüddecke, B., Ewert, S., et al.**, 2009, "Optimisation of gasoline engine performance and fuel consumption through combination of

technologies " MTZ worldwide, Vol. 70(11), pp. 30-36

[65] **Bickerstaffe, S.**, "Ford's three-cylinder gasoline turbo cuts carbon to 109g/km in the C-segment Focus", Caspian Medias, 2012, Automotive Engineer, Vol. 37(1)

[66] **Christopher, R.**, 2012, "Ricardo Information Services New Engine News," Ricardo plc

[67] **Porsche Cars Great Britain Ltd**, [Access date]. *Porsche 911 Turbo S Technical Specs* [online]. Available from: http://www.porsche.com/uk/models/911/911-turbo-s/featuresandspecs/

[68] **King, J. and Böcher, O.**, "Multiple Injection and Boosting Benefits for Improved Fuel Consumption on a Spray Guided Direct Injection Gasoline Engine," FISITA 2012 World Automotive Congress, Beijing, 2012

[69] **King, J., Heaney, M., Bower, E., et al.**, "HyBoost - An intelligently electrified optimised downsized gasoline engine concept," 10th International Conference on Turbochargers and Turbocharging, London, 2012

[70] **Lumsden, G., OudeNijeweme, D., Fraser, N., et al.**, 2009, "Development of a Turbocharged Direct Injection Downsizing Demonstrator Engine," SAE Int. J. Engines 2(1):1420-1432, 2009, doi:10.4271/2009-01-1503

[71] **Giles, K., Lewis, A., Akehurst, S., et al.**, "The Effect of Advanced Combustion Control Features on the Performance of a Highly Downsized Gasoline Engine," FISITA 2012 World Automotive Congress, Beijing, China, 2012

[72] **Salamon, C., McAllister, M., Robinson, R., et al.**, "Improving Fuel Economy by 35% through combined Turbo and Supercharging on a Spark Ignition Engine," 21st Aachen Colloquium Automobile and Engine Technology 2012, Aachen, 2012

[73] **Pournazeri, M.**, 2012, "Development of a New Fully Flexible Hydraulic Variable Valve Actuation System," PhD thesis, University of Waterloo

[74] **Murphy, T.**, "Fiat breathing easy with Multiair", Ward's Communicationss, 2010, Ward's Auto World, Vol. 46

[75] **Luttermann, C., Schünemann, E. and Klauer, N.**, 2006, "Enhanced VALVETRONIC technology for meeting SULEV emission requirements," SAE Technical Paper 2006-01-0849, 2006, doi:10.4271/2006-01-0849

[76] **Parvate-Patil, G. B., Hong, H. and Gordon, B.**, 2003, "An assessment of Iintake and exhaust philosophies for variable valve timing," 2003-32-0078

[77] **Bickerstaffe, S.**, "Perspective", Caspian Medias, 2012, Automotive Engineer, Vol. 37(5)

[78] **Coltman, D., Turner, J. W. G., Curtis, R., et al.**, 2008, "Project Sabre: A Close-Spaced Direct Injection 3-Cylinder Engine with Synergistic Technologies to Achieve Low CO2 Output," SAE Int. J. Engines 1(1):129-146, 2009, doi:10.4271/2008-01-0138

[79] **Carey, C., McAllister, M., Sandford, M., et al.**, "Extreme engine downsizing," Innovations in Fuel Economy and Sustainable Road Transport, Pune, India, 2011

[80] **Kirwan, J. E., Shost, M., Roth, G., et al.**, 2010, "3-Cylinder Turbocharged Gasoline Direct Injection: A High Value Solution for Low CO2 and NOx Emissions," SAE Int. J. Engines 3(1):355-371, 2010, doi:10.4271/2010-01-0590

[81] **Turner, J. W. G., Pearson, R. J., Curtis, R., et al.**, 2008, "Improving Fuel

Economy in a Turbocharged DISI Engine Already Employing Integrated Exhaust Manifold Technology and Variable Valve Timing," SAE Technical Paper 2008-01-2449, 2008, doi:10.4271/2008-01-2449

[82] **Cairns, A., Fraser, N. and Blaxill, H.**, 2008, "Pre Versus Post Compressor Supply of Cooled EGR for Full Load Fuel Economy in Turbocharged Gasoline Engines," SAE Technical Paper 2008-01-0425, 2008, doi:10.4271/2008-01-0425

[83] **Luckert, P., Waltner, A., Rau, E., et al.**, 2006, "The New V6 Gasoline Engine with Direct Injection by Mercedes-Benz," MTZ 11 | 2006, Volume 67

[84] **Schwarz, C., Schünemann, E., Durst, B., et al.**, 2006, "Potentials of the Spray-Guided BMW DI Combustion System," SAE Technical Paper 2006-01-1265, 2006, doi:10.4271/2006-01-1265

[85] **Osborne, R., Rouaud, C., Andersson, J., et al.**, "Development of lean stratified turbocharged gasoline engines for 2018 SOP," SIA The Spark Ignition Engine of the Future, Strasbourg, 2013

[86] **Schmidt, L., Seabrook, J., Stokes, J., et al.**, 2011, "Multiple Injection Strategies for Improved Combustion Stability under Stratified Part Load Conditions in a Spray Guided Gasoline Direct Injection (SGDI) Engine," SAE Technical Paper 2011-01-1228, 2011, doi:10.4271/2011-01-1228

[87] **Lake, T., Stokes, J., Murphy, R., et al.**, 2004, "Turbocharging Concepts for Downsized DI Gasoline Engines," SAE Technical Paper 2004-01-0036, 2004, doi:10.4271/2004-01-0036

[88] **Yang, S. and Wang, L.-S.**, 2008, "Modeling of Two Charge-air Cooling Turbo-charging Systems for Spark Ignition Engines," SAE Int. J. Fuels Lubr. 1(1):1195-1205, 2009, doi:10.4271/2008-01-1702

[89] **Serrano, J. R., Climent, H., Dolz, V., et al.**, "Analysis of variable geometry turbine and variable valve timing combined potential in a GTDI engine using 1D simulation," The Spark Ignition Engine of the Future, Strasbourg, France, 2011

[90] **Kaiadi, M., Tunestål, P. and Johansson, B.**, 2011, "Reducing Throttle Losses Using Variable Geometry Turbine (VGT) in a Heavy-Duty Spark-Ignited Natural Gas Engine," SAE Technical Paper 2011-01-2022, 2011, doi:10.4271/2011-01-2022

[91] **Ericsson, G., Angstrom, H.-E. and Westin, F.**, 2010, "Optimizing the Transient of an SI-Engine Equipped with Variable Cam Timing and Variable Turbine," SAE Int. J. Engines 3(1):903-915, 2010, doi:10.4271/2010-01-1233

[92] **Flärdh, O.**, 2012, "Modeling, Control and Optimization of the Transient Torque Response in Downsized Turbocharged Spark Ignited Engines," PhD thesis, KTH Royal Institute of Technology

[93] **Turner, J. W. G., Popplewell, A., Patel, R., et al.**, 2014, "Ultra Boost for Economy Extending the Limits of Extreme Engine Downsizing," SAE Int. J. Engines 7(1):387-417, 2014, doi:10.4271/2014-01-1185

[94] **Reyes-Belmonte, M. A.**, 2013, "Contribution to the Experimental Characterization and 1-D Modelling of Turbochargers for IC Engines," PhD thesis, Universidad Polite´cnica de Valencia

[95] **Chen, H. and Winterbone., D.**, "A Method to Predict Performance of Vaneless Radial Turbine Under Steady and Unsteady Flow Conditions," 4th International Conference on Turbocharging and Turbochargers, London, 1990

[96] **Chen, H., Hakeem, I. and Martinez-Botas, R.**, 1996, "Modelling of a

Turbocharger Turbine under Pulsating Inlet Conditions," Proceedings of the Institution of Mechanical Engineers, Part A: Journals of Power and Energy, Vol. 210, pp. 397-408

[97] **Fajardo, P.**, 2012, "Methodology for the Numerical Characterization of a Radial Turbine under Steady and Pulsating Flow," PhD thesis, Universitat Politècnica de València

[98] **Luján, J. M., Galindo, J. and Serrano, J. R.**, 2001, "Efficiency Characterization of Centripetal Turbines under Pulsating Flow Conditions," SAE Technical Paper 2001-01-0272, 2001, doi:10.4271/2001-01-0272

[99] **Shaaban, S.**, 2004, "Experimental Investigation and Extended Simulation of Turbocharger Non-adiabatic Performance," PhD thesis, University of Hannover

[100] **Rautenberg, M., Mobarak, A. and Molababic, M.**, "Infuence of Heat Transfer Between Turbine and Compressor on the Performance of Small Turbochargers," ASME International Gas Turbine Congress, Tokyo, 1983

[101] **Serrano, J., Olmeda, P., Arnau, F., et al.**, 2013, "Importance of Heat Transfer Phenomena in Small Turbochargers for Passenger Car Applications," SAE Int. J. Engines 6(2):716-728, 2013, doi:10.4271/2013-01-0576

[102] **Tang, H., Burke, R., Akehurst, S., et al.**, "Predicting the Trade-off Between Turbine Inlet Temperature and Engine Fuel Economy in a Turbocharged Gasoline Engine," IAV International Congress on Engine Processes, Berlin, 2013

[103] **Cormerais, M., Hetet, J. F., Chesse, P., et al.**, 2006, "Heat Transfer Analysis in a Turbocharger Compressor: Modelling and Experiments," SAE Technical Paper 2006-01-0023, 2006, doi:10.4271/2006-01-0023

[104] **Burke, R. D., Olmeda, P., Arnau, F. J., et al.**, "Modelling of Turbocharger Heat Transfer under Stationary and Transient Engine Operating Conditions," 11th International Conference on Turbochargers and Turbocharging, London, 2014

[105] **Bellis, V. D., Bozza, F., Schernus, C., et al.**, 2013, "Advanced Numerical and Experimental Techniques for the Extension of a Turbine Mapping," SAE Int. J. Engines 6(3):1771-1785, 2013, doi:10.4271/2013-24-0119

[106] **Capobianco, M. and Marelli, S.**, 2011, "Experimental Analysis of Unsteady Flow Performance in an Automotive Turbocharger Turbine Fitted with a Waste-gate Valve," Proceedings of the Institution of Mechanical Engineers, Part D: Journal of Automobile Engineering, Vol. 225

[107] **Capobianco, M. and Marelli, S.**, 2007, "Waste-Gate Turbocharging Control in Automotive SI Engines: Effect on Steady and Unsteady Turbine Performance," SAE Technical Paper 2007-01-3543, 2007, doi:10.4271/2007-01-3543

[108] **Capobianco, M. and Marelli, S.**, 2005, "Transient Performance of Automotive Turbochargers: Test Facility and Preliminary Experimental Analysis," SAE Technical Paper 2005-24-066, 2005, doi:10.4271/2005-24-066

[109] **Serrano, J. R., Arnau, F. J., Fajardo, P., et al.**, 2012, "Contribution to the Modeling and Understanding of Cold Pulsating Flow Influence in the Efficiency of Small Radial Turbines for Turbochargers," ASME Journal of Engineering for Gas Turbines and Power, Vol. 134

[110] **Galindo, J., Serrano, J. R., Guardiola, C., et al.**, 2006, "Surge Limit

Definition in a Specific Test Bench for the Characterization of Automotive Turbochargers " Experimental Thermal and Fluid Science, Vol. 30, pp. 449-462

[111] **Margot, X., Gil, A., Tiseira, A., et al.**, 2008, "Combination of CFD and Experimental Techniques to Investigate the Flow in Centrifugal Compressors Near Surge Line," SAE Technical Paper 2008-01-0300, 2008, doi:10.4271/2008-01-0300

[112] **Karamanis, N. and Martinez-Botas, R. F.**, 2002, "Mixed-flow turbines for automotive turbochargers: Steady and unsteady performance," International Journal of Engine Research, Vol. 3

[113] **Copeland, C. D., Martinez-Botas, R. and Seiler, M.**, "Unsteady Performance of A Double Entry Turbocharger Turbine With A Comparison to Steady Flow Conditions," ASME Turbo Expo, Berlin, 2008

[114] **Copeland, C. D., Martinez-Botas, R. and Seiler, M.**, 2012, "Unsteady Performance of a Double Entry Turbocharger Turbine With a Comparison to Steady Flow Conditions," ASME Journal of Turbomachinery, Vol. 134

[115] **Szymko. S, McGlashan, N. R., Martinez-Botas, R.**, and **Pullen, K. R.**, 2006, "The Development of a Dynamometer for Torque Measurement of Automotive Turbocharger Turbines," Proceedings of the Institution of Mechanical Engineers, Part D: Journal of Automobile Engineering, Vol. 221(2), pp. 225–239

[116] **Benz, A., Riess, M., Sens, M., et al.**, "Studies on Using Intake Valve Lift Strategies for Generating Turbulence," IAV International Congress on Engine Processes, Berlin, 2013

[117] **Gamma Technologies**, 2014, "GT-Suite Flow Theory Manual version 7.4"

[118] **Ricardo**, 2014, "Wave Build V8.3 Help System,"

[119] **Neumeister, J. and Hattrell, T.**, "Development of an advanced Quasi-Dimensional SI Engine Combustion Model," GT-Power User Conference, Frankfurt, 2005

[120] **Stone, R.**, 1999, "Introduction to Internal Combustion Engines", 3rd ed. London: Macmillan Press Ltd. 0-333-74013-0

[121] **Suyabodha, A., Pennycott, A. and Brace, C. J.**, 2013, "A Preliminary Approach to Simulating Cyclic Variability in a Port Fuel Injection Spark Ignition Engine," Proceedings of the Institution of Mechanical Engineers, Part D: Journal of Automobile Engineering, Vol. 227(5), pp. 665–674

[122] **Burke, R.**, 2011, "Investigation into the Interactions between Thermal Management, Lubrication and Control Systems of a Diesel Engine," PhD thesis, University of Bath

[123] **Lee, B.**, 2009, "Dual-Stage Boosting Systems: Modeling of Configurations, Matching and Boost Control Options," PhD thesis, University of Michigan

[124] **Yang, M. Y., Martinez-Botas, R., Padzillah, M. H., et al.**, "Comparison of the Influence of Unsteadiness between Nozzled and Nozzleless Mixed Flow Turbocharger Turbines," 11th International Conference on Turbochargers and Turbocharging, London, 2014

[125] **Chen, H. and Winterbone, D. E.**, "A One-Dimentional Performance Model for Turbocharger Turbine Under Pulsating Inlet Condition," 11th International Conference on Turbochargers and Turbocharging, London, 2014

[126] **Schwarz, J. B. and Andrews, D. N.**, "Recommended Practices for Contemporary Turbocharger Gas Stand Testing," 11th International

Conference on Turbochargers and Turbocharging, London, 2014

[127] **Bolz, H., Rinaldi, A. and Kaufmann, A.**, "Critical Aspects in Turbocharger Testing," 11th International Conference on Turbochargers and Turbocharging, London, 2014

[128] **Tang, H., Burke, R., Akehurst, S., et al.**, "Predicting the Trade-off Between Turbine Inlet Temperature and Engine Fuel Economy in a Turbocharged Gasoline Engine," IAV International Congress on Engine Processes, Berlin, 2013

[129] **Tang, H., Akehurst, S., Brace, C., et al.**, "Gasoline Engine Load Control Using Variable Geometry Turbine Turbochargers," The Spark Ignition Engine of the Future, Strasbourg, France, 2013

[130] **Tang, H., Akehurst, S., Brace, C. J., et al.**, "Optimisation of transient response of a gasoline engine with variable geometry turbine turbocharger," 11th International Conference on Turbochargers and Turbocharging, London, 2014

[131] **Burke, R. D., Brace, C. J. and Hawley, J. G.**, 2011, "Critical Evaluation of On-Engine Fuel Consumption Measurement," Proceedings of the Institution of Mechanical Engineers, Part D: Journal of Automobile Engineering, Vol. 225(6), pp. 829-844